NORTHWESTERN UNIVERSITY

Molecular-Level Design of Supramolecular Compounds and Nanomaterials

A DISSERTATION

SUBMITTED TO THE GRADUATE SCHOOL

IN PARTIAL FULFILLMENT OF THE REQUIREMENTS

for the degree

DOCTOR OF PHILOSOPHY

Field of Chemistry

By

Andrea Ivana d'Aquino

EVANSTON, ILLINOIS

March 2020

ABSTRACT

Molecular Level Design of Supramolecular Compounds and Nanomaterials

Andrea Ivana d'Aquino

Molecules are highly social: they recognize one another and form bonds with those they are attracted to and repel those they are not. Some molecules establish strong bonds, while others form weak, transient associations. These interactions are ubiquitous in Nature and are integral to life. For at the basis of many biological processes lies the ability of molecules to recognize and respond to one another. Molecular chaperonins and G-protein-coupled receptors, for example, rely on the reversible binding of molecules and proteins to guide crucial cellular functions ranging from protein folding to signal transduction. To achieve these tasks, the proteins assemble to form binding sites that reversibly and selectively bind guests through weak, intermolecular interactions known as supramolecular interactions. These supramolecular interactions render proteins *allosteric*, which enables them to adapt their structure and activity in response to changing chemical environments and, as a result, facilitate complex chemical processes. Nature's ability to orchestrate such complex chemistries, has inspired chemists to develop synthetic enzyme mimics capable of allosteric regulation.

Coordination chemistry has emerged as a powerful means to design inorganic constructs that exploit supramolecular interactions. This thesis describes the design and synthesis of bioinspired, stimuli-responsive coordination constructs, assembled via the Weak-Link approach (WLA). The WLA represents one of the few sets of fundamental reactions in inorganic chemistry that allow one to synthesize spatially defined, stimuli-responsive, and multi-component frameworks in high to quantitative yields and with remarkable functional group tolerance. The

WLA enables access to distinctly different structural states via small-molecule reactions at a metal node, which affect the coordination of hemilabile ligands. The generality and applications of this approach are demonstrated in Chapter 1. In Chapter 2, an allosterically regulated macrocycle reminiscent of a protein binding pocket, is designed and characterized. As described in Chapter 3, this system can access four distinct states and may be used in the construction of sophisticated stimuli-responsive sensors and receptors. In Chapters 4 and 5, we show that the principles of the WLA may be extended to the design and synthesis of stimuli-responsive materials. Finally, in Chapter 6, new types of stimuli-responsive WLA systems are explored.

_____

Professor Chad A. Mirkin

ACKNOWLEDGEMENTS

Our achievements are never our own—they are shared by the many people who have supported, encouraged and believed in us throughout our journey. I am privileged to have had so many people join me on my journey through graduate school and am indebted to them for their unconditional love and support and for believing in me at times when it was difficult to believe in myself. This work would not have been possible without my family, friends and mentors; therefore, I would like to specifically acknowledge the many people who have made this dissertation possible. I am grateful for their contributions and support.

From the beginning, my family committed to joining me on my journey through graduate school, and they have afforded me unwavering support, love, and compassion. Thank you to my mom and dad, Katherine and João d'Aquino, for their unconditional love, encouragement, and unfaltering confidence in me. You have instilled within me—and all your children—a truly indomitable will; you taught us to be ambitious and to persist. You have both made great sacrifices in order to give your kids opportunities, and I am so grateful for your courage, selflessness and love. Thank you to my twin sister, Anne, for being my encouragement, inspiration, and my very best friend throughout my life and graduate school. You are an exemplary scholar and teacher, and you constantly inspire me to do the best I can. You have been my compass, and I don't know where I would be without you. Thank you to my sisters, Aurea and Valentina, for their unwavering love and support and for teaching me how to be strong in the face of great adversity. You both inspire me with your resilience and tenacity. And thank you to my brother, Anthony, for being a mentor to me and for encouraging me to never give up on my dreams. You faced so many challenges as the oldest sibling and our only brother, and I am forever grateful for everything you have taught

me and for all the time you spent watching over your sisters. You have given me the strength to push forward. Thank you to Dion, Sandy, Aaron, Luis, Ashlee and Drew, for being a part of my life and my family; I am fortunate to have received so much love and support from each of you.

I would like to express a profound appreciation for my advisor, Professor Chad Mirkin, for his support, advice, mentorship, and supervision throughout the completion of my PhD. Professor Mirkin has been an invaluable source of guidance and encouragement and has always been supportive of my academic interests. The insightful criticisms and suggestions he has offered throughout my research has shaped its direction and outcome considerably. Thank you to my other committee members, Professor Emily Weiss and Professor Thomas Meade, for providing me with constructive feedback and support throughout my PhD. I also thank my undergraduate advisor, Professor Mark Bussell. I would not be where I am without Professor Bussell's kindness and mentorship during my time as an undergraduate at Western Washington University.

My intellectual and professional development has been greatly shaped by my fellow graduate students and peers at Northwestern. Thank you to all of my collaborators, who have made this work possible, including Dr. Jose Mendez-Arroyo, Ho Fung (Edmund) Cheng, Dr. Abha Gosavi, Dr. Lisa Cole, Dr. Lam-Kiu Fong, Dr. Charlotte Stern, Oliver Hayes, Dr. Andy Wang, Dr. Mike McGuirk, Yuan Liu, Ben Coleman and McKinley Paul. Thank you to Professor Joaquin Baroso Flores, for your invaluable computational work that significantly enhanced the research we published. Special thanks to my mentor, Dr. Jose Mendez-Arroyo, who taught me how to think like a chemist and to critically evaluate my work and the work of others. Thank you for helping me to see the value in my work even when I, in moments of self-doubt, had lost sight of it. I also

thank all other members of the Organometallic Subgroup (past and present) and the Mirkin Laboratory for their help, inspiration, and countless scientific discussions.

Thank you to my friends who, without them, I would be lost. Thank you to Anne d'Aquino, Steven Swick, Ellie Page, Drew Bauman, Lam-Kiu Fong, Lisa Cole, Kevin Metcalf, and Ryan Ross, for always being there for me, and helping guide me when I lost direction. Discussions with each of you have always filled me with a sense of clarity and energy for doing science and positively changing the world. In addition to providing me with your knowledge and expertise, every interaction I have had with each of you, reminds me of what a pleasure it is to think with others about chemistry, science, and life. Each of you have motivated me to not be content in approaching a problem with one set of techniques and from the perspective of one field of inquiry, but rather to approach a problem using any technique that might be illuminating and with help from any field that might be relevant. Special thanks to Lam-Kiu, who patiently supported me in my science and life, as I tried to navigate my way through countless challenges throughout graduate school. I am so lucky to call you each my friend.

Thank you to Edmund Cheng and Oliver Hayes, for being great friends and lab mates to me during graduate school. You came to graduate school as mentees, but there were many times when I felt that I was the one being mentored. I have greatly benefited from conversations and scientific discussions with each of you and am grateful to have had the opportunity to learn and grow from you both. Thank you to Christine Laramy and Matt O'Brien for the wonderful beach volleyball games, book clubs, food discussions, and appetizer nights. Thank you to Jose Mendez Arroyo and Alyssa Chinen, for your guidance, mentorship, and friendship. I am incredibly fortunate to have had great mentors to look up to.

Thank you to Professor Jennifer Lackey and all the members of Northwestern's Prison Education Program (NPEP): Anne d'Aquino, Steven Swick, Hansen Breitling, Magda Boutros, Charlotte Rosen, Jonas Rosenbrück, Jake Rothschild, Ari Tolman, Oliver Hayes, Riki Drout, Dr. Anya Degenshein, Dr. Lauren Leydon-Hardy and, of course, Professor Barron Reed (who was often working behind the scenes). Working alongside the members of NPEP was the most enriching experience of my graduate school career. Thank you to our students at Stateville Correctional Center, who have an unrelenting desire to learn and who, on a daily basis, inspire me with their fortitude, intellect, and perspectives of the world. I will deeply miss seeing you, and learning from you all each week.

Thank you to the members of NU BonD (past and present), Lam-Kiu Fong, Abdallah Diagne, Kedy Edme, Alicia McGeachy, Dana Westmoreland, Ariana Gray Bé, Jiaqi Li, Oliver Hayes, Zachary Urbach, Waleed Helweh, Nic Watkins, Sam Harvey, Emily McClure, and Naomi Dalchand. Thank you for sharing your identities and perspectives with me and for your passion in fighting to bring change and equity to science. Thank you to Jonathan, Madison and Laura, for always advocating for students and for all the work you have done to help me—and many other graduate students—through innumerable challenges we have faced here as graduate students at Northwestern, over the years.

Finally, I would like to thank Steven Swick for being an incredible partner, teacher, listener, and friend. You have been a source of companionship, laughter, love, and encouragement, and you taught me the true meaning of success: happiness. Your loving support and sage advice got me through some of the most trying aspects of graduate school. Thank you for believing in me at times when I didn't believe in myself, and for always challenging me and inspiring me. I greatly

appreciate the sacrifices you have made for us over the past five years, and I look forward to writing the next chapter of our lives together. We will never stop dreaming together.

It is the friendships I have found in graduate school that kept me afloat, and it is these friendships that I will always cherish and remember. My friends and family have given my life value and direction, and for that, I am eternally grateful.

"Nothing in life is to be feared, it is only to be understood." – Marie Curie

LIST OF ABBREVIATIONS

BAr^F_4	tetrakis[3,5-bis(trifluoromethyl)phenyl]borate
Calcd	calculated
CCD	charge coupled device
cod	1,5-cyclooctadiene
DBA	Directional Bonding Approach
DCM	dichloromethane
DFT	discrete Fourier transform
DMF	dimethylformamide
DMSO	dimethylsulfoxide
DOSY	diffusion ordered spectroscopy
EM	electron microscopy
ESI-MS	electrospray ionization mass spectrometry
Et_2O	diethyl ether
GGA	generalized gradient approximation
HPLC	high performance liquid chromatography
HR-MS	high-resolution electrospray ionization mass spectrometry
K_a	binding affinity
LC-TOF	liquid chromatography-time of flight
MeCN	acetonitrile
MeOH	methanol
NBO	natural bond orbital
NBODel	natural bond orbital deletion
NHC	N-heterocyclic carbene
NHC,S	N-heterocyclic carbene thioether
NMR	nuclear magnetic resonance
P,S	phosphine thioether
PPN	bis(triphenylphosphine)iminium
R_H	hydrodynamic radius
SIA	Symmetry Interaction Approach
STEM	scanning tunneling electron microscopy
THF	tetrahydrofurane
WLA	Weak-Link Approach

TABLE OF CONTENTS

ABSTRACT 3

ACKNOWLEDGEMENTS 5

LIST OF ABBREVIATIONS 10

TABLE OF CONTENTS 11

LIST OF TABLES AND FIGURES 18

CHAPTER 1 25

Introduction 25

1.1 Allosteric Regulation in Nature 26

1.1.1 Molecular Recognition in Nature 29

1.1.2 Nature's Reactive Cavities and Binding Pockets 30

1.2 Synthetic Enzyme Mimics 31

1.2.1 Molecular Recognition with Synthetic Receptors and Cages 31

1.2.2 Synthetic, Organic Receptors and Cages 33

1.2.3 Synthetic, Coordination-Based Receptors and Cages 35

1.3 Approaches to Coordination-Based Supramolecular Architectures 37

1.4 The Weak-Link Approach to Supramolecular Coordination Chemistry 39

1.4.1 WLA Structures Based Upon Hemilabile Ligands 40

1.4.2 General Approach to the Synthesis of Air-Stable Pt(II) WLA Architectures 41

1.4.3 Step-wise Construction of Heteroligated Pt(II) WLA Complexes 42

1.5 Allosterically-Regulated, Weak-Link Approach Macrocycles and Receptors 43

1.5.1 An Allosterically-Regulated Molecular Receptor with Switchable Selectivity 43

1.5.2 Reversible and Selective Encapsulation of Dextromethorphan and β-Estradiol Using an Asymmetric Molecular Capsule Assembled via the Weak-Link Approach 45
1.6 Introduction to Dissertation Topics 46
1.6.1 An Allosterically-Regulated Four State Macrocycle 46
1.6.2 Complex Switching Behavior in a Four State WLA Macrocycle 47
1.6.3 Design, Synthesis and Characterization of Infinite-Coordination Polymers Bearing Weak-Link Approach Building Blocks 48
1.6.4 Reconfigurable, Bio-Inspired Coordination Polymers Assembled *via* the Weak-Link Approach 48
CHAPTER 2 50
An Allosterically Regulated, Four-State Macrocycle 50
2.1 Introduction 51
2.2 Results and Discussion 55
2.2.1 Model WLA Macrocycle Design 55
2.2.2 WLA Macrocycle Synthesis and Characterization 56
2.2.3 The Solid-State Structure of 13a 62
2.2.4 Computational Studies of Complexes 13a-c 62
2.3 Conclusions 64
2.4 Experimental Methods 65
2.4.1 General Methods and Instrument Details 65
2.4.2 Synthesis 66
2.4.2.1 Synthesis of Benzimidazolium Salt (14) 66

2.4.2.2 [$Pt_2Cl_4(\kappa^1{:}\mu{:}\kappa^1$–NHC,S)$(C_2H_6OS)_2$] (12-DMSO) 66

2.4.2.3 1,4-bis(diphenylphosphino)ethylthiobenzene (10)..... 67

2.4.2.4 Synthesis of [cis–$Pt_2Cl_4(\kappa^1{:}\mu{:}\kappa^1$–NHC,S)($\kappa^1{:}\mu{:}\kappa^1$–P,S)], [trans–$Pt_2Cl_4(\kappa^1{:}\mu{:}\kappa^1$–NHC,S)($\kappa^1{:}\mu{:}\kappa^1$–P,S)], and [cis–$PtCl_2(\kappa^1{:}\mu{:}\kappa^1$–NHC,S)($\kappa^1{:}\mu{:}\kappa^1$–P,S)–trans–$PtCl_2(\kappa^1{:}\mu{:}\kappa^1$– NHC,S)($\kappa^1{:}\mu{:}\kappa^1$–P,S)] (13a-c). 67

2.4.2.5 [cis–$Pt_2Cl_4(\kappa^1{:}\mu{:}\kappa^1$–NHC,S)($\kappa^1{:}\mu{:}\kappa^1$–P,S)] (13a) 68

2.4.3 X-ray Crystallography 68

2.4.3.1 Crystal Structures of Complexes 12 and 13a 68

2.4.4 NMR Spectra of all Compounds and Complexes 70

2.4.5 Mass Spectra of all Complexes 75

CHAPTER 3 77

Complex Switching Behavior in a Four State WLA Macrocycle 77

3.1 Introduction 78

3.2 Results and Discussion 78

3.2.1 Formation of the Semi-Open WLA Macrocycle 78

3.2.2 Formation of a New WLA Intermediate State 82

3.2.3 Formation of the Fully Closed State 84

3.2.4 Accessing Each of the Reversible States 87

3.3 Conclusions 88

3.4 Experimental Methods 89

3.4.1 General Methods and Instrument Details 89

3.4.2 Synthesis 90

3.4.2.1 [cis–$Pt_2Cl_2(\kappa^1{:}\mu{:}\kappa^1$–NHC,S)($\kappa^2{:}\mu{:}\kappa^2$–P,S)][Cl]$_2$ (14). 90

3.4.2.2 [cis–$Pt_2(\kappa^1{:}\mu{:}\kappa^2$–NHC,S)($\kappa^2{:}\mu{:}\kappa^2$–P,S)$CD_3OD$][$BF_4$]$_4$ (15). 90

3.4.2.3 [cis–$Pt_2(\kappa^2{:}\mu{:}\kappa^2$–NHC,S)($\kappa^2{:}\mu{:}\kappa^2$–P,S)][$BF_4$]$_4$ (16). 91

3.4.3 Computational Details 91

3.4.3.1 Energy Minimized Models of 14, 15 and 16 92

3.4.3.2 Bond Energies Calculated for Complexes 14, 15 and 16 92

3.4.3.3 Fukui Indices Calculated for Complex 14 93

3.4.3.4 Diastereomers of 14 and 16 93

3.4.4 Reversible Opening and Closing of the WLA Macrocycle 94

3.4.4.1 General Procedure for Re-Opening 15 to Form Semi-Open Macrocycle 14 . 94

3.4.5 NMR Spectra of all Compounds and Complexes 96

3.4.6 Mass Spectra of all Complexes 101

CHAPTER 4 102

Infinite Coordination Polymer Particles Composed of Stimuli-Responsive Coordination Complex Subunits 102

4.1 Introduction 103

4.2 Results and Discussion 104

4.2.1 Synthesis and Characterization 104

4.2.2 Synthesis of Monomeric Building Blocks: 18-Pt-Open and 18-Pt-Closed 105

4.2.3 Synthesis of Coordination Polymers: 19-Pt-Open and 19-Pt-Closed 107

4.2.4 Synthesis of Infinite Coordination Polymer Particles 108

4.2.5 Synthesis of Pd^{II}-Based Coordination Polymers and Particles 109

4.3 Conclusions 112

4.4 Experimental Methods 112

4.4.1 General Methods 112

4.4.2 Synthesis 114

4.4.2.1 Synthesis of 4'-[4-(mercaptomethyl)phenyl]-2,2':6',2''-terpyridine 114

4.4.2.2 Synthesis of 18-Pt-Open 115

4.4.2.3 Synthesis of 18-Pt-Closed 116

4.4.2.4 Synthesis of 18-Pd-Closed 117

4.4.2.5 Synthesis of 18-Pd-Open 118

4.4.2.6 Synthesis of 19-Pd-Closed 119

4.4.2.7 Synthesis of 19-Pd-Open 120

4.4.2.8 Synthesis of 19-Pt-Closed 120

4.4.2.9 Synthesis of 19-Pt-Open 121

4.4.3 X-Ray Crystal Data 122

4.4.4 Characterization of Coordination-Polymers Bearing WLA Subunits 123

4.4.4.1 ^{1}H NMR and ^{1}H DOSY Spectra of Coordination Polymers 124

4.4.5 DFT Calculations 126

4.4.6 Post Polymerization Switching of States 126

4.4.7 Infinite Coordination Polymer Particle Characterization 131

4.4.8 ICP Particles Synthesis in Varying Conditions 132

4.4.9 NMR Spectra of all Compounds and Complexes 133

4.4.10 Mass Spectra of all Complexes 138

CHAPTER 5 143

Design of Reconfigurable, Bio-Inspired Coordination Polymers 143

Assembled *via* the Weak-Link Approach 143

5.1 Introduction 144

5.2 Results and Discussion 146

5.2.1 Design of CP Building Blocks Possessing Coordinating Hemilabile Ligands 146

5.2.2 Synthesis 149

5.2.2.1 Synthesis of the Closed Pd^{II} Monomer, Complex 23 149

5.2.2.2 Synthesis of the Crystalline Coordination Polymer Chain (24) 150

5.2.3 The Solid-State Structure of Coordination Polymer 24 152

5.2.4 Formation of Coordination Polymers Composed of Monomer 23 and Pt^{II} Metal Salts 153

5.2.5 Structural Studies of Pt^{II} Tweezer Monomer Analogs 154

5.3 Conclusions 155

5.4 Experimental Methods 156

5.4.1 General Methods 156

5.4.2 Synthesis 157

5.4.2.1 Synthesis of Hemilabile P,S–Pyr Ligand (22) 157

5.4.2.2 Synthesis of $Pd(P,S–Pyridine)_2(BF_4)_2$ (23) 158

5.4.2.3 Synthesis of Coordination Polymer 24 158

5.4.2.4 Synthesis of $Pt(P,S–Pyridine)_2Cl_2$ 158

5.4.3 Opening the Fully Closed Pd^{II} Complex 23 159

5.4.3 NMR Spectra of all Complexes 160

5.4.5 X-Ray Crystal Data 163

5.4.6 Computational Details 166

CHAPTER 6 167

Dissertation Overview and Future Outlook 167

6.1 Dissertation Overview 168

6.2 Summary and Conclusions 170

6.3 Future Directions 174

6.3.1 Towards a Library of Allosteric, Multi-State Receptors 175

6.3.2 1-D, 2-D and 3-D Coordination Polymer Materials via Chemically Tunable Metal–Ligand Interactions 180

CHAPTER 7 181

Conclusion 181

REFERENCES 183

LIST OF TABLES AND FIGURES

CHAPTER 1

Table 1.1 Common Non-Covalent Interactions and their Associated Strengths in kJ mol^{-1} 27

Figure 1.1 Hydrogen bonding present in alpha helices is an example of a non-covalent interaction employed by Nature. The hydrogen bonding between base pairs defines the helical structure. .. 28

Figure 1.2 The basic principle of allosteric regulation in proteins can be illustrated with the binding of oxygen to hemoglobin isolated from red blood cells. The hemoglobin protein displays cooperative binding between subunits. 29

Figure 1.3 Chaperonin proteins consist of two stacked rings of subunits that enclose separate cavities for the binding of substrates. The chaperonin protein facilitates protein re-folding. 31

Figure 1.4 Some of the early synthetic, organic host-guest architectures (from left to right): cryptands, spherands and crown ethers. 32

Figure 1.5 Binding induced conformational changes in a synthetic receptor (**1**) possessing two distinct binding sites: the polyether which binds alkali metal ions and the 2,2'-bipyridyl function which binds transition metals..... 34

Figure 1.6 Many organic receptors have been developed through the assembly of cavitands such as calixarene, resorcinarene and cyclodextrin derivatives. 35

Figure 1.7 Coordination-based supramolecular capsule (**2**) developed by the Fujita group. The capsule facilitates the pair-selective encapsulation of 9-hydroxymethylanthrancene and *N*-cyclohexyl maleimide, within cage **2** and the subsequent Diels-Alder reaction. 37

Figure 1.8 Approaches to coordination-based supramolecular constructs: A) The Directional Bonding Approach for the synthesis of squares, B) the Symmetry Interaction Approach for the synthesis of tetrahedrons, and C) the Weak-Link Approach for the synthesis of macrocycles.... 38

Figure 1.9 Depiction of tweezers, macrocycles and triple-decker complexes that can be assembled via the WLA. Such structures employ d^8 metal centers and hemilabile ligands. 39

Figure 1.10 The weak-link approach (WLA) to supramolecular chemistry employs hemilabile ligands and metal ions to make condensed, or closed, structures in high yield. These closed complexes can be interconverted between open, flexible states through small molecule coordination chemistry..... 40

Figure 1.11 Selective and reversible encapsulation of *N*-methylpyridinium (blue) and *N*-oxide pyridine (red) is achieved using a multi-state ion-regulated molecular receptor capable of accessing a closed state (**3**), a semi-open state (**4**) and a fully state (**5**). 45

Figure 1.12 An allosterically regulated, asymmetric receptor featuring a binding cavity large enough to accommodate three-dimensional pharmaceutical guest molecules as opposed to planar,

rigid aromatics, was synthesized via the WLA. This architecture is capable of switching between an expanded, flexible “open” configuration and a collapsed, rigid “closed” one..... 46

..... 131

CHAPTER 2

Figure 2.1 The Weak-Link Approach (WLA) to coordination-driven supramolecular (a) macrocycles, (b) tweezers, and (c) triple-decker complexes. For the sake of this example, complexes with Pd^{II} and Pt^{II} metal centers are illustrated, but the WLA works with many other metal systems including Rh^{I}, Cu^{I} and Ir^{I}.[91-94] 52

Scheme 2.1 (a) Step-Wise Approach to the Synthesis of WLA Tweezer and Triple-Decker Complexes, (b) Step-Wise Assembly of a WLA Heteroligated Pt^{II} Macrocyclic Capsule (c) The Scope of this Work Applies this Approach to the Synthesis of an Allosterically-Regulated, Multi-State, Heteroligated Macrocycle.[a] 54

Scheme 2.2 a) Heteroligated Pt(II) WLA complexes containing weakly donating ligands (P,O through P,S-tetrafluoroaryl) are kinetically labile, resulting in ligand scrambling; b) The strategy described here takes advantage of strong NHC-Pt(II) interactions to assemble heteroligated Pt(II) macrocycles..... 55

Figure 2.2 The design of a heteroligated WLA macrocycle bearing a ditopic bidentate NHC,S–based ligand (**12**) in conjunction with a traditional ditopic bidentate P,S–based ligand (**10**). 56

Scheme 2.3 Synthesis of Fully Open Heteroligated Macrocycles **13a-13c**. Reaction conditions: (i) 2 eq. $PtCl_2$(cod); 1 eq. Ag_2O; 6:1 CH_2Cl_2:MeOH, 24 h, 60 °C. (ii) 1:1 MeOH:CH_2Cl_2, 25 °C. (iii) CH_2Cl_2, 25 °C. 57

Figure 2.3. Single crystals obtained of complex **12-DMSO**..... 58

Figure 2.4 (a) ^{31}P NMR spectrum of complex mixture **13** in CD_2Cl_2, (b) ^{31}P NMR spectrum of single crystals of the fully open *cis* complex, **13a**, dissolved in CD_2Cl_2, (c) ^{31}P NMR spectrum of **13a** after several hours, indicating the reappearance of resonances attributable to the *cis* (**13a**), trans (**13b**), and *cis/trans* (**13c**) species. 60

Figure 2.5 Crystal structure of **13a**, drawn with a 50% thermal ellipsoid probability. Solvent molecules and hydrogen atoms have been omitted for clarity. Selected bond lengths [Å] and angles [deg]: Pt1–Cl2 2.360(2), Pt1–Cl2 2.352(2), Pt2–Cl3 2.340(2), Pt2–Cl4 2.357(2), Cl1–Pt1–Cl2 90.57(6), Cl3–Pt2–Cl4 89.42(6). 61

Figure 2.6 Energy-minimized models of complexes **13a–13c**, obtained from DFT calculations. 63

Table 2.1 Free Energies (kcal/mol) of **13a–13c** Obtained from DFT Calculations. 64

Table 2.2 Crystallographic Data for Complex **12-DMSO** and **13a** 69

CHAPTER 3

Scheme 3.1 Formation of the Semi-Open WLA Macrocycle. Reaction conditions: (i) Room temperature, MeOH, 25 °C. (ii) CH_2Cl_2, 25 °C. 79

Figure 3.1 ^{1}H DOSY NMR spectra of a sample containing complex **14** in methanl-*d*$_4$. The region corresponding to the semi-open species is indicated by the dotted red line. Asterisks denotes a diastereomer of **14**. The average diffusion coefficient of complex **14** in methanol, was determined to be $8x10^{-6}$ cm^2s^{-1}. 80

Figure 3.2 (a) ^{31}P NMR spectra of each distinct state accessible by the WLA macrocycle, namely, a fully open (**13**) a semi-open (**14**), a new intermediate state (**15**) with one Pt^{II} node in the closed state and the other in a semi-open state, and a fully closed state (**16**). (b) MALDI–TOF spectra compared with ISOPRO simulation of the molecular ion $[M–BF_4]^+$ of complex **16**. 81

Figure 3.3 ^{31}P NMR spectra of complex **14** in methanol-*d*$_4$ from 213 K to 330 K. Coalescence of the major resonance (36 ppm) and the corresponding diastereomer' resonance (37 ppm) is observed at high temperature, consistent with the presence of rapidly interconverting diastereomers. 82

Scheme 3.2 Formation of (a) the New Intermediate WLA Macrocycle State (**15**), and (b) the Fully Closed Macrocycle (**16**). Reaction conditions: (i) 4 equiv. $AgBF_4$, methanol-*d*$_4$. (ii) 1. High vacuum to remove methanol-*d*$_4$ (MeOD), 2 h; 2. CH_3NO_2-*d*$_3$. (iii) 4 equiv. $AgBF_4$, CH_3NO_2-*d*$_3$. 84

Figure 3.4 ^{31}P NMR spectra of complex **16** in CD_3NO_2 from 253 K to 338 K. Coalescence is observed at high temperature, consistent with the presence of rapidly interconverting diastereomers at elevated temperature. 85

Figure 3.5. ^{1}H NMR spectra of complex **16** in CD_3NO_2 from 253 K to 338 K. Coalescence is observed at high temperature, consistent with the presence of rapidly interconverting diastereomers at elevated temperature. 86

Scheme 3.3 The Reversible Closing and Re-Opening of the WLA Multi-State Macrocycle. MeOD = methanol-*d*$_4$. 88

Figure 3.6 Energy minimized DFT models of (a) semi-open complex **14**, (b) semi-open/fully closed complex **15**, and (c) fully closed complex **16**. 92

Table 3.1 Free Energies (kcal/mol) of **14**, **15** and **16** Obtained from DFT Calculations. 92

Table 3.2 Selected Bond Energies (kcal/mol) of **14**, **15** and **16** Obtained from DFT Calculations. 92

Table 3.3 Selected Fukui Indices for complex **14** Obtained from DFT Calculations.[a] 93

Figure 3.7 ChemDraw structures (top) and corresponding DFT models (bottom) showing the two possible diastereomers of **14**. 93

Figure 3.8 ChemDraw structures (top) and corresponding DFT models (bottom) showing top-down views of the two possible diastereomers of **16**. 94

Figure 3.8 ^{31}P NMR spectra of complexes **13a-c**, **14**, and **15** upon reopening and closing. 95

CHAPTER 4

Scheme 4.1 WLA complexes containing hemilabile coordinating motifs can be toggled between open (flexible) (A) and closed (rigid) states (B) (counterions omitted for clarity). Coordination-based assembly of these subunits results in extended structures (C,D). 105

Figure 4.1. (A) Molecular building blocks used in the synthesis of ICP particles bearing WLA subunits. (B) The X-ray crystal structure of complex **18-Pt-Closed**, drawn with 50% thermal ellipsoid probability. Hydrogens, solvent molecules, and anions have been omitted for clarity (black, Pt; orange, sulfur; purple, phosphorous; grey, carbon; blue, nitrogen). 106

Figure 4.2 (A) Proposed repeat unit, coordination polymer structure (top) and STEM micrographs (bottom) of ICPs bearing open and (B) closed WLA subunits at different concentrations. 109

Figure 4.3 (A) Proposed repeat unit structure (top) and STEM micrographs (bottom) of ICPs bearing open and (B) closed palladium WLA subunits. 111

Figure 4.4 Crystal structures of (a) **18-Pt-Closed** (obtained from the slow diffusion of ether into acetonitrile) and (b) the **18-Pd-Closed** (obtained from the slow diffusion of ether into DCM) drawn with 50% thermal ellipsoid probability. Hydrogen atoms, solvent molecules, and anions have been omitted for clarity. 122

Table 4.1 Crystal data and structural refinement for **18-Pt-Closed** and **18-Pd-Closed**. 122

Figure 4.5 ^{1}H NMR spectra of monomer **18-Pt-Closed** before (top) and after (bottom) the addition of one equivalent of $Fe(BF_4)_2 \bullet 6H_2O$ to form **19-Pt-Closed**. Dashed lines and boxes show free terpyridine resonances shifting to regions indicative of iron binding.[131] 124

Figure 4.6 ^{1}H NMR spectra of monomer **18-Pt-Open** before (top) and after (bottom) the addition of one equivalent of $Fe(BF_4)_2 \bullet 6H_2O$ to form **19-Pt-Open**. Dashed lines and boxes show free terpyridine resonances shifting to regions indicative of iron binding.[131] 124

Figure 4.7 ^{1}H DOSY NMR spectra of monomer **18-Pt-Closed** ($D = 7.9 \bullet 10^{-6}$ cm^2s^{-1}) before (left) and after (right) the addition of $Fe(BF_4)_2 \bullet 6H_2O$ to form **19-Pt-Closed**. The Spectrum of **19-Pt-Closed** indicates the complete consumption of the starting monomer and the formation of oligomeric species with diffusion coefficients reduced by up to a factor of four. 125

Figure 4.8 ^{1}H DOSY NMR spectra of monomer **18-Pt-Closed** ($D = 7.9 \bullet 10^{-6}$ cm^2s^{-1}) before (left) and after (right) the addition of $Fe(BF_4)_2 \bullet 6H_2O$ to form **19-Pt-Closed**. The Spectrum of **19-Pt-Closed** indicates the complete consumption of the starting monomer and the formation of oligomeric species with diffusion coefficients reduced by up to a factor of four. 125

Figure 4.9 Density function theory (DFT) energy minimized models of A) **19-Pd-Closed** and B) **19-Pt-Closed**. The lowest energy conformation of **19-Pt-Closed** resembles cyclic oligomers. 126

Figure 4.10 ^{1}H NMR spectra of coordination polymer **19-Pd-Open** (bottom) converted to **19-Pd-Closed** (middle) *via* abstraction of chloride post-polymerization, and **19-Pd-Closed** (middle) switched to **19-Pd-Open** (top) *via* addition of chloride post polymerization. All NMR spectra were taken in CD_3CN. 127

Figure 4.11 $^{31}P\{^{1}H\}$ NMR spectra of coordination polymer **19-Pd-Open** (bottom) converted to **19-Pd-Closed** (middle) *via* abstraction of chloride post-polymerization, and **19-Pd-Closed** (middle) switched to **19-Pd-Open** (top) *via* addition of chloride post polymerization. All spectra were taken in CD_3CN..... 128

Figure 4.12 ^{1}H DOSY spectrum, taken in CD_3CN, of resulting **19-Pd-Open** from **19-Pd-Closed**, indicating the formation of one polymeric species. 129

Figure 4.13 ^{1}H DOSY spectrum, taken in CD_3CN, of resulting **19-Pd-Closed** from **19-Pd-Open**, indicating the formation of one polymeric species. 129

Figure 4.14 ^{1}H NMR spectra of coordination polymer **19-Pt-Closed** (bottom) converted to **19-Pt-Open** (middle) *via* addition of chloride post-polymerization, and **19-Pt-Open** (middle) switched to **19-Pt-Closed** (top) *via* abstraction of chloride post polymerization. All NMR spectra were taken in CD_3CN. 130

Figure 4.15 Representative EDS spectra for ICPs composed of **19-Pt-Closed** (top) and **19-Pt-Open** (bottom) showing the presence of Cl, which is indicative of the fully open complex. 131

Figure 4.16 Representative DLS trace for colloidally stable ICPs composed of 19-Pt-Open synthesized from a 2 mM solution ($Diameter_{number\ average}$ = 164 nm, $Diameter_{Z\text{-}average}$ = 195 nm, PDI = 0.089). 131

Figure 4.17 ICP particles composed of 19-Pt-Closed containing A) 0 equiv. of chloride, B) 0.5 equiv. of chloride, and C) 1 equiv. of chloride. 132

Figure 4.18 ICP particle synthesis from a 2 mM solution of 19-Pt-Closed, at ~5 °C, resulting in ill-defined aggregates of small spheres. 132

CHAPTER 5

Figure 5.1 The goal of this work: design and synthesis of CP building blocks possessing hemilabile ligands coordinated to metal ions. 146

Figure 5.2 WLA tweezer complexes bearing hemilabile ligands and d^8 metal centers can reversibly access multiple, distinct structural states upon introduction of an allosteric effector. 147

Figure 5.3 General design of tunable WLA building blocks with different possible chelators for coordination to metal ions in the assembly of responsive coordination polymers. The WLA is an ideal platform for the synthesis of stimuli-responsive coordination polymer materials, owing to its highly tunable platform and modularity. Metal-ligand binding strength, orientation, and geometry may be tuned by changing the coordinating end group on the P,S ligand (terpyridine, pyridine, carboxylate, are discussed). 148

Scheme 5.1 Synthesis of (A) hemilabile P,S–Pyr ligand (**22**) and (B) WLA complex **23**..... 150

Scheme 5.2 (a) Reaction of $Cu^{II}(BF_4)_2 \cdot 6H_2O$ with the Pd^{II} monomer (**23**) in MeCN to give the compound [(P,S–pyr)[$Cu(OH)_2$--$(MeCN)_2$--] (**24**). (b) Crystal structure of the tweezer monomers, and (c) the coordination mode of the monomers within the coordination polymer, and (d) the coordination mode of the Cu^{II} metal node within the coordination polymer. Drawn with a 50% thermal ellipsoid probability. Solvent molecules and hydrogen atoms have been omitted for clarity. 151

Figure 5.4 ^{1}H NMR titration of **23** with $Cu^{II}(BF_4)_2 \cdot 6H_2O$ in methanol at (a) 0.0 equiv., (b) 0.2 equiv., (c) 0.4 equiv., (d) 0.6 equiv., (e) 0.8 equiv. and (f) 1.0 equiv. of $Cu^{II}(BF_4)_2 \cdot 6H_2O$..... 152

Figure 5.5 Packing of crystalline 1-D coordination polymer (**24**) bearing $Pd(P,S–Pyridine)_2(BF_4)_2$ monomers. Drawn with a 50% thermal ellipsoid probability. Solvent molecules and hydrogen atoms have been omitted for clarity. 153

Scheme 5.3 Formation of CP particles bearing complex **23** building blocks polymerized in the presence of Pt^{II} salt **25**..... 154

Figure 5.6 Crystal structure of fully open complex **26**, drawn with a 50% thermal ellipsoid probability. Solvent molecules and hydrogen atoms have been omitted for clarity. 155

Table 5.1 Crystallographic Data for Coordination Polymer **24** 163

Table 5.2 Crystallographic Data for Fully Open Monomer $Pt(P,S–Pyridine)_2Cl_2$ (**25**)..... 164

Table 5.3 Crystallographic Data for Semi-Open Pt^{II} Monomer..... 165

CHAPTER 6

Figure 6.1 An allosterically-regulated macrocycle capable of reversibly accessing four distinct structural states, assembled via the WLA. 171

Figure 6.2 A new class of infinite coordination polymer particles bearing Weak-Link Approach subunits can be chemically addressed in the solution phase with small molecule effectors. Through the introduction or abstraction of anions, the local geometry of the metal subunits can be controlled, manifested by macroscopic morphological changes in the polymer particles. 173

Figure 6.3 ICP particles synthesized by the assembly of modular Weak-Link Approach-based coordination chemistry construct building-blocks, capable of undergoing morphological changes. 174

Scheme 6.1 a) Heteroligated Pt^{II} WLA complexes traditionally synthesized *via* the halide-induced ligand rearrangement reaction in which differences in electron density at the "weak-link" (chalcoether or amine) controls heteroligated complex formation; A ≠ A′. b) The step-wise approach leverages a strong ligand–metal interaction (NHC–Pt^{II}) in order to assemble asymmetric WLA systems where the relative donating abilities of the "weak links" are not important..... 175

Scheme 6.2 Synthesis of an extended NHS,S-based ligand for the construction of larger, two-component macrocycles..... 176

Figure 6.4 Characterization of an extended NHS,S-based ligand for the construction of larger, two-component macrocycles 176

Scheme 6.3 The (top) synthesis and (bottom) ^{31}P NMR characterization of an expanded, two-component, WLA macrocycle accessed via step-wise assembly. 177

Figure 6.5 Library of hemilabile WLA ligands for use in the assembly of multi-state receptors. 177

Scheme 6.4 (a) The synthesis of a four-component, heteroligated WLA square, bearing 90° corners as confirmed by (b) single crystals suitable for X-ray diffraction of a tweezer complex bearing phenyl ring end groups. The solid-state crystal structure shown from the side view and (c) the top view, indicate the presence of a 90° angle. 178

Figure 6.6 Future work is focused on developing crystalline, 3-D frameworks that can undergo structural transitions that enable a "breathing" architecture 180

CHAPTER 1

Introduction

1.1 Allosteric Regulation in Nature

Nature has afforded us with the most functionally diverse molecules we know: Proteins. Nature uses proteins such as enzymes and ribosomes to build molecules step by step, seamlessly making and breaking bonds with unprecedented precision. These proteins are Nature's most formidable machines as they perform complex chemistry with unmatched properties with respect to substrate recognition, signaling and catalysis. At the heart of every enzyme is a complex arrangement of proteins, called the active site. The active site is a highly organized binding pocket, whose size, shape and binding motifs allow for the selective recognition and binding of specific substrates.[1-3] Processes such as self-replication, cellular signaling, and metabolism are essential to life and rely on a protein's ability to recognize and bind substrates within their active site. The process of molecular recognition is ubiquitous in many biological systems and can be understood by one unifying concept: non-covalent interactions.[4-6] The non-covalent interactions characteristic of biological molecules provide the flexibility and specificity required in most important biological processes.[2-3, 7] They provide a sharp contrast with covalent biochemical compounds which supply the structural firmness and the energy reservoir for living systems.

The thermodynamics of biological molecular recognition are primarily governed by weak, non-covalent interactions such as hydrogen bonding, van der Waals forces, or hydrophobic effects while, the highly organized nature of their cavity minimizes the entropic penalties of binding (Table 1).[3, 6, 8] Unlike covalent bonds, which are bonds that hold atoms together *within* molecules through shared electrons, non-covalent interactions are attractive forces *between* molecules (Figure 1.1).[5] The energy released in the formation of noncovalent bonds is only 1–5 kcal/mol, much less than the bond energies of single covalent bonds.[6] Because the average kinetic energy of

molecules at room temperature (25 °C) is about 0.6 kcal/mol, many molecules will have enough energy to break noncovalent interactions.[6]

Table 1.1 Common Non-Covalent Interactions and their Associated Strengths in kJ mol^{-1}

Interaction	Strength (kJ mol^{-1})
Covalent	200–400
Ion–Ion	100–360
Ion–Dipole	50–200
Dipole–Dipole	5–50
H–Bonding	4–120
Cation–π	5–80
π–π	0–50
Van der Waals	< 5 (variable)
Hydrophobic	Related to solvent-solvent interaction energy

Although the strengths of non-covalent interactions are much less than those of covalent bonds, the former play critically important roles in biological systems. Multiple noncovalent bonds often act together to produce highly stable and specific associations between different parts of a large molecule or between different macromolecules (Figure 1.1).[6] It is these interactions which in Nature allow for the exquisite control of structure that is required for biological reactions to proceed and for life to exist. Peptides, for example, can be written as a simple linear chain of amino acid residues. This does not, however, give any idea of the complex three-dimensional nature of these moieties, which is vital to their function. The intricate structure of these molecules, which is essential to their function, is based on a combination of many weak, non-covalent interactions.

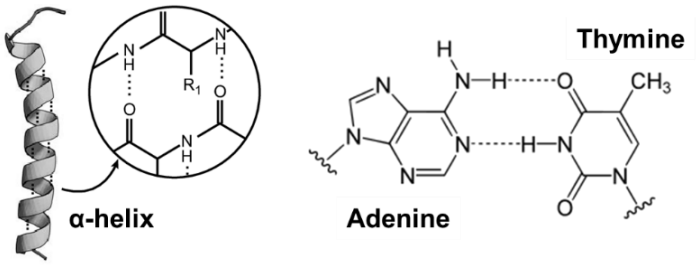

Figure 1.1 Hydrogen bonding present in alpha helices is an example of a non-covalent interaction employed by Nature. The hydrogen bonding between base pairs defines the helical structure.

A consequence of assembling protein binding pockets with non-covalent interactions that can easily be broken and reformed, is that they are structurally addressable such that they can readily undergo structural changes. These structural changes allow enzymes to be *allosterically-regulated*.[9] Of the various regulatory tools used by biological systems, the most widely used is the cooperative binding strategy called allosteric regulation (Figure 1.2).[9-10] Allosteric regulation involves the binding of a small molecule effector to an allosteric site (a site that is not the active site), which then causes a structural change in the active site, allowing for the "on" or "off" regulation of enzyme activity.[10-13]

In nature, allosteric regulation is a recognition-based process, which allows enzymes and other proteins to adapt their functional capabilities and activities in response to changing chemical environments, thereby constituting an integral mechanism of cellular homeostasis.[11-13] Importantly, allosteric regulation allows for precise biochemical control of protein activity by exploiting changes in structure that arise from a chemical recognition event, thereby changing the shape and, consequently, the functionality of the active site.[11-16]

An example of an allosterically regulated protein is hemoglobin (Figure 1.2). The binding of oxygen to one of hemoglobin's four heme sites, induces conformational changes that are relayed to the other subunits and raises their affinity for the oxygen molecule.[10, 17] In this particular case,

the binding of oxygen to hemoglobin is said to be cooperative.[18] The cooperative binding of oxygen by hemoglobin enables it to deliver 1.7 times as much oxygen as it would if the sites were independent, dramatically increasing its oxygen-carrying capacity.[10, 17, 19-20]

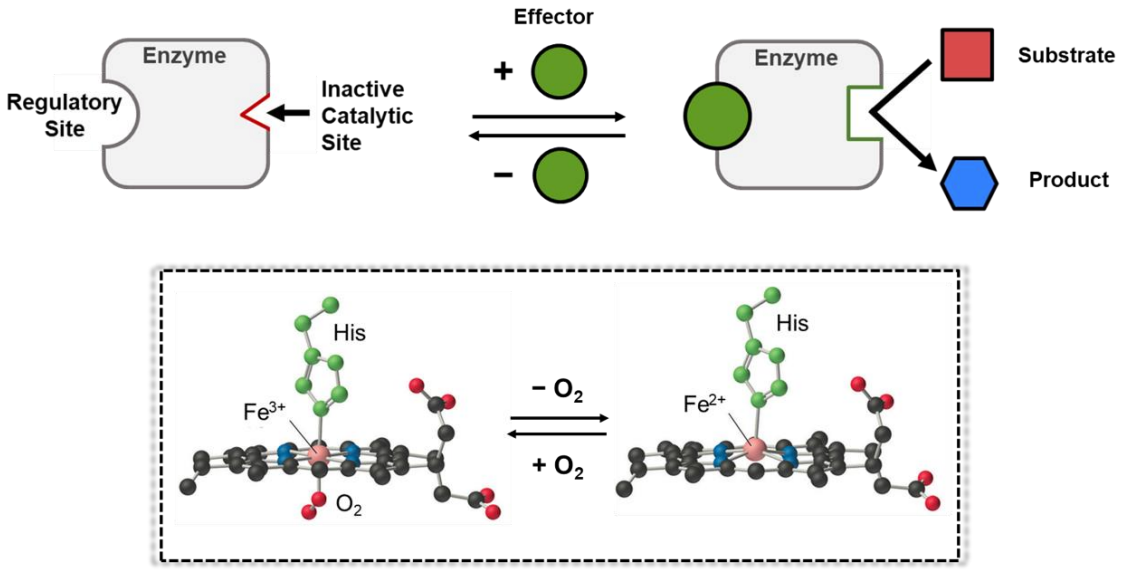

Figure 1.2 The basic principle of allosteric regulation in proteins can be illustrated with the binding of oxygen to hemoglobin isolated from red blood cells. The hemoglobin protein displays cooperative binding between subunits.

1.1.1 Molecular Recognition in Nature

At the basis of many biological processes lies the ability of molecules to recognize each other and to form well-defined complexes. Well-known examples are substrates bound to enzymes, signal substances bound to receptors, antibodies bound to antigens and metal ions bound to ionophores.[11] Proteins almost always interact with other molecules in performing their biological functions. These interactions include the binding of ligands in receptor sites, allosteric binding, the binding of antibodies to antigens, protein-DNA interactions, protein-protein interactions, multimerization, and protein-carbohydrate interactions.[21] The key factors in all these interactions are the shape and chemical properties of a protein's surface.

1.1.2 Nature's Reactive Cavities and Binding Pockets

Protein surfaces have evolved to incorporate numerous cavities, pockets and protrusions, which offer unique microenvironments for molecule and ligand binding.[22] In proteins, a cavity on the surface or in the interior of a protein that possesses suitable properties for binding a ligand is typically referred to as a binding pocket, or a binding site.[21] As previously mentioned, allosteric regulation involves the binding of a molecular effector to an allosteric site (a binding site that is not the active site), which results in a structural change in the active site, allowing for the regulation of enzyme activity.[10-13] Binding sites exploit weak, non-covalent interactions, imbuing the ligand-binding site with high chemical specificity and affinity for molecules, ions or protein ligands.[23] The set of amino acid residues around a binding pocket determines its physicochemical characteristics and, together with its shape and location in a protein, defines its functionality.[23] The dynamics of protein binding pockets are crucial for their interaction specificity. Structural flexibility allows proteins to adapt to their individual molecular binding partners and facilitates the binding process.[23] Importantly, these physiochemical features are made possible by non-covalent, supramolecular interactions, which enable the structural flexibility and addressability of these systems, while also rendering them highly specific for guest molecules. Such molecular recognition systems are termed "host-guest" systems.

A classic example of an allosterically regulated, host-guest protein is the chaperonin protein. Chaperonins form a double ring structure stacked back-to-back, which forms the protein's cleft opening where peptide folding is facilitated (Figure 1.3).[24] The substrate-binding domain is thin and brick-shaped with the cleft capped by a mobile α-helical lid. Both the lid and the cleft open to allow substrate binding, which can then be trapped by closing of the lid (Figure 1.3).[25] The

nucleotide state of the ATPase domain affects the opening (stimulated by ATP binding) and shutting (after ATP hydrolysis) of the substrate-binding site. The flexible linker, located at the base of the two domains remote from the cleft opening, is a key site in allosteric regulation.[25]

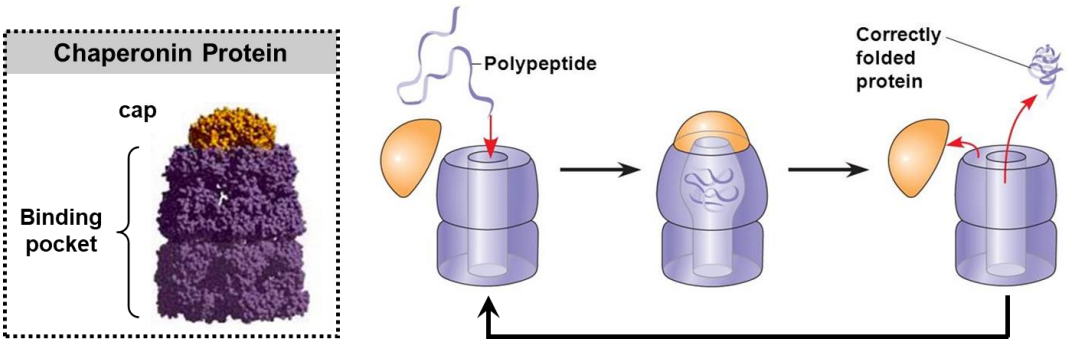

Figure 1.3 Chaperonin proteins consist of two stacked rings of subunits that enclose separate cavities for the binding of substrates. The chaperonin protein facilitates protein re-folding.

Nature's ability to orchestrate complex chemical reactions and processes using relatively weak, non-covalent interactions, has inspired chemists to mimic Nature's design with synthetic systems. Specifically, the highly selective molecular recognition inherent to enzymes has given chemists impetus to develop abiotic analogues, possessing reactive cavities, which operate under the same principles as biology.

1.2 Synthetic Enzyme Mimics

1.2.1 Molecular Recognition with Synthetic Receptors and Cages

The supramolecular organization of protein active sites heralds unprecedented properties, motivating chemists to develop generalizable strategies for the design of systems with similar control over local environment. Despite the prevalence of non-covalent interactions in the chemistry and biology of living systems, synthetic chemists did not begin to explicitly use weak, non-covalent interactions in the assembly of synthetic complexes capable of molecular

recognition, until the relatively recent emergence of the field of supramolecular chemistry. Supramolecular chemistry is the chemistry encompassing assemblies of molecules that bond or organize through non-covalent interactions.[26-28]

In 1987 the Nobel Prize in chemistry was awarded to Professor Donald J Cram,[29] Professor Jean-Marie Lehn[27] and Professor Charles J Pedersen,[30] for their work which inspired molecules with structure-specific, and highly selective interactions.[27-28, 30-31] Twenty years prior to the award, Charles J. Pedersen published two works describing methods of synthesizing cyclic polyethers, which he named crown ethers (Figure 1.4).[30] Pedersen showed that these compounds had remarkable and unexpected properties and that they could bind the alkali metal ions of lithium, sodium, potassium, rubidium and cesium into complexes. He found that, depending on the structure of the crown ether, potassium could for instance be bound before cesium, determining that different crown ethers possessed binding pockets of different sizes, into which different spherical metal ions selectively fit.[30-31] These crown ethers have been recognized as the first reported synthetic host-guest architectures which exploit the intermolecular bond.

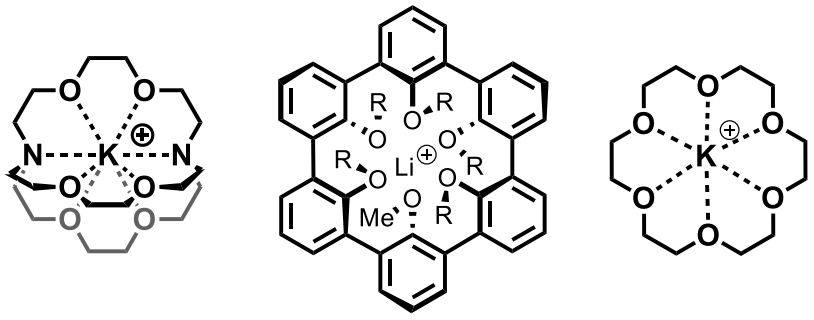

Figure 1.4 Some of the early synthetic, organic host-guest architectures (from left to right): cryptands, spherands and crown ethers.

By attaching bridges within the crown ether ring, Dr. Lehn constructed reinforced crown ethers called cryptands (Figure 1.4).[32] As a result of the complementary fit between the guest cation

and the intramolecular cavity of the host, these stable molecules strongly and selectively bind cations, including such toxic heavy metals as cadmium, lead and mercury.[33]

Together, the now laureates, were recognized for their pioneering work synthesizing organic compounds capable of binding cations, anions and neutral molecules, in a specific and selective manner. Importantly, they established factors that determine the ability of the molecules to recognize each other and, ultimately, pioneered the field of supramolecular chemistry: the chemistry of the intermolecular bond.[26, 30] Now, supramolecular chemists exploit these weak interactions with an aim of controlling chemical structure and reactivity in chemical systems.[28]

Efforts to mimic biological molecular recognition fall under the purview of supramolecular host-guest chemistry. The field of supramolecular, host-guest chemistry—in which a molecule (host) can bind another molecule (guest) to produce a "host-guest" complex—has led to the development of a vast array of host complexes and architectures.[34-35] Among these architectures, molecular "capsules" and "cages" are of particular interest owing to their well-defined cavities, which provide constrained environments reminiscent of biological active sites.

1.2.2 Synthetic, Organic Receptors and Cages

One of the first example of an allosteric supramolecular receptor was described by Rebek and co-workers in 1979.[36-39] The group designed and synthesized 2,2'-bipyridine (bpy) to which a crown ether moiety was attached in 3,3'-positions (Figure 1.5, compound **1**).[37] A tungsten tetracarbonyl ($W(CO)_4L_2$) salt was then introduced and behaves as an allosteric effector when coordinated to the bidentate bpy site and affects interaction of Na^+ with the crown ether site. The affinity of the crown ether for Na^+ is reduced about 5-fold by coordination of a $W(CO)_4$ fragment to the 2,2'-bipyridine unit. The group later went on to report ion "transport" selectivity in this

receptor, as the sites are mechanically coupled. The binding at one site forces conformational restrictions, which alter receptivity at the remote site (Figure 1.5).[38]

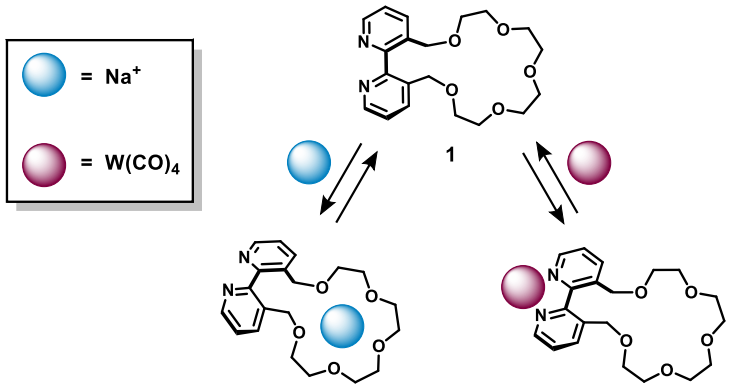

Figure 1.5 Binding induced conformational changes in a synthetic receptor (**1**) possessing two distinct binding sites: the polyether which binds alkali metal ions and the 2,2'-bipyridyl function which binds transition metals.

Since this early discovery, many groups have developed synthetic receptors through the use of covalent, organic chemistry. These organic receptors have found broad applications in small-molecule binding and catalysis, primarily, and the receptor−substrate interactions include aromatic π-stacking, solvophobic interactions, hydrogen bonding, and electrostatic interactions.

More recently, chemists have sought to expand the scope of synthetic organic receptors and have thus turned to assembling cavitands via non-covalent intermolecular forces (Figure 1.6). Unlike their covalently linked counterparts, such systems enable guest release upon disruption of the network of non-covalent interactions holding the cavitands together. For example, Gibb reported the self-assembly of two hydrophobic capsules, in water and in the presence of hydrophobic guest, to form a larger bicapsule.[40-42] This capsule has been used in photodimerizations of aryl alkenes and photo-oxidations of cycloalkenes by singlet oxygen to give the corresponding hydroperoxides.[43] However, since the formation of these capsules requires the presence of a guest molecule in polar solvents, their utility is limited. In addition, Rebek and

coworkers[44] have also developed a capsule that self-assembles via the formation of hydrogen bonds between two building blocks and shows interesting reactivity (this molecular vessel can encapsulate phenyl azide and phenyl acetylene with the right orientation to produce a 1,3-dipolar cycloaddition between the two substrates)[44], however, this system is limited by solvent choice. The synthetic and solubility challenges posed by purely organic receptors, have motivated chemists to employ coordination-based methods for the rapid assembly of supramolecular macrocycles, capsules, cages and receptors.

Figure 1.6 Many organic receptors have been developed through the assembly of cavitands such as calixarene, resorcinarene and cyclodextrin derivatives.

1.2.3 Synthetic, Coordination-Based Receptors and Cages

Current work has been focused on developing new methodologies for assembling sophisticated host-guest systems for molecular recognition. Most recently, coordination-based chemistry—the chemistry involving metal-ligand coordination bonds—has emerged as a means to direct the assembly of supramolecular host complexes. Through the use of a range of diverse functional ligands, coordination-driven self-assembly has proved to be a powerful tool to construct supramolecular architectures with controlled shapes and sizes.

Supramolecular coordination chemistry uses metal-ligand bonds with moderate energies that can be synthesized under thermodynamic control.[45-46] This oftentimes yields a single product

dictated by the coordination geometry of a metal center, while utilizing bonding motifs that yield potentially addressable structures—structures which can undergo structural changes.[47] To this end, various design principles and synthetic methodologies underpinning coordination-driven supramolecular assembly have emerged in the past 25 years.[46]

An example of a functional coordination-based assembly was demonstrated by Fujita and coworkers, who assembled a cage with Pd(II) nodes and four tridentate pyridyl ligands (Figure 1.7, **2**).[48] The addition of anthracene and maleimide derivatives to a solution of the cage lead to the inclusion of the small molecules via hydrophobic interactions. Interestingly, when this ternary complex was heated at 100 °C for 8 hours, a Diels-Alder reaction occurred between the anthracene and maleimide substrates resulting in the unusual *syn* product rather than the *anti* product.[48] The unusual regioselectivity and reactivity can be attributed to preorganization of the substrates within the cage, as no Diels-Alder reaction occurs in the absence of the cage. The restrictive cavity aligns the reactants in close proximity to each other in a hypothesized exo transition state, where the dienophile is positioned above the unsubstituted six-membered diene ring. The confines of the cage preclude substrate rearrangement, leading to the formation of the single *syn* product (Figure 1.7).[48] Importantly, this work demonstrates that supramolecular architecture can not only be used to facilitate reactions that would not normally proceed but also to make unusual product regioselectivities possible, much in the way that enzymes catalyze unfavorable reactions efficiently and selectively.

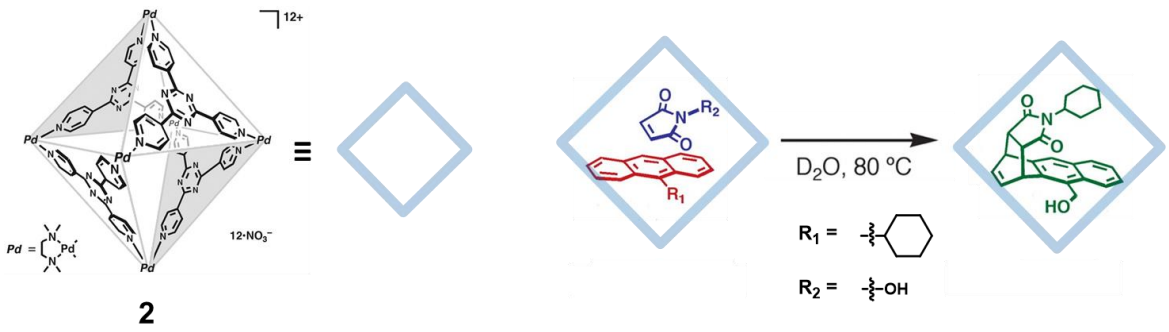

Figure 1.7 Coordination-based supramolecular capsule (**2**) developed by the Fujita group. The capsule facilitates the pair-selective encapsulation of 9-hydroxymethylanthrancene and *N*-cyclohexyl maleimide, within cage **2** and the subsequent Diels-Alder reaction.

1.3 Approaches to Coordination-Based Supramolecular Architectures

Since the concept of host-guest chemistry was first described, it has captured the imagination of chemists and has evolved into a field with exciting implications for many areas of molecular science. Numerous hosts have already been synthesized, but researchers continue to develop host molecules with properties matched to specific guest compounds. As well, efforts are under way to design more complex host molecules with the potential to incorporate several active substances. As previously mentioned, a long-standing goal of chemists has been to develop synthetic protein mimics for realizing the next generation of catalysts, signal amplifiers, and nanomaterials. Proteins possess remarkable catalytic and stimuli-responsive properties, which arise from their ability to control their supramolecular environment and resulting properties, through allosteric regulation. The supramolecular interactions that dictate protein structure and properties have inspired work on developing abiotic enzyme systems that mimic the highly selective and structurally dynamic, reactive cavities found in proteins and enzymes.

Coordination-driven supramolecular chemistry has emerged as a powerful means to assemble large and complex macrocycles, cages, and capsules, with general methods developed

by several groups, including our own, for assembling such multicomponent structures.[47] The methods for the metal-directed assembly of supramolecular constructs fall within three categories: the Directional Bonding Approach (DBA), the Symmetry-Interaction Approach (SIA) and the Weak-Link Approach (WLA).[47, 49] The DBA and SIA rely on the assembly of rigid ligands and metal centers, to form rigid supramolecular cages. In contrast, the WLA employs flexible ligands resulting in structurally flexible systems that can interconvert between rigid, "closed" and flexible, "open" structures through reversible binding events that occur at the metal center (Figure 1.8).[49-50] Among the different approaches, the WLA is a powerful method for synthesizing complexes that can undergo reversible, small-molecule-induced structural changes and therefore be toggled between a "closed" rigid state and an "open" flexible state.[47, 49, 51] Work carried out in the Mikrin group exploits the WLA to design systems which mimic the best aspects of enzymes as it allows for the construction of *allosterically-regulated* systems.

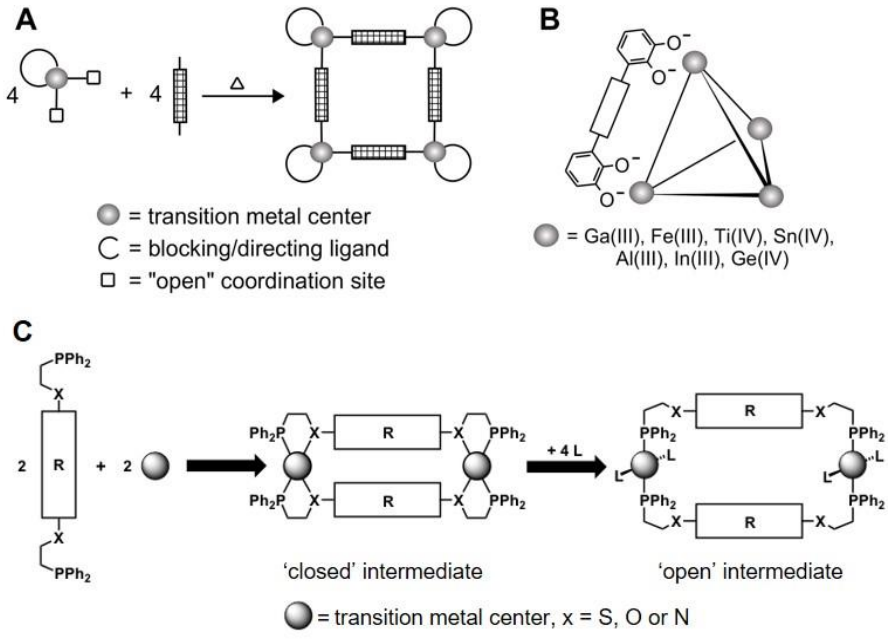

Figure 1.8 Approaches to coordination-based supramolecular constructs: A) The Directional

Bonding Approach for the synthesis of squares, B) the Symmetry Interaction Approach for the synthesis of tetrahedrons, and C) the Weak-Link Approach for the synthesis of macrocycles.

1.4 The Weak-Link Approach to Supramolecular Coordination Chemistry

The WLA to coordination-driven supramolecular chemistry, is a powerful means to construct allosteric enzyme mimics. The diverse toolbox of metals and ligands explored by our group have allowed for the construction of complex structures including tweezers, triple deckers, and macrocycles (Figure 1.9).[47]

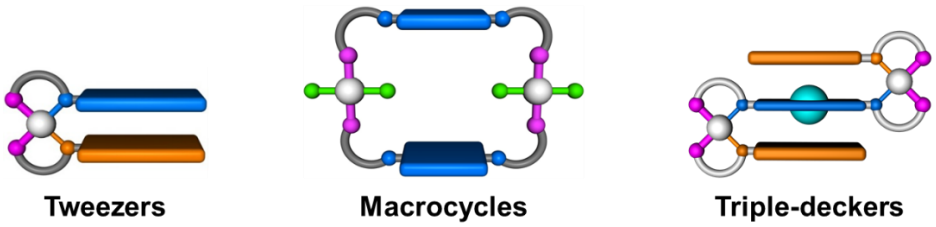

Figure 1.9 Depiction of tweezers, macrocycles and triple-decker complexes that can be assembled via the WLA. Such structures employ d^8 metal centers and hemilabile ligands.

The ability of these structures to flexibly switch between structural configurations is unique to the WLA, and results from the use of hemilabile ligands—ligands which employ a strongly binding atom, and a weakly binding atom (Figure 1.10). The difference in bond strength allows one to retain the "strong" bonds while selectively cleaving the "weak" bonds by the binding of small molecule "effectors" to the metal sites.[2] WLA complexes typically are defined by a molecular architecture where two hemilabile ligands, bearing both a "strong-link" moiety (typically a phosphine) and a "weak-link" moiety (typically a chalcoether or amine) are bound to a d^8 metal center (Figure 1.10). Introduction of a coordinating ligand, such as CO, CN^-, halide anions or acetate, results in the breaking of one or both "weak-links", and converts a rigid, condensed species to an extended, flexible one.

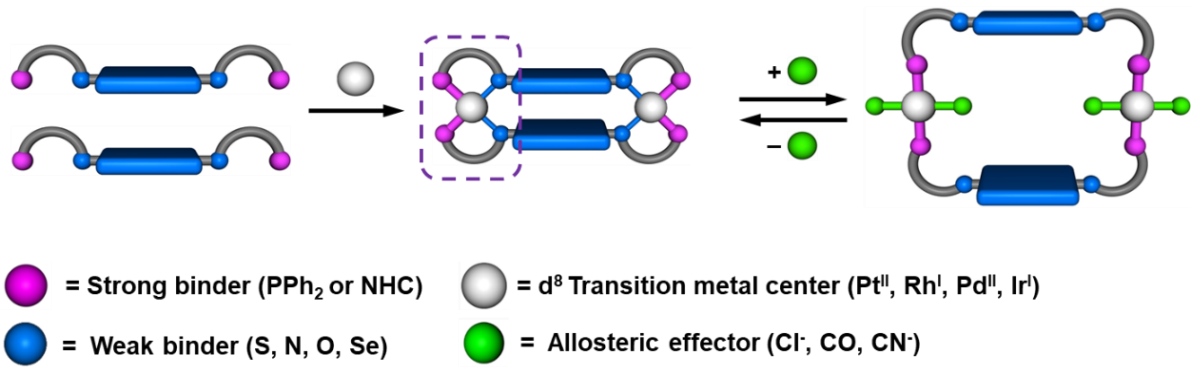

Figure 1.10 The weak-link approach (WLA) to supramolecular chemistry employs hemilabile ligands and metal ions to make condensed, or closed, structures in high yield. These closed complexes can be interconverted between open, flexible states through small molecule coordination chemistry.

The WLA, therefore, provides not only a method to synthesize cage structures that mimic the environment of biological receptors, but also affords them the structural flexibility required to modulate their activity, rendering them synthetic *allosteric receptors*. Through the modular and convergent assembly of metal ions and multidentate hemilabile ligands, the WLA provides a platform to deliberately engineer molecular selectivity and stimuli-responsiveness into supramolecular complexes. WLA-based supramolecular systems are attractive as they offer 1) chemical access to multiple structural states with tailorable selectivity and binding affinities, 2) high functional group tolerance, and 3) modularity, including access to structures with a wide variety of metal nodes and ligand types.

1.4.1 WLA Structures Based Upon Hemilabile Ligands

Our group has focused on the synthesis of novel metallo-supramolecular complexes via the WLA. As previously mentioned, these structures are based upon hemilabile ligands and allow one to build macrocyclic, triple-decker, and tweezer-based complexes, in which structural changes can

be induced by displacement of the weak binding group of the hemilabile ligand at the metal hinge sites with small molecules and elemental ions. The WLA has allowed us to design a wide variety of molecules with catalytic and biomimetic properties, in terms of allosteric regulation and recognition, which have also led to the development of sensors for small molecules and elemental ions reminiscent of amplification schemes used in molecular biology, such as ELISA (Enzyme Linked Immuno Sorbent Assays) and PCR (Polymerase Chain Reaction).[52]

1.4.2 General Approach to the Synthesis of Air-Stable Pt(II) WLA Architectures

WLA complexes typically are defined by a molecular architecture where two hemilabile ligands, bearing both a "strong-link" moiety (typically a phosphine) and a "weak-link" moiety (typically a chalcoether or amine) are bound to a d^8 (typically) metal center. Introduction of a coordinating ligand, such as CO, CN^-, halide anions or acetate, results in the breaking of one or both "weak-links", and converts a rigid, condensed species to an extended, flexible one. Furthermore, if the "weak-links" are of sufficiently different electron donating ability, then heteroligated structures can be selectively formed under thermodynamic control via a halide induced ligand rearrangement (HILR) pathway.[53-55] The WLA has enabled researchers to develop novel molecular systems capable of allosterically regulated catalysis,[56-58] sensing,[59-61] and signal amplification.[62] Until recently, such systems relied heavily on the use of air-sensitive Rh(I) metal centers, which excluded uses that required them to operate under ambient conditions. As a result, we began targeting WLA complexes based on Pt(II) due to their air-stability and analogous coordination chemistry to Rh(I), as the basis for WLA chemistry.[50]

To this end, we sought to develop a general approach to the synthesis of air-stable Pt(II) WLA complexes. Initially, we reported that heteroligated Pt(II) tweezer and triple-decker

complexes can be formed using traditional P,S-ligands, with the requirement that the ligands bear "weak-link" thioether moieties of considerably different electron donating ability, and that the reaction be performed in polar solvents (i.e. MeOH), which favors the formation of dicationic product complexes with outer-sphere counterions.[50] While this approach allowed us to bring Pt(II)-based WLA chemistry to the bench top, the ditopic tetrafluorophenyl thioether P,S-ligands proved too weakly binding, and/or too kinetically labile, to allow for the clean formation of heteroligated macrocycles (though homoligated macrocycles are accessible).[50, 63-64]

1.4.3 Step-wise Construction of Heteroligated Pt(II) WLA Complexes

The single-step assembly of Pt(II) heteroligated complexes has been shown to rely on having an appreciable energetic difference in binding between the two P,S-ligands,[50, 53, 55, 64-65] however, in the case of macrocycles, the "weak-links" are so weakly coordinating that the resulting complexes are kinetically unstable. As a result, we turned toward more strongly donating ligands by employing N-heterocyclic carbene thioether (NHC,S) ligands in conjunction with traditional P,S-ligands to obtain heteroligated structures.[66]

With respect to the WLA chemistry,[50, 53] this new synthetic approach operates nearly identically to traditional systems, however, they are synthesized by a vastly different step-wise assembly procedure.[64] The key to this approach is to first coordinate the NHC,S hemilabile ligand, essentially irreversibly, to $PtCl_2$. This occurs in the presence of Ag_2O, which acts as both a base and an Ag^+ source to generate a silver-carbene intermediate *in situ*, before transmetalation occurs, to form the more thermodynamically stable Pt–carbene bond.[64, 67-68] In the second step, a traditional monotopic, or ditopic, P,S-ligand is coordinated to yield a heteroligated structure in quantitative yield. We have used this procedure to demonstrate the step-wise assembly of benchtop stable WLA

tweezers and triple-decker complexes, which are functionally identical to previous Rh(I) systems, however immune to the dynamic ligand scrambling processes resulting from the HILR under thermodynamic control, observed in the purely P,S–Pt(II) heteroligated complexes. This new methodology for the synthesis of heteroligated Pt(II) WLA constructs has enabled current work by providing us routes to previously inaccessible heteroligated structures that combine multiple functional moieties into a single complex.

1.5 Allosterically-Regulated, Weak-Link Approach Macrocycles and Receptors

1.5.1 An Allosterically-Regulated Molecular Receptor with Switchable Selectivity

Previous work in the Mirkin group used the unique properties imparted on systems assembled by the WLA, to demonstrate the synthesis of a supramolecular allosteric receptor capable of selectively binding guest molecules (Figure 1.11).[69] This system was synthesized with a calix[4]arene cavitand (a cyclic molecule that has a cavity in which a guest molecule may fit) and was able to achieve three distinct states that discriminated guests based on size and charge.[69] The host–guest properties of the ion-regulated receptor were found to be highly dependent upon the coordination of the Pt(II) center, which is controlled through the reversible coordination of small molecule effectors. Formation of inclusion complexes was determined by ^{1}H NMR titration of guests and the binding stoichiometry of host–guest complexes was determined by using Job plots. The closed complex (**3**) was unable to bind any guest molecules due to its restricted binding cavity size. Semi-open complex **4**, could be reversibly accessed upon introduction of chloride and, in contrast, was able to selectively bind the neutral molecule *N*-oxide pyridine. Only the positively charged semi-open complex **4** is able to encapsulate the neutral guest molecule in the form of a 1:1 inclusion complex. Interestingly, it was determined that the formation of this inclusion

complex is driven by dipole-dipole interactions between the positively charged, cationic complex, and the negatively charged oxygen of *N*-oxide pyridine. Upon introduction of cyanide (CN^-), the complex can be opened to a neutral, fully open complex (**5**). The fully open complex is able to selectively bind the guest molecule, *N*-methylpyridinium. Interestingly, in the host-guest complex formed with receptor **5** and *N*-methylpyridinium, the most significant interactions found were π–π stacking interactions (1.05 kcal/mol) between the bonding orbital of the calix[4]arene phenyl ring and the antibonding orbital of β and γ carbons in the guest molecule. Importantly, the formation of a 1:1 host–guest complex can only be observed between cationic guest, *N*-methylpyridinium, and the neutral, fully open configuration. This indicates that the electrostatic repulsion between **5** and the positively charged guest, plays a major role dictating the host–guest selectivity.

By controlling the coordination environment around a Pt(II) regulatory center via the use of small coordinating anions, the authors showed that three independent supramolecular configurations could be accessed, each with unique properties based on overall cavity size and charge. Importantly, the authors demonstrated that the coordination geometry at the regulatory site dictates the size of the cavity and the nature of the possible electrostatic and dipole interactions, giving rise to selective substrate binding.

Although an impressive example of an allosterically regulated host-guest system, this molecular receptor was limited to relatively small guest molecules and could only reversibly access two structural states, with the third state being irreversible. A significant advance would be to rationally design systems that can selectively recognize and bind a greater variety of sophisticated substrates and control chemical reactivity, in a reversible manner.

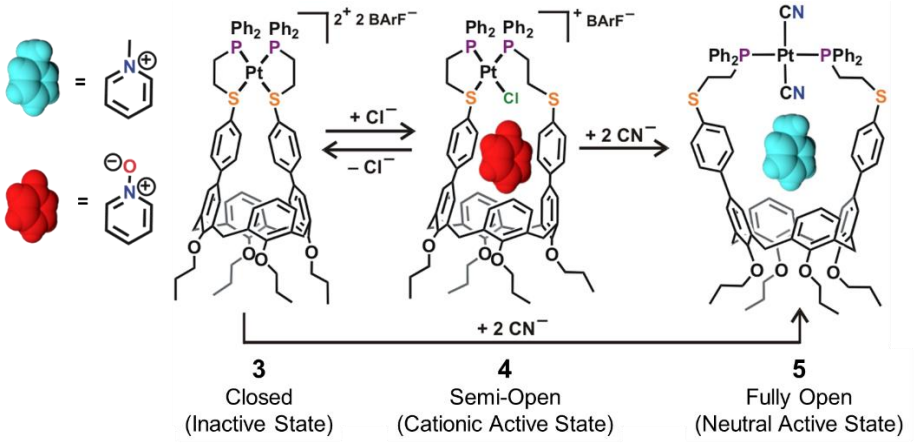

Figure 1.11 Selective and reversible encapsulation of *N*-methylpyridinium (blue) and *N*-oxide pyridine (red) is achieved using a multi-state ion-regulated molecular receptor capable of accessing a closed state (**3**), a semi-open state (**4**) and a fully state (**5**).

1.5.2 Reversible and Selective Encapsulation of Dextromethorphan and β-Estradiol Using an Asymmetric Molecular Capsule Assembled via the Weak-Link Approach

More recently, our group was able to demonstrate the design and synthesis of an allosterically-regulated, asymmetric receptor featuring a binding cavity large enough to accommodate molecular entities was synthesized via the WLA (Figure 1.12).[70] This architecture is capable of switching between an expanded, flexible "open" configuration (**7**) to a collapsed, rigid "closed" one (**6**). The molecular receptor can be completely modulated *in situ* through the use of simple ionic effectors, which reversibly control the coordination state of the Pt(II) metal hinges to open and close the molecular receptor. The substantial change in binding cavity size and electrostatic charge between the two configurations is used to modulate the host-guest properties of the receptor, in the presence of two pharmaceuticals: dextromethorphan (**6**) and β-estradiol (**9**).[70]

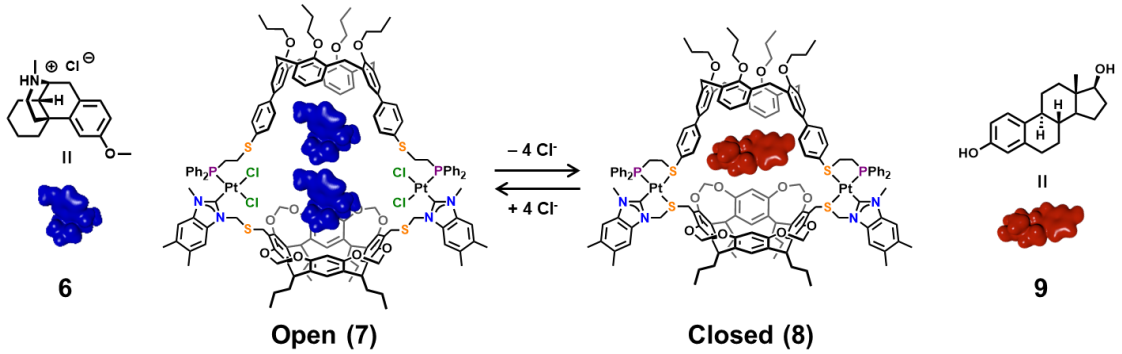

Figure 1.12 An allosterically regulated, asymmetric receptor featuring a binding cavity large enough to accommodate three-dimensional pharmaceutical guest molecules as opposed to planar, rigid aromatics, was synthesized via the WLA. This architecture is capable of switching between an expanded, flexible "open" configuration and a collapsed, rigid "closed" one.

Each configuration was demonstrated to have an affinity for a different type of guest pharmaceutical, which arises from the electrostatic and dipole interactions each assembly can provide in the recognition process. In addition to studying the unusual binding properties of this structure, the authors reported the reversible capture and release of guest molecules by switching between closed and open configurations *in situ*. The nature of the host-guest interactions was explored using Job plots, ^{1}H NMR titrations, and DFT computational studies and, importantly, detailed the synthesis of the first asymmetric receptor employing *N*-heterocyclic carbene (NHC) ligands, assembled via the WLA. This work paved the way for future asymmetric receptors and was key to demonstrating the irreversible nature of the Pt^{II}–NHC bond. This work inspired the projects that will be discussed in the future chapters of this thesis.

1.6 Introduction to Dissertation Topics

1.6.1 An Allosterically-Regulated Four State Macrocycle

In Chapter 2 of this dissertation, a molecular receptor capable of emulating the reversible conformational changes of a protein's binding cavity was designed, synthesized and assembled via

the Weak-Link Approach (WLA). Macrocycles capable of host-guest chemistry are an important class of structures that have attracted considerable attention due to their utility in chemical separations, analyte sensing, signal amplification, and drug delivery. The deliberate design and synthesis of such structures are rate-limiting steps in utilizing them for such applications, and coordination-driven supramolecular chemistry has emerged as a promising tool for rapidly making large classes of such systems with attractive molecular recognition capabilities and, in certain cases, catalytic properties. A particularly promising subset of such systems are stimuli-responsive constructs made from hemilabile ligands via the Weak-Link Approach (WLA) to supramolecular coordination chemistry. Such structures can be reversibly toggled between different shapes, sizes, and charges based upon small molecule and elemental anion chemical effectors. In doing so, one can deliberately change their recognition properties and both stoichiometric and catalytic chemistries, thereby providing mimics of allosteric enzymes. The vast majority of structures made to date involve two-state systems, with a select few being able to access three different states. Herein, we describe the synthesis of a new allosterically-regulated macrocycle assembled via the WLA. The target structure was made via the step-wise assembly of ditopic bidentate hemilabile *N*-heterocyclic carbene-thioether (NHC,S) and phosphino-thioether (P,S) ligands at Pt^{II} metal nodes. Importantly, each complex was fully characterized by multinuclear NMR spectroscopy and, in some cases, single-crystal X-ray diffraction studies and DFT computational models.

1.6.2 Complex Switching Behavior in a Four State WLA Macrocycle

In Chapter 3 of this dissertation, the switching behavior of the relatively simple macrocycle designed in Chapter 2, is explored. The WLA macrocycle displays complex dynamic behavior when addressed with small molecule effectors, and structural switching can be achieved with

several distinct molecular cues. Importantly, each state was fully characterized by multinuclear NMR spectroscopy and, in some cases, single-crystal X-ray diffraction studies and DFT computational models. The driving forces for switching are elucidated and the structure-property relationships discussed. This new structure opens the door to complex multi-cue switching reminiscent of multi-state chemoswitches that could be important in controlling stoichiometric and catalytic transformations as well as generating molecular logic systems.

1.6.3 Design, Synthesis and Characterization of Infinite-Coordination Polymers Bearing Weak-Link Approach Building Blocks

In Chapter 4 of this dissertation, a family of infinite coordination polymer (ICP) particles was synthesized by the assembly of modular Weak-Link Approach-based coordination chemistry construct building-blocks. Chloride ions can be used to chemically interconvert these building blocks between rigid, closed and flexible, semi-open states either pre- or post-polymerization. These changes in molecular geometry manifest themselves as morphological changes in the ICP particles. Furthermore, scanning transmission electron microscopy, energy-dispersive X-ray spectroscopy, and dynamic light scattering data suggest that the resulting particle morphology is highly dependent not only on the structure of the soluble precursors but also on the bond strengths and the dissociation kinetics of the metal-ligand coordination bonds in the polymer chain.

1.6.4 Reconfigurable, Bio-Inspired Coordination Polymers Assembled *via* the Weak-Link Approach

In Chapter 5 of this dissertation, a new class of materials is described in which WLA complexes act as building blocks for crystalline coordination polymer chains. The ability to engineer the responsive properties of nanoscale coordination polymers (CPs) at the molecular level

holds promise for the development of sophisticated, multifunctional materials. To realize this goal, CP building blocks must be capable of responding to molecular stimuli, while producing structural changes in the ligand geometry or orientation in a reversible manner. Herein, we report the design and synthesis of a reconfigurable, bio-inspired CP assembled *via* the Weak-Link Approach (WLA). Reaction of copper(II) tetrafluoroborate hexahydrate (Cu^{II} $(BF_4)_2$•$6H_2O$) with stimuli-responsive organometallic monomers bearing hemilabile phosphino-thioether pyridine ligands (P,S–pyr) in acetonitrile (MeCN) gave the compound [(P,S–pyr)[$Cu(OH)_2(MeCN)_2$]. The coordination environment at the regulatory metal node dictates the charge and the structural conformation of the assembly, resulting in two distinct structural states that correspond to two morphological phases: one closed, crystalline phase and one open, amorphous phase. Together, single crystal X-ray diffraction, NMR spectroscopy and mass spectrometry were used to study the formation and binding modes of the coordination complex monomers and resulting coordination polymers in the solution and solid state. Additionally, electron microscopy studies confirm that the assembly can undergo a transition from a crystalline single-chain to an amorphous state upon the introduction of a small molecule effector (Cl^-). Single crystal X-ray diffraction studies in conjunction with DFT calculations, reveal that ligand geometry and bond strength effects are important molecular parameters which drive the formation of either single-chain, or amorphous, coordination polymers. Taken together, this work represents a promising method for the construction of reconfigurable CP materials, possessing properties reminiscent of biological systems.

CHAPTER 2

An Allosterically Regulated, Four-State Macrocycle

The work presented in this chapter is based upon work published in:

d'Aquino, A. I.; Cheng, H. F.; Barroso-Flores, J.; Kean, Z. S.; Mendez-Arroyo, J. E.; McGuirk, C. M.; Mirkin, C. A. An Allosterically-Regulated, Four-State Macrocycle. *Inorg. Chem*. **2018**, *57*, 3568–3578. DOI: 10.1021/acs.inorgchem.7b02745

2.1 Introduction

The rational design of supramolecular systems, which undergo reversible structural changes, has been a long-standing goal of chemists due to the potential for developing technologically useful catalysts, switches, and sensors.[71-72] Coordination-driven supramolecular chemistry has emerged as a powerful means to assemble large and complex macrocycles, cages, and capsules, with general methods developed by the Stang,[73] Fujita,[74] Raymond,[75-76] Nitschke,[77-78] Mirkin,[47, 50, 79] and other groups,[80-82] for assembling such multicomponent structures. Among the different approaches to coordination-driven supramolecular constructs, the Weak-Link Approach (WLA) has emerged as a powerful means for synthesizing complexes that can undergo reversible small molecule-induced structural changes and therefore be toggled between "closed" rigid states and "open" flexible ones (Figure 2.1 a–c).[47, 50, 52] Through the modular and convergent assembly of metal ions and hemilabile ligands, the WLA provides a platform for engineering molecular selectivity and stimuli-responsiveness with deliberate control. WLA-based supramolecular systems are attractive as they offer: (1) chemical access to multiple different states with tailorable selectivity and binding affinities,[69-70] (2) high functional group tolerance,[50, 83] and (3) modularity, including access to structures with a wide variety of metal nodes and ligand types.[47, 79, 83] Many stimuli-responsive systems have been developed based on this platform, through the incorporation of catalytic,[84-88] redox-active,[89-90] and host-guest recognition sites[69] into the ligands in such a way that small-molecule induced structural changes result in marked changes in the properties of these complexes.

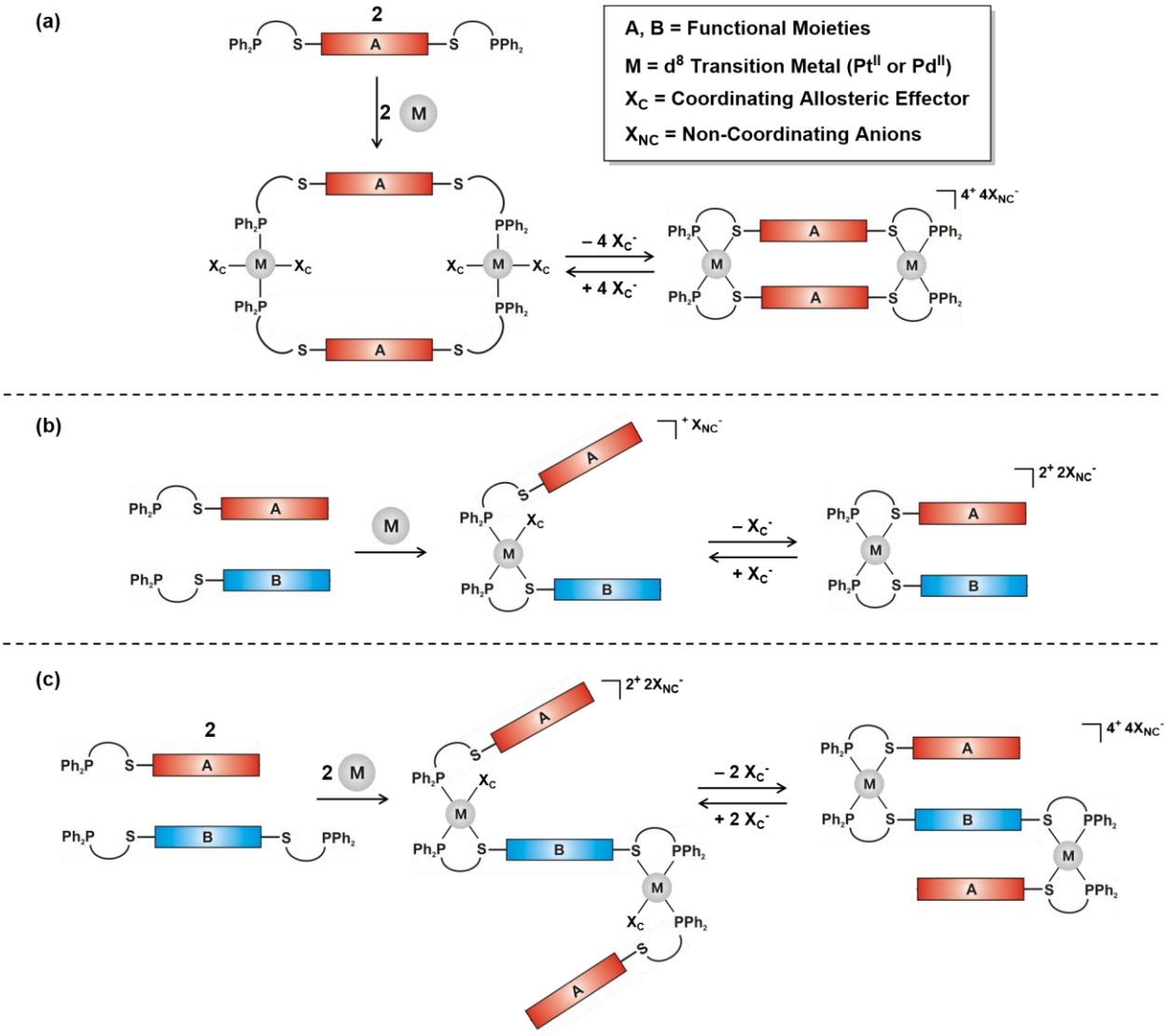

Figure 2.1 The Weak-Link Approach (WLA) to coordination-driven supramolecular (a) macrocycles, (b) tweezers, and (c) triple-decker complexes. For the sake of this example, complexes with Pd^{II} and Pt^{II} metal centers are illustrated, but the WLA works with many other metal systems including Rh^{I}, Cu^{I} and Ir^{I}.[91-94]

The addressable nature of these structures arises from the hemilabile phosphinoalkyl−chalcoether or –amine (P,X; P = $Ph_2PCH_2CH_2$–, X = O, S, Se, N) ligands typically coordinated to d^8 transition metals (such as Rh^{I}, Pd^{II} or Pt^{II}). These complexes can reversibly access

three distinct states, a fully open, semi-open and fully closed state through the removal and introduction of small molecules coordinating ligands (X_C) or elemental anions, which can easily displace the metal–S bond ("weak-link", in this example), while preserving the metal–P bond ("strong-link") (Figure 2.1; for simplicity the semi-open macrocycle is not shown in Figure 2.1a, and the fully open states are omitted from Figure 2.1b and 2.1c). Recently, our group reported the step-wise synthesis of heteroligated Pt^{II} WLA tweezer and triple-decker complexes with monotopic bidentate hemilabile *N*-heterocyclic carbene-thioether (NHC,S) and phosphino-thioether (P,S) ligands (Scheme 2.1a).[95] This strategy allowed for the assembly of air-stable heteroligated structures without the requirement of different electron donating abilities at the "weak-links", a requisite for previous heteroligated Pt^{II} WLA systems.[96] This step-wise approach was demonstrated in the synthesis of heteroligated tweezer and triple-decker complexes.[95] Recently, this approach was used to synthesize a switchable molecular receptor that can access two distinct structural states: flexible "open" and a rigid "closed" states (Scheme 2.1b).[70] Although this construct was the first example of a heteroligated Pt^{II} macrocyclic system, the limited structural states accessible by this complex prevented the switching between multiple binding pockets, each capable of binding a different guest molecule or exhibiting a different, but complementary function. Developing allosterically regulated structures that can access multiple states with different properties is a fundamental challenge and remains an important synthetic goal. The structures reported herein are the first step toward the development of multi-state, stimuli-responsive receptors, catalysts and chemoswitches, with fundamentally interesting functions relating to their different chemically tunable structures.

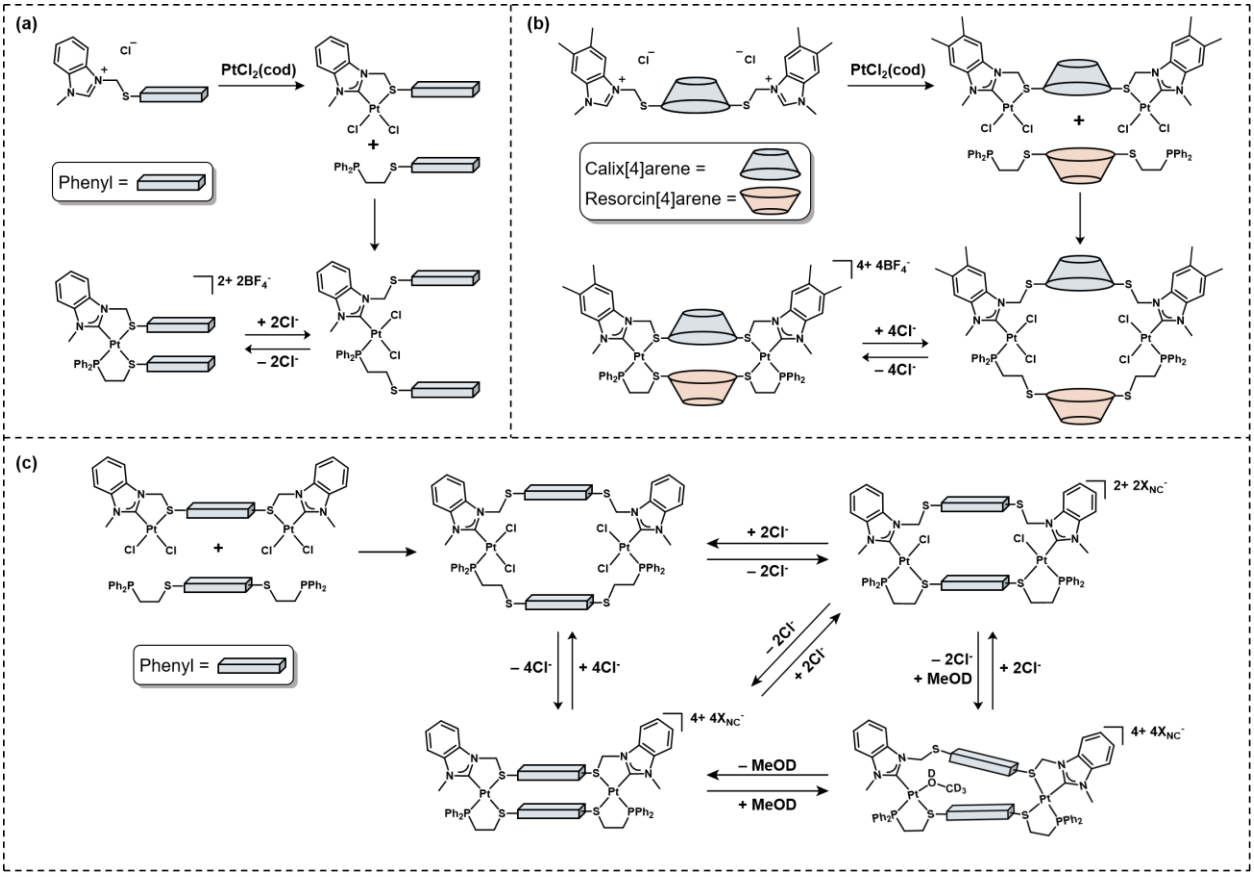

Scheme 2.1 (a) Step-Wise Approach to the Synthesis of WLA Tweezer and Triple-Decker Complexes, (b) Step-Wise Assembly of a WLA Heteroligated Pt^{II} Macrocyclic Capsule (c) The Scope of this Work Applies this Approach to the Synthesis of an Allosterically-Regulated, Multi-State, Heteroligated Macrocycle.[a]

Herein, we apply this step-wise approach to the synthesis of a heteroligated multi-state macrocycle, possessing two different ditopic bidentate ligands bridging two Pt^{II} metal nodes, which exhibits four-state switching behavior, considerably more complex than previously reported for WLA systems (Scheme 2.1c). Experimental and computational evidence suggests that, while the addressability of the system arises from the coordination chemistry, the resulting complexity of the macrocycle behavior is a function of multiple factors, including: geometry, strain, strength of coordination bonds and electronics. This is in contrast with previously reported WLA systems

that rely on the use of weakly chelating ligands to achieve the assembly of heteroligated structures, which are too unstable to form significantly strained structures.[50]

2.2 Results and Discussion

2.2.1 Model WLA Macrocycle Design

The Mirkin group has historically synthesized heteroligated macrocycles using a Rh(I) metal center bearing one P,S and one P,O ligand, the different donating abilities of which allow for the formation of heteroligated structures as the thermodynamic products. A significant drawback, however, of the Rh(I) complexes is their instability under ambient conditions and limited accessible solvents and guests.[97] In order to synthesize bench-top stable complexes, our group turned to Pt(II) as the coordination center. Unfortunately, a drawback of this Pt(II) chemistry is that the more weakly donating ligands (P,O through P,S-tetrafluoroaryl) are now kinetically labile, resulting in ligand scrambling and largely limiting the available ligands to form stable structures (Scheme 2.2A).[19,21]

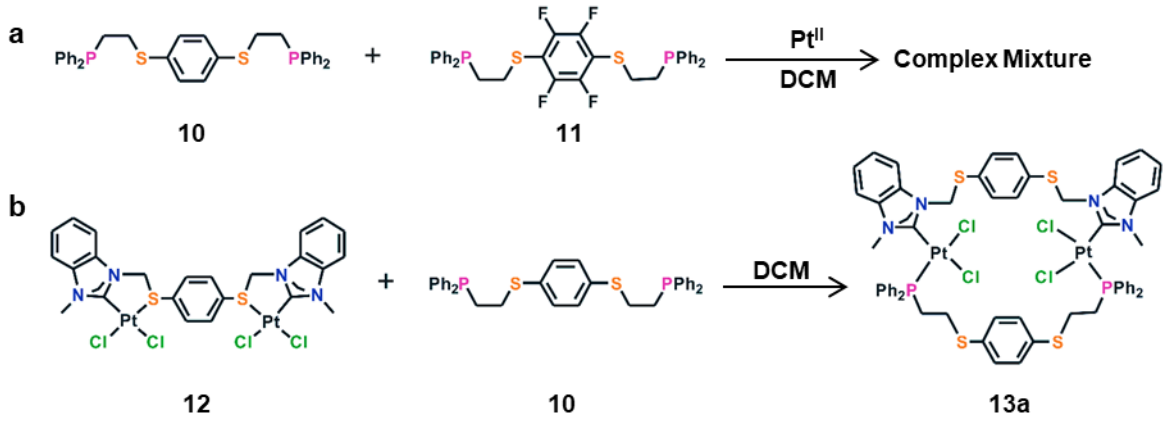

Scheme 2.2 a) Heteroligated Pt(II) WLA complexes containing weakly donating ligands (P,O through P,S-tetrafluoroaryl) are kinetically labile, resulting in ligand scrambling; b) The strategy described here takes advantage of strong NHC-Pt(II) interactions to assemble heteroligated Pt(II) macrocycles.

As a solution, the Mirkin group developed a methodology for the stepwise assembly of heteroligated Pt(II) complexes based on *N*-heterocyclic carbene-thioether (NHC,S) and (P,S-aryl) ligands. NHCs are strong sigma donors and are more strongly donating than even the most donating phosphines, which allows them to be bound to the Pt(II) center in a monoligated fashion in the first step. Subsequent addition of a P,S–Aryl ligand allows for the formation of kinetically stable and structurally rigid heteroligated Pt(II) complexes.[66] We hypothesize that this synthetic strategy is generalizable and can, therefore, be applied to the synthesis of higher-order heteroligated complexes and used this strategy to design a heteroligated macrocycle bearing both a P,S-based ligand (**10**) and an NHC-based ligand (Figure 2.2, **12**).

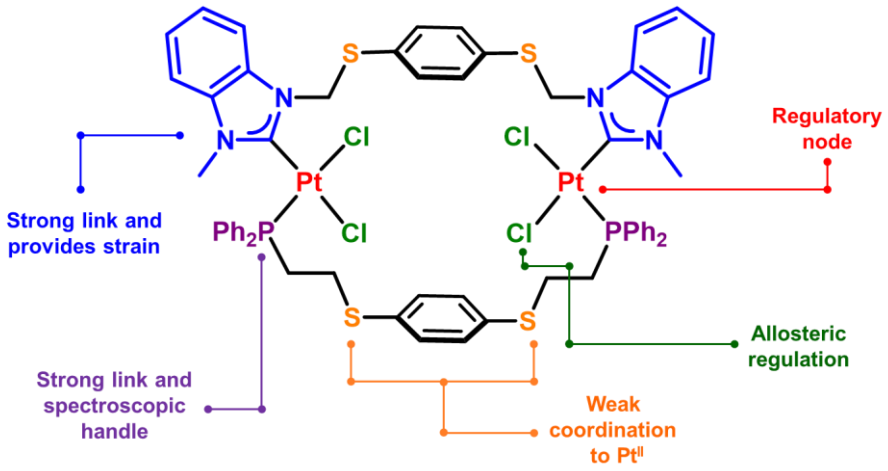

Figure 2.2 The design of a heteroligated WLA macrocycle bearing a ditopic bidentate NHC,S–based ligand (**12**) in conjunction with a traditional ditopic bidentate P,S–based ligand (**10**).

2.2.2 WLA Macrocycle Synthesis and Characterization

In order to synthesize the Pt^{II} heteroligated WLA macrocycle, we utilized a previously reported step-wise approach employing a ditopic bidentate NHC,S–based ligand in conjunction with a traditional ditopic bidentate P,S–based ligand, both of which bind Pt^{II} strongly enough to

result in kinetically stable structures. Benzimidazolium chloride salt **14** was treated with two equivalents of dichloro(1,5-cyclooctadiene)platinum(II) ($PtCl_2$(cod)) and one equivalent of silver(I) oxide (Ag_2O) in dichloromethane (CH_2Cl_2) to produce complex **12** [$Pt_2Cl_4(\kappa^1{:}\mu{:}\kappa^1$–NHC,S)] as an insoluble white solid (Scheme 2.3).

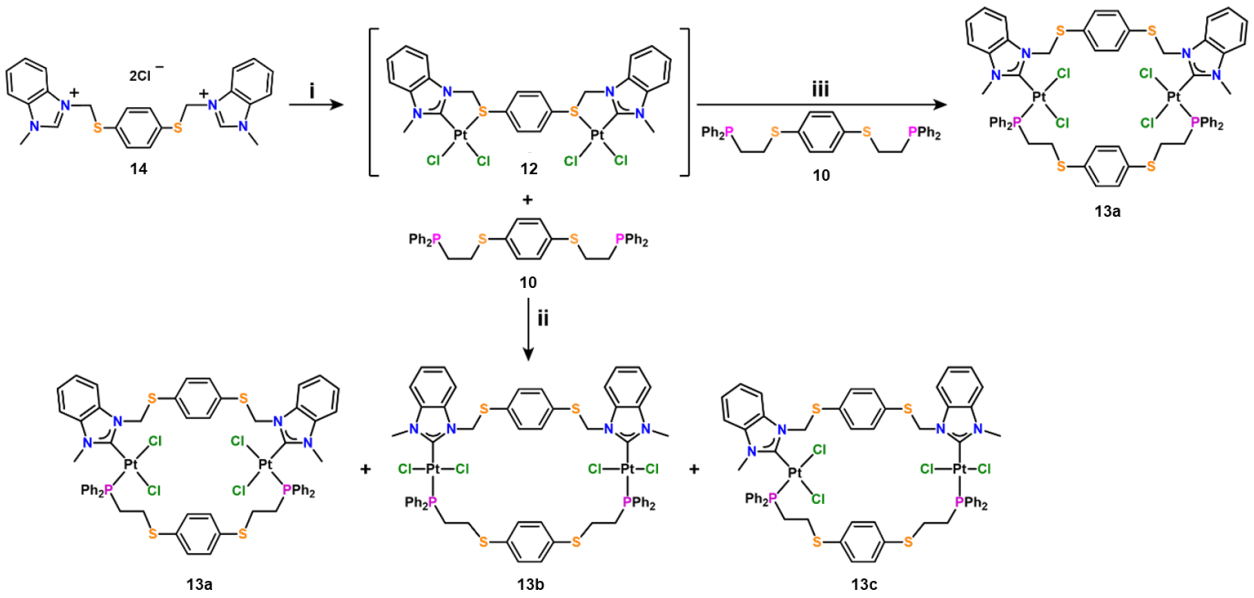

Scheme 2.3 Synthesis of Fully Open Heteroligated Macrocycles **13a-13c**. Reaction conditions: (i) 2 eq. $PtCl_2$(cod); 1 eq. Ag_2O; 6:1 CH_2Cl_2:MeOH, 24 h, 60 °C. (ii) 1:1 MeOH:CH_2Cl_2, 25 °C. (iii) CH_2Cl_2, 25 °C.

In order to confirm that the metalation reaction of **14** with Ag_2O and the subsequent transmetalation reaction with $PtCl_2$(cod) were successful, complex **12** was characterized by matrix-assisted laser desorption ionization-time of flight mass spectrometry (MALDI−TOF MS), with monoisotopic mass and isotopic distribution matching those of the molecular ion $[M–Cl]^+$. Due to the low solubility of complex **12** in CH_2Cl_2, single crystals suitable for X-ray diffraction were obtained by slow diffusion of diethyl ether into a solution of complex **12** in dimethyl sulfoxide (DMSO). The solid-state structure reveals a complex with DMSO ligands coordinated

to the metal center, displacing the weakly bound thioether groups on the NHC,S hemilabile ligand (Figure 2.3).

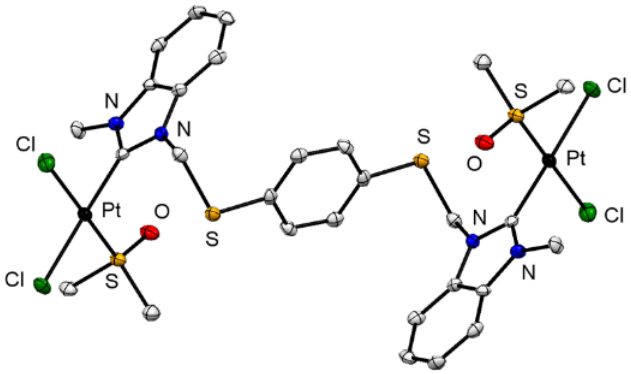

Figure 2.3. Single crystals obtained of complex **12-DMSO**.

The irreversible metalation–transmetalation reaction at the NHC ligand allows the subsequent use of strongly binding P,S-ligands without the occurrence of previously observed ligand exchange reactions.[96, 98] Due to the low solubility of **12** in CH_2Cl_2, complex **12** was dissolved in a 1:1 mixture of dichloromethane and methanol (MeOH) and reacted with one equivalent of P,S–aryl–S,P ligand **10** (Scheme 2.3). Characterization of the resulting product by ^{1}H and ^{31}P nuclear magnetic resonance (NMR) spectroscopy revealed that the fully open macrocycle was obtained as a mixture of isomers (**13a**–**13c**) when synthesized under homogenous conditions in a 1:1 mixture of MeOH and CH_2Cl_2 (Scheme 2.3). Consistent with this observation, a high-resolution mass spectrum (HRMS) of the sample exhibited a peak with a mass to charge (*m/z*) ratio corresponding to the molecular ion $[M–Cl]^+$.

^{31}P NMR spectroscopy was used to further characterize the resulting compounds since it is highly diagnostic of coordination environment. Additionally, the resonance shifts and platinum–phosphorus coupling patterns were consistent with the presence of a combination of *cis*- (**13a**),

trans- (**13b**) and combined *cis/trans* (**13c**) fully open complexes (Figure 2.4a).[99-101] As summarized in Figure 2.4, the fully open *trans* species **13b** [*trans*–Pt_2Cl_4(κ^1:μ:κ^1–NHC,S)(κ^1:μ:κ^1–P,S)] contains two platinum nodes in which the phosphine and carbene are *trans* to one another; this configuration is evidenced by a resonance at 9.7 ppm with a $J_{P–Pt}$ coupling constant of 2300 Hz. The presence of the *cis* complex **13a** [*cis*–Pt_2Cl_4(κ^1:μ:κ^1–NHC,S)(κ^1:μ:κ^1–P,S)] is evidenced by a resonance at 1.8 ppm with a larger $J_{P–Pt}$ of 3740 Hz. Downfield from each of the two major resonances are additional sets of signals at 2.5 and 10.5 ppm, which are of equal intensity relative to one another (Figure 2.4a). We proposed that they correspond to a species which has both *cis* and *trans* nodes in one complex, **13c** [*cis*–$PtCl_2$(κ^1:μ:κ^1–NHC,S)(κ^1:μ:κ^1–P,S)–*trans*–$PtCl_2$(κ^1:μ:κ^1–NHC,S)(κ^1:μ:κ^1–P,S)]. This assignment is supported by the $^{31}P–^{195}Pt$ coupling constants that are comparable to that of the purely *cis* and purely *trans* isomers (Figure 2.4). The relative chemical shifts along with the $^{31}P–^{195}Pt$ coupling constants reveal important information about the *trans* influence inherent to these structures.[100-102] In the case of strongly donating ligands, the chemical shift typically appears further downfield,[101] such as in *trans* complex **13b**. Between isostructural complexes, larger $^{31}P–^{195}Pt$ coupling constants are indicative of a more weakly coordinating ligand *trans* to the phosphine ligand, while smaller coupling constants indicate the presence of a more strongly coordinating ligand. The NHC is a more strongly donating ligand than the chloride; therefore, the coupling constant of the *trans* complex **13b** ($J_{P–Pt}$ = 2300 Hz) is significantly smaller than that of the *cis* complex **13a** ($J_{P–Pt}$ = 3740 Hz). The *cis/trans* species (**13c**) follow the same trend, with one Pt^{II} node in the *cis* configuration and the other in the *trans* orientation, each having a chemical shift and coupling constant in the same region of the spectrum as the fully *cis* and *trans* counterparts, respectively. The resonance at 2.5 ppm has a larger coupling

constant (J_{P-Pt} = 2943 Hz), while the resonance of equal intensity further downfield at 10.5 ppm, has a smaller coupling constant (J_{P-Pt} = 2270 Hz).

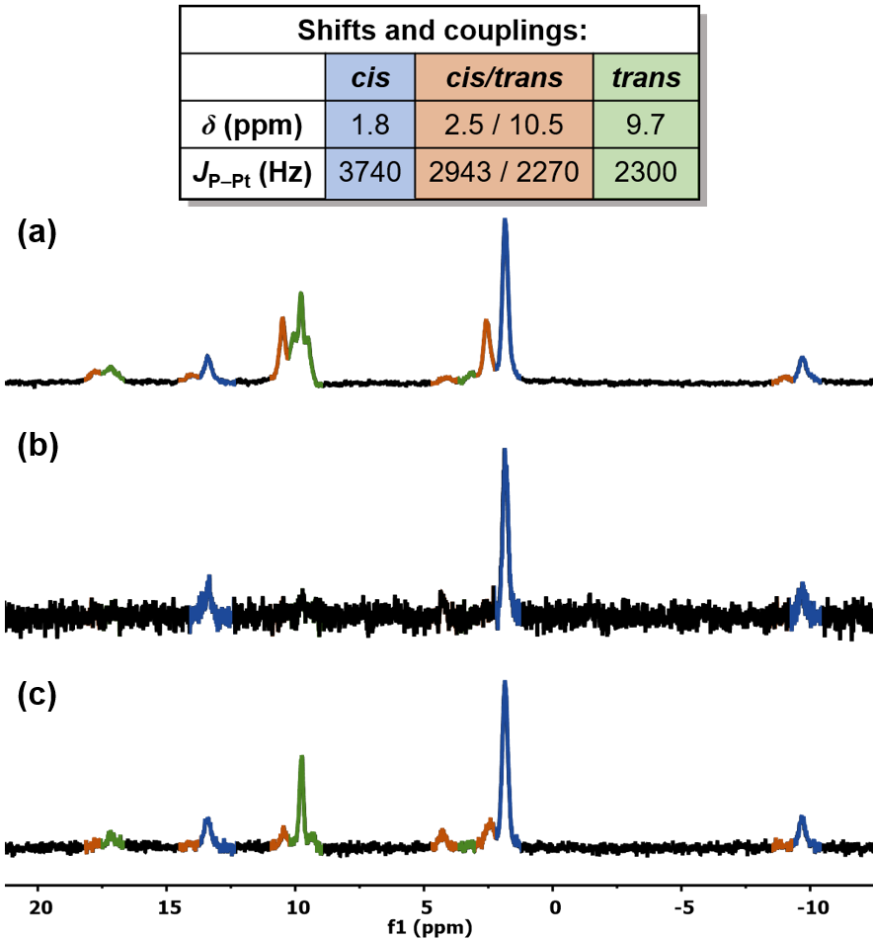

Figure 2.4 (a) ^{31}P NMR spectrum of complex mixture **13** in CD_2Cl_2, (b) ^{31}P NMR spectrum of single crystals of the fully open *cis* complex, **13a**, dissolved in CD_2Cl_2, (c) ^{31}P NMR spectrum of **13a** after several hours, indicating the reappearance of resonances attributable to the *cis* (**13a**), trans (**13b**), and *cis/trans* (**13c**) species.

When the solvent from the solution of **13a**–**c** was slowly evaporated, single crystals composed exclusively of **13a** were isolated. The solid-state structure of **13a** is consistent with the solution-phase spectroscopic characterization of the fully open *cis* isomer, with one κ^1:μ:κ^1–P,S ligand and one κ^1:μ:κ^1–NHC,S ligand coordinated to Pt^{II} through the phosphines and carbenes,

respectively (Figure 2.5). We hypothesized that the *cis* fully open structure would dynamically equilibrate back to the **13a**–**c** complexes initially observed in solution, an indication of fully open isomers similar in energy. To assess the kinetic stability of **13a**, its crystals were dissolved in CD_2Cl_2 and the corresponding ^{31}P NMR spectrum was collected (Figure 2.4b), confirming our assignment of the 1.8 ppm shift belonging to **13a**. Over time, we observed the reappearance of resonances attributable to the *trans* (**13b**) and *cis/trans* (**13c**) species, in addition to *cis* **13a**, indicating the complex undergoes isomerization in solution (Figure 2.4c). Consistent with an equilibrium that involves small energetic differences between isomers, we observed strong solvent effects in the synthesis of **13a-c**. In an alternative procedure, we reacted **12** with **10** in dichloromethane under heterogeneous conditions (Scheme 2.3), resulting in the selective formation of **13a** as confirmed by ^{1}H and ^{31}P NMR spectroscopy and HRMS. These results suggest that solvent effects play a key role in lowering the kinetic barriers to establish an equilibrium between isomers **13a-c**.

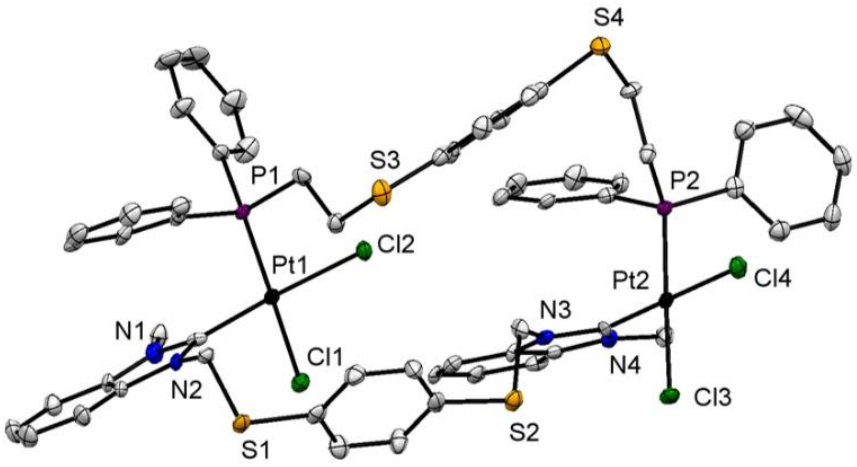

Figure 2.5 Crystal structure of **13a**, drawn with a 50% thermal ellipsoid probability. Solvent molecules and hydrogen atoms have been omitted for clarity. Selected bond lengths [Å] and angles [deg]: Pt1–Cl2 2.360(2), Pt1–Cl2 2.352(2), Pt2–Cl3 2.340(2), Pt2–Cl4 2.357(2), Cl1–Pt1–Cl2 90.57(6), Cl3–Pt2–Cl4 89.42(6).

2.2.3 The Solid-State Structure of 13a

The solid-state structure of **13a** confirms that the *cis* fully open complex contains two inner sphere chloride atoms in the *cis* orientation. Complex **13a** crystallized in the triclinic centrosymmetric space group *P*ī, and the asymmetric unit contains distinct Pt–Cl bond lengths and angles (Figure 2.5) comparable to those found in literature.[50, 95] The Pt^{II} metal nodes adopt a square planar geometry [Cl1–Pt1–Cl2 = 90.57(6)°], with the phosphine moieties *cis* to the carbene moieties [P1–Pt1–C1 = 94.6(2)°] (Figure 2.5). The solid-state structure supports the assignments made in the ^{1}H and ^{31}P NMR spectra.

2.2.4 Computational Studies of Complexes 13a-c

In order to further investigate and understand the intramolecular interactions and relative energies of each fully open isomer in solution, we explored the electronic structures of **13a**, **13b** and **13c** and their possible diastereomers with Density Functional Theory (DFT) calculations in the gas phase. DFT calculations were carried out on the solid-state structure of **13a** with Gaussian 09 suite of programs at the B97D/LANL2DZ level of theory. The selected functional B97D empirically includes dispersion effects, which allows for a better description of the electronic structure. The geometry optimized model of **13a** provided the basis for developing the energy minimized models of **13b** and **13c** and their respective isomers. Bond lengths and angles of model **13a** are nearly identical to those measured in the solid-state crystal structure. All structures correspond to local minima on the potential energy surfaces and, therefore, are chemically accessible states. Population analysis was performed within the Natural Bond Orbitals (NBO) formalism to provide a localized, pairwise, description of the electron density.

We hypothesized that complexes **13a–13c** would be relatively close in their free energies, owing to the observation of rapid and dynamic conversion from the purely *cis* state to the mixture of *cis*, *trans* and *cis/trans* states. Energy minimized models (Figure 2.6) were obtained for each complex (**13a–13c**), and their respective frontier orbitals were identified, as they point to the identity of the orbitals involved in WLA bonding. Relative HOMO and LUMO energies were calculated, and free energies were compared across different structures. Table 2.1 summarizes the free energies calculated from the DFT results.

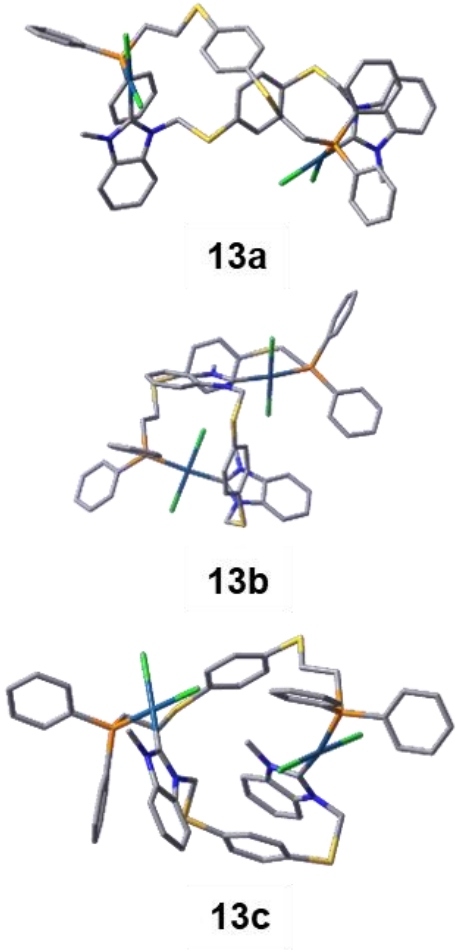

Figure 2.6 Energy-minimized models of complexes **13a–13c**, obtained from DFT calculations.

Table 2.1 Free Energies (kcal/mol) of **13a–13c** Obtained from DFT Calculations.

Compound	Free Energy (kcal/mol)	Relative Free Energy (kcal/mol)
13a	-2811.3087	0.0
13b	-2811.3029	0.006
13c	-2811.3018	0.007

Computational modeling of the fully open states suggests that the overall free energy of the three states are close enough that there is no strong preference to form one isomer over the others. This is consistent with a system that has very small energy differences between isomers, suggesting that **13a–13c** are nearly isoenergetic.

2.3 Conclusions

A primary goal of supramolecular coordination chemistry—drawing inspiration from biology—is the synthesis of three-dimensional structures with highly organized and addressable reactive compartments. Herein we demonstrate the synthesis and assembly of a macrocycle containing two types of hemilablile coordinating ligands, with the aim of advancing the scope and function of such biomimetic compartments. Specifically, the macrocycle is composed of: (1) a strongly chelating, *N*-heterocyclic carbene–thioether (NHC,S) ligand which has been synthesized and its structure characterized using NMR spectroscopy in solution, and single–crystal X-ray diffraction in the solid state, and (2) a phosphinoalkyl–thioether (P,S) ligand. The allosterically addressable heteroligated macrocycle is assembled in a stepwise fashion by chelating each ligand to a Pt(II) metal center as confirmed by NMR spectroscopy. This macrocycle represents the first

example of a stable yet structurally addressable heteroligated macrocycle which is suitable for use under ambient conditions. The methodology developed so far will allow access to far more complex allosterically regulated, supramolecular host-guest capsules for applications in molecular recognition and beyond.

2.4 Experimental Methods

2.4.1 General Methods and Instrument Details

Commercially available chemicals were purchased as reagent grade from Sigma-Aldrich, Acros, and Alfa Aesar, unless otherwise noted, and used as received. Unless otherwise stated, all solvents were purchased anhydrous and degassed under a stream of argon prior to use. All glassware and magnetic stirring bars were thoroughly dried in an oven (180 °C). Reactions were monitored using thin layer chromatography (TLC), and commercial TLC plates (silica gel 254, Merck Co.) were developed and the spots were visualized under UV light at 254 or 365 nm. Flash chromatography was performed using SiO_2-60 (230–400 mesh ASTM, 0.040–0.063 mm; Fluka). Deuterated solvents were purchased from Cambridge Isotope Laboratories and used as received. ^{1}H, ^{31}P, $^{31}P\{^{1}H\}$ and $^{19}F\{^{1}H\}$ NMR spectra were recorded on a Bruker Avance 400 MHz and chemical shifts (δ) are given in ppm. ^{1}H NMR spectra were referenced internally to residual proton resonances in the deuterated solvents (dichloromethane-d_2 = δ 5.32; nitromethane-d_3 = δ 4.33; methanol-d_4 = δ 3.31). ^{31}P and $^{31}P\{^{1}H\}$ NMR spectra were referenced to an external 85% H_3PO_4 standard (δ 0). High resolution electrospray ionization mass spectrometry (HR–MS) measurements were recorded on an Agilent 6120 LC-TOF instrument in positive ion mode. Electrospray ionization mass spectrometry (ESI–MS) was recorded on a Micromas Quatro II triple quadrapole mass spectrometer. Matrix assisted laser desorption ionization–time of flight mass spectrometry

(MALDI–TOF MS) was recorded on a Bruker Autoflex III smartbeam in reflectron and positive ion mode.

2.4.2 Synthesis

2.4.2.1 Synthesis of Benzimidazolium Salt (14)

In a modified procedure,[95] a solution of 1,4-bis[(chloromethyl)thio]benzene (50 mg, 0.209 mmol) and 1-methylbenzimidazole (74.09 mg, 0.627 mmol) were dissolved in 5 mL of anhydrous dimethylformamide (DMF). The reaction mixture was stirred and heated at 100 ℃ for 24 h in a Schlenk flask under N_2 gas. The solvent was reduced to ca. 1 mL in *vacuo* with heptane. The product was then washed with diethyl ether and dichloromethane and dried in *vacuo* to obtain a white solid (66.3 mg, 0.132 mmol, 63% yield). ^{1}H NMR (400 MHz, DMSO-d_6): δ 9.85 (s, 2H), 7.68 (dtd, J = 15.7, 7.4, 6.3 Hz, 4H), 7.72–7.64 (m, 4H); 7.37 (s, 4H), 6.17 (s, 4H), 4.05 (s, 6H). ^{13}C NMR (126 MHz, DMSO-d_6) δ 142.32, 132.31, 131.98, 131.67, 130.12, 126.79, 126.67, 114.06, 113.91, 49.83, 33.42.

2.4.2.2 [$Pt_2Cl_4(\kappa^1{:}\mu{:}\kappa^1$–NHC,S)$(C_2H_6OS)_2$] (12-DMSO)

A solution of benzimidazolium salt (**1**) (100 mg, 0.199 mmol) in a solvent mixture of DCM:MeOH at a ratio of 6:1 (4 mL), was combined with Ag_2O (46 mg, 0.199 mmol) and the mixture was stirred at 60 ℃ until the solution became murky and the black Ag_2O powder disappeared. After ten minutes, a solution of $PtCl_2$(cod) (149 mg, 0.397 mmol) in the solvent mixture of DCM:MeOH at a ratio of 6:1 (6 mL) was added to the mixture, which was then stirred at 60 ℃ over 24 h. The suspension was centrifuged, washed with Et_2O (10 mL x 3), and dried in *vacuo*. The product was obtained as an off-white powder (115 mg, 0.120 mmol, 60% yield). ^{1}H NMR (400 MHz, DMSO-d_6): δ 7.74 (dd, J = 8.2, 3.7 Hz, 2H), 7.41 (d, J = 1.7 Hz, 4H), 7.35 (t, J

= 7.7 Hz, 2H), 7.29–7.16 (m, 4H), 6.20–6.02 (m, 4H); 4.19 (d, J = 3.6 Hz, 6H). ^{13}C NMR (126 MHz, DMSO-d_6) δ 155.68 (d, $^{1}J_{C\text{-}Pt}$ = 4.2 Hz), 133.17 (s), 133.05 (s), 132.73 (s), 132.66 (s), 124.02 (s), 123.89 (s), 111.69 (s), 111.36 (s), 111.31 (s), 51.37 (s), 34.83 (s). MALDI–TOF MS (Matrix: dithranol). Calcd for $[M–Cl]^+$: 926.961 *m/z*. Found: 926.803 *m/z*.

2.4.2.3 1,4-bis(diphenylphosphino)ethylthiobenzene (10)

In a modified procedure,[103-104] benzene-1,4-dithiol (0.340 mg, 2.36 mmol) was combined with AIBN (catalytic amount) in a Schlenk flask in THF (15 mL) under N_2 gas. Diphenylvinyl phosphine ($KPPh_2$, 1.0 g, 4.71 mmol) was added drop-wise to the reaction mixture, *via* syringe, under N_2 gas over the course of 30 min. The solution turned from yellow to red. The reaction was refluxed for 18 h under N_2 gas. After stirring for 18 h, the reaction solution was concentrated in vacuo to give a yellow oil. The crude product was washed with hexanes (10 mL x 3) followed by MeOH (10 mL x 3), filtered and dried under high vacuum. The pure product appeared as an off-white solid powder (1.18 g, 90% yield). ^{1}H NMR (400 MHz, CD_2Cl_2): δ 7.41–7.35 (m, 8H), 7.34–7.31 (m, 12H), 7.10 (s, 4H), 2.96–2.90 (m, 4H), 2.36–2.32 (m, 4H). ^{31}P NMR (162 MHz, CD_2Cl_2): δ -17.36.

2.4.2.4 Synthesis of [cis–Pt_2Cl_4(κ^1:μ:κ^1–NHC,S)(κ^1:μ:κ^1–P,S)], [trans–Pt_2Cl_4(κ^1:μ:κ^1–NHC,S)(κ^1:μ:κ^1–P,S)], and [cis–$PtCl_2$(κ^1:μ:κ^1–NHC,S)(κ^1:μ:κ^1–P,S)–trans–$PtCl_2$(κ^1:μ:κ^1– NHC,S)(κ^1:μ:κ^1–P,S)] (13a-c).

A solution of **10** (81.3 mg, 0.143 mmol) in CD_2Cl_2/CD_3OD (1:1, 2.5 mL) was added to a suspension of complex **12** (115 mg, 0.120 mmol) in CD_2Cl_2/CD_3OD (1:1, 0.7 mL) in a glass vial in the glove box. The mixture was then stirred at room temperature for 48 h, during which the yellow murky solution became clear and a dark precipitate formed (AgCl). The supernatant was

then dried in *vacuo* to obtain a pale yellow solid powder as the product (114 mg, 0.0745 mmol, 62% yield). ^{1}H NMR (400 MHz, CD_2Cl_2): δ 8.06–6.95 (m, 38H), 4.27–3.82 (m, 4H), 3.35–3.10 (br, 8H), 1.26 (s, 6H). ^{31}P NMR (162 MHz, CD_2Cl_2): δ 10.45 (d, $^{1}J_{P-Pt}$ = 2270 Hz); 9.73 (d, $^{1}J_{P-Pt}$ = 2300 Hz); 2.53 (d, $^{1}J_{P-Pt}$ = 2943 Hz); 1.81 (d, $^{1}J_{P-Pt}$ = 3740 Hz). HRMS (ESI+). Calcd for $[M-Cl]^{+}$: 1493.1039 *m/z*. Found: 1493.1051 *m/z*.

2.4.2.5 [cis–Pt_2Cl_4(κ^1:μ:κ^1–NHC,S)(κ^1:μ:κ^1–P,S)] (13a)

Crystals of complex **13a** were obtained by slow diffusion of Et_2O into a CH_2Cl_2 solution of **13a-c**. ^{1}H NMR (400 MHz, CD_2Cl_2): δ 8.06–8.00 (m, 4H), 7.75 (s, 4H), 7.60–7.48 (m, 10H), 7.35 (s, 4H), 7.30–7.11 (m, 11H), 7.01–6.98 (m, 9H), 6.03–5.84 (d, 13.54 Hz, 2H), 5.78–5.57 (d, 13.51 Hz, 2H), 3.82 (s, 6H), 3.45–3.22 (dt, 6.16, 6.16, 11.32 Hz, 4H), 3.19–2.92 (m, 4H). ^{31}P NMR (162 MHz, CD_2Cl_2): δ 1.84 ($^{1}J_{P-Pt}$ = 3740 Hz).

2.4.3 X-ray Crystallography

Suitable crystals were selected and the crystals were each mounted on MITIGEN holders in Paratone oil on a Kappa Apex 2 diffractometer. Using Olex2,[105] the structures were solved with the ShelXT[106] structure solution program using Direct Methods and refined with the ShelXL[107] refinement package using Least Squares minimization.

2.4.3.1 Crystal Structures of Complexes 12 and 13a

Single crystals of **12-DMSO** and **13a** were mounted on a MITIGEN holder in Paratone oil on a Kappa Apex 2 diffractometer. All measurements were made with graphite-monochromated Cu Kα radiation and all structures were solved with ShelXT structure solution program using Direct Methods and refined with the ShelXL refinement package using Least Squares minimization.

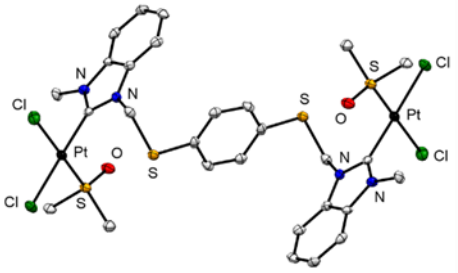

12-DMSO

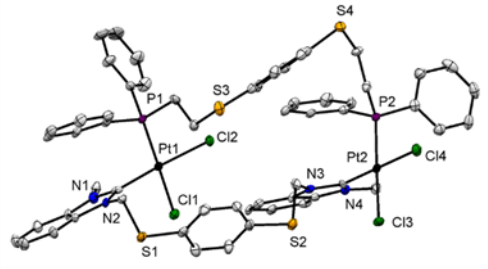

13a

Table 2.2 Crystallographic Data for Complex **12-DMSO** and **13a**

	12-DMSO	**13a**
Empirical formula	$C_{40}H_{70}Cl_4N_4O_8Pt_2S_{10}$	$C_{62}H_{62}Cl_{12}N_4P_2Pt_2S_4$
Formula weight	1587.58	1868.91
Temperature / K	100.06	100.0
Crystal system	triclinic	triclinic
Space group	P-1	P-1
a / Å	9.2837(3)	11.3838(5)
b / Å	11.1950(4)	17.4837(7)
c / Å	14.3816(5)	18.1658(8)
α/°	91.703(2)	84.972(3)
β/°	90.044(2)	74.501(3)
γ/°	104.747(2)	79.960(3)
Volume / Å^3	1444.77(9)	3427.5(3)
Z	1	2
ρ_{calc} / mg mm^{-3}	1.825	1.811
μ / mm^{-1}	14.412	13.749
F(000)	786	1832
Crystal size / mm^3	0.253 × 0.164 × 0.015	0.212 × 0.025 × 0.015
2Θ range for data collection	6.148 to 130.288°	7.05 to 133.55°

Index ranges	$-10 \leq h \leq 10, -13 \leq k \leq 12, -16 \leq l \leq 16$	$-12 \leq h \leq 13, -20 \leq k \leq 20, 0 \leq l \leq 21$
Reflections collected	11518	11971
Independent reflections	4844[R(int) = 0.0334]	11971[R(int) = 0.0731]
Data/restraints/parameters	4844/0/316	11971/0/777
Goodness-of-fit on F^2	1.044	1.077
Final R indexes [I>2σ (I)]	$R_1 = 0.0317$, $wR_2 = 0.0939$	$R_1 = 0.0464$, $wR_2 = 0.1028$
Final R indexes [all data]	$R_1 = 0.0331$, $wR_2 = 0.0952$	$R_1 = 0.0667$, $wR_2 = 0.1093$
Largest diff. peak/hole / e $Å^{-3}$	2.338/-1.249	2.399/-1.460

2.4.4 NMR Spectra of all Compounds and Complexes

^{1}H NMR Spectrum of Benzimidazolium chloride salt (14)

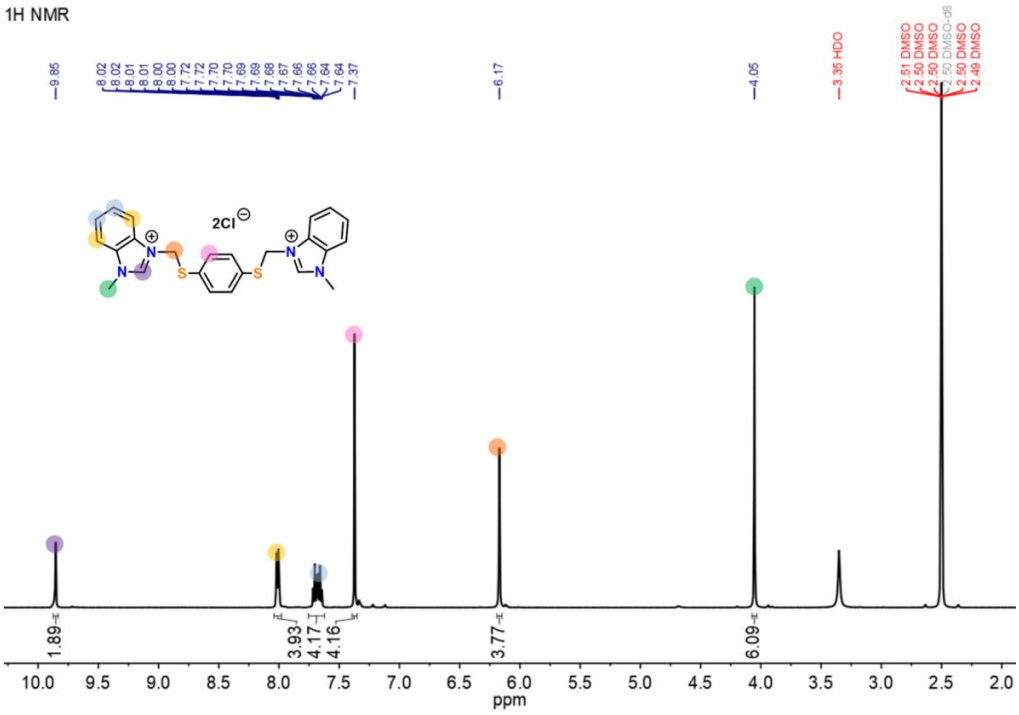

^{13}C NMR Spectrum of Benzimidazolium chloride salt (14)

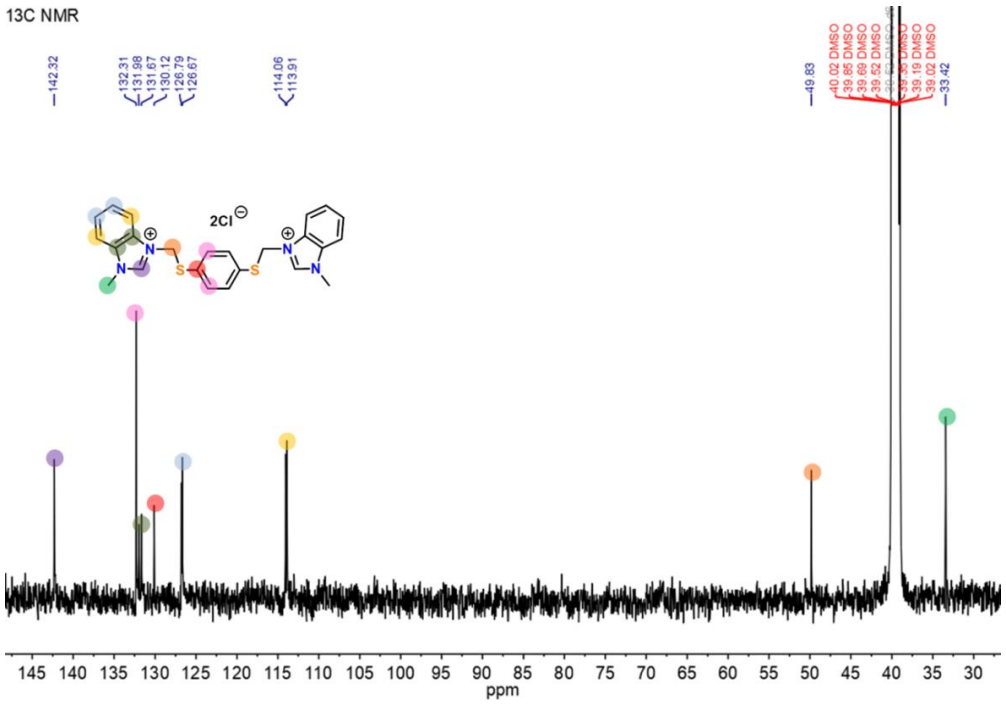

^{1}H NMR Spectrum of Monoligated Complex [$Pt_2Cl_4(\kappa^1{:}\mu{:}\kappa^1$–NHC,S)($C_2H_6OS)_2$] (12-DMSO)

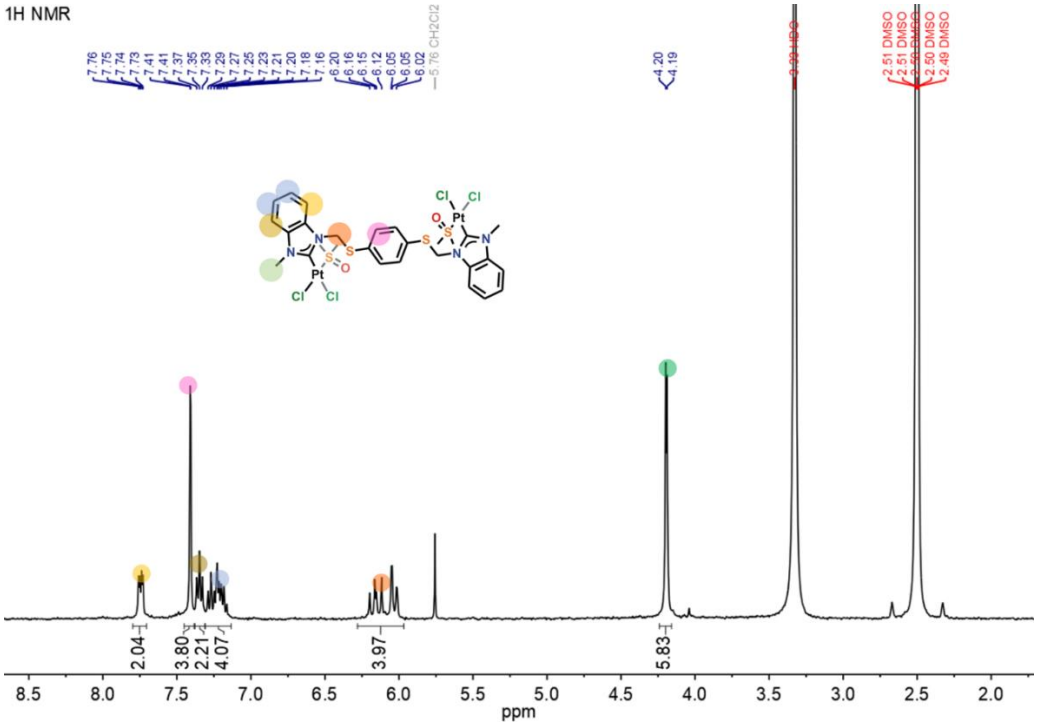

^{13}C NMR Spectrum of Monoligated Complex [$Pt_2Cl_4(\kappa^1{:}\mu{:}\kappa^1$–NHC,S)$(C_2H_6OS)_2$] (12-DMSO)

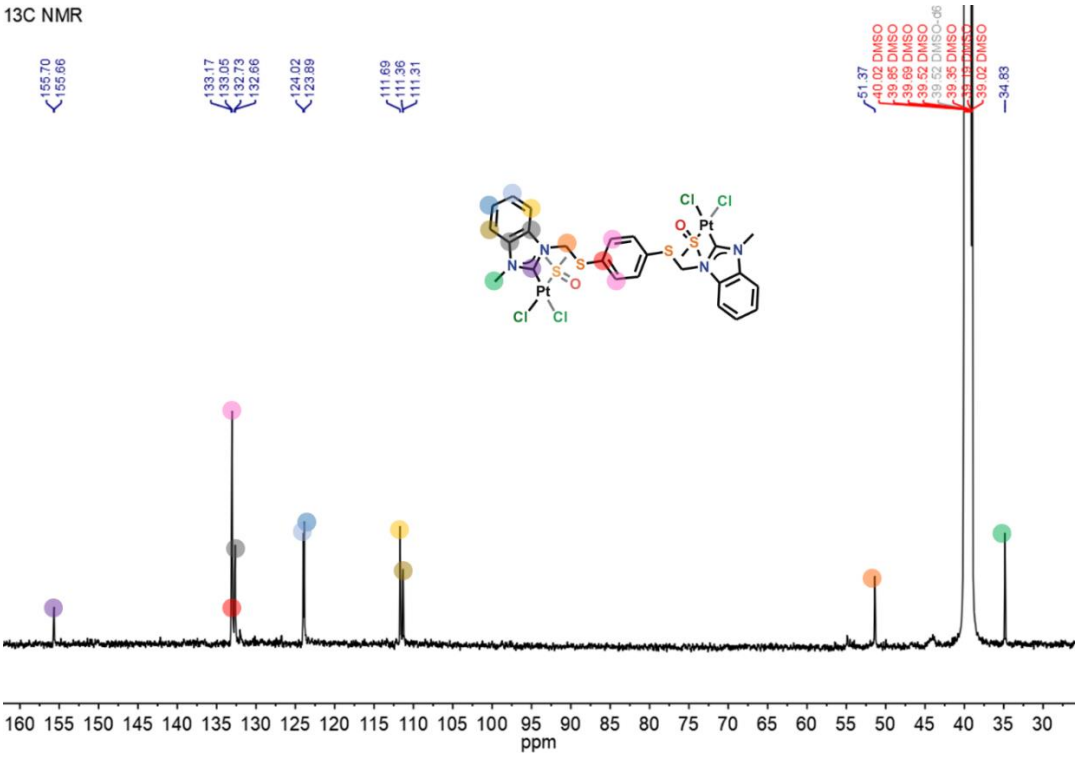

^{1}H NMR Spectrum of 1,4-bis(diphenylphosphino)ethylthiobenzene (10)

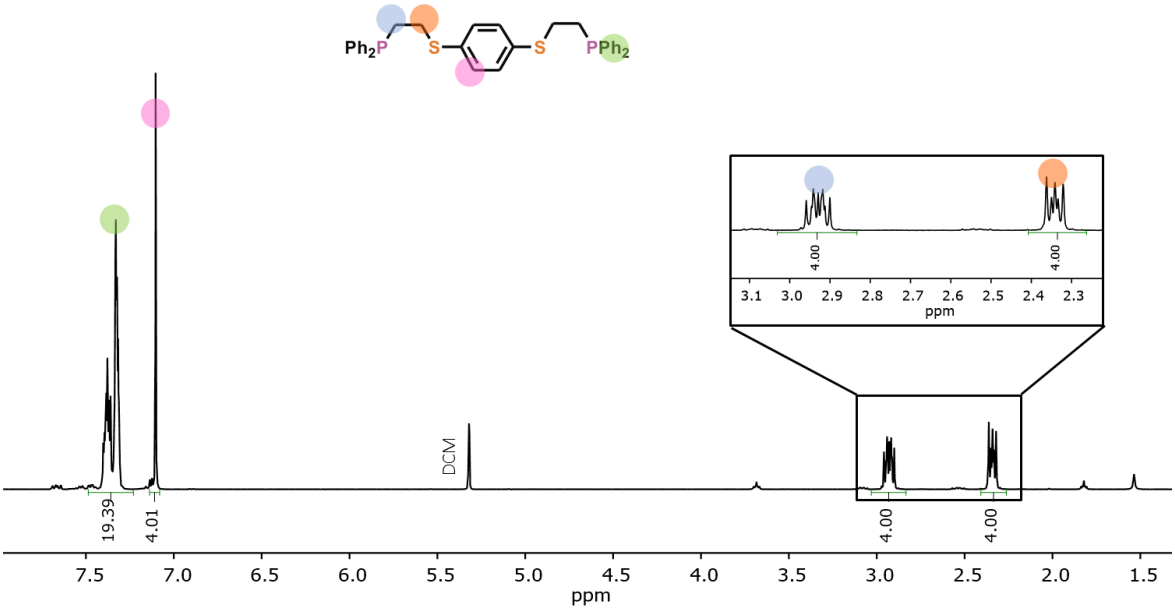

^{31}P NMR Spectrum of 1,4-bis(diphenylphosphino)ethylthiobenzene (10)

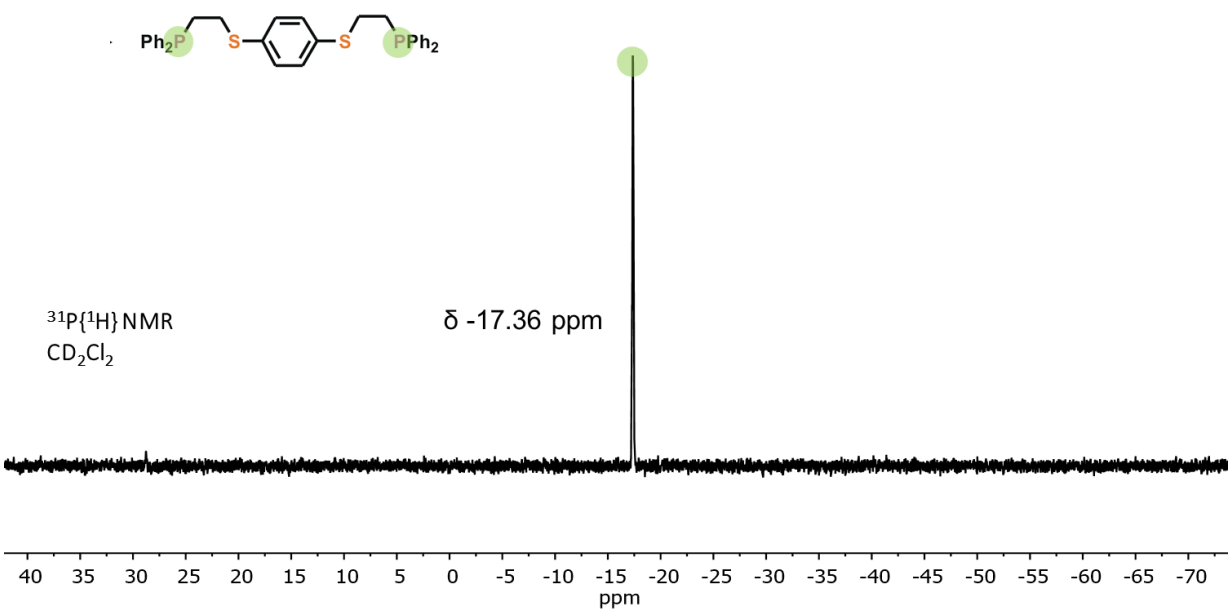

^{1}H NMR Spectra of Fully Open Macrocycle Isomers (13a-c)

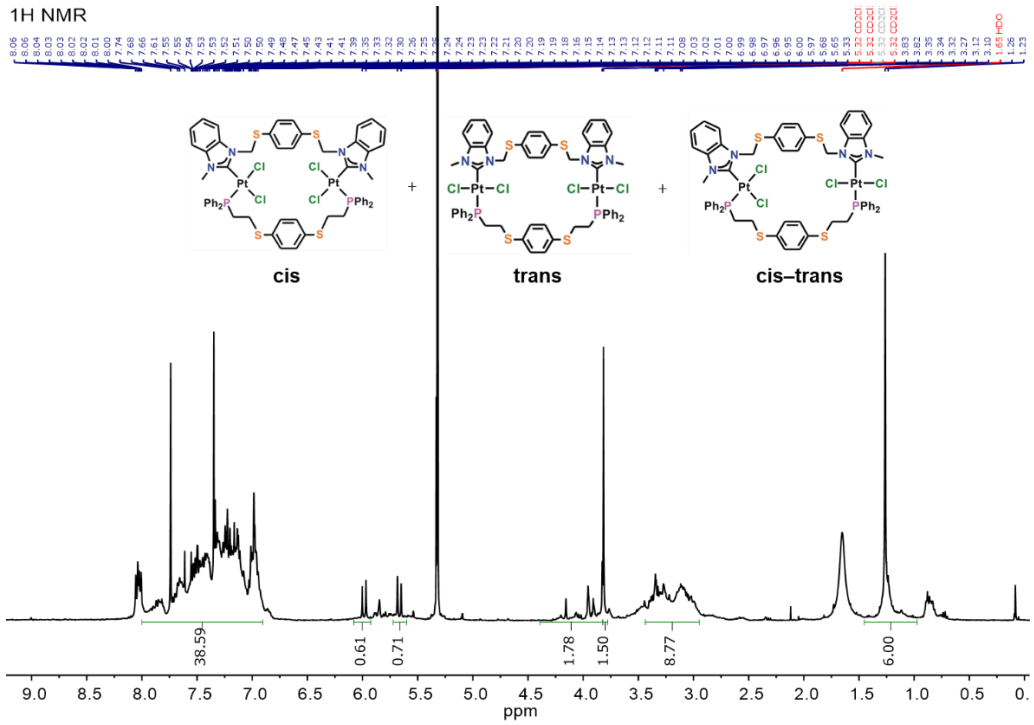

^{31}P NMR Spectra of Fully Open Macrocycle Isomers (13a-c)

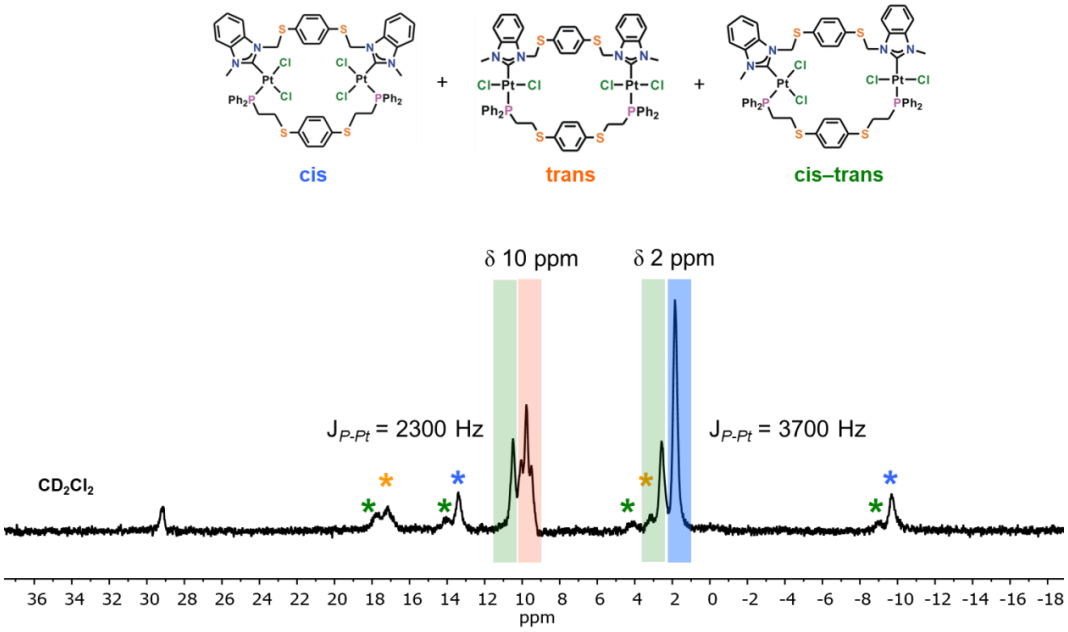

^{1}H NMR Spectrum of Fully Open Macrocycle Crystals [cis–Pt_2Cl_4(κ^1:μ:κ^1–NHC,S)(κ^1:μ:κ^1–P,S)] (13a)

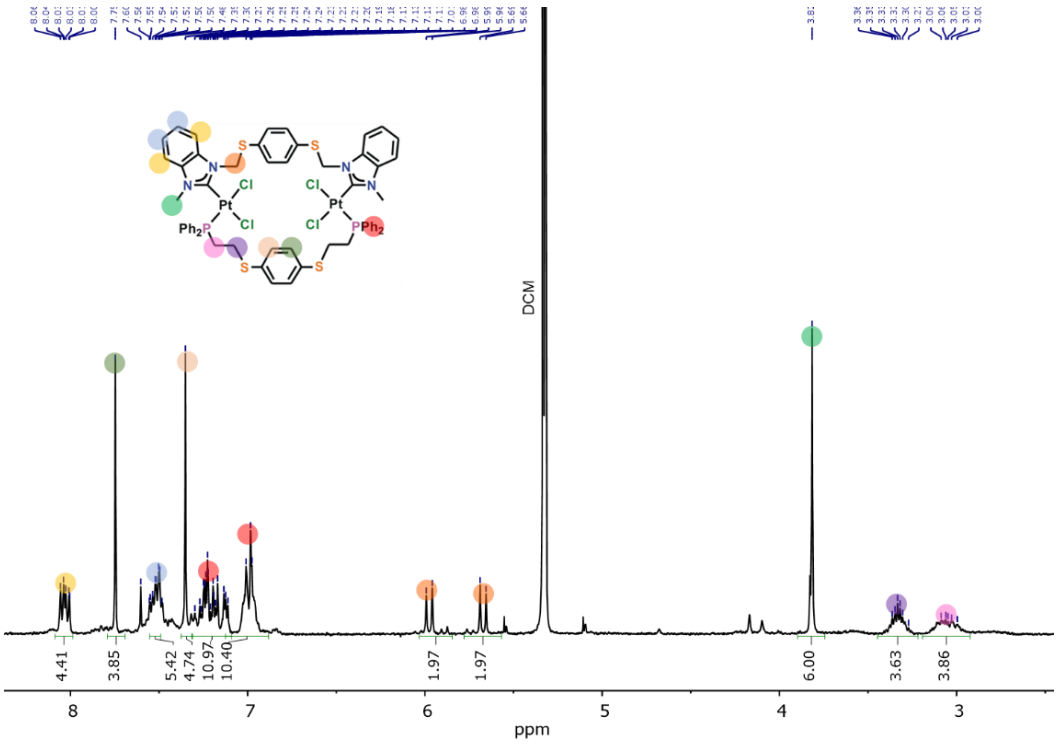

^{31}P NMR Spectrum of Fully Open Macrocycle Crystals [cis–Pt_2Cl_4(κ^1:μ:κ^1–NHC,S)(κ^1:μ:κ^1–P,S)] (13a)

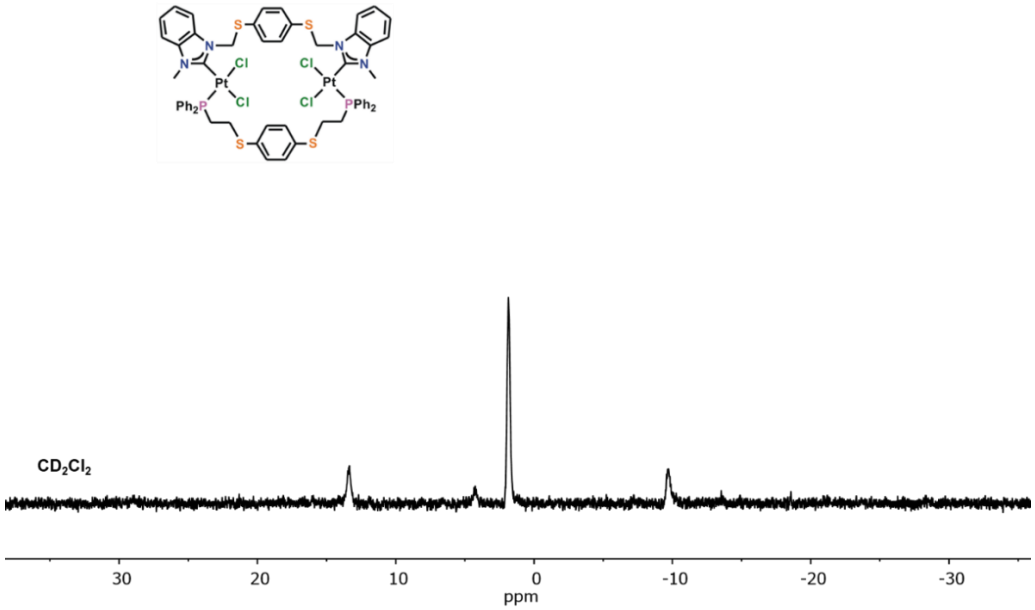

2.4.5 Mass Spectra of all Complexes

MALDI-TOF MS of [Pt_2Cl_4(κ^1:μ:κ^1–NHC,S)] (12)

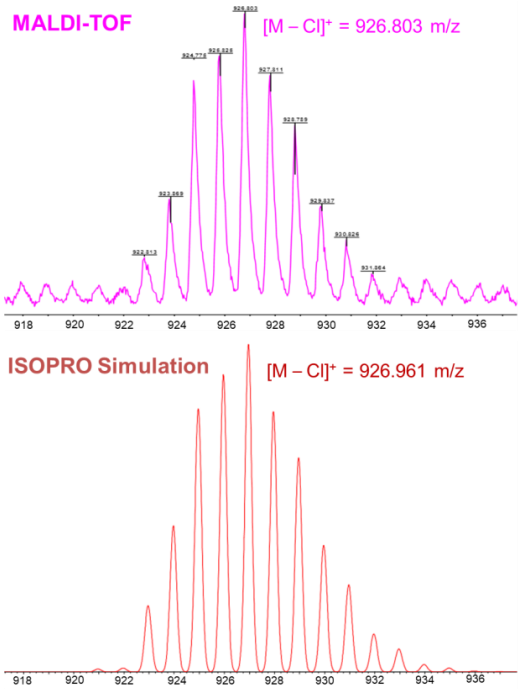

HRMS (ESI+) of Fully Open Macrocycle (13)

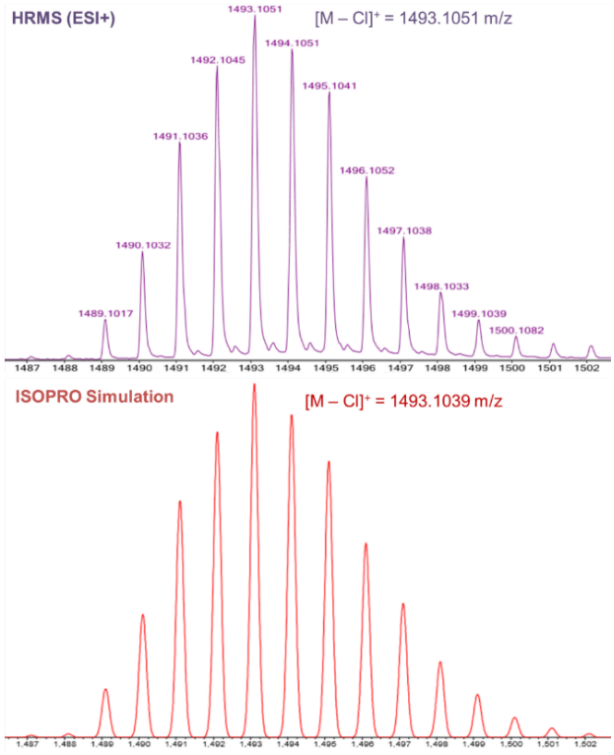

CHAPTER 3

Complex Switching Behavior in a Four State WLA Macrocycle

The work presented in this chapter is based upon work published in:

d'Aquino, A. I.; Cheng, H. F.; Barroso-Flores, J.; Kean, Z. S.; Mendez-Arroyo, J. E.; McGuirk, C. M.; Mirkin, C. A. An Allosterically-Regulated, Four-State Macrocycle. *Inorg. Chem*. **2018**, *57*, 3568–3578. DOI: 10.1021/acs.inorgchem.7b02745

3.1 Introduction

Molecular capsules assembled through coordination chemistry have long been used as scaffolds to explore new types of molecular interactions in constrained geometries and have potential applications in catalysis, drug delivery and separations. However, these assemblies are rigid, usually trapping guests within the cavity or are effective only in a limited set of conditions. These systems can be greatly enhanced by introducing principles from biology such as allosteric regulation to expand the capabilities and reduce the shortcomings of such assemblies. To overcome this limitation, the Weak-Link Approach (WLA) is used to assemble a heterodimeric molecular receptor in this work. Herein, we apply this step-wise approach to the synthesis of a heteroligated multi-state macrocycle, possessing two different ditopic bidentate ligands bridging two Pt^{II} metal nodes, which exhibits four-state switching behavior, considerably more complex than previously reported for WLA systems. Experimental and computational evidence suggests that, while the addressability of the system arises from the coordination chemistry, the resulting complexity of the macrocycle behavior is a function of multiple factors, including: geometry, strain, strength of coordination bonds and electronics. This is in contrast with previously reported WLA systems that rely on the use of weakly chelating ligands to achieve the assembly of heteroligated structures, which are too unstable to form significantly strained structures.[50]

3.2 Results and Discussion

3.2.1 Formation of the Semi-Open WLA Macrocycle

Upon exposing the neutral, fully open state **13a** (or the mixture of **13a-c**) to MeOH, the dicationic, semi-open complex [*cis*–$Pt_2Cl_2(\kappa^1{:}\mu{:}\kappa^1$–NHC,S)($\kappa^2{:}\mu{:}\kappa^2$–P,S)][Cl]$_2$ (**14**) was formed via the transfer of a chloride anion from the inner coordination sphere of each Pt^{II} center to the

outer coordination sphere (Scheme 3.1). In polar protic solvents such as MeOH, outer-sphere chloride counterions are stabilized by hydrogen bonding, and the overall charge of the complex is stabilized by the polar solvent, thus favoring the semi-open state. This transformation is enthalpically driven and has been observed in similar systems.[50, 108-109]

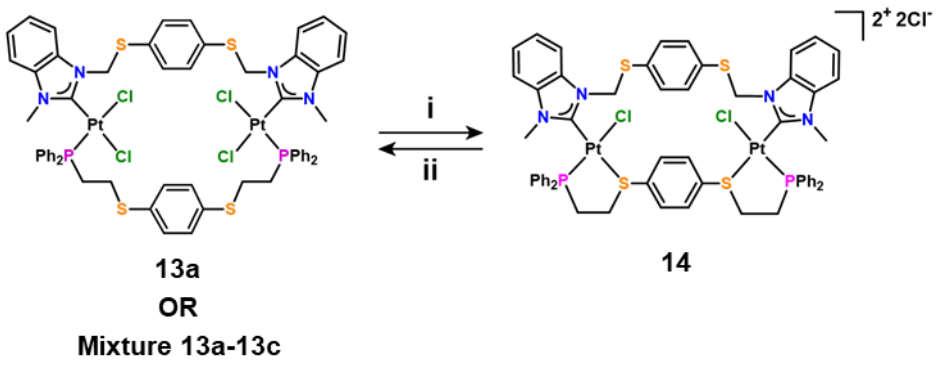

Scheme 3.1 Formation of the Semi-Open WLA Macrocycle. Reaction conditions: (i) Room temperature, MeOH, 25 °C. (ii) CH_2Cl_2, 25 °C.

The driving force of the switching from the fully open to the semi-open state is two-fold: (i) the two outer-sphere chloride ions and the charged complex are stabilized by the polar solvent and (ii) the structure is able to relieve ring strain by adopting the semi-open configuration as evidenced by DFT calculations. Complex **14** was thoroughly characterized via ^{1}H and ^{31}P NMR spectroscopy, diffusion ordered spectroscopy (DOSY, Figure 3.1), two-dimensional correlation spectroscopy and HRMS.

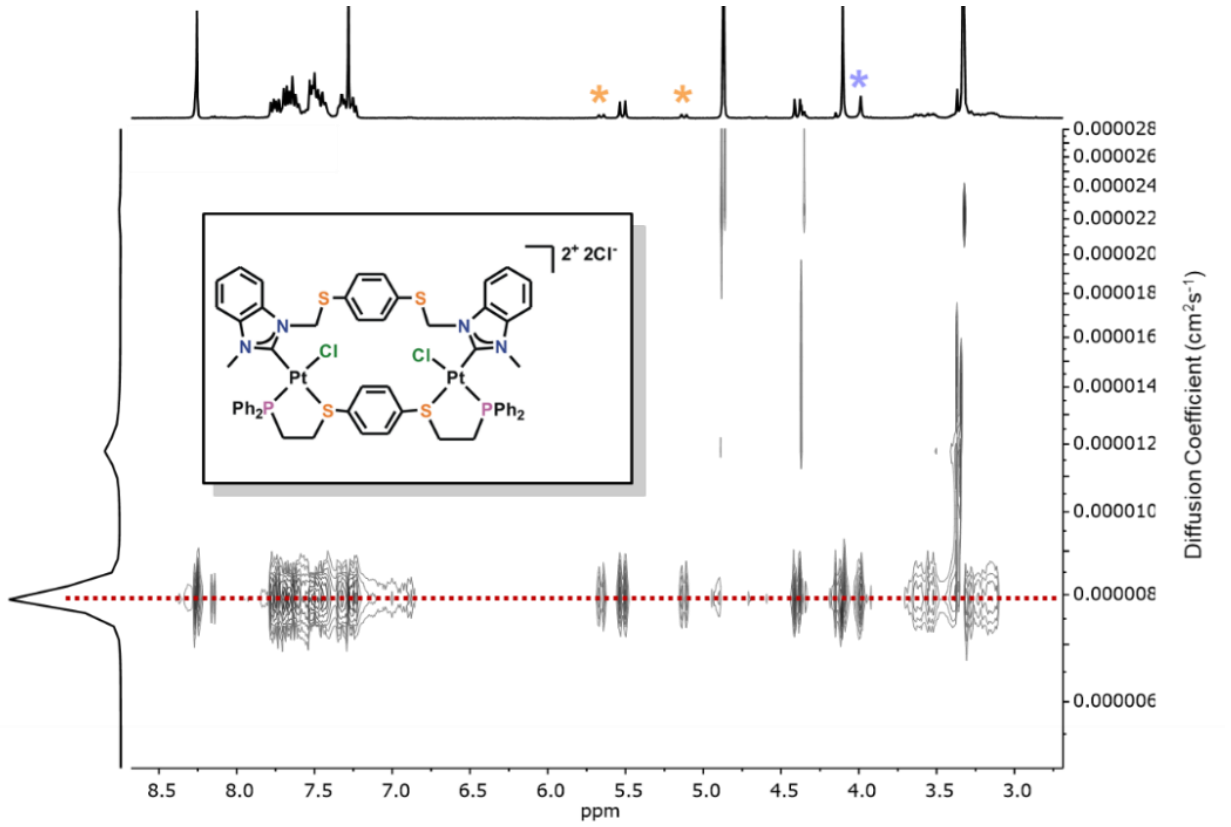

Figure 3.1 ^{1}H DOSY NMR spectra of a sample containing complex **14** in methanl-d_4. The region corresponding to the semi-open species is indicated by the dotted red line. Asterisks denotes a diastereomer of **14**. The average diffusion coefficient of complex **14** in methanol, was determined to be $8x10^{-6}$ cm^2s^{-1}.

The chemical shift observed in the ^{31}P NMR spectrum of complex **14** (δ 36 ppm) is shifted dramatically downfield from that of the fully open Pt^{II} complexes with a concurrent decrease in the coupling constant ($J_{P\text{-}Pt}$ = 3421 Hz) (Figure 3.2a). The downfield chemical shift and the decrease in $J_{P\text{-}Pt}$ are consistent with increased back donation from the platinum atoms in the semi-open state in which the P,S-ligand is fully chelated with the phosphine moiety *trans* to the chloride. Additionally, this downfield shift is diagnostic of phosphine-containing ligands forming a five-membered ring.[110]

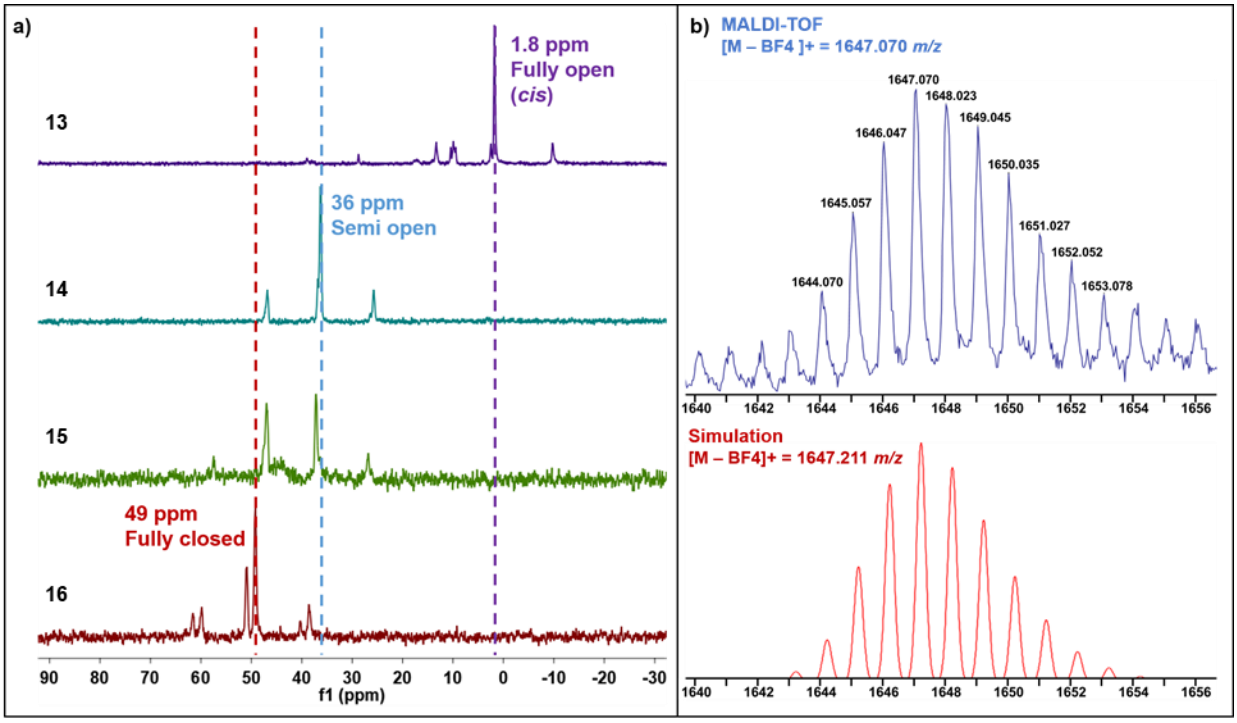

Figure 3.2 (a) ^{31}P NMR spectra of each distinct state accessible by the WLA macrocycle, namely, a fully open (**13**) a semi-open (**14**), a new intermediate state (**15**) with one Pt^{II} node in the closed state and the other in a semi-open state, and a fully closed state (**16**). (b) MALDI–TOF spectra compared with ISOPRO simulation of the molecular ion $[M–BF_4]^+$ of complex **16**.

A small shoulder at 37 ppm, hypothesized to be due to the presence of diastereomers, is present just downfield of the major resonance at 36 ppm in the ^{31}P NMR spectrum. Previous reports have shown that stereoisomers in WLA tweezer complexes with two phosphinoalkyl–thioether ligands, as well as in WLA complexes bearing NHC,S and P,S-ligands, can be observed via ^{1}H and ^{31}P NMR spectroscopy.[50, 95] This is attributed to the intramolecular inversion of the thioether moiety *trans* to a ligand with a strong trans effect (such as phosphines).[111-112] A variable temperature (VT) ^{31}P NMR study revealed the two signals (36 ppm and 37 ppm) present at room temperature coalesce at high temperature (330 K) in methanol-d_4, indicating rapid interconversion

of the diastereomers in solution (Figure 3.3). These results were further supported by energy minimized DFT calculations of the two diastereomers.

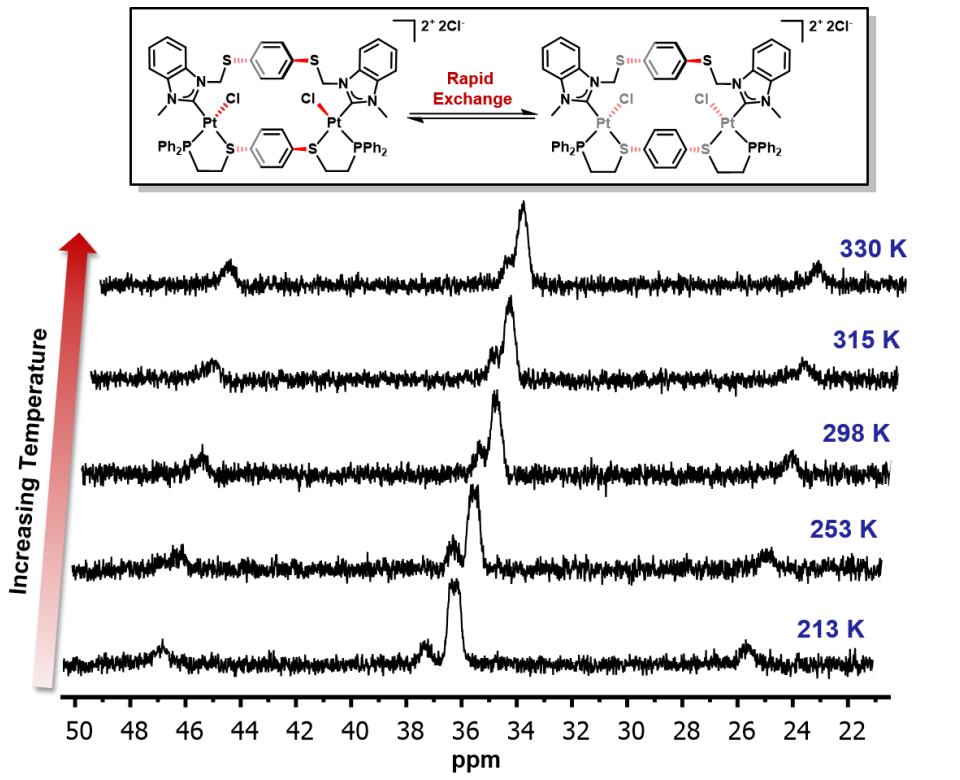

Figure 3.3 ^{31}P NMR spectra of complex **14** in methanol-d_4 from 213 K to 330 K. Coalescence of the major resonance (36 ppm) and the corresponding diastereomer' resonance (37 ppm) is observed at high temperature, consistent with the presence of rapidly interconverting diastereomers.

3.2.2 Formation of a New WLA Intermediate State

Semi-open complex **14** was then reacted with four equivalents of silver tetrafluoroborate ($AgBF_4$) in methanol to abstract the four chlorides (two inner sphere and two outer sphere) and form the fully closed complex with fully chelated ditopic bidentate P,S- and NHC,S-ligands (Scheme 3.2a). Despite being a widely reported method for closing WLA complexes, the reaction did not result in a fully closed complex as evidenced by ^{31}P NMR and MALDI–TOF MS. Instead, the signals in the ^{31}P NMR spectrum indicate a seemingly non-symmetric product, displaying two

distinct ^{31}P resonances of equal intensity: one at 37 ppm and the other at 47 ppm (Figure 3.2a, **15**). The signal at 37 ppm is consistent with previously reported Pt^{II} semi-open complexes bearing NHC,S-ligands,[95] while the resonance downfield at 47 ppm is characteristic of a fully closed complex.[95] Given that the peaks were of approximately equal intensity, we hypothesized that a new WLA structural state was obtained, namely, a macrocycle with one Pt^{II} metal center in a fully closed state and the other in a semi-open state with methanol-d_4 bound to the platinum center rather than the expected thioether moiety ([*cis*–$Pt_2(\kappa^1{:}\mu{:}\kappa^2$–NHC,S)$(\kappa^2{:}\mu{:}\kappa^2$–P,S)$CD_3OD][BF_4]_4$, **15**, Scheme 3.2a). This hypothesis was supported by the observation that the relative intensities of the two peaks did not change when additional $AgBF_4$ was added, indicating that the reaction had gone to completion and that the signal at 37 ppm does not belong to residual starting material. Although single crystals suitable for X-ray diffraction were not obtained, ^{1}H and ^{31}P NMR spectroscopy, MALDI–TOF MS and DFT calculations support the formation of complex **15**. MALDI–TOF MS analysis of complex **15** revealed a peak at 1767.308 *m/z*, which matches the simulated mass of the molecular ion $[M+H]^+$. Additionally, DFT calculations were used to calculate the strength of the Pt^{II}–$OHCH_3$ bond, for comparison to the traditional Pt^{II}–S bond. The Pt^{II}–$OHCH_3$ interaction was calculated to be 30.70 kcal/mol, which is comparable to that of the Pt^{II}–S bond energy in the same compound (42.25, 57.10 and 63.77 kcal/mol), further supporting the formation of **15**.

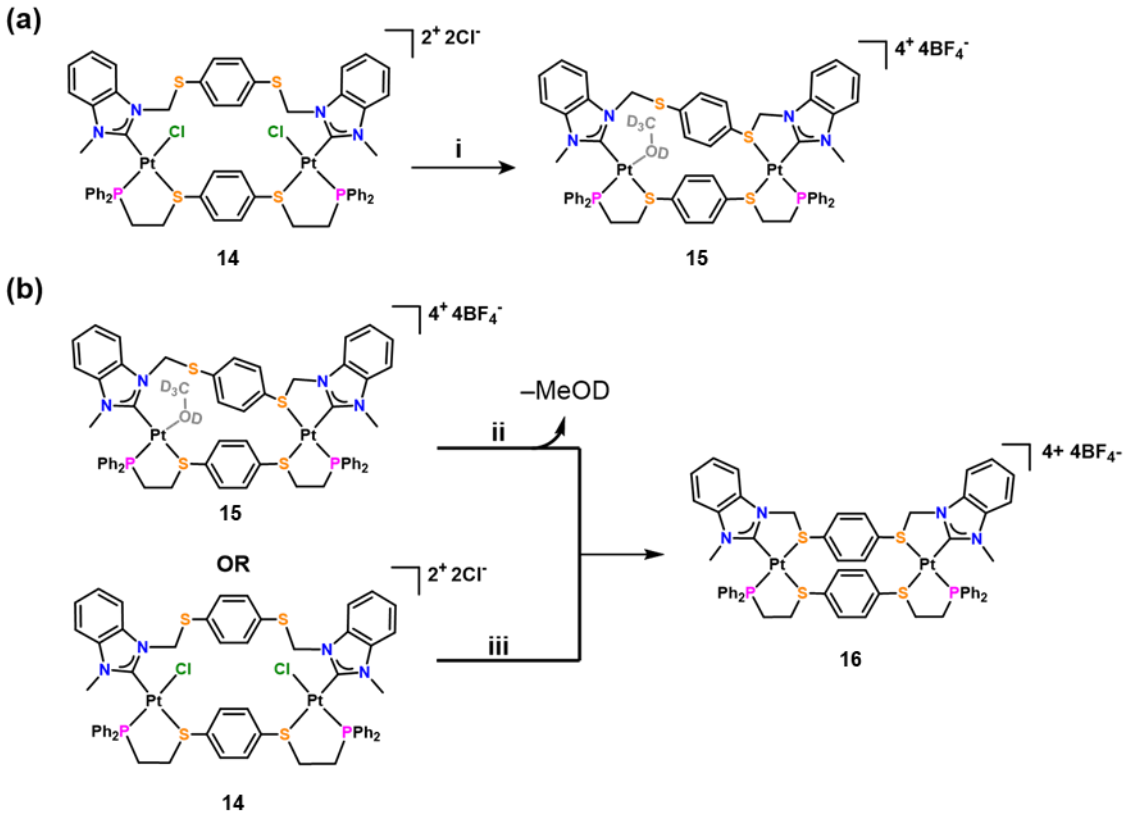

Scheme 3.2 Formation of (a) the New Intermediate WLA Macrocycle State (**15**), and (b) the Fully Closed Macrocycle (**16**). Reaction conditions: (i) 4 equiv. $AgBF_4$, methanol-d_4. (ii) 1. High vacuum to remove methanol-d_4 (MeOD), 2 h; 2. CH_3NO_2-d_3. (iii) 4 equiv. $AgBF_4$, CH_3NO_2-d_3.

3.2.3 Formation of the Fully Closed State

In order to fully close the macrocycle, complex **15** was subjected to high vacuum for two hours to liberate what was hypothesized to be a methanol-d_4 molecule bound to the Pt^{II} metal center and form the κ^2:μ:κ^2–NHC,S and κ^2:μ:κ^2–P,S coordinated complex (Scheme 3.2b). Characterization by ^1H and ^{31}P NMR spectroscopy (Figure 3.2a, **16**), MALDI–TOF MS and DFT calculations confirmed the formation of the fully closed state. Specifically, when the fully dried product was dissolved in a non-coordinating deuterated solvent (nitromethane- d_3) and analyzed by ^{31}P NMR spectroscopy (Figure 3.2a, **16**), two major resonances at 49 ppm ($J_{P\text{-}Pt}$ = 3450 Hz)

and 51 ppm ($J_{P\text{-}Pt}$ = 3450 Hz) were observed with an integral ratio of 2:1. This result is consistent with the formation of the fully closed complex **16** with a 2:1 mixture of diastereomers, as was the case in the semi-open complex. Complex **16** was further investigated by a VT ^{31}P NMR spectroscopy study from room temperature to 338 K, a temperature range in which thioether inversion was previously observed (Figure 2.8).[95, 108]

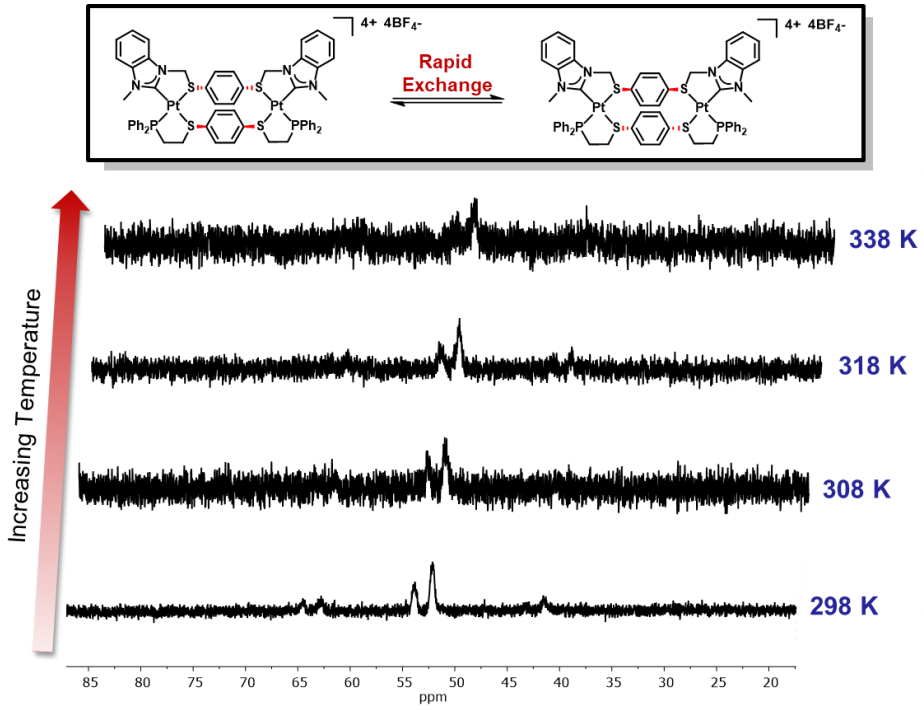

Figure 3.4 ^{31}P NMR spectra of complex **16** in CD_3NO_2 from 253 K to 338 K. Coalescence is observed at high temperature, consistent with the presence of rapidly interconverting diastereomers at elevated temperature.

The coalescence of the two signals at high temperature confirmed that the two peaks stem from the two diastereomers of the fully closed complex **16**. This was further confirmed via VT ^{1}H NMR spectroscopy (Figure 3.5).

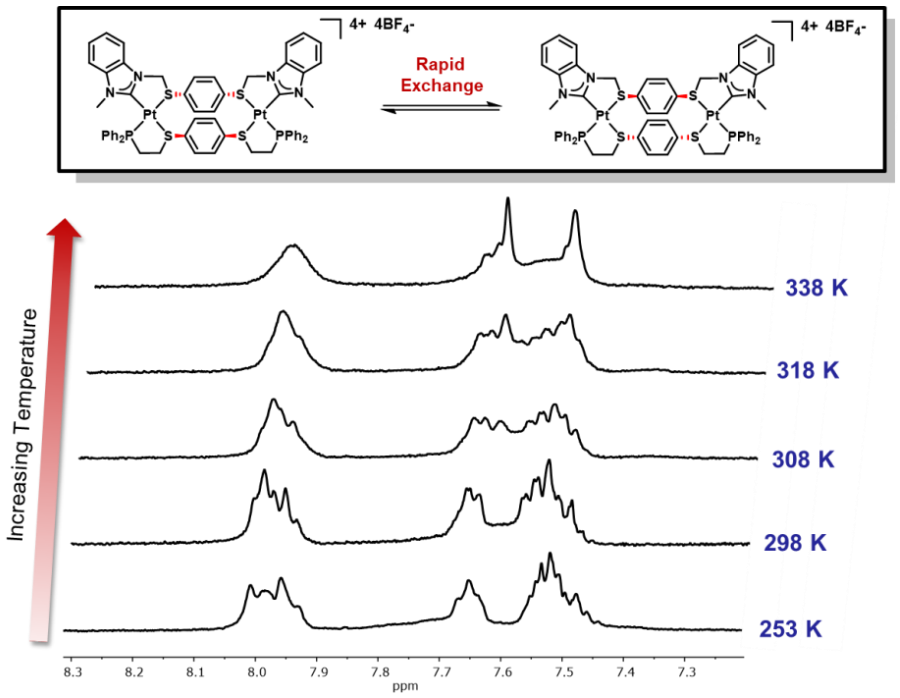

Figure 3.5. ^{1}H NMR spectra of complex **16** in CD_3NO_2 from 253 K to 338 K. Coalescence is observed at high temperature, consistent with the presence of rapidly interconverting diastereomers at elevated temperature.

To further investigate the structures and energies of the two diastereomers, energy minimized models were calculated by DFT and their relative energies were obtained. The energy minimized models suggest that both diastereomers are structurally accessible states and are comparable in their free energies, consistent with the nearly equal proportion observed in the ^{31}P NMR spectrum. The presence of complex **16** was further confirmed by MALDI–TOF MS with a peak at 1647.070 *m/z*, which matches the simulated isotopic distribution of the molecular ion $[M–BF_4]^+$ (Figure 3.2b). Additionally, Complex **16** can also be obtained directly from the semi-open complex **14** via reaction with four equivalents of $AgBF_4$ in the non-coordinating solvent nitromethane (Scheme 3.2b).

3.2.4 Accessing Each of the Reversible States

As previously mentioned, WLA complexes are unique in their ability to be allosterically regulated in a reversible manner. As such, we sought to re-open complex **16** and reform each of the previously accessed states (Scheme 3.3). Complex **15** was readily regenerated from complex **16** by dissolution in methanol. Upon addition of four equivalents of a soluble chloride source, namely bis(triphenylphosphoranylidene)ammonium chloride (PPNCl), complex **15** was converted to semi-open complex **14**. The opening was evidenced by the disappearance of the signal at 47 ppm and the concomitant appearance of signals at 36 ppm and 37 ppm, corresponding to the two diastereomers of complex **14**. Upon dissolving the fully dried complex **14** in CD_2Cl_2, fully-open complex **13a** was regenerated, completing the closing and re-opening cycle. The ^{31}P NMR spectrum of the resulting product shows the disappearance of the resonances at 36 ppm and 37 ppm and the reappearance of the signal at 1.8 ppm ($J_{P-Pt} = 3740$ Hz), consistent with the formation of the *cis* complex **13a**.

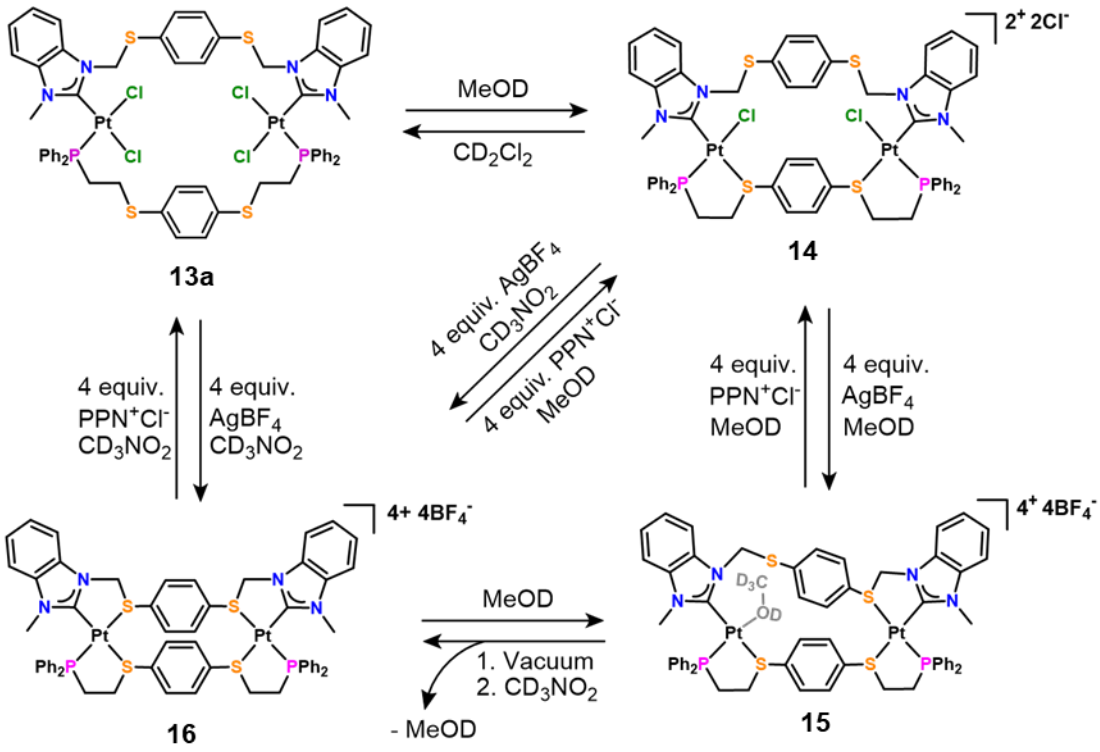

Scheme 3.3 The Reversible Closing and Re-Opening of the WLA Multi-State Macrocycle. MeOD = methanol-*d*4.

3.3 Conclusions

Of the various supramolecular architectures that have been synthesized through coordination-driven supramolecular assembly, the macrocycle continues to be an important architecture due to its defined cavity, making it useful for host-guest chemistry, designed molecular recognition, and catalysis.[72] Additionally, macrocyclic architectures have paved the way for the synthesis of larger, more sophisticated structures with three-dimensional cavities. The addressable construct described here is a potentially useful building block for the construction of higher order, chemically addressable complexes with multi-state switching capabilities. Key to the success of the step-wise formation of heteroligated WLA macrocycles is the kinetic stability of the

complexes where the “weak-link” thioether is a relatively strong donor. The consequence of this strong bonding is illustrated by the formation of semi-open/fully closed complex **15**, in which a methanol molecule occupies one of the empty coordination sites. The methanol molecule displaces a single thioether and alleviates some of the fully closed structure’s strain energy, which has been investigated by DFT calculations. The ring strain present in this system suggests that the WLA may allow us to design systems in which strain can be exploited to enable the use of allosteric effectors that are not anionic. The result is a macrocyclic structure that can adopt new intermediate states previously not observed in traditional WLA systems, making it the first platinum-based system to require multiple cues or stimuli to be switched between states and the only known four-state WLA system.

3.4 Experimental Methods

3.4.1 General Methods and Instrument Details

Commercially available chemicals were purchased as reagent grade from Sigma-Aldrich, Acros, and Alfa Aesar, unless otherwise noted, and used as received. Unless otherwise stated, all solvents were purchased anhydrous and degassed under a stream of argon prior to use. All glassware and magnetic stirring bars were thoroughly dried in an oven (180 °C). Reactions were monitored using thin layer chromatography (TLC), and commercial TLC plates (silica gel 254, Merck Co.) were developed and the spots were visualized under UV light at 254 or 365 nm. Flash chromatography was performed using SiO_2-60 (230–400 mesh ASTM, 0.040–0.063 mm; Fluka). Deuterated solvents were purchased from Cambridge Isotope Laboratories and used as received. ^{1}H, ^{31}P, $^{31}P\{^{1}H\}$ and $^{19}F\{^{1}H\}$ NMR spectra were recorded on a Bruker Avance 400 MHz and chemical shifts (δ) are given in ppm. ^{1}H NMR spectra were referenced internally to residual proton

resonances in the deuterated solvents (dichloromethane-d_2 = δ 5.32; nitromethane-d_3 = δ 4.33; methanol-d_4 = δ 3.31). ^{31}P and ^{31}P{^{1}H} NMR spectra were referenced to an external 85% H_3PO_4 standard (δ 0). High resolution electrospray ionization mass spectrometry (HR–MS) measurements were recorded on an Agilent 6120 LC-TOF instrument in positive ion mode. Electrospray ionization mass spectrometry (ESI–MS) was recorded on a Micromas Quatro II triple quadrapole mass spectrometer. Matrix assisted laser desorption ionization–time of flight mass spectrometry (MALDI–TOF MS) was recorded on a Bruker Autoflex III smartbeam in reflectron and positive ion mode.

3.4.2 Synthesis

3.4.2.1 [cis–Pt$_2$Cl$_2$(κ^1:μ:κ^1–NHC,S)(κ^2:μ:κ^2–P,S)][Cl]$_2$ (14).

Complex mixture **13a-c** (or single crystals of **13a**) was fully dried and then dissolved in CD_3OD. ^{1}H NMR (400 MHz, methanol-d_4): δ 8.25 (s, 4H); 7.78–7.60 (m, 12H); 7.57–7.43 (m, 12H); 7.35–7.30 (m, 4H); 7.28 (s, 4H); 7.27–7.24 (m, 2H); 5.51 (d, J = 14.0 Hz, 2H); 4.40 (d, J = 14.0 Hz, 2H); 4.10 (s, 6H); 3.63–3.52 (m, 4H); 3.28–3.11 (m, 4H). ^{31}P NMR (162 MHz, methanol-d_4): δ 36.83(d, $^{1}J_{P-Pt}$ = 3421 Hz); 36.29. HRMS (ESI+). Calcd for $[M–2Cl]^{2+}$: 729.0677 *m/z*. Found: 729.0680 *m/z*.

3.4.2.2 [cis–Pt$_2$(κ^1:μ:κ^2–NHC,S)(κ^2:μ:κ^2–P,S)CD_3OD][BF_4]$_4$ (15).

Four equivalents of $AgBF_4$ was added to a solution of **14** in methanol. The solution was allowed to stir for 30 min. ^{1}H NMR (400 MHz, methanol-d_4): δ 8.54–7.17 (m, 36H), 6.19–5.94 (br, 2H), 4.08–4.02 (s, 2H), 3.68–3.57 (m, 4H), 3.20–2.94 (br, 4H). ^{31}P NMR (162 MHz, methanol-d_4): δ 37.16 (semi-open); δ 46.95 (fully-closed). MALDI–TOF MS (Matrix: α-cyano-4-hydroxycinnamic acid). Calcd for $[M+H]^+$: 1767.249 *m/z*. Found: 1767.308 *m/z*.

3.4.2.3 [cis–$Pt_2(\kappa^2{:}\mu{:}\kappa^2\text{–NHC,S})(\kappa^2{:}\mu{:}\kappa^2\text{–P,S})][BF_4]_4$ (16).

Complex **15** was subjected to high vacuum for two hours to remove the MeOH molecule hypothesized to be bound to the Pt^{II} metal node. The fully dried powder was then dissolved in deuterated nitromethane (CD_3NO_2). ^{1}H NMR (400 MHz, CD_3NO_2): δ 8.51 (s, 4H), 8.16–7.92 (m, 10H), 7.69 (s, 6H), 7.65–7.43 (m, 16H), 6.32–5.84 (m, 4H), 4.02–3.77 (m, 2H), 3.62 (d, J = 19.7 Hz, 6H), 3.34–3.14 (m, 2H), 2.98–2.70 (m, 4H). ^{31}P NMR (162 MHz, CD_3NO_2): δ 50.93 (d, $^1J_{P–Pt}$ = 3450 Hz; diastereomer); δ 49.21 (d, $^1J_{P–Pt}$ = 3450 Hz);. MALDI–TOF MS (Matrix: 2,5-dihydroxybenzoic acid): Calcd for $[M–BF_4]^+$: 1647.211 *m/z*. Found: 1647.070 *m/z*.

3.4.3 Computational Details

All structures were optimized at the B97D/lanl2dz level of theory. Functional B97D includes dispersion effects albeit empirically. The Lanl2dz basis set was used with a pseudopotential for Pt^{II} and Cl because we can expand their core electrons and include some relativistic affects when studying the platinum bonding. Population analysis was performed within the Natural Bond Orbitals (NBO) formalism. NBO allows for a localized, pairwise, description of the electron density and is more reliable than the Mulliken's default. Interaction energies were calculated with the NBODel (deletion) procedure. This takes the Fock matrix and finds the elements that connect orbitals from one atom to those of another and sets their values to zero (deletion); the resulting matrix is re-diagonalized and the associated energy value increases with respect to the original non-deleted one. The change in energy is ascribed to the interaction energy.

3.4.3.1 Energy Minimized Models of 14, 15 and 16

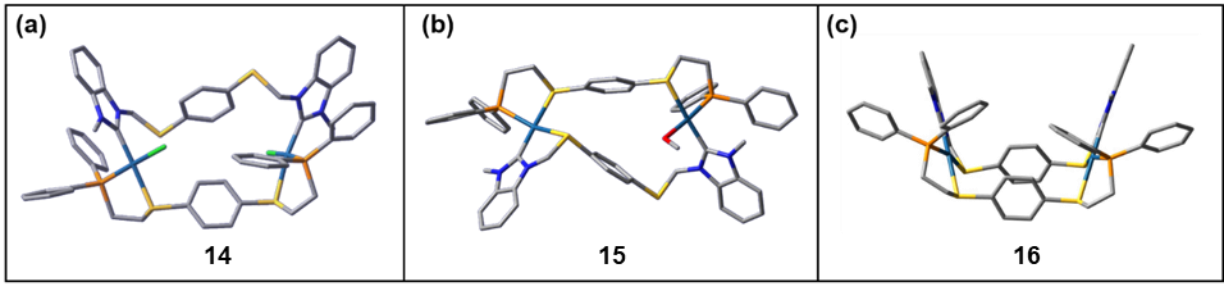

Figure 3.6 Energy minimized DFT models of (a) semi-open complex **14**, (b) semi-open/fully closed complex **15**, and (c) fully closed complex **16**.

Table 3.1 Free Energies (kcal/mol) of **14**, **15** and **16** Obtained from DFT Calculations.

Compound	Free Energy (kcal/mol)
14	-2780.8563
15	-2865.6565
16	-2750.0284

3.4.3.2 Bond Energies Calculated for Complexes 14, 15 and 16

Table 3.2 Selected Bond Energies (kcal/mol) of **14**, **15** and **16** Obtained from DFT Calculations.

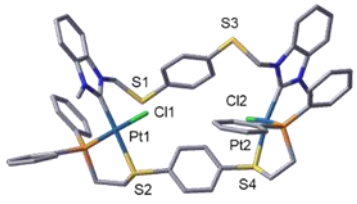

14

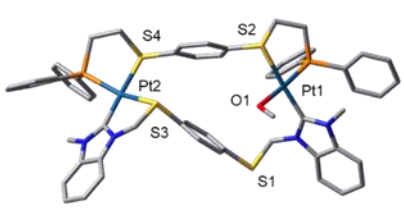

15

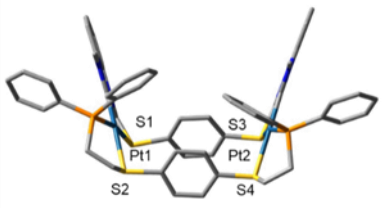

16

Bond	Δ Energy (kcal/mol)	Bond	Δ Energy (kcal/mol)	Bond	Δ Energy (kcal/mol)
Pt1–S2	61.239	Pt1–S2	42.255	Pt1–S1	59.529
Pt1–Cl1	88.486	Pt1–O1	30.704	Pt1–S2	63.514

Pt2–S4	62.264	Pt2–S4	63.771	Pt2–S3	64.226
Pt2–Cl2	92.227	Pt2–S3	57.102	Pt2–S4	58.440

3.4.3.3 Fukui Indices Calculated for Complex 14

Table 3.3 Selected Fukui Indices for complex **14** Obtained from DFT Calculations.[a]

Atom	Fukui Indice
Cl1	**0.54**
Cl2	**0.54**
Pt1	**0.045**
Pt2	**0.051**
S1	**0.13**
S3	**0.14**

[a]Fukui indices indicate the electrophilic and nucleophilic sites. Electrophilic sites are highlighted in blue in Table 3.3, while nucleophilic sites are highlighted in red.

3.4.3.4 Diastereomers of 14 and 16

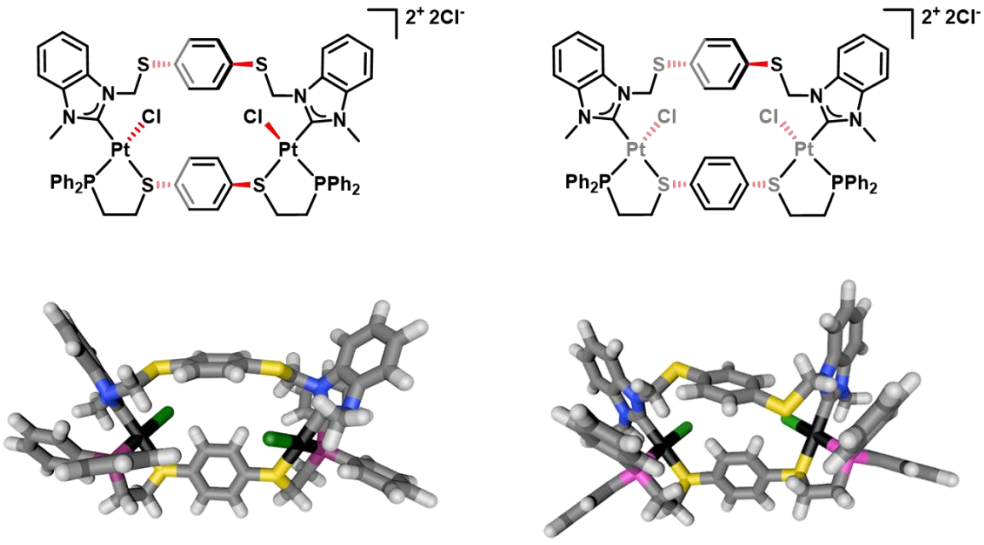

Figure 3.7 ChemDraw structures (top) and corresponding DFT models (bottom) showing the two possible diastereomers of **14**.

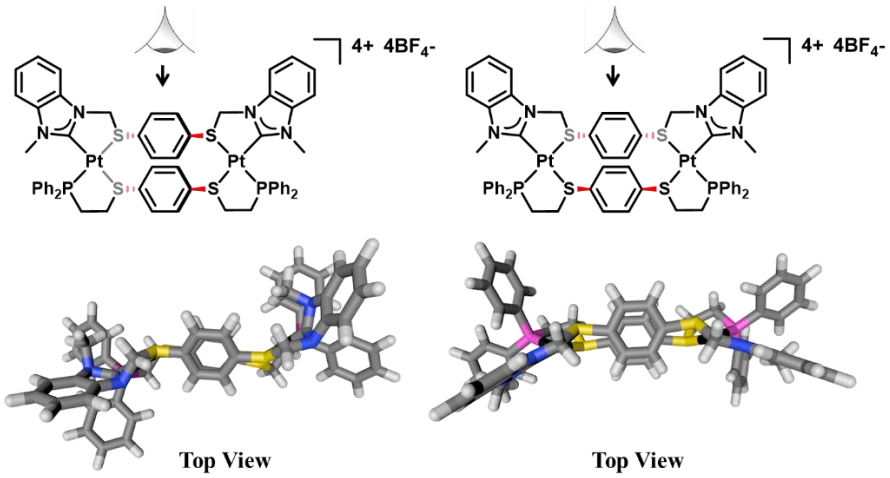

Figure 3.8 ChemDraw structures (top) and corresponding DFT models (bottom) showing top-down views of the two possible diastereomers of **16**.

3.4.4 Reversible Opening and Closing of the WLA Macrocycle

3.4.4.1 General Procedure for Re-Opening 15 to Form Semi-Open Macrocycle 14

Four equivalents of bis(triphenylphosphoranylidene)ammonium chloride (PPNCl) was added to a sample of complex **15** in methanol-*d*$_4$. The complex was characterized by ^{1}H and ^{31}P NMR spectroscopies and HR-MS.

3.4.4.2 General Procedure for Re-Opening 14 to Form Fully Open Macrocycle 13a

Fully dried complex **14** was dissolved in CD_2Cl_2 to form complex **13a**. The complex was characterized by ^{1}H and ^{31}P NMR spectroscopies and HR-MS.

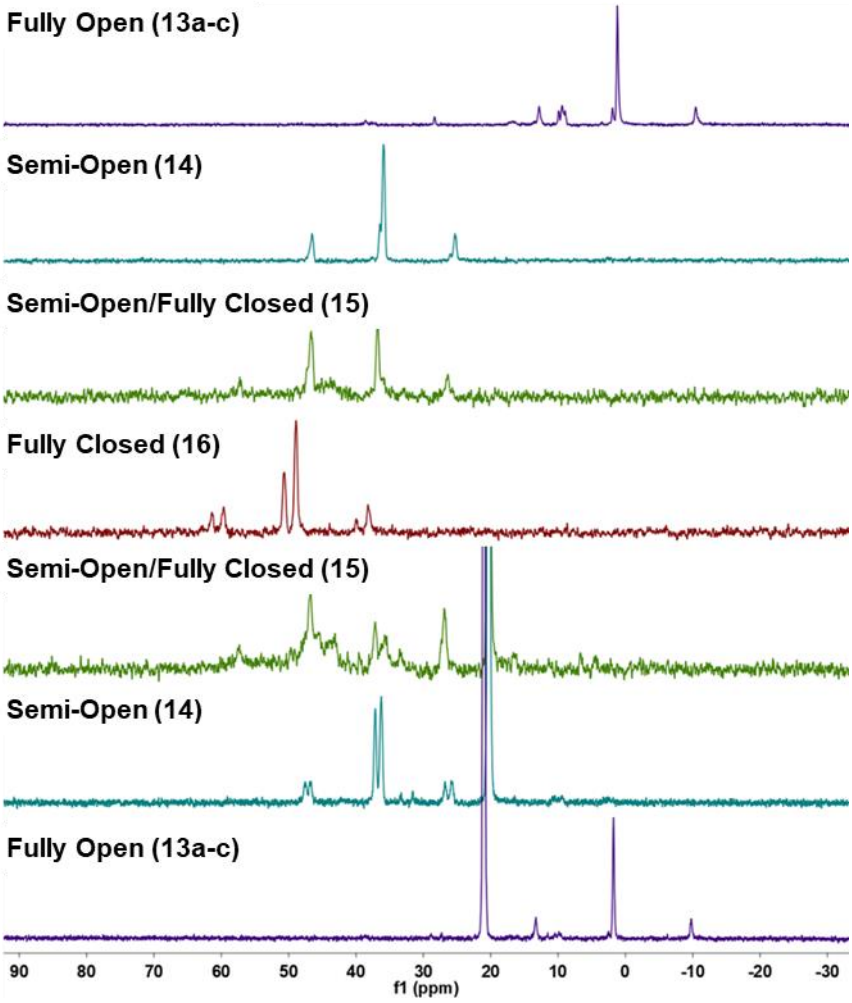

Figure 3.8 ^{31}P NMR spectra of complexes **13a-c**, **14**, and **15** upon reopening and closing.

3.4.5 NMR Spectra of all Compounds and Complexes

^{1}H NMR Spectrum of Semi-Open [*cis*–$Pt_2Cl_2(\kappa^1{:}\mu{:}\kappa^1$–NHC,S)($\kappa^2{:}\mu{:}\kappa^2$–P,S)][Cl]$_2$ (14)

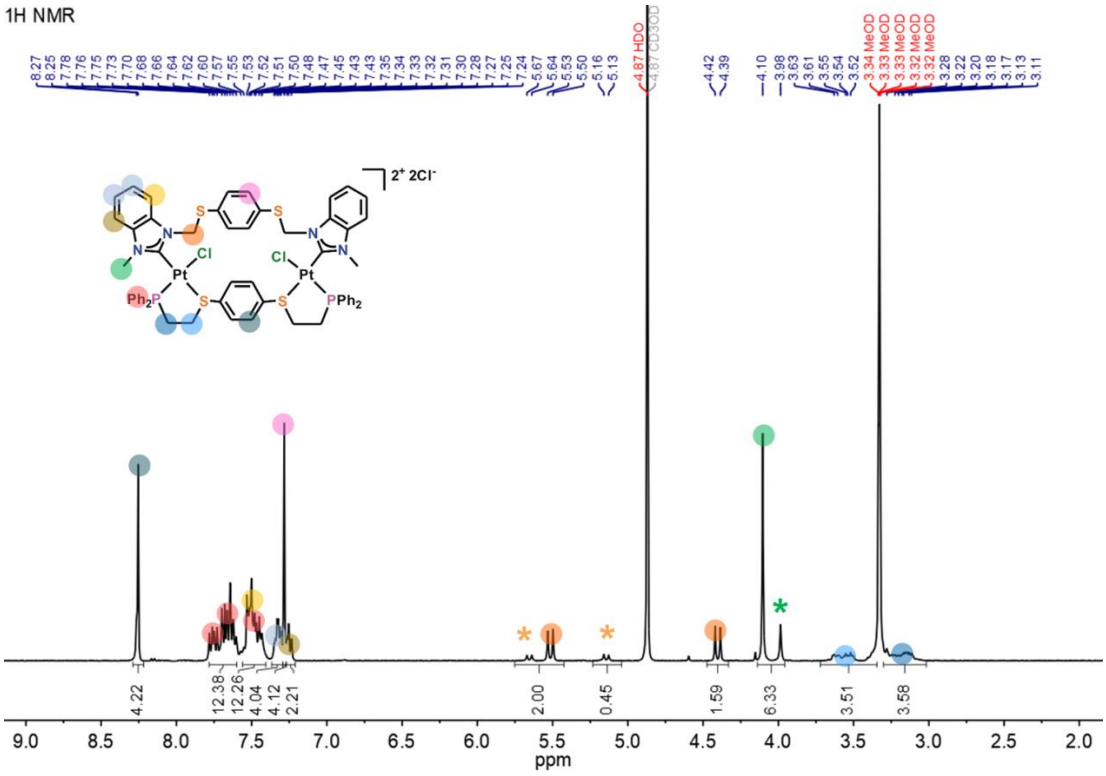

^{31}P NMR Spectrum of Semi-Open [*cis*–$Pt_2Cl_2(\kappa^1{:}\mu{:}\kappa^1$–NHC,S)($\kappa^2{:}\mu{:}\kappa^2$–P,S)][Cl]$_2$ (14)

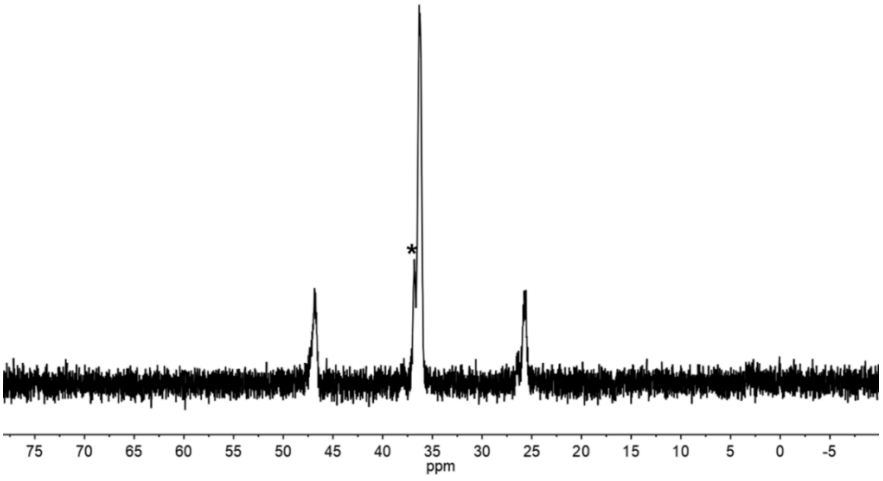

*Diastereomer of **14**.

^{1}H and ^{31}P NMR Spectra of Fully Closed/Semi-Open Complex [*cis*–Pt$_2$(κ^1:μ:κ^2–NHC,S)(κ^2:μ:κ^2–P,S)CD$_3$OD][BF$_4$]$_4$ (15)

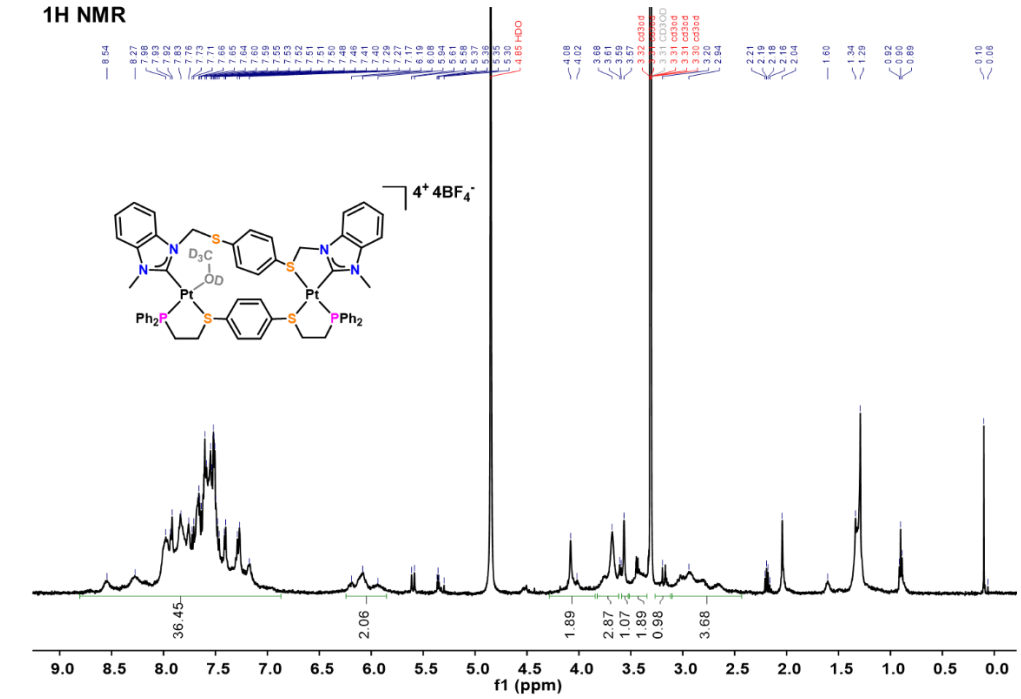

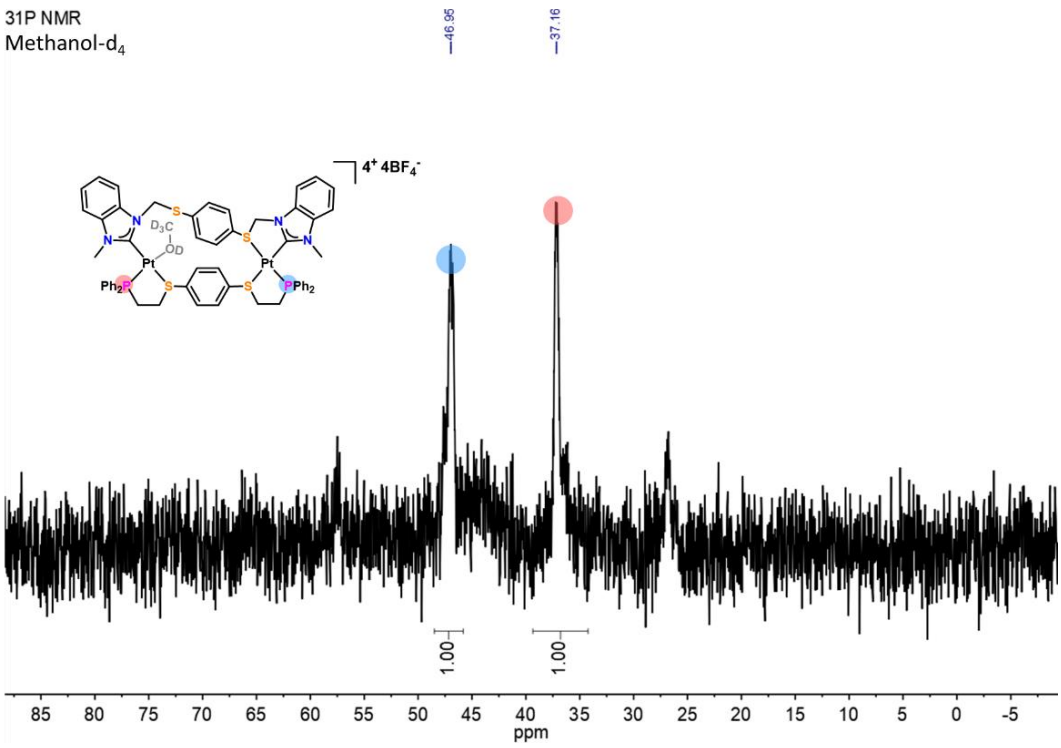

^{1}H and ^{31}P NMR Spectra of Fully Closed Macrocycle [*cis*–Pt$_2$(κ^2:μ:κ^2–NHC,S)(κ^2:μ:κ^2–P,S)][BF$_4$]$_4$ (16)

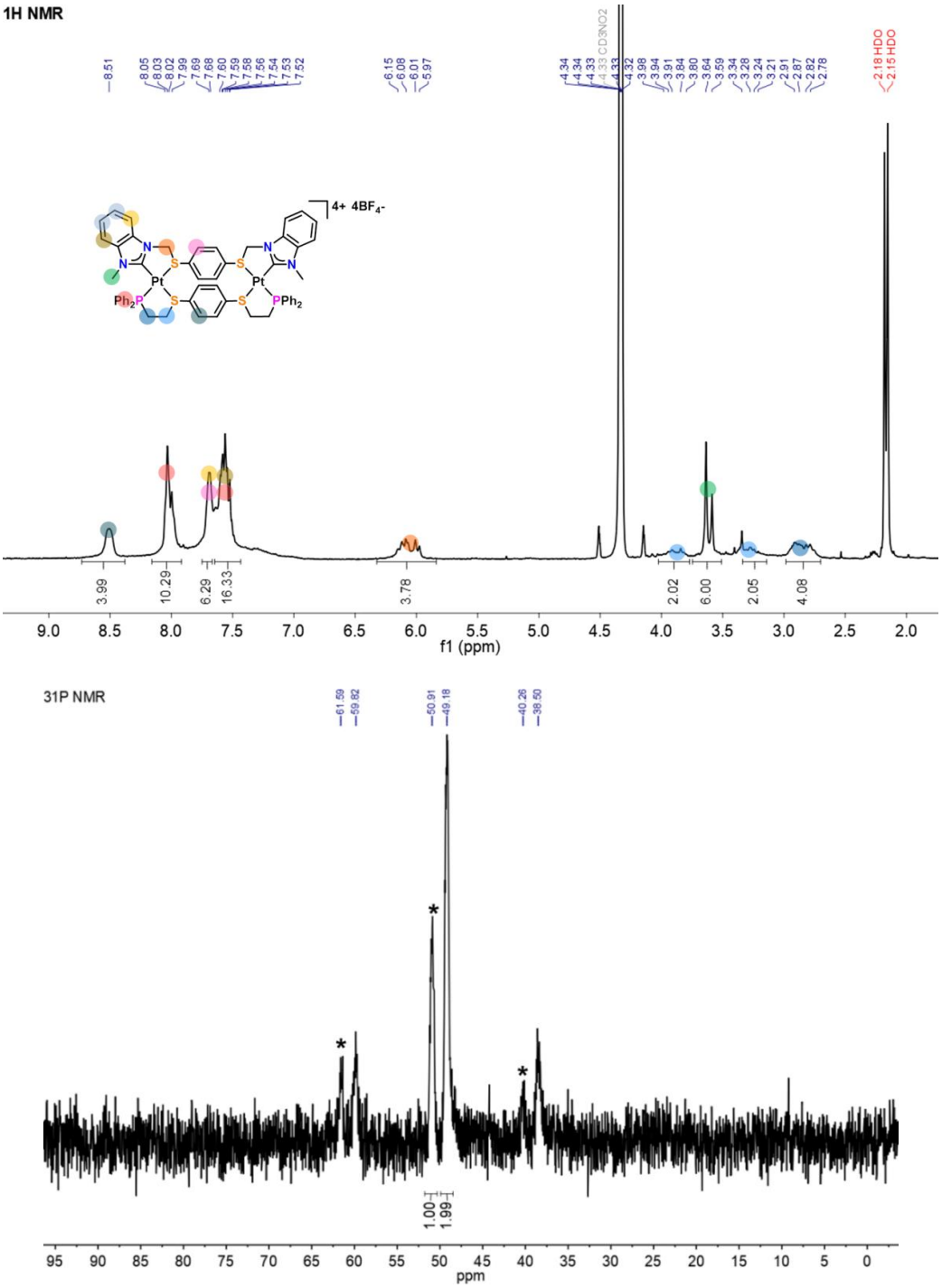

*Diastereomers of **16**.

Re-opening 15 to form [*cis*–Pt$_2$(κ^1:μ:κ^1–NHC,S)(κ^2:μ:κ^2–P,S)][Cl]$_2$ (14)

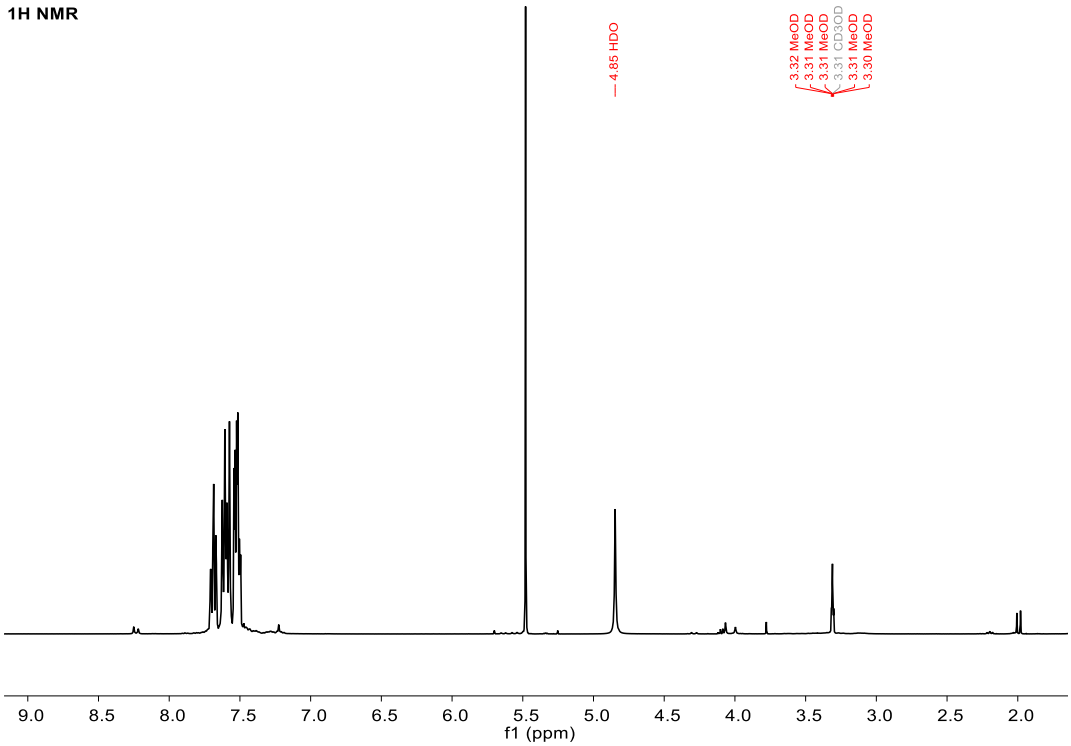

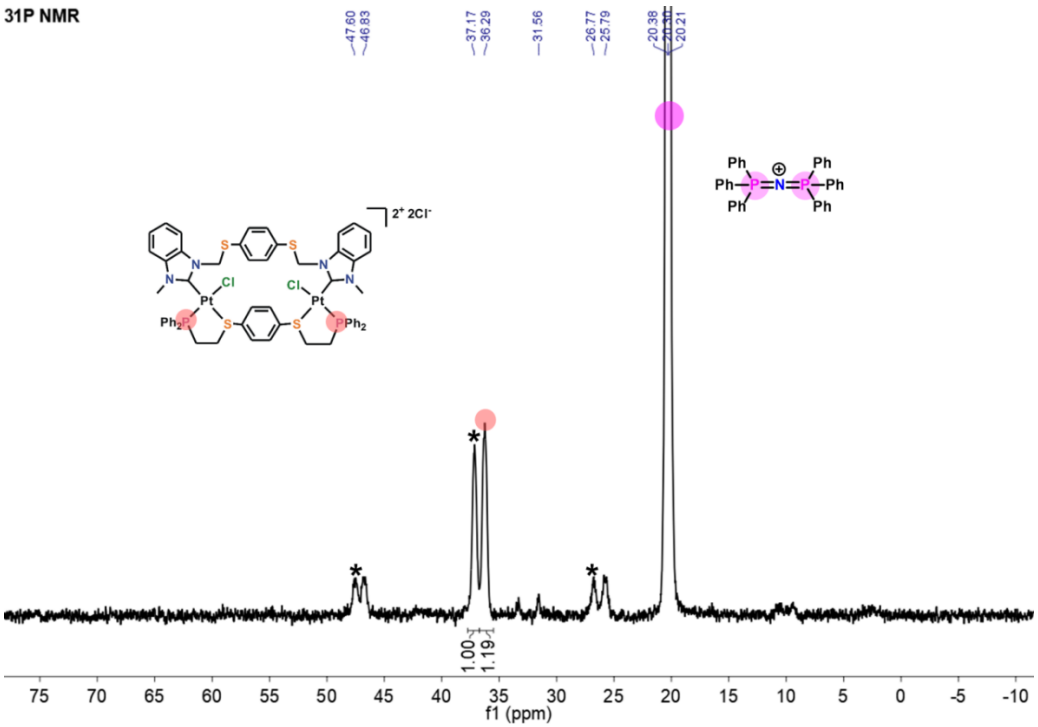

*Diastereomers of **14**.

Re-opening (14) to form [*cis*–Pt_2Cl_4(κ^1:μ:κ^1–NHC,S)(κ^1:μ:κ^1–P,S)] (13a)

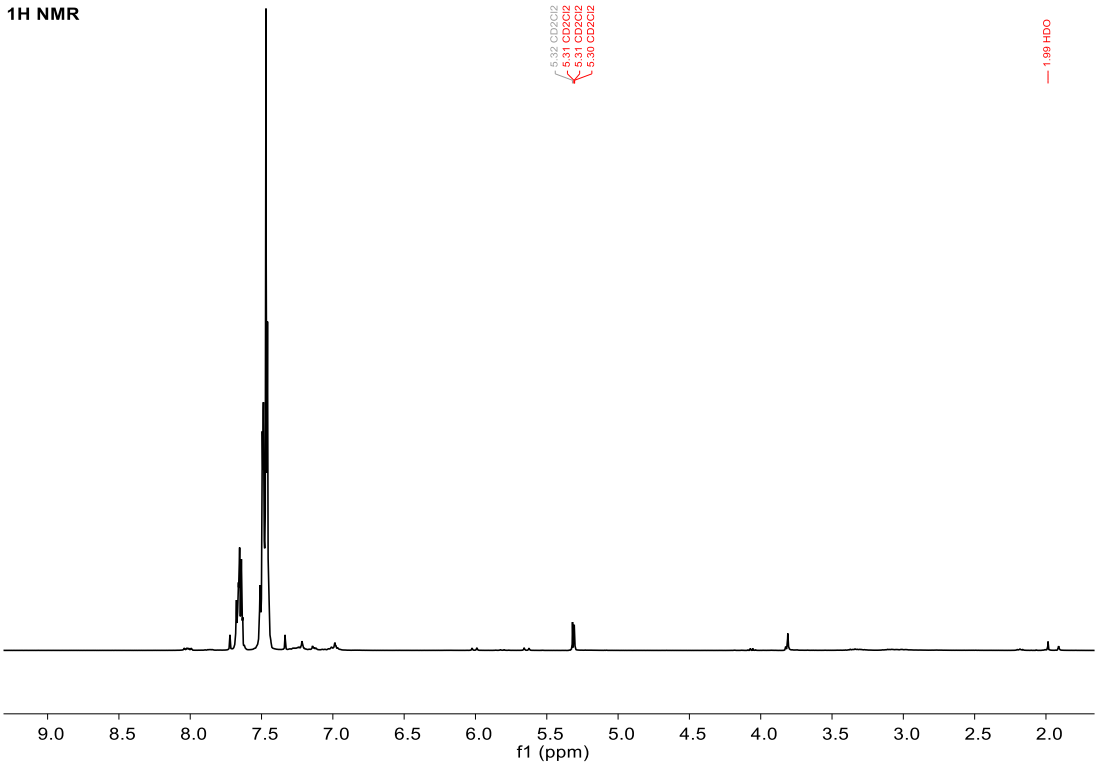

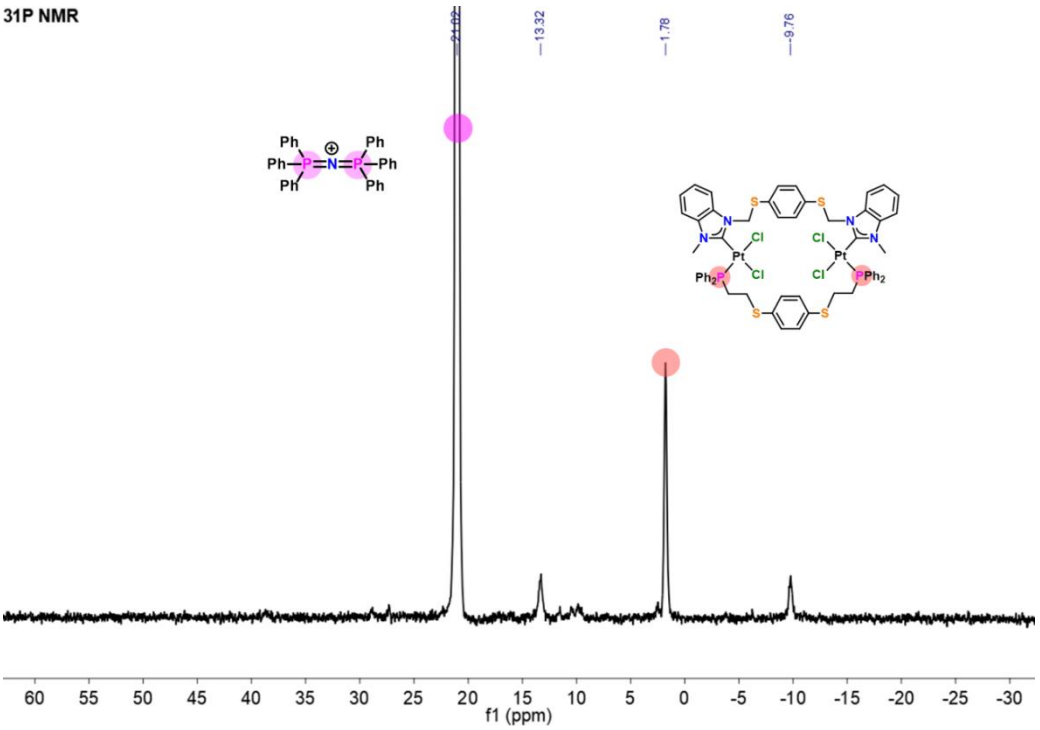

3.4.6 Mass Spectra of all Complexes

HR-MS (ESI+) of Semi-Open Macrocycle [*cis*–$Pt_2Cl_2(\kappa^1{:}\mu{:}\kappa^1$–NHC,S)($\kappa^2{:}\mu{:}\kappa^2$–P,S)][Cl]$_2$ (14)

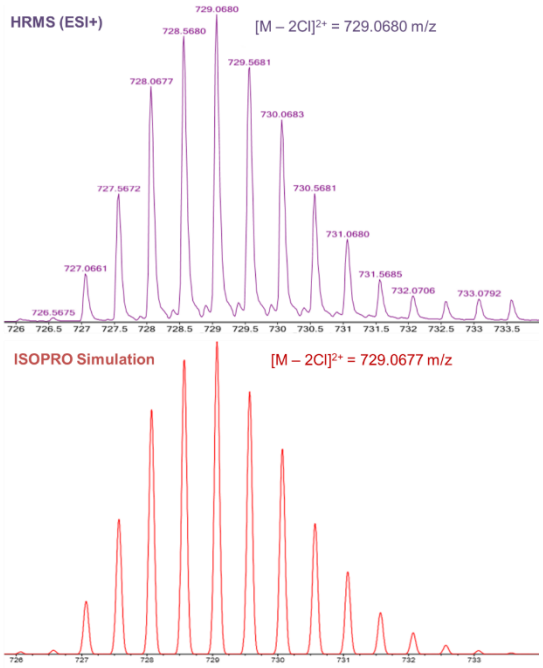

MALDI-TOF MS of Fully Closed/Semi-Open Complex [*cis*–$Pt_2(\kappa^1{:}\mu{:}\kappa^2$–NHC,S)($\kappa^2{:}\mu{:}\kappa^2$–P,S)$CH_3OH$][$BF_4$]$_4$ (15)

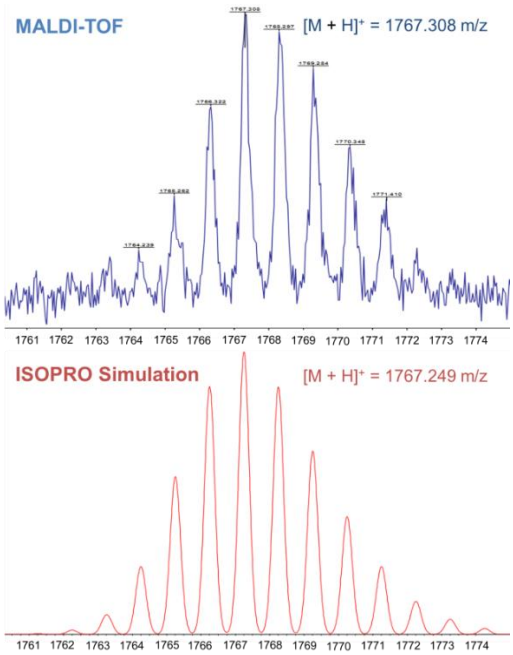

CHAPTER 4

Infinite Coordination Polymer Particles Composed of Stimuli-Responsive Coordination Complex Subunits

The work presented in this chapter is based upon work published in:

d'Aquino, A. I.; Kean, Z. S.; Mirkin, C. A. Infinite Coordination Polymer Particles Composed of Stimuli-Responsive Coordination Complex Subunits. *Chem. Mater*. **2017**, *29*, 10284–10288.

DOI: 10.1021/acs.chemmater.7b03638

4.1 Introduction

Infinite coordination polymer particles (ICPs) are organic-inorganic hybrid materials in which repeating ligand units are connected *via* metal ion nodes into one-, two-, or three-dimensional structures.[113] Interest in ICPs stems from their modularity, ease in which organic components can be interchanged within them, and how changes in molecular structure can result in changes in porosities,[114] as well as catalytic,[115] biological,[116] and spectroscopic properties.[117] While this broad class of materials encompasses polymers with regular repeat units, such as crystalline metal-organic frameworks (MOFs) and other nano or porous coordination polymers (NCPs or PCPs), the scope of ICPs is not limited to crystalline materials. Work by our group,[118-120] and others[121-123] has shown that amorphous ICPs can be formed under the kinetically controlled precipitation of soluble precursors. The ability to assume an amorphous state enables the formation of nano- and micron-sized particles where shape is not dictated by crystal packing forces but instead by the interfacial free energy between the particles and the solvent.[124] Initial work from our group and others,[119, 121] reported the first methods for synthesizing spherical ICP particles. Since this initial work, the library of building blocks and ICP particles accessible through this approach has grown significantly[119, 125-127] and, importantly, these studies have demonstrated that the chemical and physical properties of these materials are highly morphology-dependent.

An attractive feature of ICP particles is their ability to incorporate a wide variety of complex building blocks, including ones that render such structures stimuli-responsive.[128] One class of architectures, yet to be explored in the context of ICP particles are ones made from Weak-Link Approach (WLA) building blocks. WLA complexes are supramolecular coordination compounds that are assembled from transition metal precursors (typically d^8 metal centers) and

hemilabile ligands. They are defined by both open (flexible) and closed (rigid) structural states that may be interconverted through the introduction or removal of chemical effectors (Scheme 4.1A,B).[47] They have shown promise in amplified chemical sensing,[60-62] catalysis,[129] and molecular recognition.[69] Although they have not yet been studied in polymeric systems and ICPs in particular, they could prove to be valuable modalities for modulating both the chemical and physical properties of such structures in a post-synthetic manner, as they provide precise chemical control over molecular geometry, charge and flexibility of the molecular subunits and resulting oligomers. Herein, we report the design and synthesis of a new class of ICP particles consisting of ferric ions and chemically addressable WLA complex building blocks. These structures have been characterized in the presence and absence of an elemental ion effector (Cl^-), which changes the local coordination environment of the metal nodes within the polymer, in addition to the mesoscopic structural fate of the particle.

4.2 Results and Discussion

4.2.1 Synthesis and Characterization

Proof-of-concept WLA-based ICPs were synthesized from monomers composed of: (1) either square-planar Pt^{II} or Pd^{II} metal cores bound to hemilabile phosphino–thioether (P,S) ligands appended with (2) a secondary terpyridine ligand. The terpyridine moieties allow such complexes to be oligomerized and polymerized in the presence of Fe^{II} ions (Scheme 4.1C,D).

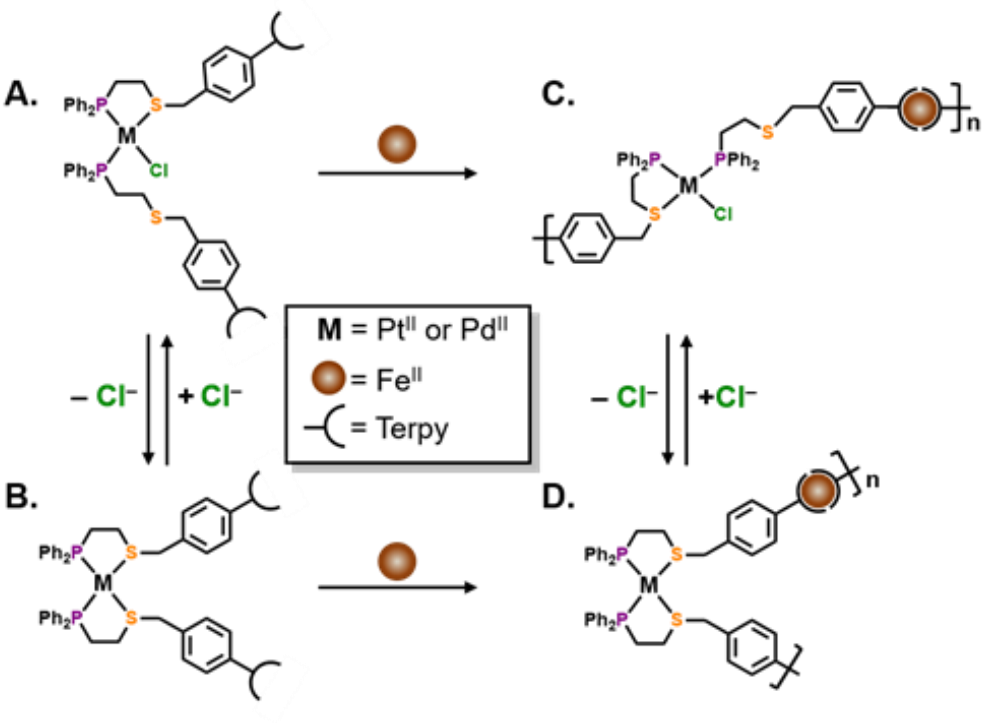

Scheme 4.1 WLA complexes containing hemilabile coordinating motifs can be toggled between open (flexible) (A) and closed (rigid) states (B) (counterions omitted for clarity). Coordination-based assembly of these subunits results in extended structures (C,D).

4.2.2 Synthesis of Monomeric Building Blocks: 18-Pt-Open and 18-Pt-Closed

We first synthesized ligand **17** (Figure 4.1A) according to a modified literature procedure from previously reported compounds (see Supporting Information).[130] We chose the terpyridine moiety for its extremely high affinity ($K_a \sim 10^8$) and selective 2:1 binding with Fe^{II} ions,[131] as well as the previously demonstrated orthogonality of this binding motif with Pt^{II}-WLA systems.[130] Ligand **17** was then reacted with dichloro(1,5-cyclooctadiene) platinum(II) ($Pt(COD)Cl_2$) in dichloromethane (CH_2Cl_2) to yield complex **18-Pt-Open** (Figure 4.1A) in quantitative yield.

The molecular structure of **18-Pt-Open** is both flexible and dynamic, whereby exchange between the thioether group and the chloride (Cl^-) bound to the Pt^{II} center occurs at room

temperature as evidenced by variable temperature ^{31}P nuclear magnetic resonance (NMR) spectroscopy. With complex **18-Pt-Open** in hand, we were able to generate the rigid complex **18-Pt-Closed** (Figure 4.1A) by chloride abstraction with thallium tetrafluoroborate ($TlBF_4$). The structure and geometry of complex **18-Pt-Closed** were confirmed in solution by ^{1}H and ^{31}P NMR spectroscopies and high-resolution electrospray ionization mass spectrometry (HR-ESI-MS), and in the solid-state by single crystal X-ray diffraction (Figure 4.1B).

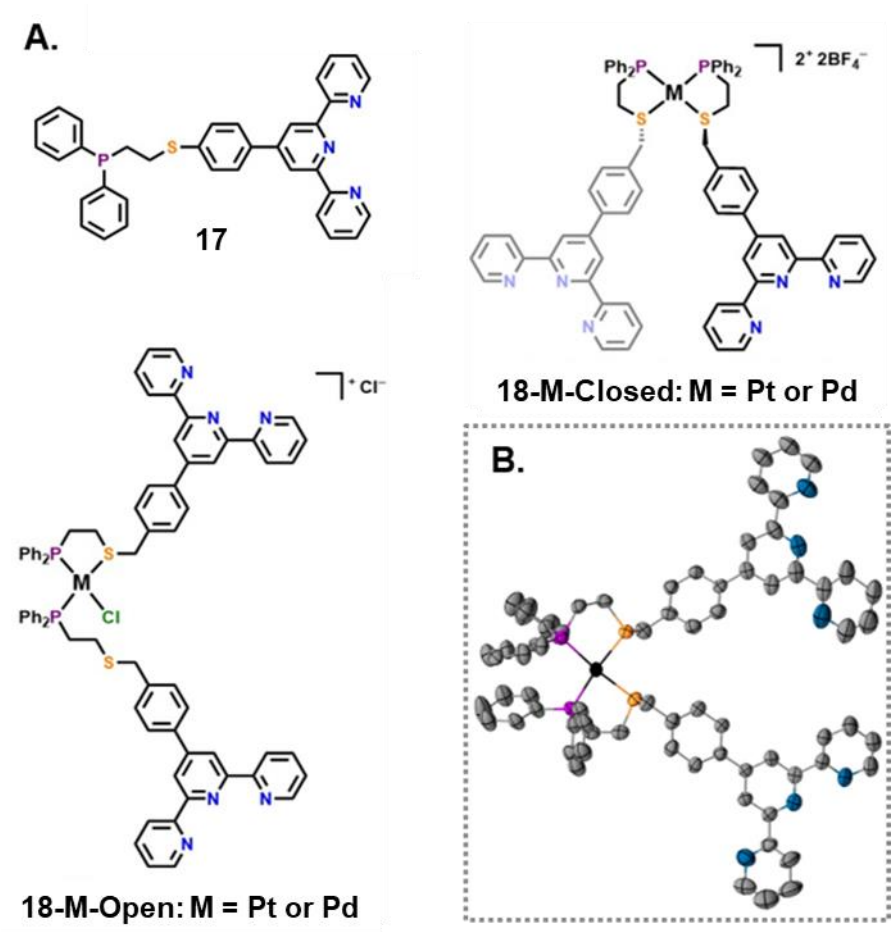

Figure 4.1. (A) Molecular building blocks used in the synthesis of ICP particles bearing WLA subunits. (B) The X-ray crystal structure of complex **18-Pt-Closed**, drawn with 50% thermal ellipsoid probability. Hydrogens, solvent molecules, and anions have been omitted for clarity (black, Pt; orange, sulfur; purple, phosphorous; grey, carbon; blue, nitrogen).

4.2.3 Synthesis of Coordination Polymers: 19-Pt-Open and 19-Pt-Closed

In order to form soluble ICP precursors, both **18-Pt-Open** and **18-Pt-Closed** were dissolved in acetonitrile (CH_3CN) and treated with one equivalent of iron(II) tetrafluoroborate ($Fe(BF_4)_2$) to polymerize the terpyridine groups to form intermediates **19-Pt-Open** and **19-Pt-Closed**, respectively (Figure 4.2), which can be switched between states post polymerization. While the ^{1}H NMR spectrum of **19-Pt-Open** was relatively nondescript, comprised of many broad peaks and consistent with the formation of high molecular weight polymer, the ^{1}H NMR spectrum of **19-Pt-Closed** exhibited well-formed narrow peaks and was more complex, consistent with more rigid and less dynamic species. In order to further characterize these structures, diffusion-ordered spectroscopy (DOSY) experiments were performed. Based on the ^{1}H DOSY experiments, the diffusion coefficient of **19-Pt-Closed** is calculated to be approximately a factor of four greater than the constituent monomer **18-Pt-Closed**, as calculated from the Stokes Einstein equation, indicating the formation of low molecular weight, cyclic, oligomers. This result is consistent with the narrow peaks present in the ^{1}H NMR spectrum of **19-Pt-Closed** and can be attributed to the nearly co-parallel orientation of the terminal terpyridine ligands. This observation is consistent with that of analogous systems,[132-135] and with density functional theory (DFT) calculations performed on the solid-state structure of **19-Pt-Closed** (see Supporting Information, Fig. S6). It is clear that the flexible nature of the monomer **18-Pt-Open** enables the formation of flexible coordination polymer **19-Pt-Open** in solution. The closed monomer (**18-Pt-Closed**), however, results in the formation of rigid cyclic oligomers (**19-Pt-Closed**) owing to the co-parallel orientation of the terminal terpyridines ligands. This co-parallel orientation is a direct result of the nearly 30° angle formed between the Pt^{II} metal node and the thioether moiety on the P/S ligand, in

the closed structure. The results observed for the soluble precursors indicate that molecular geometry strongly affects the nature of the polymeric precursors and, ultimately, particle morphology.

4.2.4 Synthesis of Infinite Coordination Polymer Particles

Next, we synthesized ICP particles by the slow precipitation method.[119, 136] In a typical experiment, a solution of either **19-Pt-Open** or **19-Pt-Closed** was prepared in CH_3CN, and diethyl ether was allowed to slowly diffuse into it over the course of 24 hours. Particle samples were then suspended in an excess of diethyl ether for storage and analysis. All samples were analyzed by scanning transmission electron microscopy (STEM) and energy-dispersive X-ray spectroscopy (EDX), indicating an elemental composition consistent with the proposed structures, while samples that formed stable suspensions were also characterized by dynamic light scattering (DLS). Importantly, the morphology of the final particles formed from **19-Pt-Open** was highly dependent on the concentration of the initial solution in CH_3CN. When particles were grown from an 8 mM solution (with respect to the monomer) of **19-Pt-Open**, the resulting particles were composed of spherical aggregates and particles of various sizes, with most spherical features being smaller than 100 nm; this is consistent with uncontrolled growth and incomplete coalescence and characteristic of conditions where growth occurs too quickly (Figure 4.2A).[119]

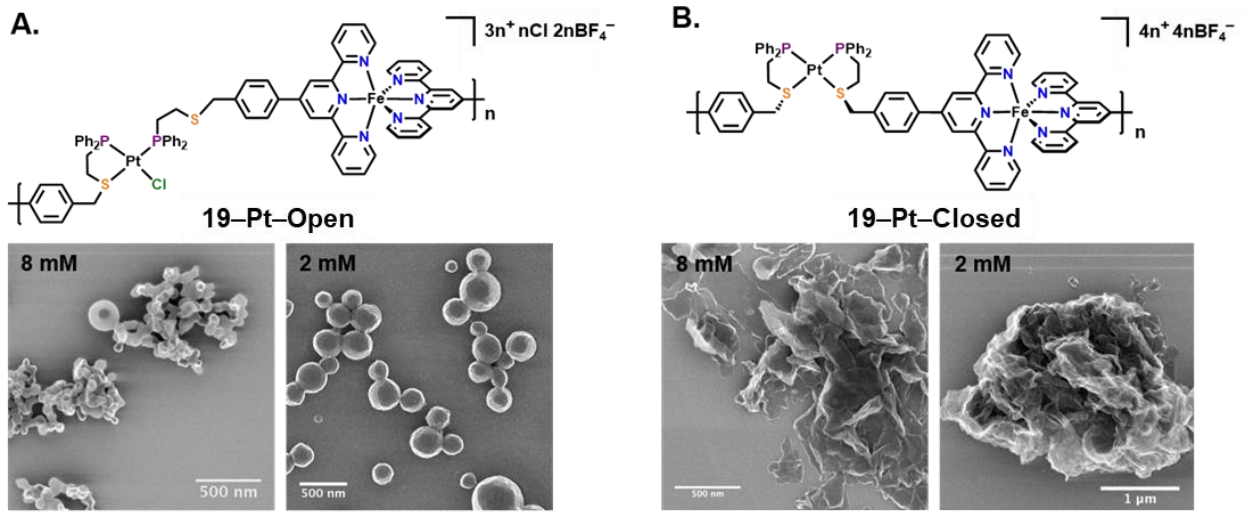

Figure 4.2 (A) Proposed repeat unit, coordination polymer structure (top) and STEM micrographs (bottom) of ICPs bearing open and (B) closed WLA subunits at different concentrations.

Alternatively, when the concentration was lowered to 2 mM, we obtained spherical particles between 200 and 500 nm in size (DLS Z-Average size = 195 nm), that while well formed, appeared to have rough surface features. While **19-Pt-Open** under 8 mM growth conditions was observed to form particles with predominantly spherical features, the oligomeric precursor **19-Pt-Closed** yielded ill-defined aggregates and sheets. Synthesis of particles were also attempted with sub-stoichiometric quantities of chloride, and two kinds of morphologies were observed: aggregates of spherical particles and sheets. When the concentration of the **19-Pt-Closed** was lowered to 2 mM, larger aggregates were formed (Figure 4.2B). While we attempted to further slow the growth process by performing the particle synthesis at ~5 °C, this simply arrested the growth process at stages that resulted in ill-defined aggregates of small spheres.

4.2.5 Synthesis of Pd^{II}-Based Coordination Polymers and Particles

In light of our inability to grow smooth, well-defined ICP particles, we looked toward adjusting the strength of the metal–ligand coordination bonds as a means of facilitating molecular

level rearrangement and more rapid coalescence of the system. Here, we hypothesized that by employing a more labile metal center, smooth spheres would form in order to minimize interfacial energy, as any rough surface topology will increase the overall surface area and thus the interfacial energy. To test this hypothesis, we took advantage of the modular nature of the WLA to assemble a new set of complexes with an isoelectronic and isostructural palladium core. Previous reports indicate that the rate of Pd-P,S-ligand exchange occurs on the timescale of seconds and minutes,[137] much faster than that for Pt-P,S-ligand exchange under identical conditions. Therefore, we utilized modified procedures to synthesize a new set of monomers, **18-Pd-Open** (Figure 4.3A) and **18-Pd-Closed**, which are qualitatively identical to the Pt derivatives, as evidenced by ^{1}H NMR spectroscopy, ^{1}H DOSY, ESI mass spectrometry, and single crystal X-ray diffraction studies. Importantly, coordination polymers **19-Pd-Open** and **19-Pd-Closed** can be synthesized and interconverted post-polymerization, which was confirmed by ^{1}H and ^{31}P NMR spectroscopy and DOSY experiments.

ICP formation was attempted, again by slow diffusion of diethyl ether into acetonitrile solutions of **19-Pd-Open** or **19-Pd-Closed** (2 and 8 mM). Intriguingly, while there were some variations in size and polydispersity, all samples led to the formation of well-formed spherical particles with smooth surface topologies (Figure 4.3). The variation in size between **19-Pd-Open** and **19-Pd-Closed**, is likely due to the difference in length between the monomers that comprise the two polymeric states. The open states, regardless of metal, are extended and more flexible than the closed states.

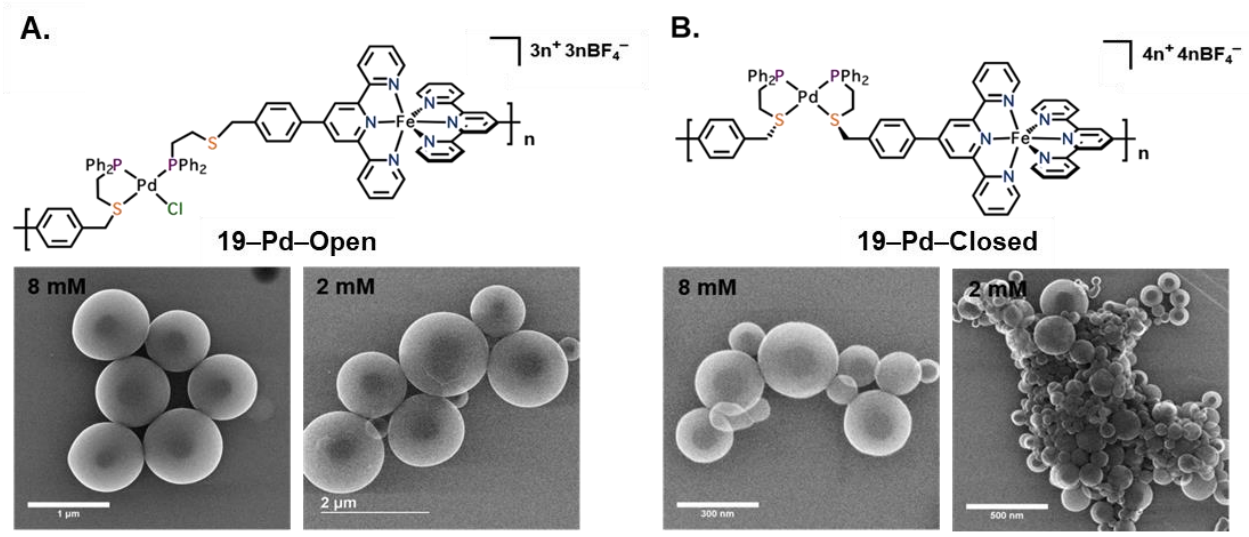

Figure 4.3 (A) Proposed repeat unit structure (top) and STEM micrographs (bottom) of ICPs bearing open and (B) closed palladium WLA subunits.

This observation not only supports our hypothesis that the formation of smooth spheres will result from employing a more labile metal center, but also rules out the potential effect of charge and counterions on the particle morphology. For example, between the open and closed systems the charge changes from 1^+ to 2^+, as do the counterions (Cl^- to BF_4^-), however this in itself has no bearing on the final morphology given that both **19-Pd-Open** or **19-Pd-Closed** form particles of the same morphology. It is important to note that the formation process, which initially involves nucleation, followed by oligomerization, aggregation, fusion and growth,[113] influences the polydispersity observed in the ICP particles. During the slow diffusion of the initiation solvent (diethyl ether), the concentration of the ligand and metal ion precursors decrease over time, resulting in a decrease in the nucleation of new particles.[113] Although physical parameters, such as concentration and temperature, were used to control the rate at which nucleation and particle

formation occur, achieving monodisperse particles remains a challenge for these amorphous materials.

4.3 Conclusions

In conclusion, when taken together, these results indicate that the ability of the system to rearrange on the molecular level dictates its ability to form fully coalesced smooth ICP particles. This study also suggests that one can use switchable molecular motifs embedded within ICPs to control morphology and that metal-heteroatom bond strength (Pt-P,S vs Pd-P,S) is an important consideration and point of tunability. Indeed, if the interactions are too weak, as in the case of the Pd system, very little differentiation at the mesoscopic particle level is observed, under all conditions tested. These observations open the door to making well defined ICP particles with stimuli responsive units embedded within and for controlling particle morphology by altering the lability of coordination bonds in particles formed under kinetic control. Such structures may lead to new motifs that could become important in the area of chemical sensing where molecularly triggered events can lead to changes in macroscopic properties that affect signaling.

4.4 Experimental Methods

4.4.1 General Methods

All chemicals were purchased from Sigma-Aldrich and used without further purification, unless otherwise stated. (2-chloroethyl)diphenylphosphine[138] and 4'-[4-(mercaptomethyl)phenyl]-2,2':6',2''-terpyridine[139] were synthesized according to literature procedures. Solvents were purchased anhydrous and degassed under a stream of argon prior to use. Flash chromatography was performed using SiliaFlash F60 SiO_2 (230–400 mesh ASTM, 0.040–0.063 mm; SiliCycle). Deuterated solvents were purchased from Cambridge Isotope Laboratories and used as received.

^{1}H and $^{31}P\{^{1}H\}$ NMR spectra were recorded on a Bruker Avance 400 MHz. ^{1}H NMR spectra were referenced to residual proton resonances (CD_2Cl_2 = δ 5.32; CD_3CN = δ 1.94) in the deuterated solvents. ^{13}C NMR spectra were referenced to the solvent peak (CD_2Cl_2 = δ 53.84; CD_3CN = δ 1.32 and 118.26) $^{31}P\{^{1}H\}$ NMR spectra were referenced to an 85% H_3PO_4 aqueous solution. All chemical shifts are reported in ppm. High resolution mass spectra measurements (HR-MS) were recorded on an Agilent 6120 LC-TOF instrument in positive ion mode. Transmission electron microscopy (TEM) imaging and energy dispersive X-ray data were performed and collected on a Hitachi HD-2300 STEM microscope operating at 200 kV, equipped with two Thermo Scientific Energy Dispersive X-ray (EDX) detectors. TEM samples were prepared by drop-casting a 5 μL Et2O solution of particles onto a carbon-coated Cu TEM grid (Ted Pella). Single crystals suitable for X-ray diffraction studies were mounted using oil (Infineum V8512) on a glass fiber. All measurements were made on a CCD area detector with graphite monochromated Mo Kα or Cu Kα radiation. Data were collected using Bruker APEXII detector and processed using APEX2 from Bruker. Dynamic light scattering (DLS) data were collected using a Zetasizer Nano ZS (Malvern Instruments Ltd). All XRD structures were solved by direct methods and expanded using Fourier techniques. The non-hydrogen atoms were refined anisotropically. Hydrogen atoms were included in idealized positions, but not refined. Their positions were constrained relative to their parent atom.

4.4.2 Synthesis

4.4.2.1 Synthesis of 4'-[4-(mercaptomethyl)phenyl]-2,2':6',2''-terpyridine

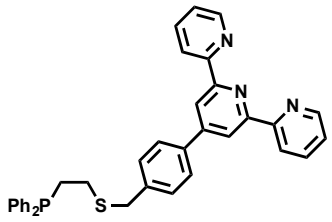

17

4'-[4-(mercaptomethyl)phenyl]-2,2':6',2''-terpyridine was prepared according to literature procedures.[2a,b] In a glove box: 4'-[4-(mercaptomethyl)phenyl]-2,2':6',2''-terpyridine (475 mg, 1.34 mmol) was transferred to a 6 mL vial with stir bar and dissolved in 7 mL CH_3CN. Potassium *tert*-butoxide (150 mg, 1.34 mmol) in 2 mL THF was added slowly while stirring rapidly to produce a light yellow suspension. (2-chloroethyl)diphenylphosphine (367 mg, 1.47 mmol) was then added as a solid and the vial was sealed, removed from the glovebox, and allowed to stir at 70 °C overnight. The solution was cooled, then passed through a short plug of neutral alumina, which was washed with an additional 50 mL of CH_2Cl_2. The solvent was removed under reduced pressure and the residue was recrystallized from CH_2Cl_2/EtOH to give **17** as fine white needles (530 mg) in 70 % yield.

^{1}H NMR (400 MHz, CD_2Cl_2): δ = 8.76 (s, 2H), 8.73 (m, 2H), 8.70 (m, 2H), 7.91 (td, *J* = 7.7, 1.8 Hz, 2H), 7.79 (d, *J* = 8.2 Hz, 2H), 7.38 (m, 8H), 7.33 (m, 6H), 3.79 (s, 2H), 2.52 (m, 2H), 2.31 (m, 2H). ^{13}C{^{1}H} NMR (101 MHz, CD_2Cl_2): δ = 156.51, 156.41, 150.11, 149.58, 140.10, 138.51 (d, J_{C-P} = 13.9 Hz), 137.54, 137.23, 133.05 (d, J_{C-P} = 18.8 Hz), 129.89, 129.12, 128.90 (d, J_{C-P} = 6.6 Hz), 127.69, 124.29, 121.48, 118.97, 36.22, 28.86 (d, J_{C-P} = 15.1 Hz), 28.08 (d, J_{C-P} = 21.6 Hz).

$^{31}P\{^{1}H\}$ NMR (162 MHz, CD_2Cl_2): δ = -17.05. ESI-HRMS (m/z): Calcd: 568.1971 [M+H]+. Found: 568.1982.

4.4.2.2 Synthesis of 18-Pt-Open

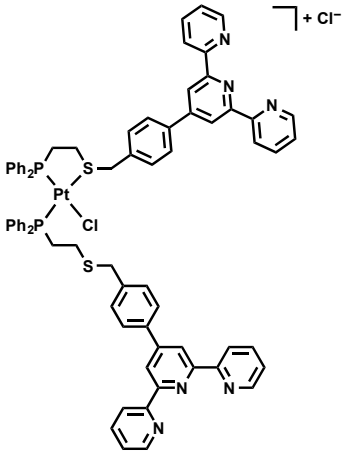

18-Pt-Open

Dichloro(1,5-cyclooctadiene)platinum(II) ($Pt(COD)Cl_2$, 65.8 mg, 0.176 mmol) was weighed into a 6 mL vial with a stir bar and 2 mL of CH_2Cl_2 was added. A solution of **17** (200 mg, 0.352 mmol) in 2 mL CH_2Cl_2 was prepared and added dropwise to the mixture containing $Pt(COD)Cl_2$ while stirring. After 10 min, the homogenous clear solution was evaporated under reduced pressure to a minimal volume and Et_2O was added to precipitate a white solid. The solid was collected by centrifugation, redissolved in CH_2Cl_2, and precipitated into Et_2O to yield **18-Pt-Open** as a microcrystalline white solid in quantitative yield.

^{1}H NMR (400 MHz, CD_2Cl_2): δ = 8.72 (s, 4H), 8.71 (m, 4H), 8.68 (m, 4H), 7.90 (td, J = 7.7, 1.8 Hz, 4H), 7.69 (d, J = 8.2 Hz, 4H), 7.62 (d, J = 7.8 Hz, 4H), 7.51 (t, J = 7.3 Hz, 4H), 7.39–7.21 (m, 20H), 4.42 (br s, 4H), 2.74 (br m, 8H). $^{31}P\{^{1}H\}$ NMR (162 MHz, T = 193 K, CD_2Cl_2): δ = 42.66

($J_{P–Pt}$ = 3595 Hz), 6.98 ($J_{P–Pt}$ = 3105 Hz). ESI-HRMS (m/z): Calcd: 1365.3132 [M–Cl]+. Found: 1365.3129

4.4.2.3 Synthesis of 18-Pt-Closed

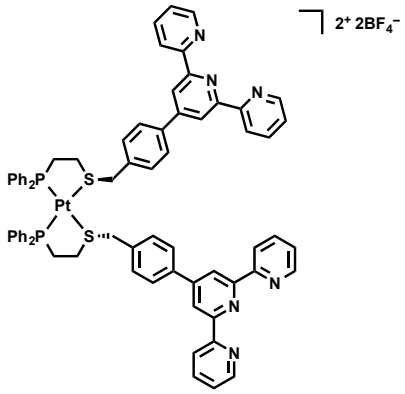

18-Pt-Closed

Thallium tetrafluoroborate ($TlBF_4$, 23 mg, 0.079 mmol) was weighed into a 2 mL vial equipped with a stir bar and 1 mL of CH_3CN was added. With stirring, **17** (54 mg, 0.039 mmol) was added as a solution in CH_2Cl_2 (4 mL) and allowed to react for 30 min. The white suspension was then filtered through celite and washed with an excess of CH_2Cl_2 to give a translucent light yellow solution. The solution was evaporated under reduced pressure and redissolved in 3 mL of CH_2Cl_2 to give a slightly cloudy suspension that was filtered through a 0.2 μm PTFE filter. The resulting solution was then evaporated under reduced pressure to give **18-Pt-Closed** (57 mg) as a yellow microcrystalline solid in 98 % yield.

^{1}H NMR (400 MHz, CD_3CN): δ = 8.60 (m, 4H), 8.57 (s, 4H), 8.54 (dt, J = 7.9, 1.1, 4H), 7.90 (d, J = 8.0 Hz, 4H), 7.88 (td, J = 7.9, 1.8 Hz, 4H), 7.66 (d, J = 8.3 Hz, 4H), 7.60–7.10 (br, 20H) 7.36

(ddd, J = 7.5, 4.8, 1.2 Hz, 4H), 4.68 (br s, 4H), 2.98 (br m, 8H). $^{31}P\{^{1}H\}$ NMR (162 MHz, CD_3CN): δ = 46.91 ($J_{P–Pt}$ = 3032 Hz). ESI-HRMS (m/z): Calcd: 1417.3473 [M–BF_4]+. Found: 1417.3505.

4.4.2.4 Synthesis of 18-Pd-Closed

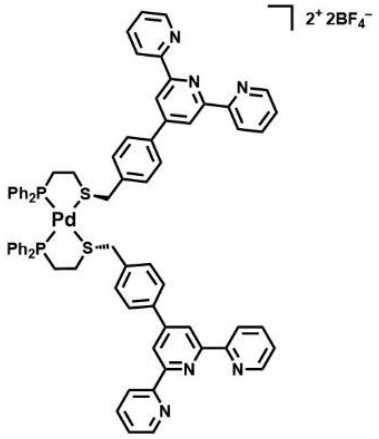

18-Pd-Closed

In the glovebox, tetrakis(acetonitrile)palladium(II) tetrafluoroborate ($Pd(MeCN)_4(BF_4)_2$, 39.2 mg, 0.088 mmol) was weighed into a 6 mL vial with a stir bar and 2 mL of CH_2Cl_2 was added. A solution of **17** (100 mg, 0.176 mmol) in 2 mL CH_2Cl_2 was prepared and added dropwise to the mixture containing $Pd(MeCN)_4(BF_4)_2$ while stirring. After 10 min, the homogenous clear, yellow solution was evaporated under reduced pressure to a minimal volume and Et_2O was added to precipitate a yellow solid. The solid was collected by centrifugation, redissolved in CH_2Cl_2, and precipitated into Et_2O to yield **18-Pd-Closed** (133 mg) as a microcrystalline yellow solid in quantitative yield.

^{1}H NMR (400 MHz, CD_2Cl_2): δ = 8.60 (m, 2H), 8.59 (m, 2H), 8.58 (s, 4H), 8.56 (d, J = 1.14, 2H), 8.54 (d, J = 1.07, 2H), 7.86 (s, 2H), 7.84 (s, 2H), 7.79 (td, J = 7.78, 1.4, 4H), 7.55 (m, 9H), 7.47

(br m, 15H), 7.25 (ddd, J = 7.45, 4.72, 1.20, 4H), 4.54 (s, 4H), 3.37 (dq, J = 10.41, 6.33, 5.85, 4H). $^{31}P\{^{1}H\}$ NMR (162 MHz, CD_2Cl_2): δ = 61.58. ESI-HRMS (m/z): Calcd: 1327.2890 $[M–BF_4]+$. Found: 1327.2875

4.4.2.5 Synthesis of 18-Pd-Open

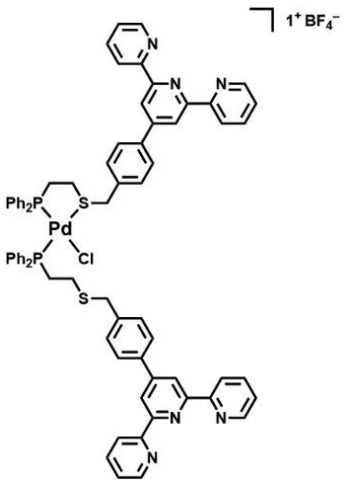

18-Pd-Open

18-Pd-Open was synthesized via two different procedures:

Chloride salt method: In a dry 6 mL vial equipped with a stir bar, **18-Pd-Closed** was dissolved in ~2 mL of CH_2Cl_2 and allowed to dissolve. In a separate vial, a solution of tetrabutylammonium chloride (8 mg, 0.029 mmol) was prepared in CH_2Cl_2 and added to the solution of **18-Pd-Closed** and allowed to react for 30 min. The resulting homogeneous, clear, yellow solution was then evaporated under reduced pressure to give **18-Pd-Open** as a yellow microcrystalline solid in quantitative yield.

Chloride resin method: **18-Pd-Closed** was measured into a falcon tube (12 mg, 0.008 mmol) and dissolved in 2 mL of CH_3CN. In a separate falcon tube, 312 mg of Dowex 1x4 chloride resin (100-200 mesh) was measured out and mixed with 3 mL of CH_3CN. The solution containing **18-Pd-**

Closed was slowly transferred (via pipette) to the flacon tube containing the Dowex chloride resin. Once completely transferred, the solution was mixed continuously for 30 min. After 30 min, solution was filtered and the resin washed with 1 mL portions of CH_3CN. The resulting homogeneous, clear, yellow solution was then evaporated under reduced pressure to give **18-Pd-Open** as a yellow microcrystalline solid in 88% yield.

^1H NMR (400 MHz, CD_3CN): δ = 8.67 (m, 13H), 7.89 (td, J = 7.76, 1.82, 4H), 7.67 (d, J = 7.99, 4H), 7.54 (m, 8H), 7.36 (m, 12H), 7.19 (dd, J = 12.40, 7.73, 8H), 4.23 (s, 4H), 3.14 (m, 9 H), 2.74 (m, 4H), 2.56 (m, 4H). $^{31}P\{^1H\}$ NMR (162 MHz, CD_3CN): δ = 65.06, 43.34. ESI-HRMS (m/z): Calcd: 1365.3186 $[M–BF_4]+$. Found: 1365.3146.

4.4.2.6 Synthesis of 19-Pd-Closed

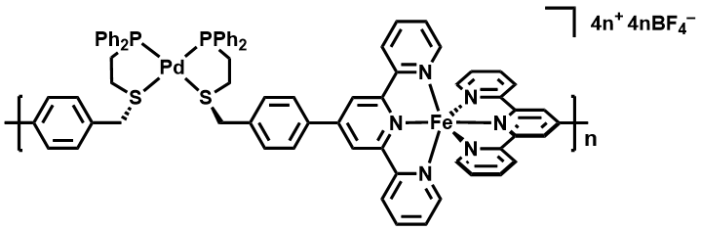

19-Pd-Closed

A solution of iron(II)tetrafluoroborate hexahydrate ($Fe(BF_4)_2•6H_2O$) was prepared by dissolving 0.0040 g of $Fe(BF_4)_2•6H_2O$ in 500 μL of CD_3CN. The prepared $Fe(BF_4)_2•6H_2O$ solution was then added to a solution of **18-Pd-Closed** (9.8 mg, 0.007 mmol) in CD_3CN until a 1:1 molar ratio was achieved (2.3 mg of $Fe(BF_4)_2$, 0.007 mmol). The solution changed from a clear, yellow solution to a dark purple solution.

4.4.2.7 Synthesis of 19-Pd-Open

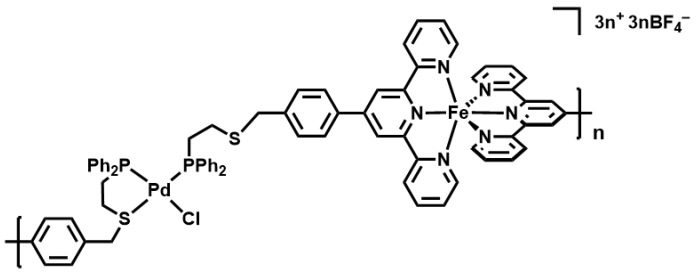

19-Pd-Open

19-Pd-Open can be prepared from **18-Pd-Open** prepared by either of the two outlined procedures, above. A solution of iron(II)tetrafluoroborate hexahydrate ($Fe(BF_4)_2 \cdot 6H_2O$) was prepared by dissolving 0.0041 g of $Fe(BF_4)_2 \cdot 6H_2O$ in 200 μL of CD_3CN. The prepared $Fe(BF_4)_2 \cdot 6H_2O$ solution was then added into a solution of **18-Pd-Open** (12.0 mg, 0.009 mmol) in CD_3CN until a 1:1 molar ratio was achieved (3.0 mg of $Fe(BF_4)_2$, 0.009 mmol) The solution changed from a clear, yellow solution to a dark purple solution.

4.4.2.8 Synthesis of 19-Pt-Closed

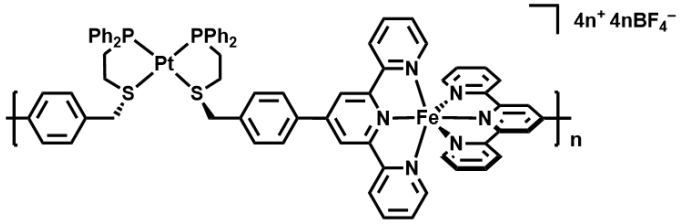

19-Pt-Closed

A solution of iron(II)tetrafluoroborate hexahydrate ($Fe(BF_4)_2 \cdot 6H_2O$) was prepared by dissolving 0.0040 g of $Fe(BF_4)_2 \cdot 6H_2O$ in 200 μL of CD_3CN. The prepared $Fe(BF_4)_2 \cdot 6H_2O$ solution was then added to a solution of **18-Pt-Closed** (3.0 mg, 0.002 mmol) in CD_3CN until a 1:1 molar ratio was

achieved (0.673 mg of $Fe(BF_4)_2$, 0.002 mmol). The solution changed from a clear, yellow solution to a dark purple solution.

4.4.2.9 Synthesis of 19-Pt-Open

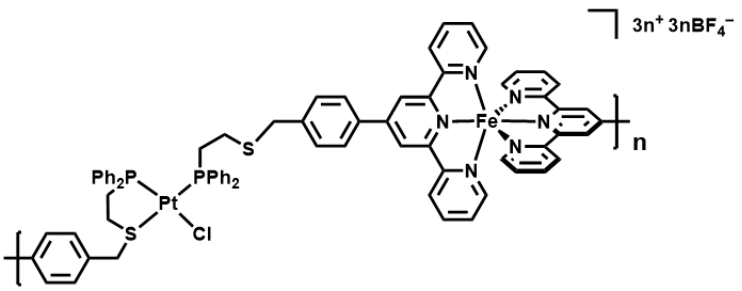

19-Pt-Open

A solution of iron(II)tetrafluoroborate hexahydrate ($Fe(BF_4)_2 \cdot 6H_2O$) was prepared by dissolving 0.0040 g of $Fe(BF_4)_2 \cdot 6H_2O$ in 300 μL of CD_3CN. The prepared $Fe(BF_4)_2 \cdot 6H_2O$ solution was then added to a solution of **18-Pt-Open** (6.0 mg, 0.004 mmol) in CD_3CN until a 1:1 molar ratio was achieved (1.44 mg of $Fe(BF_4)_2$, 0.004 mmol). The solution changed from a clear, yellow solution to a dark purple solution.

4.4.3 X-Ray Crystal Data

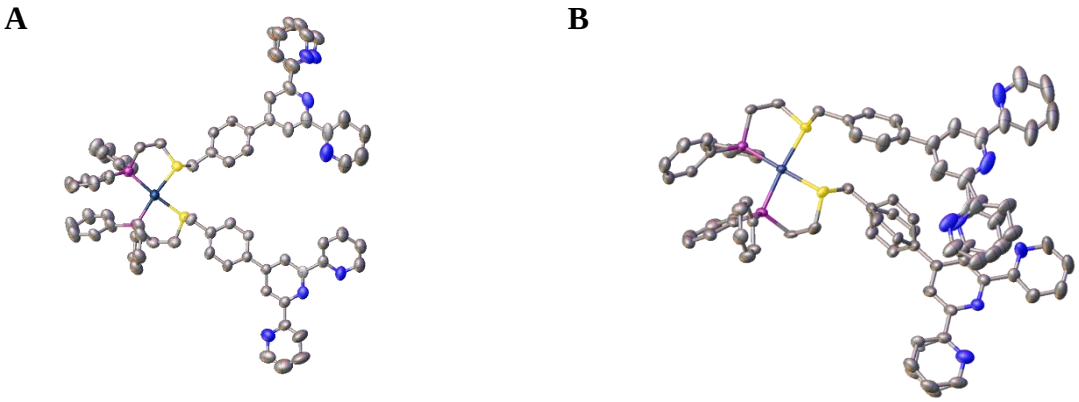

Figure 4.4 Crystal structures of (a) **18-Pt-Closed** (obtained from the slow diffusion of ether into acetonitrile) and (b) the **18-Pd-Closed** (obtained from the slow diffusion of ether into DCM) drawn with 50% thermal ellipsoid probability. Hydrogen atoms, solvent molecules, and anions have been omitted for clarity.

Table 4.1 Crystal data and structural refinement for **18-Pt-Closed** and **18-Pd-Closed**.

	18-Pt-Closed	**18-Pd-Closed**
Empirical formula	$C_{72}H_{60}F_{18}N_6P_5PtS_2$	$C_{76}H_{70}B_2F_8N_6OP_2PdS_2$
Formula weight	1765.32	1489.46
Temperature / K	100.0	149.99
Crystal system	orthorhombic	monoclinic
Space group	Ccce	$P2_1/c$
a / Å	22.614(4)	9.5073(5)
b / Å	28.042(5)	35.1644(18)
c / Å	54.989(12)	21.6818(11)
α/°	90	90
β/°	90	92.515(4)
γ/°	90	90
Volume / $Å^3$	34871(12)	7241.6(6)

Z	16	4
ρ_{calc} / mg mm^{-3}	1.345	1.366
μ / mm^{-1}	5.013	3.601
F(000)	14096	3064.0
Crystal size / mm^3	0.222 × 0.146 × 0.014	0.259 × 0.095 × 0.006
2Θ range for data collection	3.214 to 127.094°	5.026 to 136.634°
Index ranges	0 ≤ h ≤ 25, 0 ≤ k ≤ 32, 0 ≤ l ≤ 63	-11 ≤ h ≤ 10, -42 ≤ k ≤ 40, -18 ≤ l ≤ 26
Reflections collected	12624	34154
Independent reflections	12007[R(int) = 0.0000]	12892[R(int) = 0.0642]
Data/restraints/parameters	12007/1119/982	12892/534/1033
Goodness-of-fit on F^2	1.046	1.050
Final R indexes [I>2σ (I)]	R_1 = 0.0965, wR_2 = 0.2614	R_1 = 0.0605, wR_2 = 0.1515
Final R indexes [all data]	R_1 = 0.1278, wR_2 = 0.2786	R_1 = 0.0803, wR_2 = 0.1607
Largest diff. peak/hole / e Å^{-3}	1.502/-0.786	0.939/-0.938

4.4.4 Characterization of Coordination-Polymers Bearing WLA Subunits

In order to determine the stoichiometry of metal-ligand binding, we conducted a titration wherein samples each containing a fixed concentration of 230 μM **18-M-Open** or **18-M-Closed** (M = Pd^{II} or Pt^{II}) in 1 mL CD_3CN were prepared with increasing amounts of $Fe(BF_4)_2 \cdot 6H_2O$ ranging from 0 to 300 μM.

4.4.4.1 ^{1}H NMR and ^{1}H DOSY Spectra of Coordination Polymers

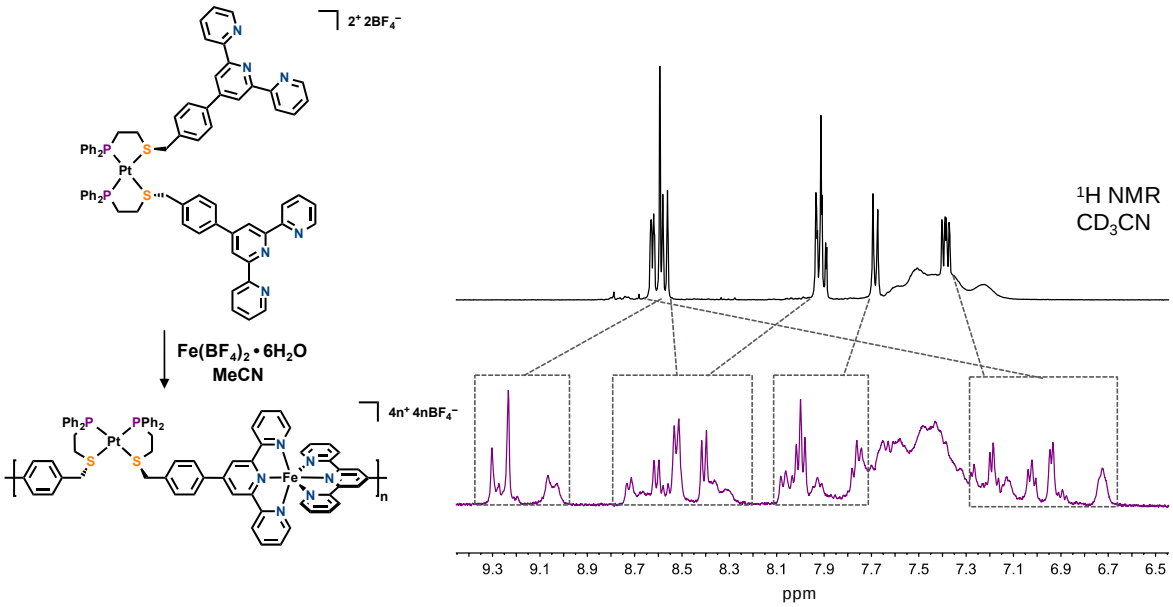

Figure 4.5 ^{1}H NMR spectra of monomer **18-Pt-Closed** before (top) and after (bottom) the addition of one equivalent of $Fe(BF_4)_2$•$6H_2O$ to form **19-Pt-Closed**. Dashed lines and boxes show free terpyridine resonances shifting to regions indicative of iron binding.[131]

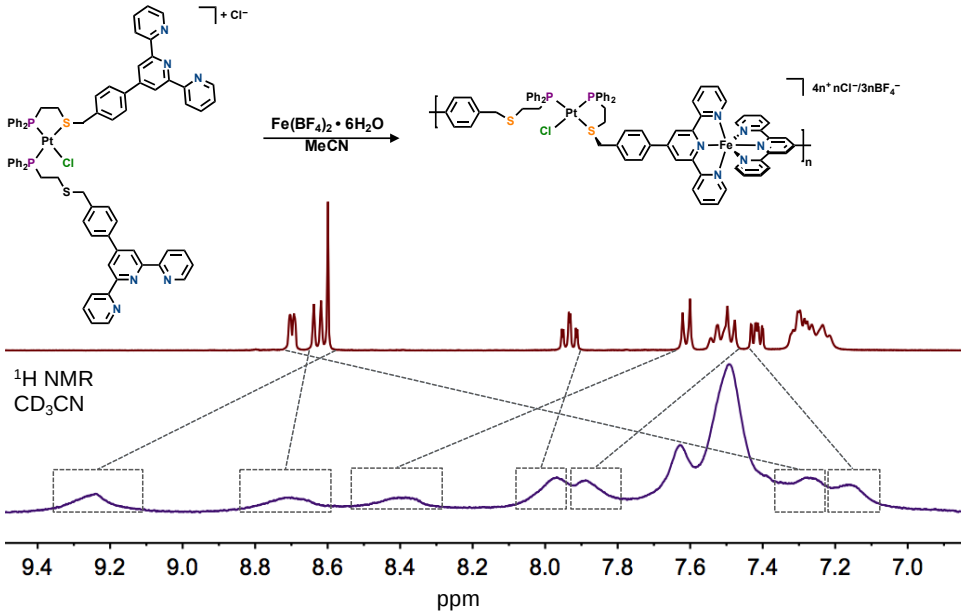

Figure 4.6 ^{1}H NMR spectra of monomer **18-Pt-Open** before (top) and after (bottom) the addition of one equivalent of $Fe(BF_4)_2$•$6H_2O$ to form **19-Pt-Open**. Dashed lines and boxes show free terpyridine resonances shifting to regions indicative of iron binding.[131]

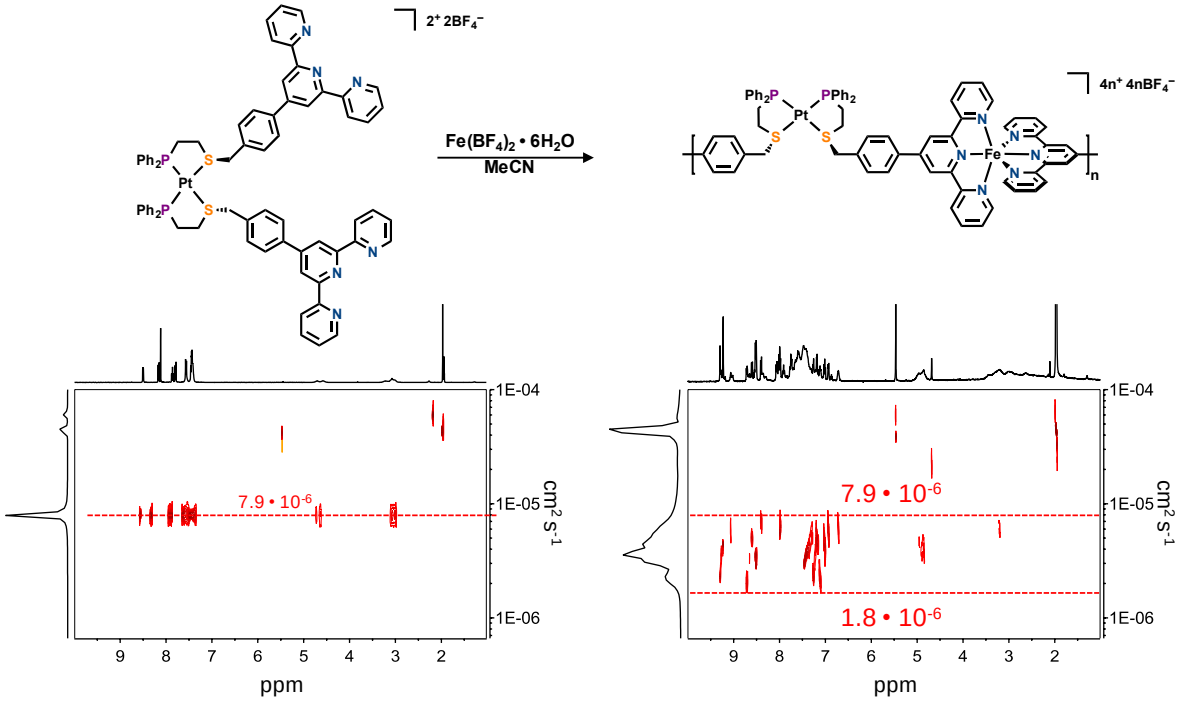

Figure 4.7 ^{1}H DOSY NMR spectra of monomer **18-Pt-Closed** (D = 7.9 • 10^{-6} cm^2s^{-1}) before (left) and after (right) the addition of $Fe(BF_4)_2$•$6H_2O$ to form **19-Pt-Closed**. The Spectrum of **19-Pt-Closed** indicates the complete consumption of the starting monomer and the formation of oligomeric species with diffusion coefficients reduced by up to a factor of four.

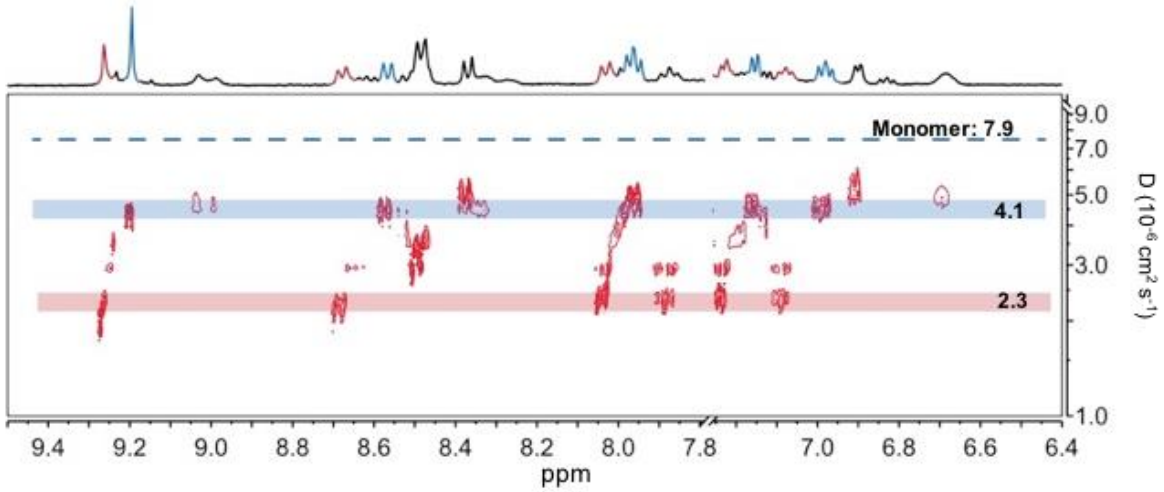

Figure 4.8 ^{1}H DOSY NMR spectra of monomer **18-Pt-Closed** (D = 7.9 • 10^{-6} cm^2s^{-1}) before (left) and after (right) the addition of $Fe(BF_4)_2$•$6H_2O$ to form **19-Pt-Closed**. The Spectrum of **19-Pt-Closed** indicates the complete consumption of the starting monomer and the formation of oligomeric species with diffusion coefficients reduced by up to a factor of four.

4.4.5 DFT Calculations

All computational calculations were carried out with the use of SCM's Amsterdam Density Functional (ADF2016.104) suite on a 12-core computational cluster. The model for **19-Pd-Closed** and **19-Pt-Closed** were built ignoring counter anions and assuming local charge(s) arising from the Pd(II) or Pt(II) metal center only. Geometry optimizations of all electrons were made by applying the generalized gradient approximation method (GGA) with bases sets containing triple-ζ functions with two polarization functions (TZ2P), and the local density approximation of Becke, Perdew and Ernzerhof (PBE).[140] Scalar relativistic effects were taken into consideration for heavy metal atoms.

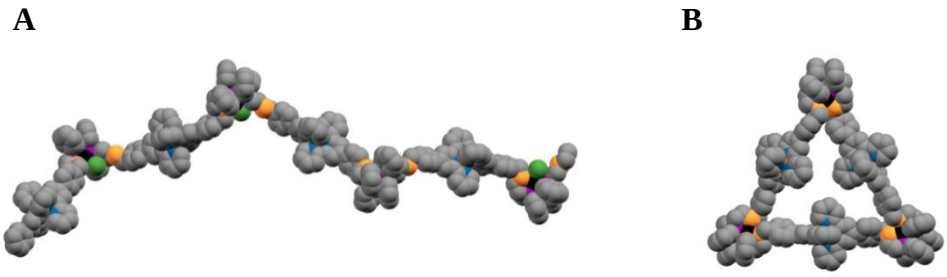

Figure 4.9 Density function theory (DFT) energy minimized models of A) **19-Pd-Closed** and B) **19-Pt-Closed**. The lowest energy conformation of **19-Pt-Closed** resembles cyclic oligomers.

4.4.6 Post Polymerization Switching of States

In order to switch from the closed Pd^{II} coordination polymer (**19-Pd-Closed**) to the open Pd^{II} coordination polymer (**19-Pd-Open**), a solution of **19-Pd-Closed** (10 mg, 0.007 mmol) in CH_3CN was treated with tetrabutylammonium chloride (TBAC, 2 mg, 0.007 mmol). The solution was filtered, and the resulting homogeneous, clear, purple solution was evaporated under reduced pressure to give **19-Pd-Open**. In an alternative approach, the closed Pd^{II} coordination polymer

(**19-Pd-Closed**) to the open Pd^{II} coordination polymer (**19-Pd-Open**), **3-Pd-Closed** (25 mg, 0.018 mmol) was dissolved in ~4 mL of CH_3CN in a falcon tube. In a separate falcon tube, 440 mg of Dowex 1x4 chloride resin (100-200 mesh) was measured out and mixed with 4 mL of CH_3CN. The solution containing **3-Pd-Closed** was slowly transferred (via pipette) to the falcon tube containing the Dowex chloride resin. Once completely transferred, the solution was mixed continuously for 30 min. After 30 min, the solution was filtered, and the resin was washed with 1 mL portions of CH_3CN. The filtrate was collected, and the resulting homogeneous, clear, purple solution was then evaporated under reduced pressure to give **3-Pd-Open**. Access to **3-Pd-Closed** from **3-Pd-Open** was achieved by addition of $Tl(BF_4)$.

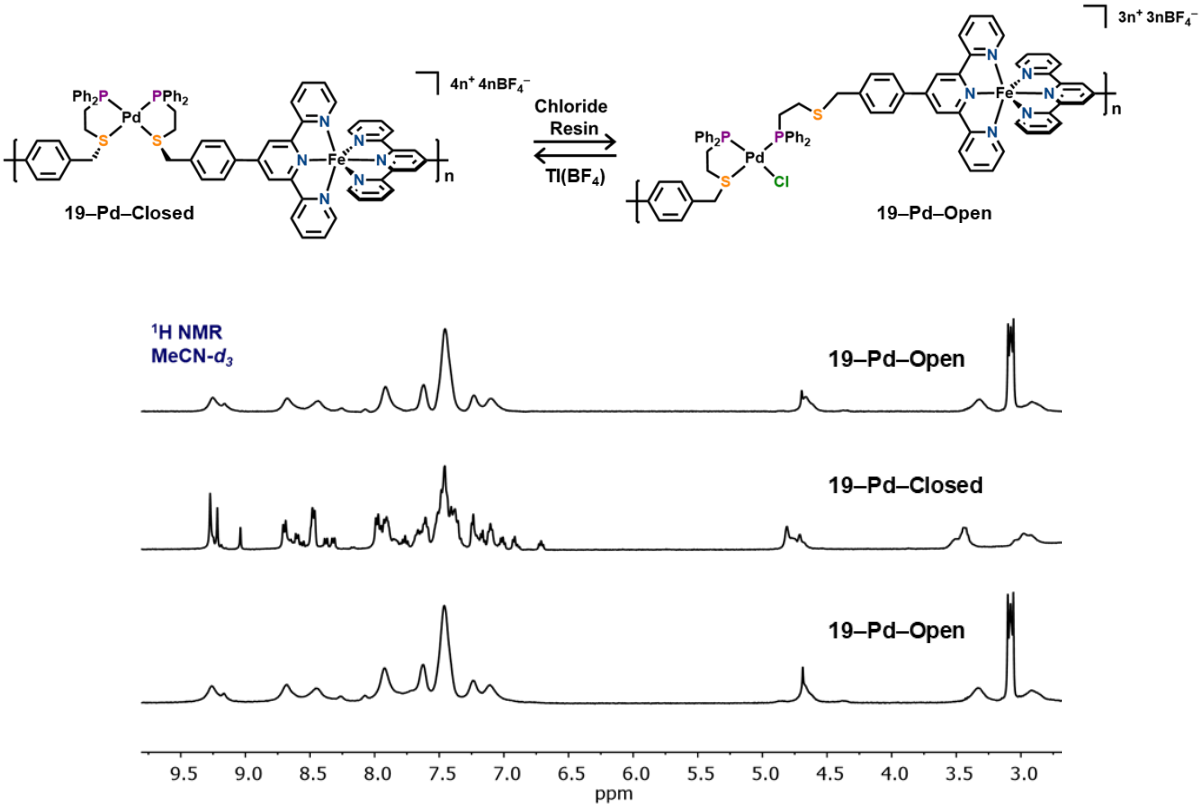

Figure 4.10 ^1H NMR spectra of coordination polymer **19-Pd-Open** (bottom) converted to **19-Pd-Closed** (middle) *via* abstraction of chloride post-polymerization, and **19-Pd-Closed** (middle) switched to **19-Pd-Open** (top) *via* addition of chloride post polymerization. All NMR spectra were taken in CD_3CN.

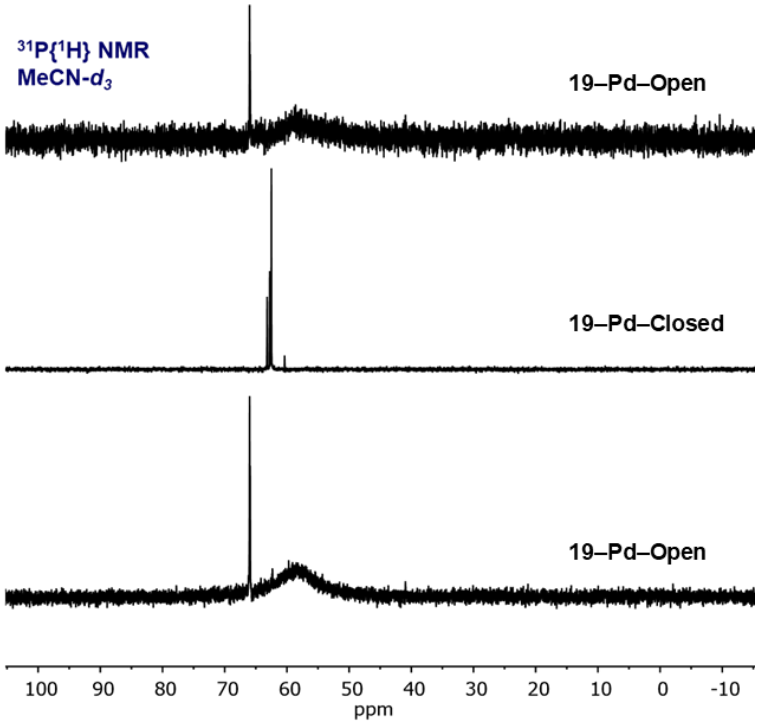

Figure 4.11 $^{31}P\{^{1}H\}$ NMR spectra of coordination polymer **19-Pd-Open** (bottom) converted to **19-Pd-Closed** (middle) *via* abstraction of chloride post-polymerization, and **19-Pd-Closed** (middle) switched to **19-Pd-Open** (top) *via* addition of chloride post polymerization. All spectra were taken in CD_3CN.

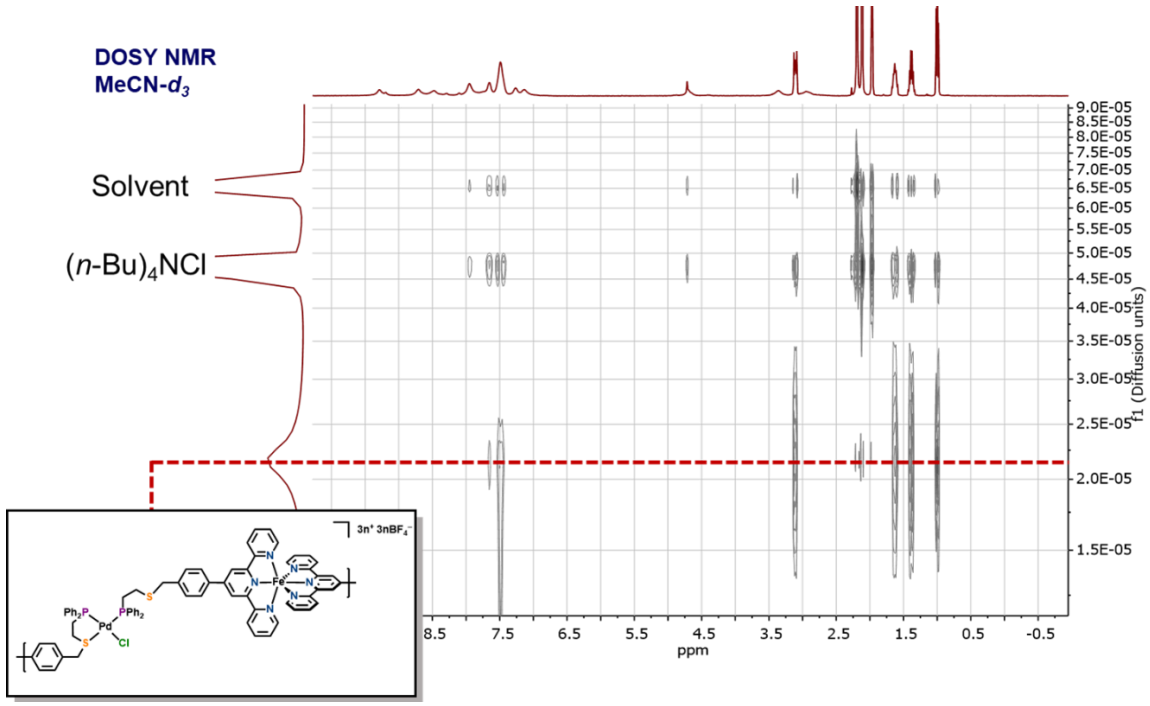

Figure 4.12 ^{1}H DOSY spectrum, taken in CD_3CN, of resulting **19-Pd-Open** from **19-Pd-Closed**, indicating the formation of one polymeric species.

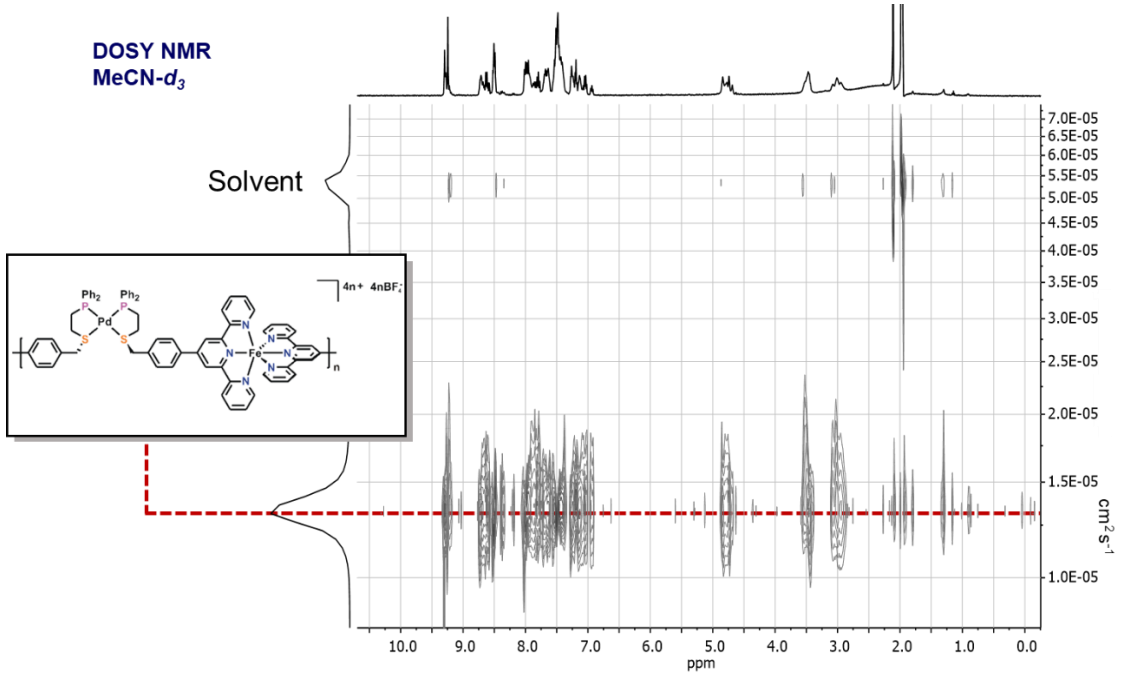

Figure 4.13 ^{1}H DOSY spectrum, taken in CD_3CN, of resulting **19-Pd-Closed** from **19-Pd-Open**, indicating the formation of one polymeric species.

In order to switch from **19-Pt-Closed** to **19-Pt-Open**, **19-Pt-Closed** (9 mg, 0.006 mmol) was dissolved in ~3 mL of CH_3CN in a falcon tube. In a separate falcon tube, 300 mg of Dowex 1x4 chloride resin (100-200 mesh) was measured out and mixed with 3 mL of CH_3CN. The solution containing **19-Pt-Closed** was slowly transferred (via pipette) to the flacon tube containing the Dowex chloride resin. Once completely transferred, the solution was stirred continuously for 30 min. After 30 min, the solution was filtered, and the resin was washed with 1 mL portions of CH_3CN. Switching from **19-Pt-Open** to **19-Pt-Closed** was achieved by dissolving **19-Pt-Open** (6 mg, 0.004 mmol) in CH_3CN and treating it with $TlBF_4$ (1.2 mg, 0.004 mmol) and the mixture was stirred for one hour.

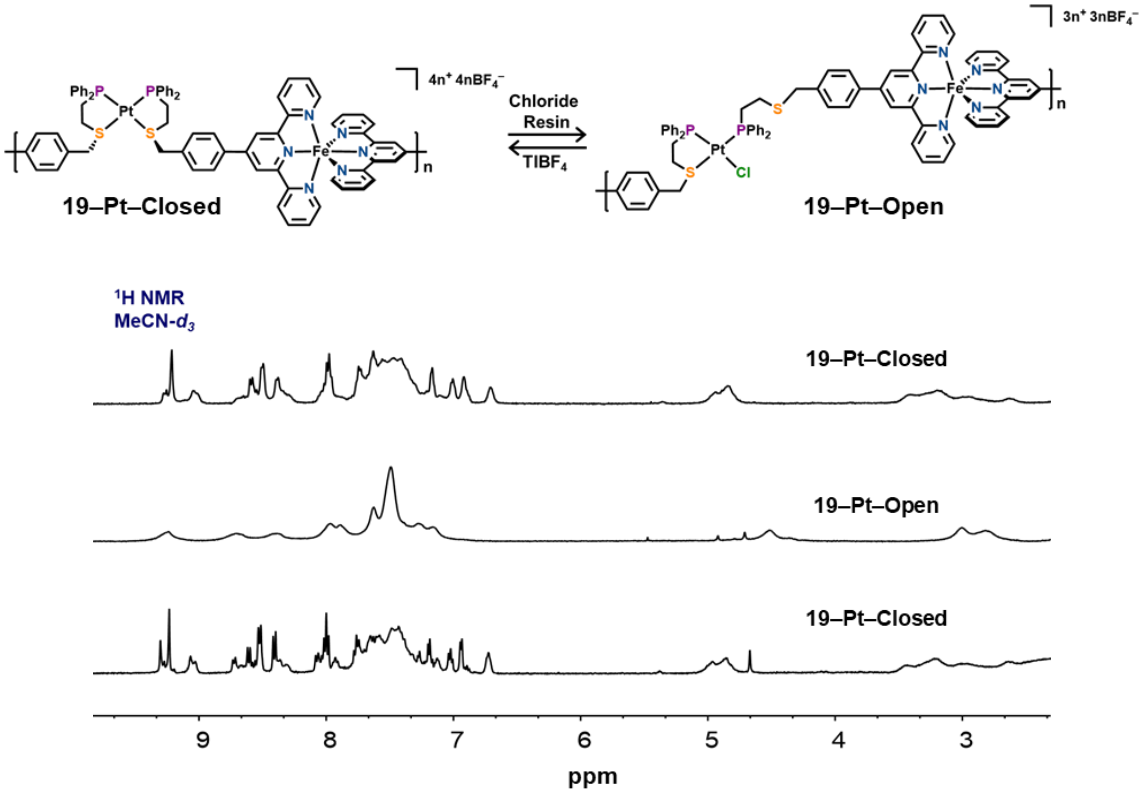

Figure 4.14 ^{1}H NMR spectra of coordination polymer **19-Pt-Closed** (bottom) converted to **19-Pt-Open** (middle) *via* addition of chloride post-polymerization, and **19-Pt-Open** (middle) switched to **19-Pt-Closed** (top) *via* abstraction of chloride post polymerization. All NMR spectra were taken in CD_3CN.

4.4.7 Infinite Coordination Polymer Particle Characterization

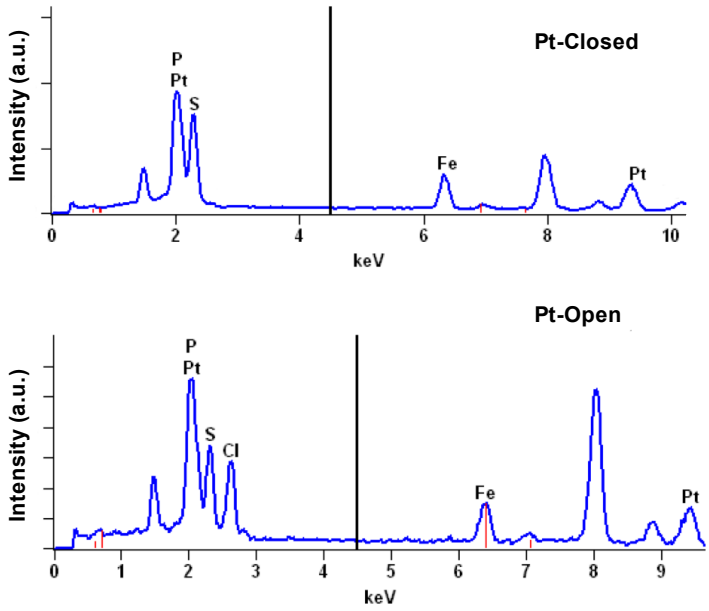

Figure 4.15 Representative EDS spectra for ICPs composed of **19-Pt-Closed** (top) and **19-Pt-Open** (bottom) showing the presence of Cl, which is indicative of the fully open complex.

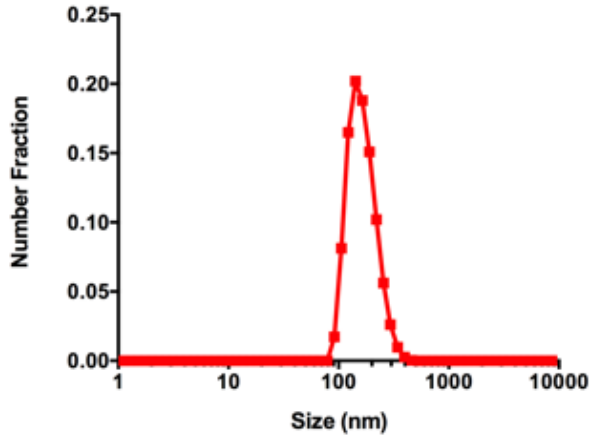

Figure 4.16 Representative DLS trace for colloidally stable ICPs composed of 19-Pt-Open synthesized from a 2 mM solution ($Diameter_{number\ average}$ = 164 nm, $Diameter_{Z\text{-}average}$ = 195 nm, PDI = 0.089).

4.4.8 ICP Particles Synthesis in Varying Conditions

ICP particles composed of **19-Pt-Closed** were prepared with sub-stoichiometric equivalents of chloride, and the resulting particle morphologies were analyzed using STEM. A solution of **19-Pt-Closed** (12 mg, 0.008 mmol) was dissolved in 4 mL of CH_3CN and tetrabutylammonium chloride (1.1 mg, 0.004 mmol) was added. Particles were synthesized from 8 mM solutions (with respect to the monomer).

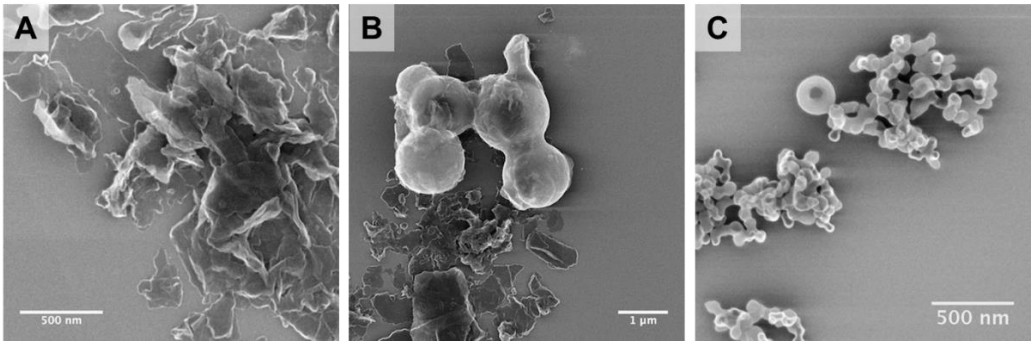

Figure 4.17 ICP particles composed of 19-Pt-Closed containing A) 0 equiv. of chloride, B) 0.5 equiv. of chloride, and C) 1 equiv. of chloride.

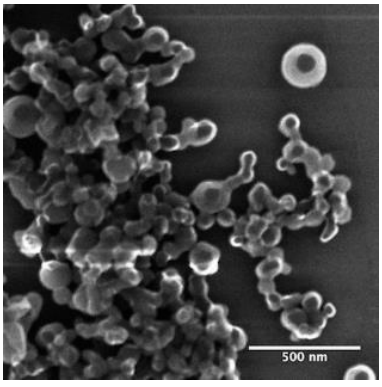

Figure 4.18 ICP particle synthesis from a 2 mM solution of 19-Pt-Closed, at ~5 °C, resulting in ill-defined aggregates of small spheres.

4.4.9 NMR Spectra of all Compounds and Complexes

^{1}H NMR and ^{31}P{^{1}H} NMR of: Ligand 17

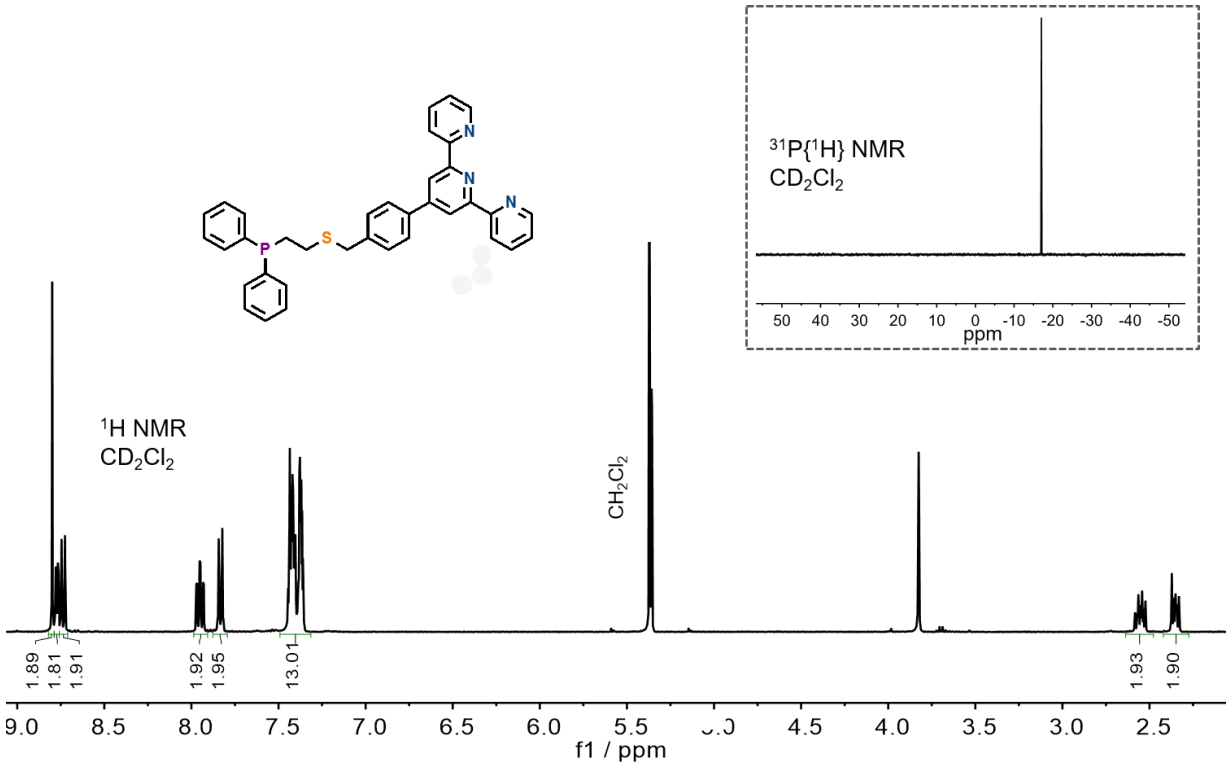

^{1}H NMR and ^{31}P{^{1}H} VT NMR of: 18-Pt-Open

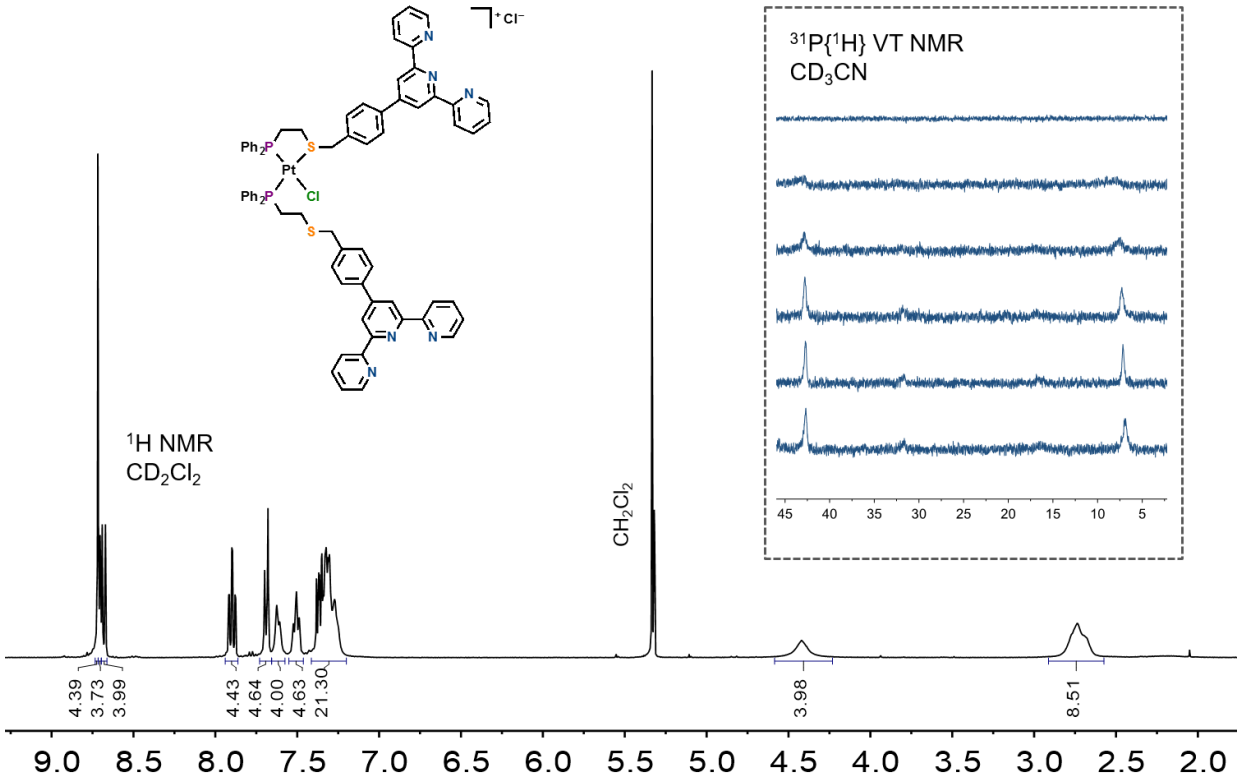

^{1}H NMR and ^{31}P{^{1}H} NMR of: 18-Pt-Closed

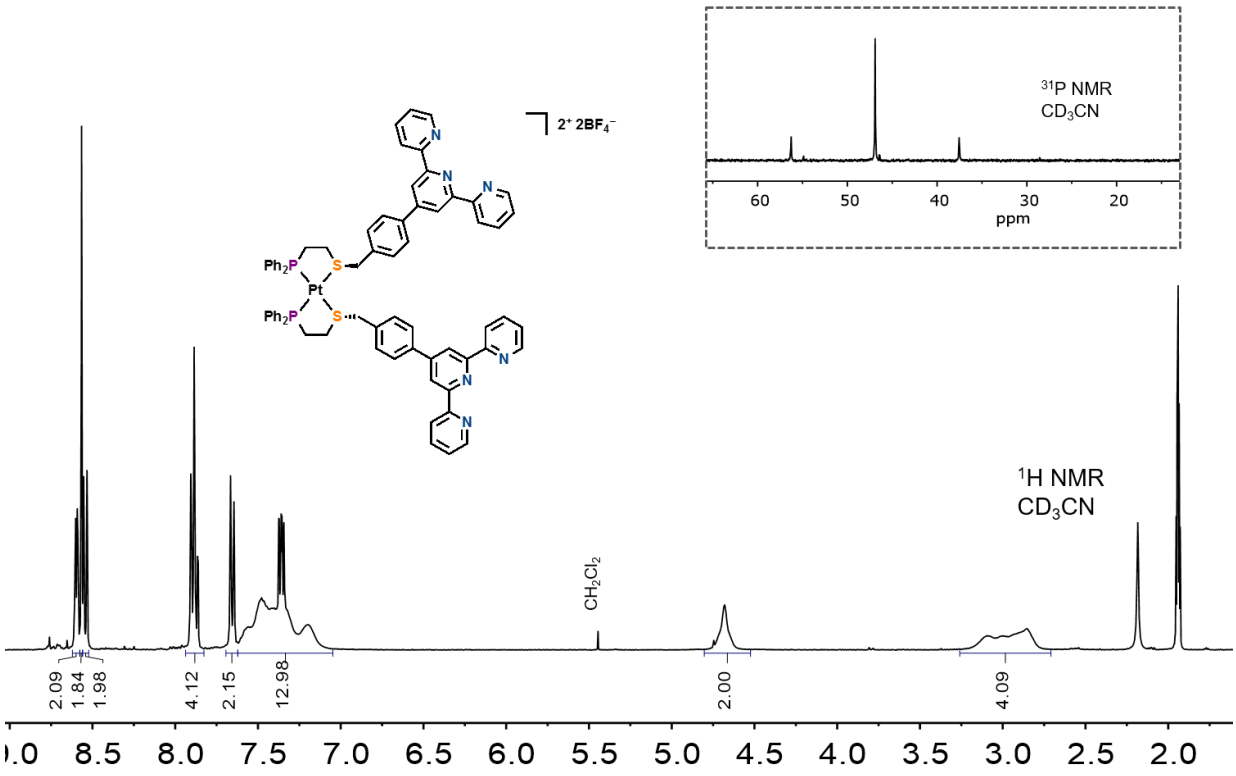

^{1}H NMR and ^{31}P{^{1}H} NMR of: 18-Pd-Closed

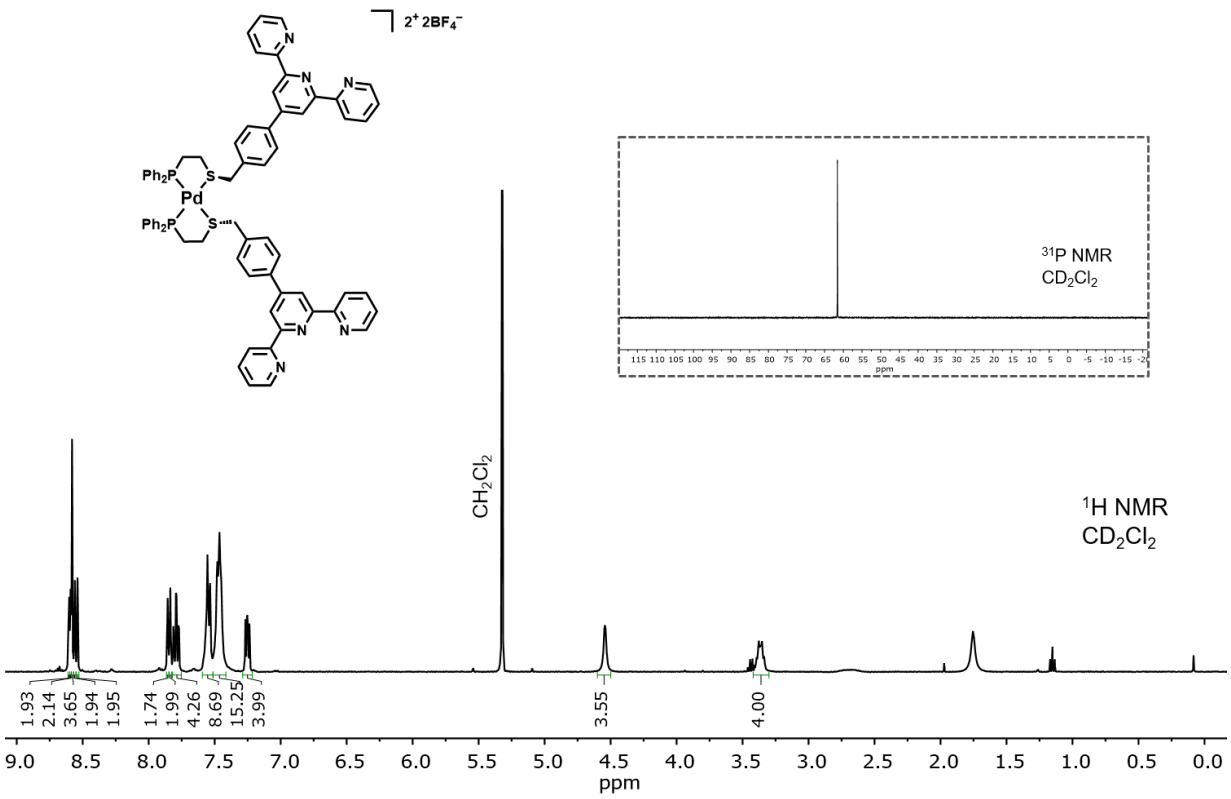

^{1}H NMR and ^{31}P{^{1}H} NMR of: 18-Pd-Open

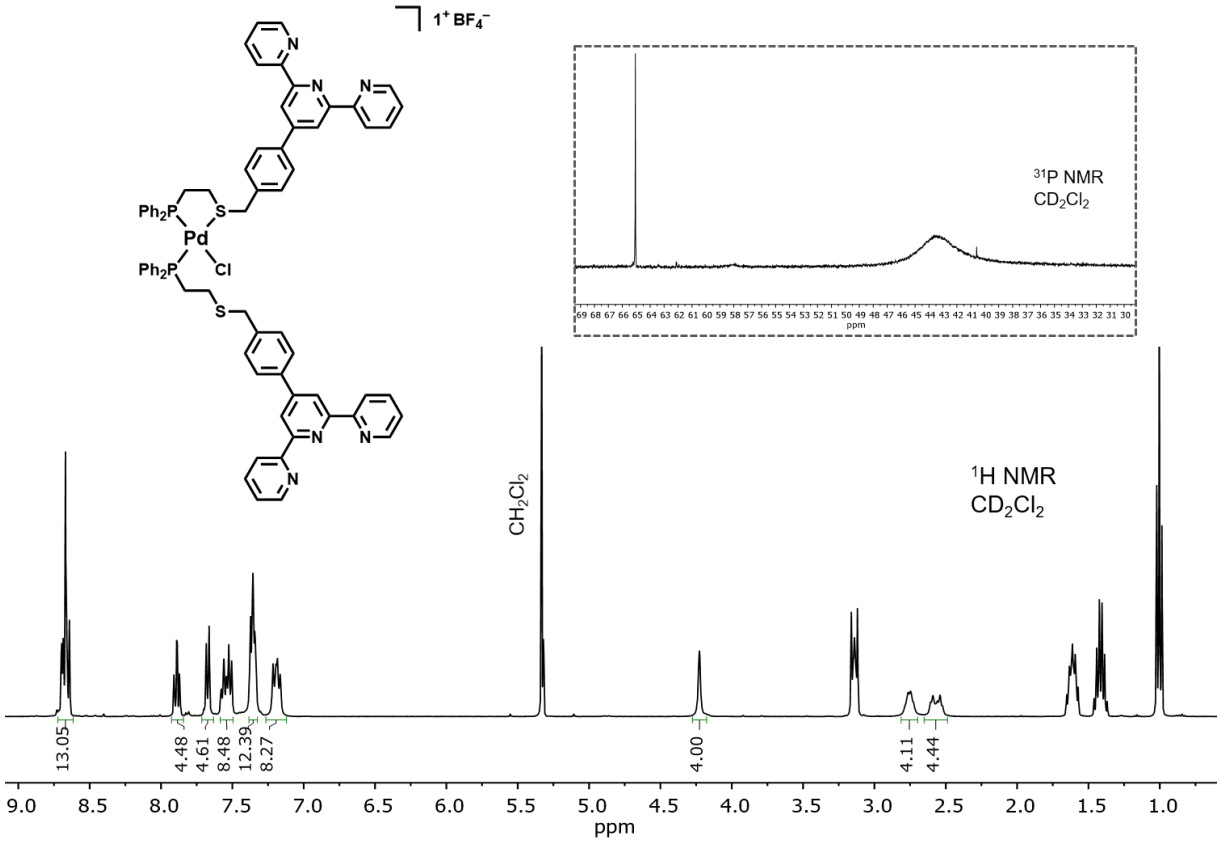

4.4.10 Mass Spectra of all Complexes

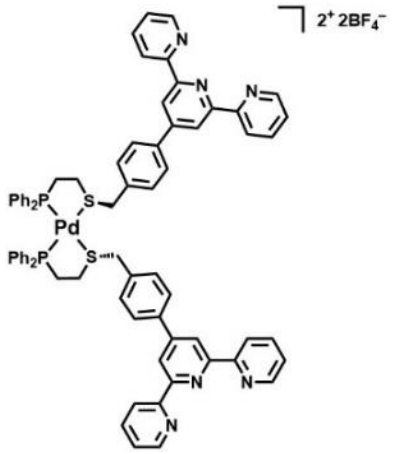

2-Pd-Closed

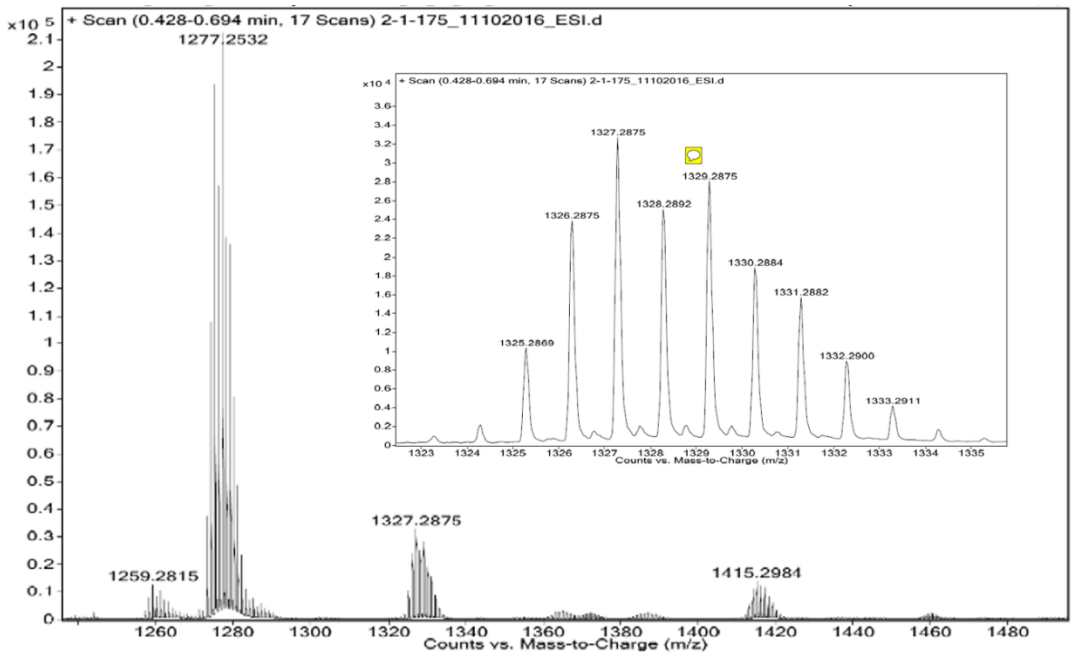

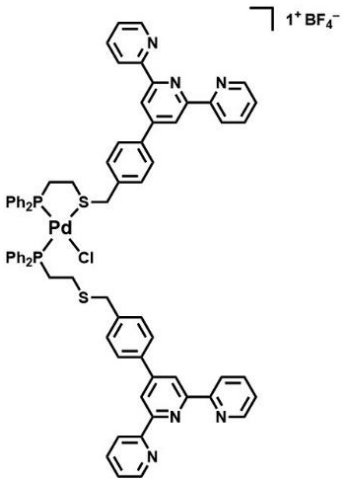
1+ BF4−
Ph2P
S
Pd
Cl
N

2-Pd-Open

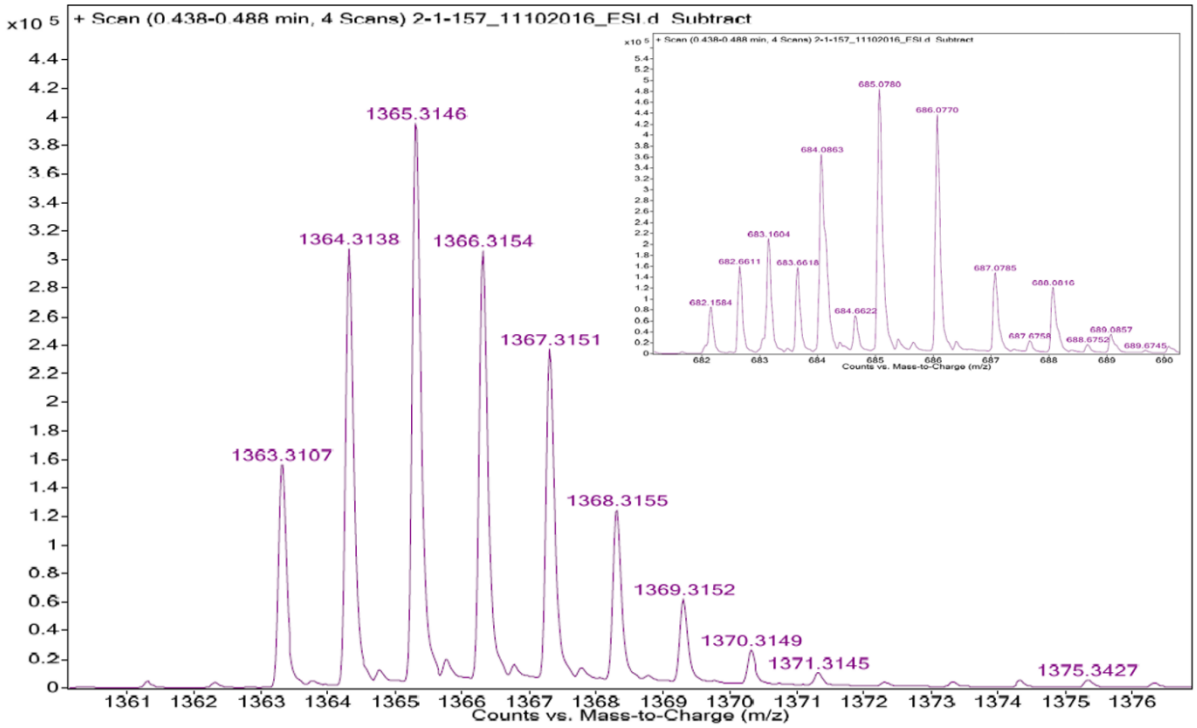
+ Scan (0.438-0.488 min, 4 Scans) 2-1-157_11102016_ESI.d Subtract
x10 5
1365.3146
1364.3138
1366.3154
1367.3151
1363.3107
1368.3155
1369.3152
1370.3149
1371.3145
1375.3427
Counts vs. Mass-to-Charge (m/z)

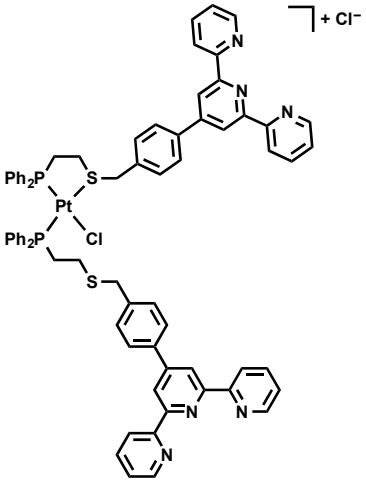
+ Cl⁻
N
N
N
Ph2P
S
Pt
Ph2P
Cl
S
N
N
N

2-Pt-Open

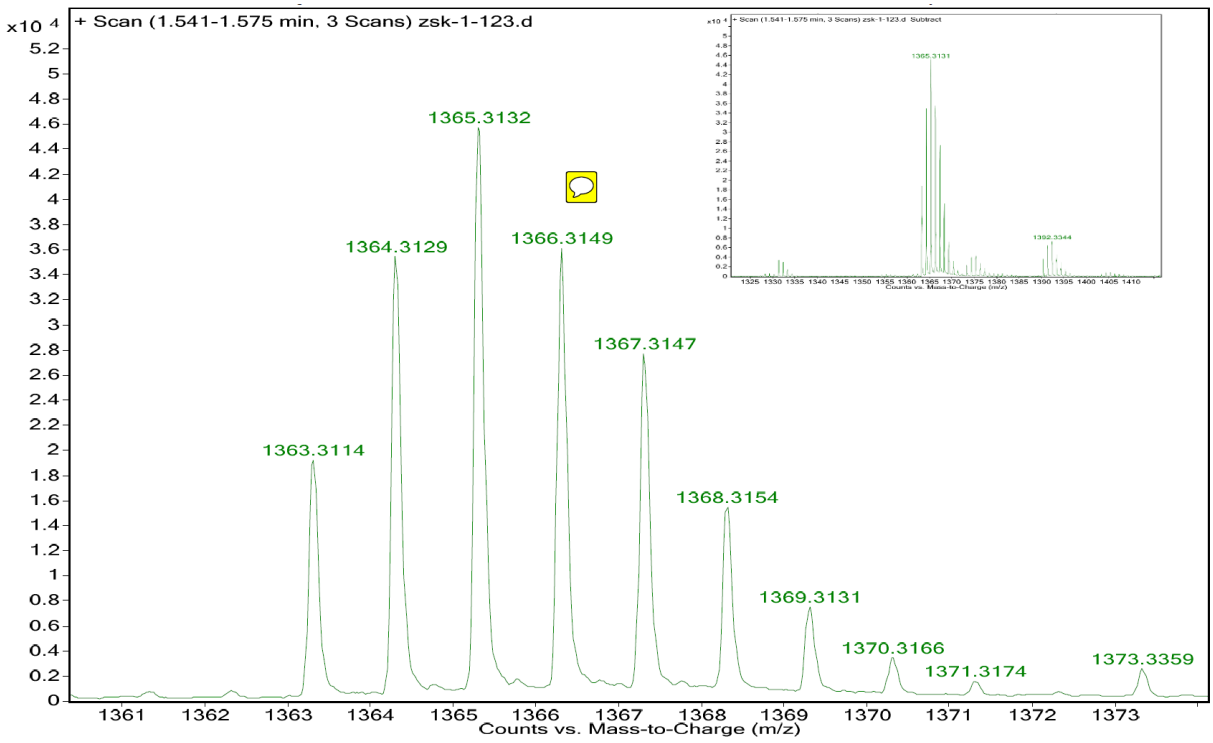
+ Scan (1.541-1.575 min, 3 Scans) zsk-1-123.d
x10 4
5.2
5
4.8
4.6
4.4
4.2
4
3.8
3.6
3.4
3.2
3
2.8
2.6
2.4
2.2
2
1.8
1.6
1.4
1.2
1
0.8
0.6
0.4
0.2
0
1365.3132
1364.3129
1366.3149
1367.3147
1363.3114
1368.3154
1369.3131
1370.3166
1371.3174
1373.3359
1361
1362
1363
1364
1365
1366
1367
1368
1369
1370
1371
1372
1373
Counts vs. Mass-to-Charge (m/z)

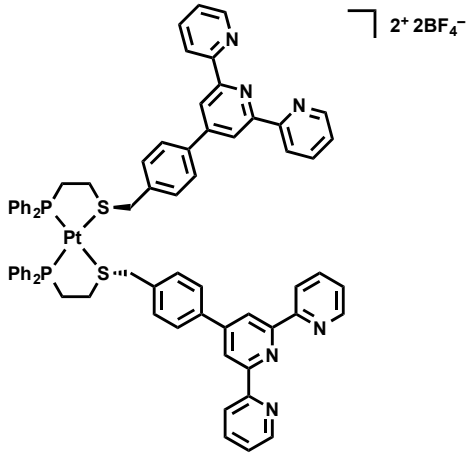
2+ 2BF4−
Ph2P
S
Pt
Ph2P
S
N
N
N
N
N
N

2-Pt-Closed

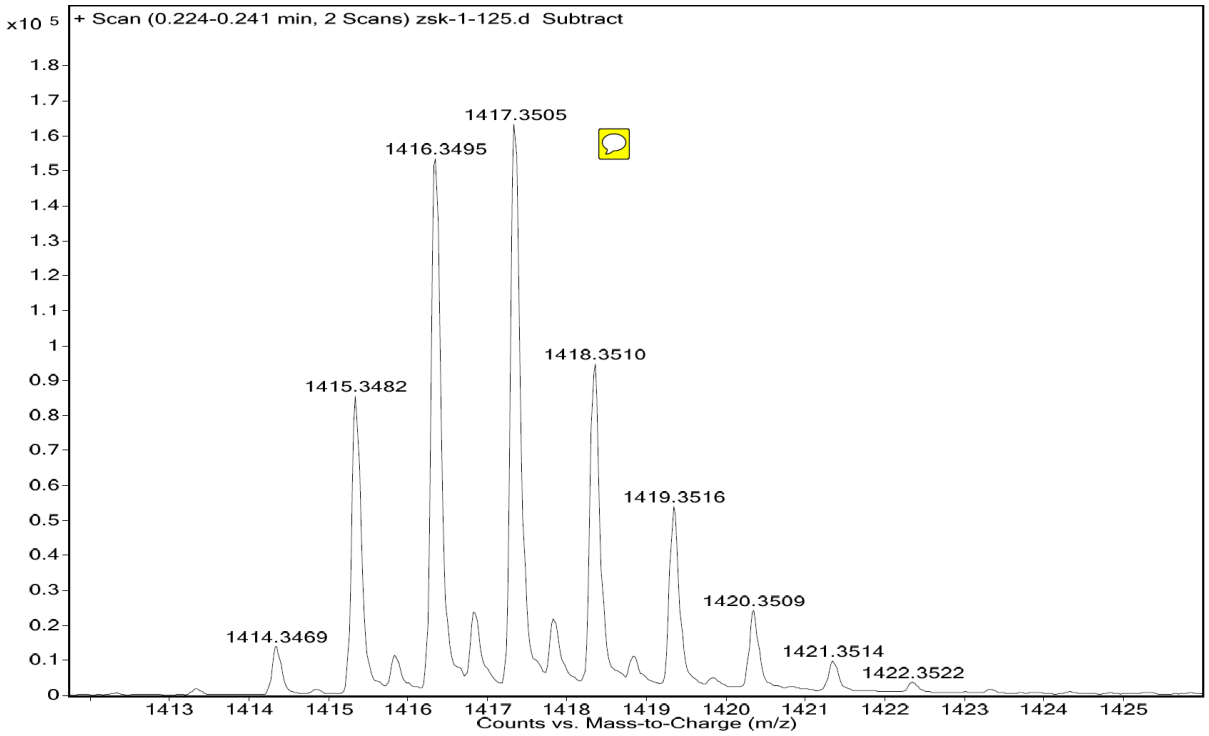
x10 5
+ Scan (0.224-0.241 min, 2 Scans) zsk-1-125.d Subtract
1.8
1.7
1.6
1.5
1.4
1.3
1.2
1.1
1
0.9
0.8
0.7
0.6
0.5
0.4
0.3
0.2
0.1
0
1417.3505
1416.3495
1418.3510
1415.3482
1419.3516
1420.3509
1414.3469
1421.3514
1422.3522
1413
1414
1415
1416
1417
1418
1419
1420
1421
1422
1423
1424
1425
Counts vs. Mass-to-Charge (m/z)

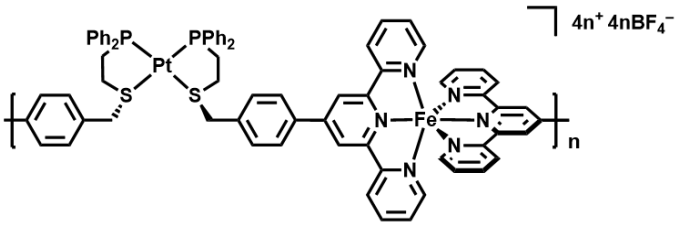

3-Pt-Closed

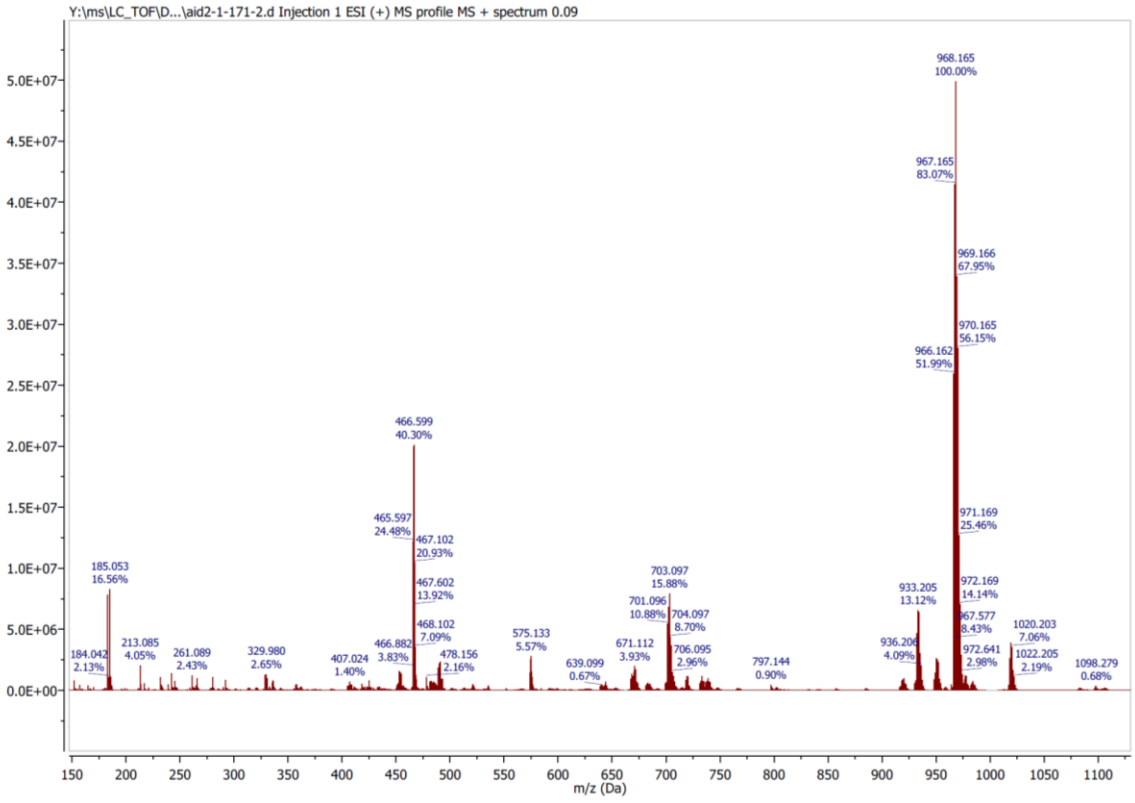

(fragments into multiple species)

CHAPTER 5

Design of Reconfigurable, Bio-Inspired Coordination Polymers Assembled *via* the Weak-Link Approach

The work presented in this chapter is unpublished.

5.1 Introduction

Proteins and other biological systems demonstrate remarkable control over their primary, secondary and tertiary structure through a complex network of relatively weak supramolecular interactions.[141] These interactions allow proteins to effectively regulate their structure and function in response to molecular effectors or stimuli, a process known as allosteric regulation, which enable their unique properties and unmatched activity.[8, 142] Chemists, therefore, have sought to adapt these same principles found in biology, to the assembly of abiotic allosteric architectures with a goal of developing the next generation of catalysts, sensors and functional materials. One versatile class of bio-inspired materials that have garnered significant interest are coordination polymers (CPs),[143-146] whose structures consist of multidentate ligands interconnected by cationic metal nodes.[113, 147] Interest in CPs have stemmed from their highly tailorable metal and ligand precursors, which exhibit microporosity and high internal surface areas, and possess a high level of structural tailorability for a broad range of applications.[113, 148]

Significant advances have been made in the development of bio-inspired CPs, with recent work demonstrating stimuli-responsive CPs that dynamically adapt their structure in response to a stimulus,[149] however, the vast majority of work in the field has focused on modulating the structure and properties of bulk materials (e.g. Metal-Organic Frameworks).[150-152] Stimuli-responsive micrometer- and nanometer-scale CPs on the other hand, are a particularly attractive—though, underdeveloped—synthetic target. It is well understood that the size and composition of microporous materials drastically affect their diffusion kinetics and electronic properties[153] for a broad range of applications such as drug delivery,[154] sensing, gas storage,[155-156] molecular separations,[157] catalysis and ion exchange.[158] Developing responsive CP building blocks,

therefore, represents a method to modulate the chemical, physical and electronic properties of these materials on the nanoscale. Though several methods exist for the synthesis of a broad range of CP materials,[113, 159] there are few established approaches for the construction of stimuli-responsive, nanoscale CPs. Therefore, a central goal of this work is to expand the scope of stimuli-responsive CP materials at the micrometer and nanometer scale.

Previous reports have shown that molecular geometry and metal-ligand coordination, influence the chemical and physical properties of CPs,[160-163] therefore, a strategy for constructing stimuli-responsive CP nanomaterials must focus on the development of monomeric building-blocks possessing: (a) Tunable structural geometry; (b) Geometrically well-defined coordination sites to induce the assembly of 1-D, 2-D or 3-D architectures[148, 164]; and (c) Modular and facile syntheses for incorporation into a wide variety of networks. On the basis of these principles, we focused on the design and synthesis of CP building blocks possessing hemilabile ligands coordinated to metal ions (Figure 5.1). Despite their extensive use in stimuli-responsive coordination-based compounds, hemilabile ligands are relatively underrepresented as constituents used in the construction of CP building blocks, until recently.[160] However, their modular design and high degree of tunability make hemilabile ligands attractive for modulating the chemical and physical properties of CP materials. As such, we sought to incorporate these versatile, hemilabile ligands into stimuli-responsive monomers *via* the Weak-Link Approach (WLA), a supramolecular strategy to assembling coordination-based architectures (Figure 5.1).[47, 49, 66, 165]

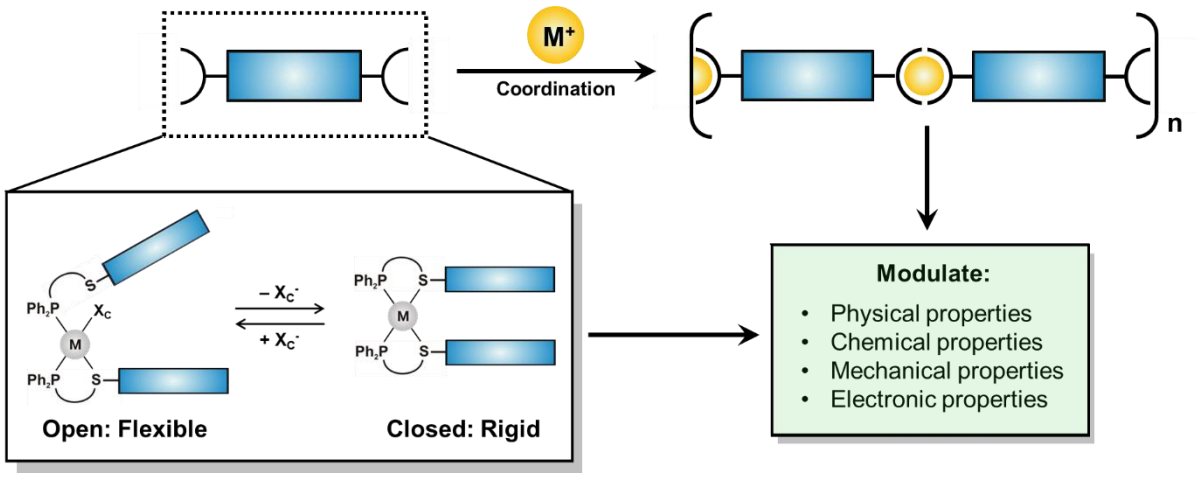

Figure 5.1 The goal of this work: design and synthesis of CP building blocks possessing hemilabile ligands coordinated to metal ions.

5.2 Results and Discussion

5.2.1 Design of CP Building Blocks Possessing Coordinating Hemilabile Ligands

WLA structures have traditionally been assembled from d^8 transition metals and hemilabile phosphino–chalcoether (P,X; X = O, S, Se) ligands, therefore, the monomer used here was based on a Pd^{II} tweezer-like complex bearing pyridine coordinating units, as shown in Figure 5.2. Such architectures give rise to stimuli-responsive building blocks that can reversibly access distinctly different structural states upon introduction to small molecule effectors or elemental anions.

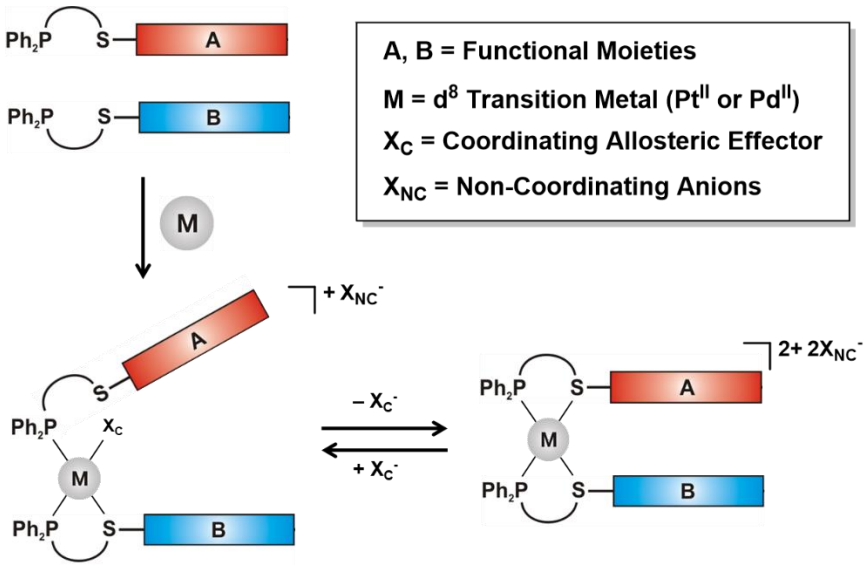

Figure 5.2 WLA tweezer complexes bearing hemilabile ligands and d^8 metal centers can reversibly access multiple, distinct structural states upon introduction of an allosteric effector.

The WLA enables structures possessing addressable structural geometry, well-defined coordination sites, tunable ligand design and offers a modular and facile syntheses of stimuli-responsive building blocks for incorporation into a wide variety of network materials.[47, 50, 52, 69] As such, the WLA lends itself to the construction of responsive, supramolecular, coordination-based materials and, importantly, meets the molecular design parameters previously described.

We, therefore, designed molecular-level building blocks for the assembly of stimuli-responsive coordination polymer materials (Figure 5.3). Drawing upon our previous work investigating the assembly of terpyridine-based WLA building blocks,[160] we sought to expand the scope of such materials to include building blocks of varying denticity, geometry, chelating strength and ligand basicity. In this way, fundamental structure–property relationships could be elucidated, and materials function could be tuned through deliberate molecular-level design.

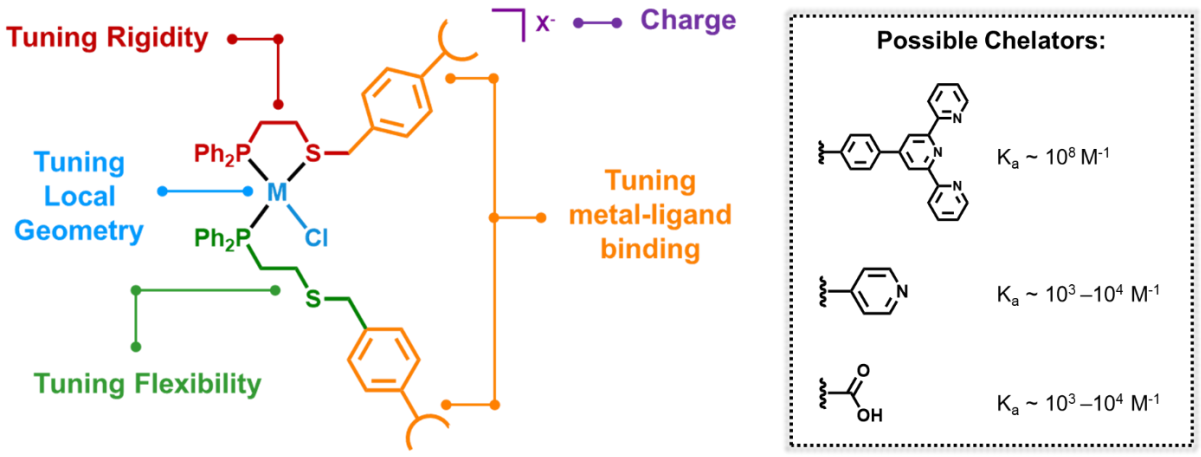

Figure 5.3 General design of tunable WLA building blocks with different possible chelators for coordination to metal ions in the assembly of responsive coordination polymers. The WLA is an ideal platform for the synthesis of stimuli-responsive coordination polymer materials, owing to its highly tunable platform and modularity. Metal-ligand binding strength, orientation, and geometry may be tuned by changing the coordinating end group on the P,S ligand (terpyridine, pyridine, carboxylate, are discussed).

Initially, we explored the effect of pyridine as the coordinating group appended to the WLA hemilabile ligands. The pyridine units allow the monomer to be polymerized via metal–ligand coordination, in the presence of metal ions such as Cu^{II}.[166-167] Upon assembly, the resulting complexes can be switched between a flexible, open state and a rigid, closed state by the stoichiometric addition or removal of allosteric effectors (such as Cl^-), which displace the weakly coordinating X moiety in the metal–X bond while retaining the strongly coordinating metal–P bond. Phosphino–thioether (P,S) ligands have been previously employed as WLA ligands with d^8 metal centers such as Pt^{II} and Pd^{II}, and are sufficiently strong to form a robust metal–thioether bond in the absence of chloride, while becoming sufficiently labile in the presence of chloride.[69, 86] The stimuli-responsive properties of these constructs render the WLA an emerging and

important tool for preparing CP materials whose structure and properties can be precisely addressed with small molecule effectors.

5.2.2 Synthesis

5.2.2.1 Synthesis of the Closed Pd^{II} Monomer, Complex 23

Model WLA-based CP building blocks were synthesized from square-planar Pd^{II} and Pt^{II} metal nodes coordinated by hemilabile phosphino–thioether (P,S) ligands appended with pyridine coordinating groups (P,S–pyr, **22**).

The P,S–pyr ligand (**22**) was synthesized from commercially available 4-mercaptopyridine (**21**) and (2-chloroethyl)diphenylphosphine precursor **20**, according to a modified literature procedure from previously reported compounds (Scheme 5.1A).[47, 66, 69, 89-90] The pyridine moiety has a moderately high binding affinity ($K_a \sim 10^4$) with Cu^{II} ions,[168-169] and is less sterically hindered than the previously reported terpyridine WLA system. These features were attractive for investigating how binding affinity and steric bulk, affect the chemical and physical properties of coordination polymer materials assembled with stimuli-responsive subunits. Two equivalents of ligand **22** were then reacted with one equivalent of tetrakis(acetonitrile)palladium(II) tetrafluoroborate ($Pd(MeCN)(BF_4)_2$) in a solution of dichloromethane (CH_2Cl_2) and methanol (MeOH) to yield complex **23** (Scheme 5.1B) in nearly quantitative yield. The polar solvent drives the formation of a closed complex, whereby the counter ions are outer sphere.

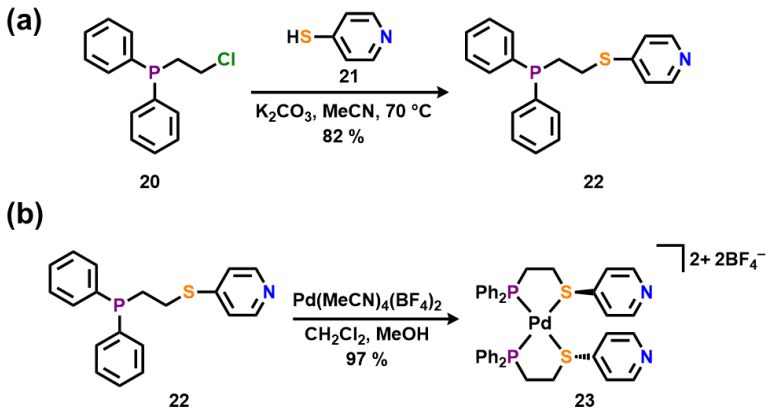

Scheme 5.1 Synthesis of (A) hemilabile P,S–Pyr ligand (**22**) and (B) WLA complex **23**.

The molecular structure of **23** was studied in solution by ^{1}H and ^{31}P NMR spectroscopies and high-resolution electrospray ionization mass spectrometry (HR-ESI-MS) and in the solid-state by single crystal X-ray diffraction. The ^{1}H and ^{31}P NMR spectra provide evidence supporting the clean formation of a fully closed complex (**23**), as the ^{31}P NMR resonance at ~64 ppm, is highly diagnostic of a fully closed complex in which the P,S-pyr ligands are fully chelated to the Pd^{II} metal node. Interestingly, when complex **23** is dissolved only in the non-polar solvent dichloromethane, the closed complex rapidly switches to the fully open state. This is evidenced by the single ^{31}P resonance that appears at ~15 ppm.

5.2.2.2 Synthesis of the Crystalline Coordination Polymer Chain (24)

In order to form soluble CP precursors, closed complex **23** was initially dissolved in acetonitrile (CH_3CN) and treated with one equivalent of $Cu^{II}(BF_4)_2 \cdot 6H_2O$ in order to polymerize the pyridine end groups. The monomers rapidly polymerize to form the coordination polymer **24** (Scheme 5.2a). To further study the polymerization behavior of **23** in the solution state, we turned to ^{1}H NMR spectroscopy titration studies. A stock solution of $Cu^{II}(BF_4)_2 \cdot 6H_2O$ and complex **23**, were prepared in methanol in order to maintain the closed structural state of **23**. $Cu^{II}(BF_4)_2 \cdot 6H_2O$

was then slowly titrated into a solution of **23**, and the ^{1}H NMR spectrum collected from zero to one equivalent of $Cu^{II}(BF_4)_2 \cdot 6H_2O$ (Figure 5.4a–f).

The ^{1}H NMR spectrum of **23** at zero equivalents (Figure 5.4a) exhibited relatively narrow peaks, representative of a molecular species possessing equivalent protons. As the concentration of $Cu^{II}(BF_4)_2 \cdot 6H_2O$ increases with increasing equivalents added, the ^{1}H NMR spectrum of significantly broadens. This broadening is highly representative of a polymeric species in which non-equivalent protons are present in similar environments.

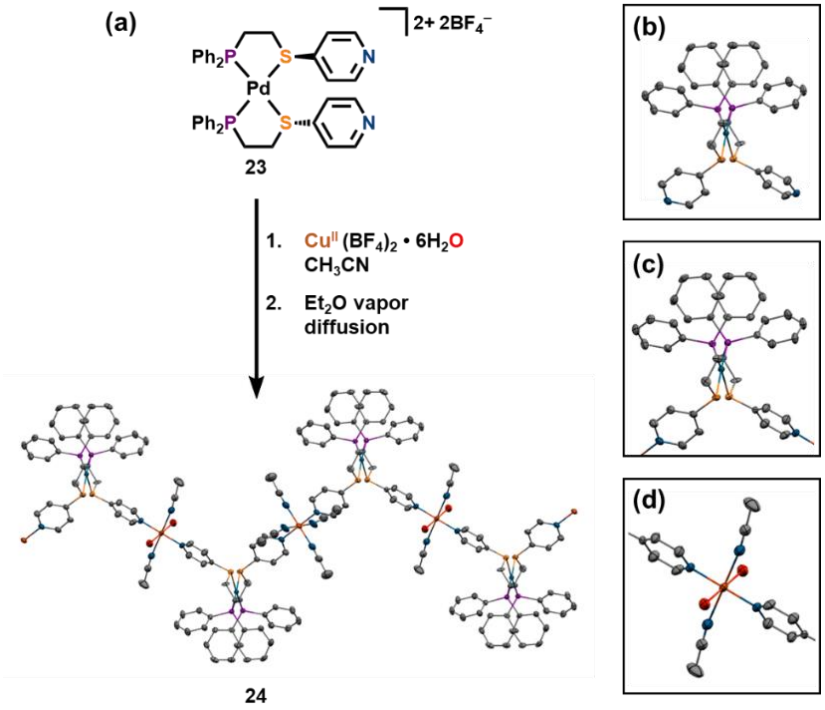

Scheme 5.2 (a) Reaction of $Cu^{II}(BF_4)_2 \cdot 6H_2O$ with the Pd^{II} monomer (**23**) in MeCN to give the compound [(P,S–pyr)[Cu(OH)$_2$--(MeCN)$_2$--] (**24**). (b) Crystal structure of the tweezer monomers, and (c) the coordination mode of the monomers within the coordination polymer, and (d) the coordination mode of the Cu^{II} metal node within the coordination polymer. Drawn with a 50% thermal ellipsoid probability. Solvent molecules and hydrogen atoms have been omitted for clarity.

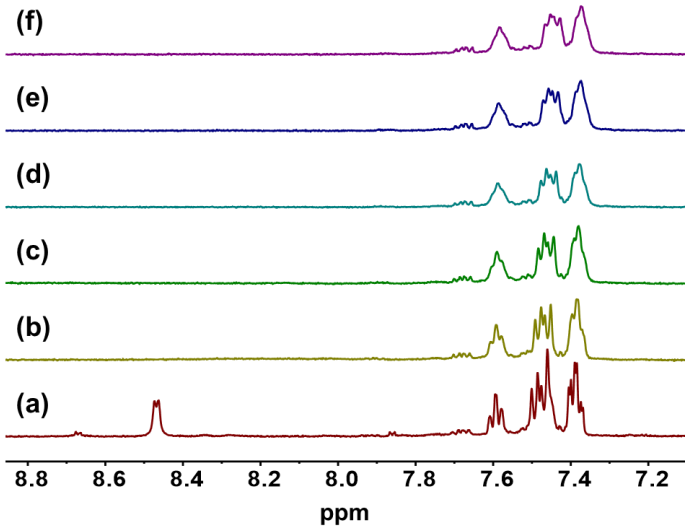

Figure 5.4 ^{1}H NMR titration of **23** with $Cu^{II}(BF_4)_2 \bullet 6H_2O$ in methanol at (a) 0.0 equiv., (b) 0.2 equiv., (c) 0.4 equiv., (d) 0.6 equiv., (e) 0.8 equiv. and (f) 1.0 equiv. of $Cu^{II}(BF_4)_2 \bullet 6H_2O$.

5.2.3 The Solid-State Structure of Coordination Polymer 24

Single crystals of polymer **24** were obtained by preparing a solution of coordination polymer **23** and a 0.42 mM solution of of $Cu^{II}(BF_4)_2 \bullet 6H_2O$ in a mixed solution of DCM and methanol (solutions were prepared in a 1:1 ratio), and slowly diffusing ether into the prepared solution (Figure 5.2 and 5.5).

Interestingly, the N–Pd–N dihedral angle formed by the monomers within the coordination polymer measures to be about 90°. This angle, in addition to the relatively little steric bulk of the pyridine ligand, favor the formation of crystalline polymer chains, whereby the copper metal node within the coordination polymer forms a nearly 180° dihedral angle (Figure 5.2 c and d). The 90° angle formed about the Pd^{II} metal nodes, in conjunction with the 180° dihedral angle formed about the Cu^{II} metal nodes, results in a distinct alternating crystal packing (Figure 5.5). Additionally, the N–Cu distance at the copper metal node, measure to be about 1.990 Å.

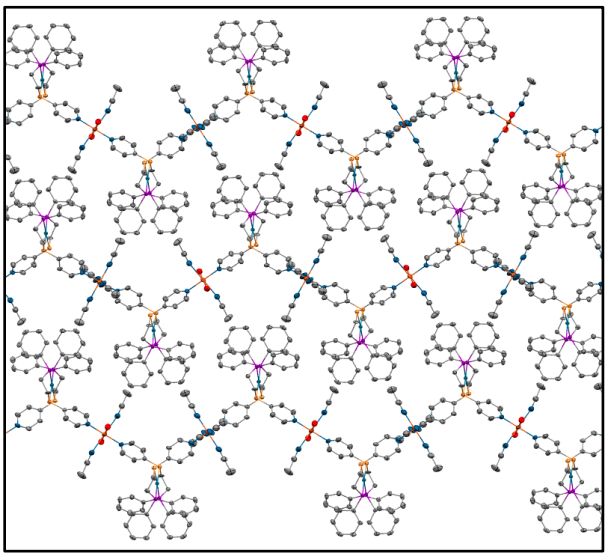

Figure 5.5 Packing of crystalline 1-D coordination polymer (**24**) bearing $Pd(P,S–Pyridine)_2(BF_4)_2$ monomers. Drawn with a 50% thermal ellipsoid probability. Solvent molecules and hydrogen atoms have been omitted for clarity.

5.2.4 Formation of Coordination Polymers Composed of Monomer 23 and Pt^{II} Metal Salts

In order to better understand the assembly conditions and dynamics of **23**, we sought to polymerize monomer **23** in the presence of other metal ions such as Pt^{II} (Scheme 5.3). We hypothesized that the geometry about the secondary metal node would affect the assembly behavior and morphology of the resulting material. Upon addition of *cis*-bis(benzonitrile)dichloroplatinum(II), WLA-based coordination polymers formed via coordination of the pyridine moieties with the Pt^{II} metal nodes. Despite many attempts to grow single crystals suitable for X-ray diffraction of the resulting coordination polymer, only amorphous coordination polymer particles formed upon the slow diffusion of ether into a concentrated solution of coordination polymer. The polymerization of 23 in the presence of 25 was studied using ^{1}H and ^{31}P NMR spectorscopies and the resulting coordination polymer particles were characterized by

electron microscopy (Scheme 5.3). The STEM images revealed the formation of spherical particles 1-2 μm in diameter.

In a separate experiment, we also investigated the assembly behavior and resulting properties of the same system in the presence of Fe^{II}. We again found that crystalline chains could not be obtained and hypothesized that this may be the case due to the size of the iron metal node and the geometry resulting from the pyridine coordination. Studies are still underway, investigating the polymeric structure.

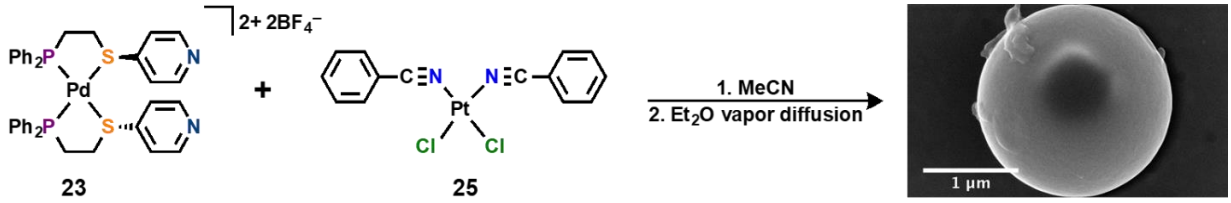

Scheme 5.3 Formation of CP particles bearing complex **23** building blocks polymerized in the presence of Pt^{II} salt **25**.

5.2.5 Structural Studies of Pt^{II} Tweezer Monomer Analogs

In light of the crystalline nature of the Pd^{II} tweezers polymerized with Cu^{II}, we were interested in the molecular structure and assembly behavior of Pt^{II} analogs, and therefore sought to generate the open and closed Pt^{II} tweezer complexes that matched the Pd^{II} system. Fully open Pt^{II} tweezer complex **26** was synthesized in an identical method to the Pd^{II} derivative, however, a Pt^{II} salt was used in place of the Pd^{II} salt. The structure and geometry of the fully open complex (**26**) was confirmed in solution by ^{1}H and ^{31}P NMR spectroscopies and high-resolution electrospray ionization mass spectrometry and in the solid-state by single crystal X-ray diffraction. Interestingly, single crystals suitable for X-ray diffraction could not be readily obtained for the

Pd^{II} fully open complex, however, crystals of the fully open Pt^{II} can be readily obtained by slow vapor diffusion (Figure 5.6).

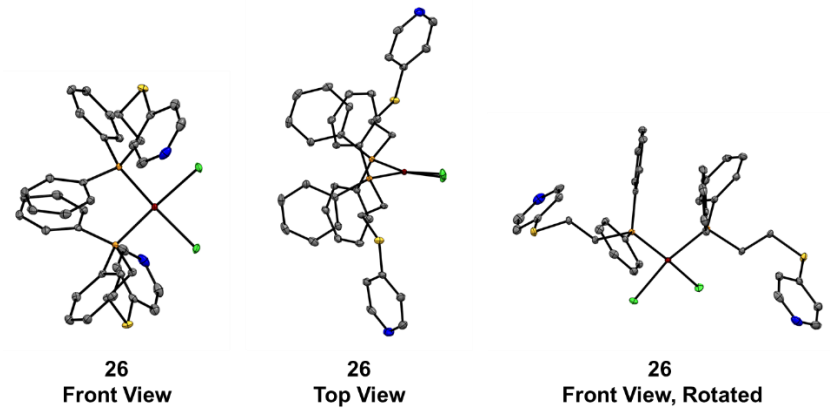

Figure 5.6 Crystal structure of fully open complex **26**, drawn with a 50% thermal ellipsoid probability. Solvent molecules and hydrogen atoms have been omitted for clarity.

5.3 Conclusions

The construction of stimuli-responsive soft materials requires non-covalent interactions that are both specific and directional to ensure that the required molecular assembly forms as intended, and that the assembly is reversible. Herein, we demonstrated the design and synthesis of stimuli-responsive coordination polymers bearing WLA subunits. Importantly, we have showed that the incorporation of switchable molecular motifs embedded within ICPs can control morphology and chemical properties, such as absorbance and fluorescence, whereby one structure can access a crystalline, single chain phase, or an amorphous, multi-chain phase. Such structures may lead to new motifs that may have applications in the area of chemical sensing where molecularly triggered events can lead to changes in macroscopic properties that affect signaling.

5.4 Experimental Methods

5.4.1 General Methods

All chemicals were purchased from Sigma-Aldrich or Fisher Scientific and used without further purification, unless otherwise stated. (2-chloroethyl)diphenylphosphine[138] (**20**) and diphenyl((4-pyridyl)thioethyl)phosphine, ligand **22**[139], were synthesized according to literature procedures. Solvents were purchased anhydrous and degassed under a stream of argon prior to use. Flash chromatography was performed using SiliaFlash F60 SiO_2 (230–400 mesh ASTM, 0.040–0.063 mm; SiliCycle). Deuterated solvents were purchased from Cambridge Isotope Laboratories and used as received. ^{1}H and $^{31}P\{^{1}H\}$ NMR spectra were recorded on a Bruker Avance 400 MHz. ^{1}H NMR spectra were referenced to residual proton resonances (CD_2Cl_2 = δ 5.32; CD_3CN = δ 1.94) in the deuterated solvents. ^{13}C NMR spectra were referenced to the solvent peak (CD_2Cl_2 = δ 53.84; CD_3CN = δ 1.32 and 118.26) and $^{31}P\{^{1}H\}$ NMR spectra were referenced to an 85% H_3PO_4 aqueous solution. All chemical shifts are reported in ppm. High resolution mass spectra measurements (HR-MS) were recorded on an Agilent 6120 LC-TOF instrument in positive ion mode. Transmission electron microscopy (TEM) imaging and energy dispersive X-ray data were performed and collected on a Hitachi HD-2300 STEM microscope operating at 200 kV, equipped with two Thermo Scientific Energy Dispersive X-ray (EDX) detectors. TEM samples were prepared by drop-casting a 5 μL Et_2O solution of particles onto a carbon-coated Cu TEM grid (Ted Pella). Single crystals suitable for X-ray diffraction studies were mounted using oil (Infineum V8512) on a glass fiber. All measurements were made on a CCD area detector with graphite monochromated Mo Kα or Cu Kα radiation. Data were collected using Bruker APEXII detector and processed using APEX2 from Bruker. Dynamic light scattering (DLS) data were collected using a Zetasizer

Nano ZS (Malvern Instruments Ltd). All XRD structures were solved by direct methods and expanded using Fourier techniques. The non-hydrogen atoms were refined anisotropically. Hydrogen atoms were included in idealized positions, but not refined. Their positions were constrained relative to their parent atom.

5.4.2 Synthesis

5.4.2.1 Synthesis of Hemilabile P,S–Pyr Ligand (22)

Diphenyl((4-pyridyl)thioethyl)phosphine, ligand **22**[139], was synthesized according to literature procedures. In a glovebox under inert atmosphere, 4-mercaptopyridine (**21**) was dissolved in 7 mL MeCN in a flask equipped with a stir bar. Potassium carbonate (150 mg, 1.34 mmol) was dissolved in 2 mL of MeCN and the solution was added slowly to **21** while stirring rapidly. (2-chloroethyl)diphenylphosphine (367 mg, 1.47 mmol) was then added as a solid and the vial was sealed, removed from the glovebox, and allowed to stir at 70 °C overnight. The solution was cooled, then passed through a short plug of neutral alumina, which was washed with an additional 50 mL of CH_2Cl_2. The solvent was removed under reduced pressure and the residue was recrystallized from CH_2Cl_2/EtOH to give **22** as fine white needles in 82 % yield. ^{1}H NMR (500 MHz, Methylene Chloride-d_2) δ 8.56 – 8.42 (m, 1H), 7.50 – 7.31 (m, 5H), 7.21 – 7.09 (m, 1H), 3.68 (s, 1H), 2.59 – 2.43 (m, 1H), 2.42 – 2.25 (m, 1H). ^{31}P NMR (162 MHz, Methylene Chloride-d_2) δ -17.35. ^{13}C NMR (101 MHz, Methylene Chloride- d_2) δ 149.87, 149.83, 147.40, 132.70, 132.51, 128.76, 128.54, 128.47, 123.80, 123.74, 35.13, 35.04, 34.95, 28.25, 27.90, 27.69.

5.4.2.2 Synthesis of $Pd(P,S–Pyridine)_2(BF_4)_2$ (23)

Tetrakis(acetonitrile)palladium(II) tetrafluoroborate ($Pd(MeCN)_4(BF_4)_2$) was weighed into a 6 mL vial with a stir bar and 2 mL of a 1:1 mixture of MeOH / CH_2Cl_2 was added. A solution of **22**, dissolved in 2 mL of the same 1:1 mixture of MeOH / CH_2Cl_2, was prepared and added dropwise to the mixture containing $Pd(MeCN)_4(BF_4)_2$ while stirring. After 10 min, the homogenous clear solution was evaporated under reduced pressure to a minimal volume and Et_2O was added to precipitate a white solid in quantitative yield. ^{1}H NMR (400 MHz, Acetonitrile-d_3) δ 8.64 (s, 2H), 7.63 (dt, J = 7.4, 4.0 Hz, 2H), 7.50 – 7.35 (m, 7H), 2.17 (s, 0H). ^{31}P NMR (162 MHz, Acetonitrile-d_3) δ 63.78.

5.4.2.3 Synthesis of Coordination Polymer 24

In order to form soluble CP precursors, closed complex **23** was initially dissolved in acetonitrile (CH_3CN) and treated with one equivalent of $Cu^{II}(BF_4)_2 \cdot 6H_2O$ in order to polymerize the pyridine end groups. The prepared $Fe(BF_4)_2 \cdot 6H_2O$ solution was then added to a solution of **23** in CD_3CN until a 1:1 molar ratio was achieved. ^{1}H NMR (500 MHz, Methanol-d_4) δ 7.58 (s, 2H), 7.51 (s, 1H), 7.44 (d, J = 12.1 Hz, 1H), 7.37 (s, 5H), 3.11 (s, 4H), 2.15 (s, 4H), 1.33 (s, 2H), 1.29 (d, J = 4.2 Hz, 1H).

5.4.2.4 Synthesis of $Pt(P,S–Pyridine)_2Cl_2$

^{1}H NMR (400 MHz, Methylene Chloride-d_2) δ 8.59 – 8.51 (m, 1H), 7.55 – 7.38 (m, 4H), 7.38 – 7.29 (m, 2H), 5.37 (s, 2H), 4.55 (s, 1H), 3.11 (s, 1H), 2.68 – 2.59 (m, 0H). ^{31}P NMR (162 MHz, Methylene Chloride-d_2) δ 50.97, 39.79, 28.61.

5.4.3 Opening the Fully Closed Pd^{II} Complex 23

The fully open Pd^{II} monomer complex was accessed by dissolving monomer **23** in dichloromethane. The formation of a fully open complex is observed in the ^{31}P NMR spectrum with the appearance of a peak at 15.34 ppm. In less polar solvent (DCM), complex **23** is stabilized with two inner sphere chlorides, rendering the overall complex neutral in charge. In slightly more polar solvent (methanol), the complex is stabilized as the fully closed complex with two outer-sphere chlorides.

5.4.3 NMR Spectra of all Complexes

^{1}H, ^{31}P{1H} and ^{13}C NMR Spectra of P,S-Pyr Ligand 22

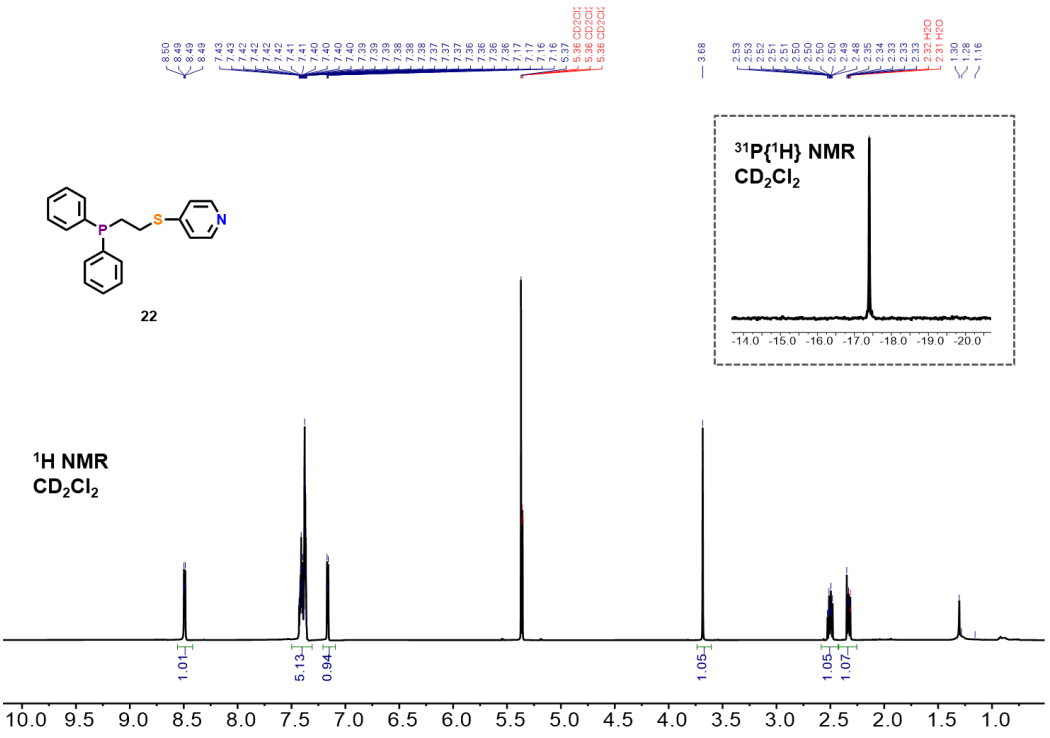

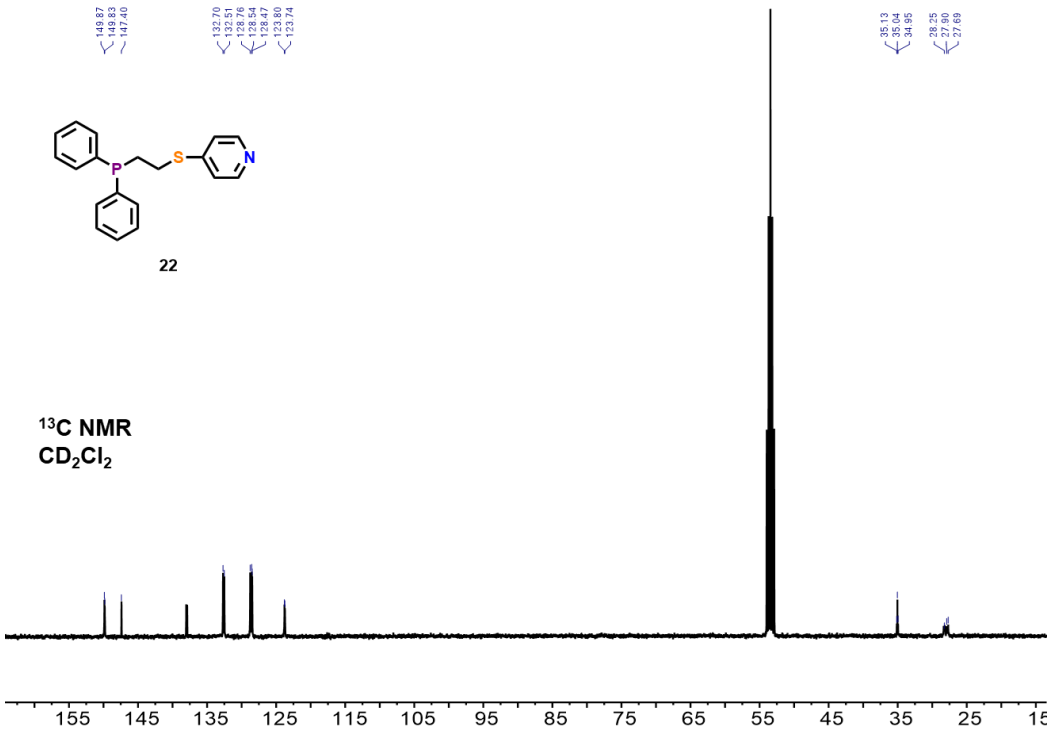

^{1}H and ^{31}P{1H} NMR Spectra of Pd(P,S–Pyridine)$_2$(BF$_4$)$_2$ (23)

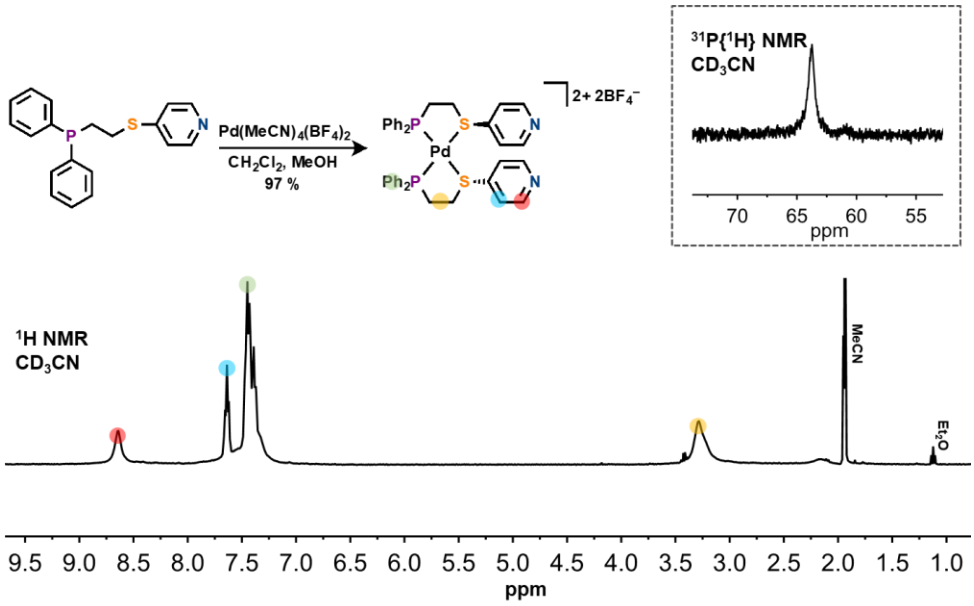

^{1}H and $^{31}P\{1H\}$ NMR Spectra of the Open Monomer $Pt(P,S–Pyridine)_2Cl_2$

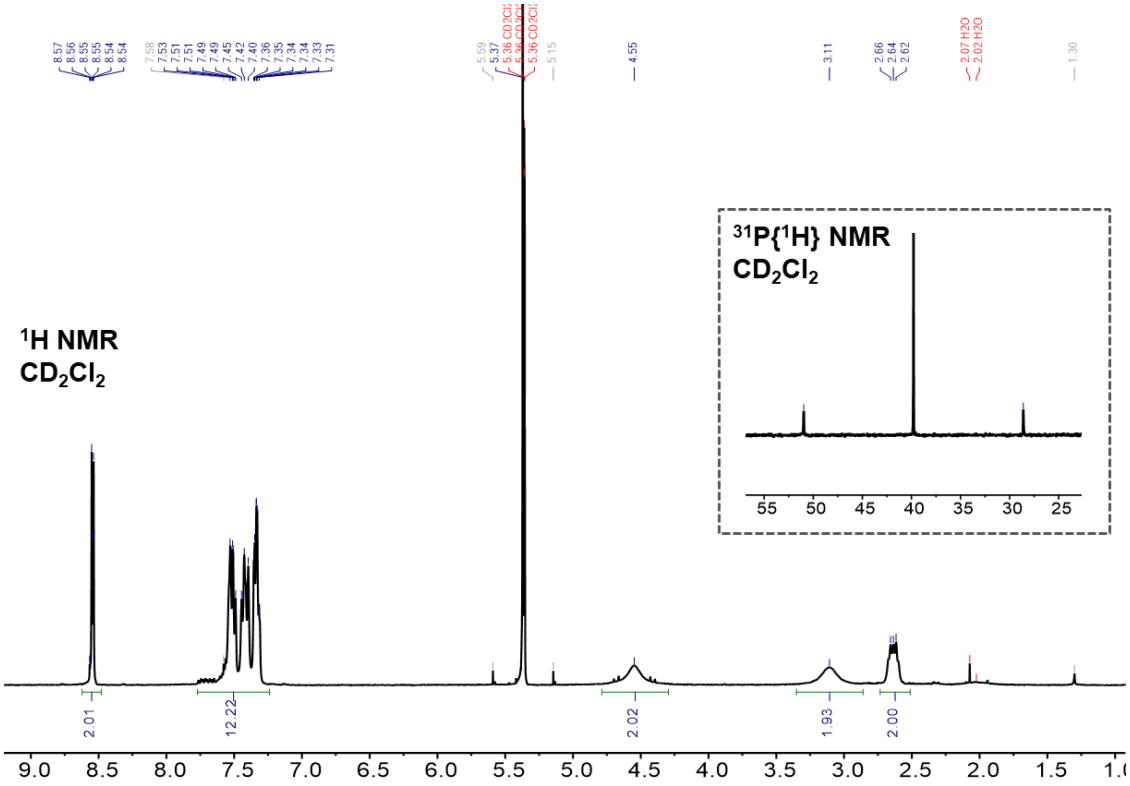

5.4.5 X-Ray Crystal Data

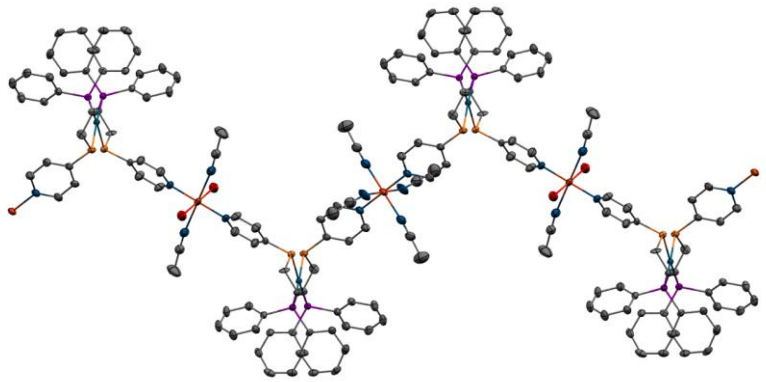

Table 5.1 Crystallographic Data for Coordination Polymer **24**

Identification code	cx0759
Empirical formula	$C_{46}H_{50}B_4CuF_{16}N_6O_2P_2PdS_2$
Formula weight	1362.16
Temperature / K	100.09
Crystal system	monoclinic
Space group	P21/n
a / Å, b / Å, c / Å	13.3903(4), 30.8825(9), 14.3575(4)
α/°, β/°, γ/°	90, 106.5840(15), 90
Volume / Å3	5690.2(3)
Z	4
ρcalc / mg mm-3	1.590
μ / mm-1	0.915
F(000)	2740
Crystal size / mm3	0.181 × 0.067 × 0.024
2Θ range for data collection	3.24 to 56.822°
Index ranges	$-17 \leq h \leq 17$, $-35 \leq k \leq 41$, $-19 \leq l \leq 19$
Reflections collected	76641
Independent reflections	14219[R(int) = 0.0565]

Data/restraints/parameters	14219/141/741
Goodness-of-fit on F2	1.050
Final R indexes [I>2σ (I)]	R1 = 0.0720, wR2 = 0.1879
Final R indexes [all data]	R1 = 0.1164, wR2 = 0.2033
Largest diff. peak/hole / e Å-3	1.332/-1.150

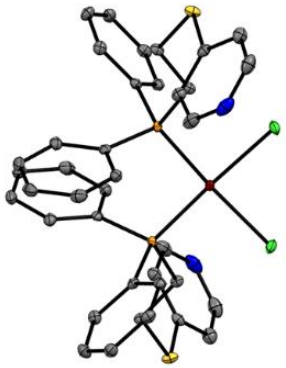

Table 5.2 Crystallographic Data for Fully Open Monomer Pt(P,S–Pyridine)$_2$Cl$_2$ (**25**)

Empirical formula	$C_{42}H_{46}Cl_4N_2OP_2PtS_2$
Formula weight	1057.76
Temperature / K	99.96
Crystal system	triclinic
Space group	P-1
a / Å, b / Å, c / Å	9.8446(5), 10.6104(5), 21.0355(10)
α/°, β/°, γ/°	83.095(4), 79.268(4), 84.615(4)
Volume / Å^3	2137.42(18)
Z	2
ρ_{calc} / mg mm^{-3}	1.644
μ / mm^{-1}	10.341
F(000)	1056

Crystal size / mm^3	0.147 × 0.046 × 0.004
2Θ range for data collection	8.416 to 130.966°
Index ranges	$-8 \leq h \leq 11$, $-12 \leq k \leq 12$, $-24 \leq l \leq 24$
Reflections collected	15128
Independent reflections	7105[R(int) = 0.0844]
Data/restraints/parameters	7105/0/490
Goodness-of-fit on F^2	1.050
Final R indexes [I>2σ (I)]	R_1 = 0.0510, wR_2 = 0.1287
Final R indexes [all data]	R_1 = 0.0734, wR_2 = 0.1364
Largest diff. peak/hole / e $Å^{-3}$	5.177/-1.479

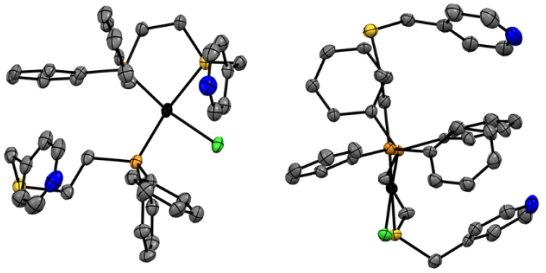

Pt–Methylpyr–Open Front View **Pt–Methylpyr–Open Side View**

Table 5.3 Crystallographic Data for Semi-Open Pt^{II} Monomer

Identification code	cx0695
Empirical formula	$C_{42}H_{46}Cl_4N_2OP_2PtS_2$
Formula weight	1057.76
Temperature / K	99.96
Crystal system	triclinic
Space group	P-1
a / Å, b / Å, c / Å	9.8446(5), 10.6104(5), 21.0355(10)
α/°, β/°, γ/°	83.095(4), 79.268(4), 84.615(4)

Volume / $Å^3$	2137.42(18)
Z	2
ρ_{calc} / mg mm^{-3}	1.644
μ / mm^{-1}	10.341
F(000)	1056
Crystal size / mm^3	0.147 × 0.046 × 0.004
2Θ range for data collection	8.416 to 130.966°
Index ranges	$-8 \leq h \leq 11$, $-12 \leq k \leq 12$, $-24 \leq l \leq 24$
Reflections collected	15128
Independent reflections	7105[R(int) = 0.0844]
Data/restraints/parameters	7105/0/490
Goodness-of-fit on F^2	1.050
Final R indexes [I>2σ (I)]	R_1 = 0.0510, wR_2 = 0.1287
Final R indexes [all data]	R_1 = 0.0734, wR_2 = 0.1364
Largest diff. peak/hole / e $Å^{-3}$	5.177/-1.479

5.4.6 Computational Details

DFT calculations were performed using the Amsterdam Density Functional (ADF2013.01) suite on a 16-core Parallel Quantum Solutions (PQS) computational cluster. The model for complex **23** and **24**, were built ignoring counter anions and assuming only local charge arising from the Pt(II) metal center. Geometry optimizations were made without restraints in the ADF GUI including all electrons and using the generalized gradient approximation method (GGA) with basis sets containing triple-ζ functions with two polarization function (TZ2P), and the local density approximations of Becke, Perdew and Ernzerhof (PBE)[140]. Scalar relativistic effects were taken into consideration for heavy Pt(II) atoms.

CHAPTER 6

Dissertation Overview and Future Outlook

6.1 Dissertation Overview

Orchestrating the dynamic assembly of complex protein subunits, requires many relatively weak non-covalent, intermolecular interactions. Nature's ability to assemble life's most formidable machines—proteins—therefore, relies on supramolecular assembly. Supramolecular assembly is the basis of forming various complex biological superstructures, such as double-stranded DNA, three-dimensionally folded proteins, and biologically active cell membranes, that are integral for life. In all of these cases, molecular recognition is key to forming precise and selective interactions with other molecular entities, which enable proteins' highly complex three-dimensional surfaces and architectures. These interactions include correct pairing between hydrogen bond donors/acceptors, electrostatic forces, induced interactions, and the hydrophobic effect, among others. Each interaction works in concert with the many other weak interactions, to form the chemically and functionally diverse proteins ubiquitous in Nature.

In this way, Nature has inspired chemists to develop abiotic systems that incorporate such supramolecular interactions, with the goal of designing the next generation of sensors, catalysts and drug-delivery vehicles. Importantly, Nature has helped lay the foundation for two fundamental concepts in supramolecular chemistry: complementarity and preorganization. Strong binding between a host and a guest occurs when there is a good match of guest shape and host binding site (complementarity), and when this match is achieved with little conformational rearrangement (preorganization), resulting in attractive pairwise interactions between host and guest. These concepts have tremendous implications on a structure's function, properties and assembly kinetics and thermodynamics. As such, developing a fundamental understanding of the molecular-level

interactions in such systems is key to understanding supramolecular assembly and resulting properties.

Supramolecular assembly has emerged as a particularly useful approach for the bottom-up assembly of nanoscale materials where a wide variety of morphologies can be achieved either in bulk or in solution ranging from cylinders and spheres to micelles and vesicles.[170] Among the different approaches, the WLA is a powerful method for synthesizing complexes that can undergo reversible, small-molecule-induced structural changes and therefore be toggled between a "closed" rigid state and an "open" flexible state. Through the modular and convergent assembly of metal ions and multidentate hemilabile ligands, the WLA provides a platform to deliberately engineer molecular selectivity and stimuli-responsiveness into supramolecular complexes. WLA-based supramolecular systems are attractive as they offer 1) chemical access to multiple structural states with tailorable selectivity and binding affinities, 2) high functional group tolerance, and 3) modularity, including access to structures with a wide variety of metal nodes and ligand types. A number of stimuli-responsive systems have been developed based on this platform, through the incorporation of catalytic, redox-active, and host−guest recognition sites into the ligands in such a way that small-molecule-induced structural changes result in marked changes in the physical or chemical properties of these complexes.

This dissertation summarizes a generalizable supramolecular coordination-based approach to the synthesis of supramolecular coordination constructs possessing switchable properties. This work represents a major advance in the design and synthesis of biomimetic constructs with promise in the fields of drug delivery, molecular sensing, chemical separations, and catalysis. Specifically, the Weak-Link Approach to supramolecular chemistry was utilized to assemble such constructs,

owing to its modular and tailorable nature. The WLA enables one to modulate conformational changes in organometallic structures through the use of small molecule effectors, rendering them allosterically regulated.

6.2 Summary and Conclusions

Macrocycles capable of host−guest chemistry are an important class of structures that have attracted considerable attention because of their utility in chemical separations, analyte sensing, signal amplification, and drug delivery. The deliberate design and synthesis of such structures are rate-limiting steps in utilizing them for such applications, and coordination-driven supramolecular chemistry has emerged as a promising tool for rapidly making large classes of such systems with attractive molecular recognition capabilities and, in certain cases, catalytic properties. A particularly promising subset of such systems are stimuli-responsive constructs made from hemilabile ligands via the weak-link approach (WLA) to supramolecular coordination chemistry. Such structures can be reversibly toggled between different shapes, sizes, and charges based upon small-molecule and elemental-anion chemical effectors. In doing so, one can deliberately change their recognition properties and both stoichiometric and catalytic chemistries, thereby providing mimics of allosteric enzymes. The design and synthesis of a new allosterically regulated four-state macrocycle was assembled via the WLA in Chapter 2. The target structure was made via the stepwise assembly of ditopic bidentate hemilabile N-heterocyclic carbene thioether (NHC,S) and phosphino thioether (P,S) ligands at Pt^{II} metal nodes. The relatively simple macrocycle displays complex dynamic behavior, which was explored in Chapter 3. When addressed with small-molecule effectors, the macrocycle undergoes structural switching which can be achieved with several distinct molecular cues (Figure 6.1). Importantly, each state was fully characterized by

multinuclear NMR spectroscopy and, in some cases, single-crystal X-ray diffraction studies and density functional theory computational models.

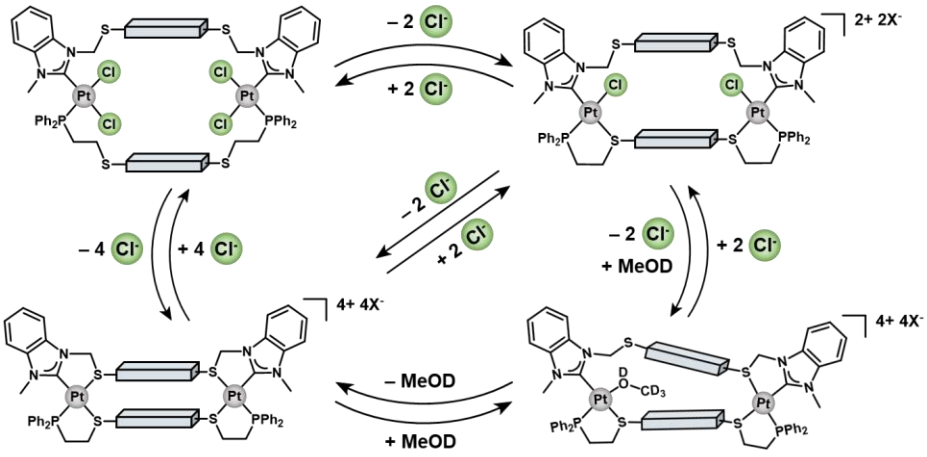

Figure 6.1 An allosterically-regulated macrocycle capable of reversibly accessing four distinct structural states, assembled via the WLA.

In summary, this work details the design, synthesis, and characterization of a multi-state WLA macrocycle bearing hemilabile *N*-heterocyclic carbene-thioether (NHC,S) and phosphino-thioether (P,S) ligands. We demonstrated: (i) the synthesis and characterization of a new class of hemilabile ligands—specifically, a more strongly chelating bi-bidentate NHC,S ligand, (ii) the incorporation of this ligand into a Pt(II) heteroligated macrocycle and (iii) the Pt(II) macrocycle was shown to not undergo dynamic ligand scrambling—as is seen in typical P,S based WLA Pt(II) systems. With this Pt^{II} WLA macrocycle, we can access four distinct reversible configurational states, distinguishing it from classical two- and three-state WLA complexes. Specifically, through small molecule and elemental anion reactions at the Pt^{II} metal nodes, we are able to control the complex geometries in the open, semi-open, mixed semi-open/fully closed, and fully closed states.

Furthermore, we thoroughly investigate the *cis/trans* isomers present in different states via spectroscopic and computational methods and study the intramolecular forces involved in the overall formation of each state. Ultimately, this class of WLA complexes may be used in the construction of functional supramolecular architectures, such as molecular capsules and receptors, and can even be thought of in terms of a multi-state switch. Work on related supramolecular host-guest capsules containing NHC,S ligands, for applications in sensing and encapsulation, is underway.

Chapter 4 details the design, synthesis, and characterization of a new class of Infinite Coordination Polymer Particles (ICPs) bearing Weak-Link Approach (WLA)-based building blocks. Infinite coordination polymer particles are organic-inorganic hybrid materials in which repeating ligand units are connected *via* metal ion nodes into one-, two-, or three-dimensional structures. Interest in ICPs stems from their modularity, ease in which organic components can be interchanged within them, and how changes in molecular structure can result in changes in porosities, as well as catalytic, biological, and spectroscopic properties. While this broad class of materials encompasses polymers with regular repeat units, such as crystalline metal-organic frameworks (MOFs) and other nano or porous coordination polymers (NCPs or PCPs), the scope of ICPs is not limited to crystalline materials. The ability to assume an amorphous state enables the formation of nano- and micron-sized particles where shape is not dictated by crystal packing forces but instead by the interfacial free energy between the particles and the solvent.

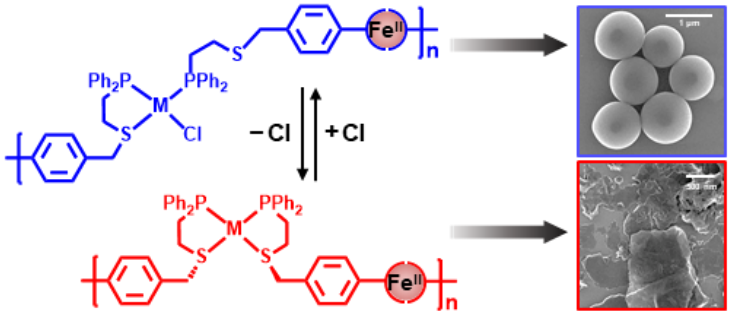

Figure 6.2 A new class of infinite coordination polymer particles bearing Weak-Link Approach subunits can be chemically addressed in the solution phase with small molecule effectors. Through the introduction or abstraction of anions, the local geometry of the metal subunits can be controlled, manifested by macroscopic morphological changes in the polymer particles.

In Chapter 5 we explore a family of ICP particles that was synthesized by the assembly of modular Weak-Link Approach-based coordination chemistry construct building-blocks. Chloride ions can be used to chemically interconvert these building blocks between rigid, closed and flexible, semi-open states either pre- or post-polymerization. These changes in molecular geometry manifest themselves as morphological changes in the ICP particles. Furthermore, scanning transmission electron microscopy, energy-dispersive X-ray spectroscopy, and dynamic light scattering data suggest that the resulting particle morphology is highly dependent not only on the structure of the soluble precursors but also on the bond strengths and the dissociation kinetics of the metal-ligand coordination bonds in the polymer chain. This work shows how stimuli-responsive systems can be used to modulate the properties of ICPs, which is important in chemical sensing, where molecularly triggered events lead to changes in macroscopic properties that affect signaling.

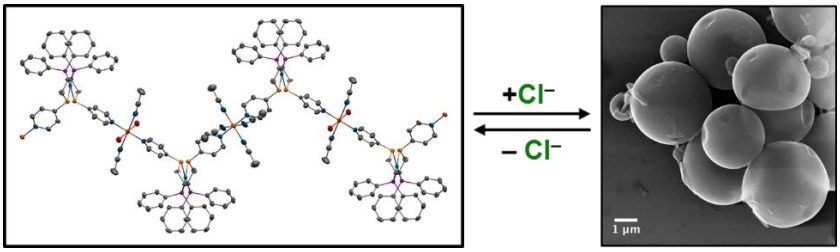

Figure 6.3 ICP particles synthesized by the assembly of modular Weak-Link Approach-based coordination chemistry construct building-blocks, capable of undergoing morphological changes.

When taken together, this work has expanded the scope of supramolecular WLA constructs by leveraging their stimuli-responsive properties for incorporation into macrocyclic constructs and nanoscale materials. Work towards developing these constructs and materials occurred through three main research projects. 1) We sought to enhance the structural and functional complexity of the WLA constructs by developing WLA macrocycles and receptors using a step-wise assembly approach for stimuli-responsive and programmable molecular receptors. This work builds upon our previously reported foundation for synthesizing structurally sophisticated heteroligated macrocycles, which can be readily modified with a variety of functional motifs. 2) We worked towards understanding how to induce changes in the coordination and structural states of WLA constructs using a broad range of stimuli. 3) We aimed to develop stimuli-responsive materials for applications in sensing, drug delivery, and remediation. Work towards this goal resulted in the design, synthesis, and assembly of stimuli-responsive building blocks, which can be incorporated into coordination polymers.

6.3 Future Directions

Moving forward, we seek to push the boundaries of this work by developing more sophisticated molecular sensors which can bind guests with high affinity and specificity. Additionally, we are working to develop methods for regulating such constructs with new kinds

of stimuli. Finally, we hope to expand upon the work detailed in Chapters 4 and 5 of this dissertation and develop functional responsive nanomaterials possessing stimuli-responsive building blocks.

6.3.1 Towards a Library of Allosteric, Multi-State Receptors

In order to expand the library of stimuli-responsive macrocycles and receptors accessible by the WLA, we have sought to develop receptors with varying sizes, functional groups, and properties. Work towards this goal has resulted in the synthesis of a library of highly tunable hemilabile ligands for the assembly of stimuli-responsive, multi-state WLA receptors. The structures were prepared via the stepwise assembly NHC,S and P,S ligands at Pt^{II} metal nodes, as previously reported by our group (Figure 6.4).

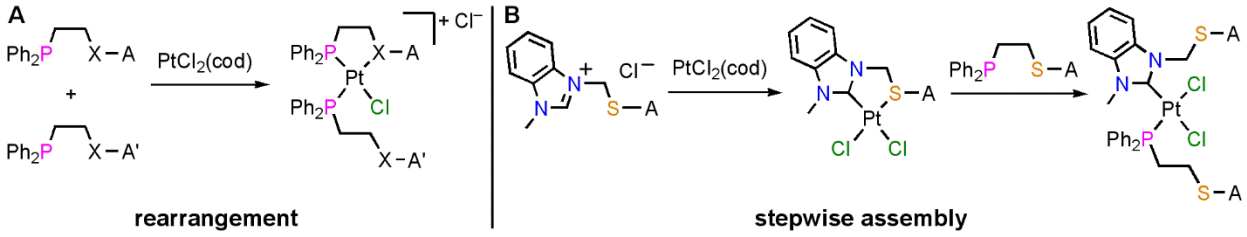

Scheme 6.1 a) Heteroligated Pt^{II} WLA complexes traditionally synthesized *via* the halide-induced ligand rearrangement reaction in which differences in electron density at the "weak-link" (chalcoether or amine) controls heteroligated complex formation; A ≠ A′. b) The step-wise approach leverages a strong ligand–metal interaction (NHC–Pt^{II}) in order to assemble asymmetric WLA systems where the relative donating abilities of the "weak links" are not important

We sought to build upon our previous work on the design and synthesis of a heteroligated multi-state macrocycle, to access larger macrocyclic host architectures. Expanding macrocyclic cavity size in a two-component system enables us to encapsulate larger guest molecules and incorporate more recognition motifs. To achieve this goal, we designed and synthesized longer P,S and NHC,S ligands by incorporating a biphenyl spacer (Scheme 6.2). The structure was fully characterized by ^{1}H NMR spectroscopy (Figure 6. 4) and HR-MS.

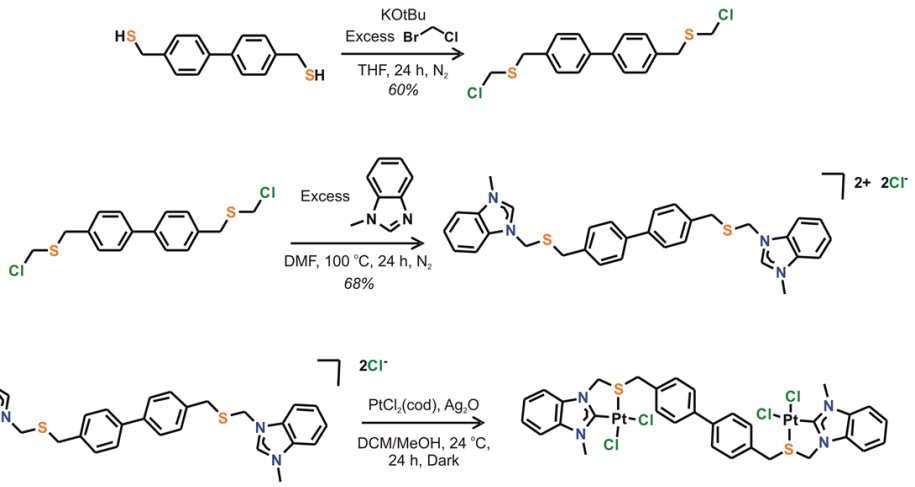

Scheme 6.2 Synthesis of an extended NHS,S-based ligand for the construction of larger, two-component macrocycles

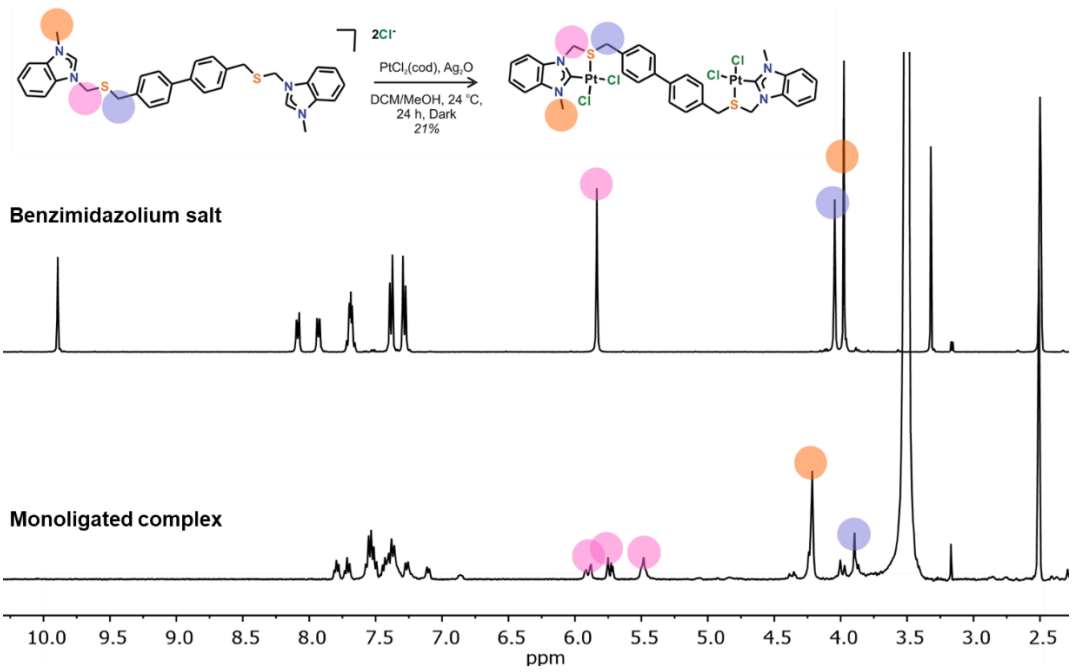

Figure 6.4 Characterization of an extended NHS,S-based ligand for the construction of larger, two-component macrocycles

To assemble the new heteroligated macrocycle, the NHC,S and P,S ligands were dissolved in dimethylsulfoxide and stirred in the dark overnight (Scheme 6.3). The resulting complex was

characterized in the solution state via ^{1}H and ^{31}P NMR spectroscopy. With the larger heteroligated, WLA macrocycles in hand, we sought to develop a library of hemilabile ligands for incorporation into multi-state receptors (Figure 6.5) and investigate their structure-property relationships to elucidate structural motifs necessary for binding specific guest molecules.

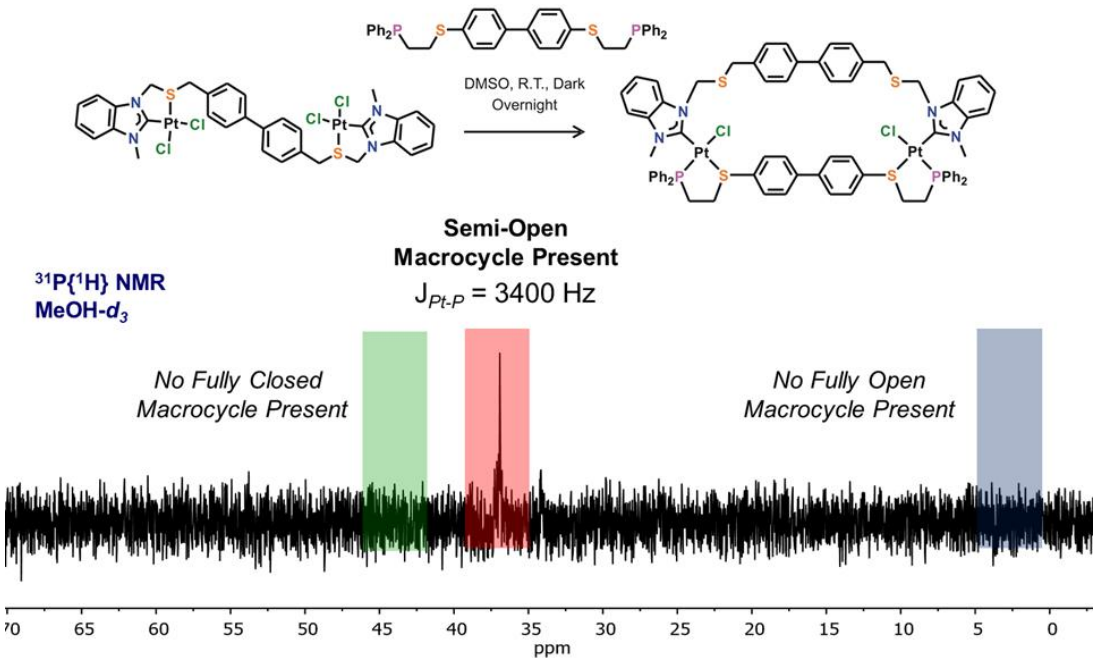

Scheme 6.3 The (top) synthesis and (bottom) ^{31}P NMR characterization of an expanded, two-component, WLA macrocycle accessed via step-wise assembly.

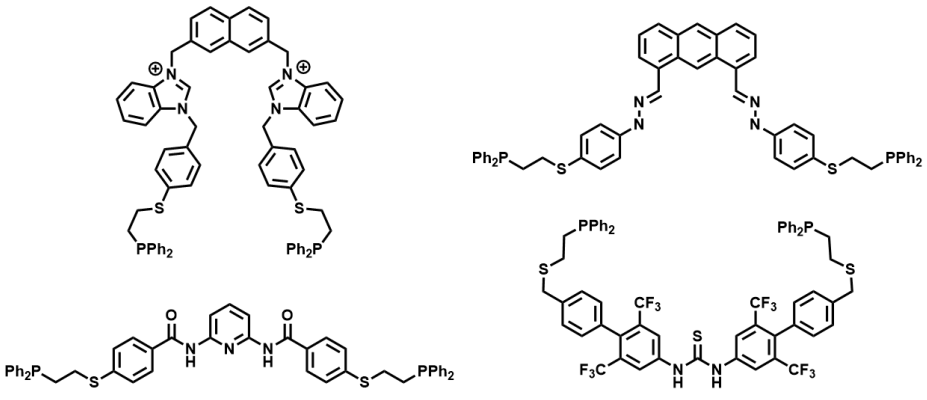

Figure 6.5 Library of hemilabile WLA ligands for use in the assembly of multi-state receptors.

Supramolecular squares were our first target as they offer large binding pockets and potentially higher binding affinity for guests. Using insight from the assembly and switching behavior of the two-component model, heteroligated macrocycle, we designed a heteroligated, tetrametallic square, which incorporates four hemilabile ligands: two traditional ditopic bidentate P,S-based ligands and two longer ditopic bidentate NHC,S-based ligands (Scheme 6.4a).

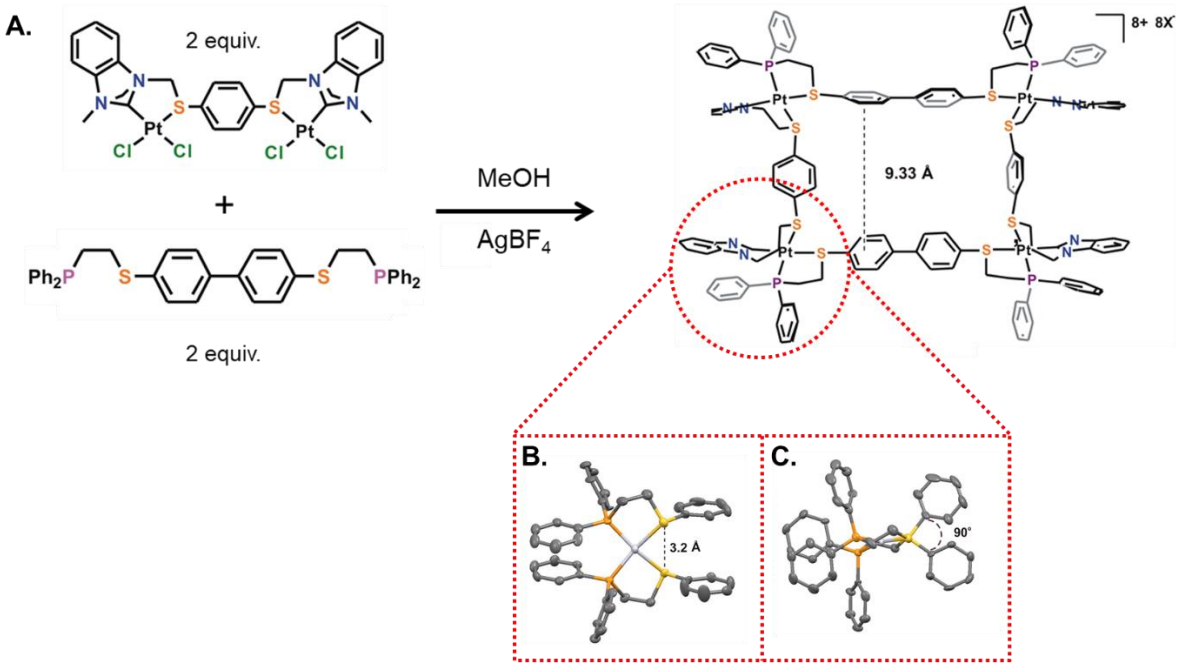

Scheme 6.4 (a) The synthesis of a four-component, heteroligated WLA square, bearing 90° corners as confirmed by (b) single crystals suitable for X-ray diffraction of a tweezer complex bearing phenyl ring end groups. The solid-state crystal structure shown from the side view and (c) the top view, indicate the presence of a 90° angle.

Longer NHC,S ligands are required to favor the formation of a four-component square opposed to a two-component macrocycle. To establish whether the ligands form 90º angles at the Pt center to enable the assembly of squares, we synthesized and characterized a heteroligated tweezer complex containing phenyl rings as end groups to elucidate the geometry, distance, and orientation of the ligands (Scheme 6.4b,c). The solid-state crystal structure revealed that the S–

aryl/S–aryl dihedral angles are ~90°, indicating that in the closed state, a square architecture is favored. Importantly, an irreversible metalation–transmetalation reaction at the NHC ligand enabled the use of strongly binding P,S-ligands without undesired ligand exchange. Characterization of the resulting ligands in solution was carried out by ^{1}H and ^{31}P NMR spectroscopy and mass spectrometry (MS).

Future work will be focused on studying structure-function relationships of the library of WLA-based receptors and macrocycles assembled. We hypothesize that by establishing the foundation for assembling larger WLA macrocycles and squares, we will be able to incorporate a variety of different ligands possessing multiple, specific functional groups. These functional groups will imbue the WLA constructs with multiple recognition elements for supramolecular sensing and binding of guest molecules. For example, we will design and synthesize ligands which provide hydrogen-bonding moieties, cation-π interactions, π–π interactions, and dipole interactions. This library of ligands will enable us to systematically study structure-function relationships in the context of host-guest systems, sensors and even catalysis. Importantly, we will develop design rules for the synthesis of highly specific receptors that bind guests with high affinity, a long-standing goal within the field. This modular platform will allow us to systematically investigate which recognition elements work cooperatively to bind guest molecules with high affinity, and expand the design space of stimuli-responsive host-guest receptors and cages. We will use techniques such as NMR spectroscopy, UV-Vis spectroscopy, FT-IR spectroscopy, and isothermal titration calorimetry (ITC) to elucidate guest binding properties through determination of host-guest binding affinities and guest orientation within the host.

6.3.2 1-D, 2-D and 3-D Coordination Polymer Materials via Chemically Tunable Metal–Ligand Interactions

Previously, a single-chain CP was formed through the coordination of stimuli-responsive metallo ligands and metal ions, and its structure-property relationships were studied. Tweezer-like, WLA-based Pd^{II} monomers possessing phosphino-thioether pyridine ligands (P,S–pyr) were designed, synthesized, and characterized, however, further work is needed to elucidate fundamental structure–property–function relationships in such materials.

Future work toward accomplishing this goal will focus on screening the conditions necessary for the assembly of higher-ordered assemblies containing WLA building blocks. Specifically, we will work to systematically study the effect of solvent, counterions, concentration, and functional groups, to determine the synthetic parameters that drive the formation of different architectures. Currently, we are able to access amorphous particles and single-chain coordination polymers; however, the ultimate goal is to design and synthesize crystalline, 3-D frameworks that can undergo structural transitions that enable a "breathing" architecture (Figure 6.6). This type of structure would enable the use of these materials in energy applications where they would be able to store and release molecular guests.

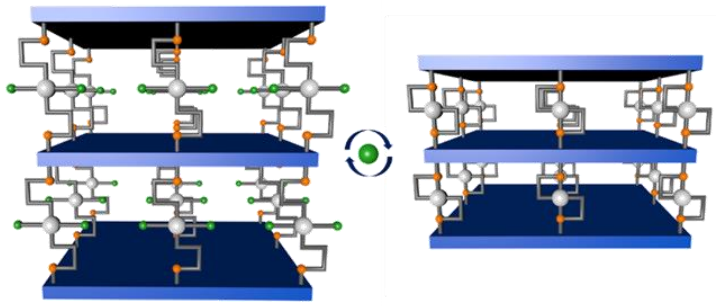

Figure 6.6 Future work is focused on developing crystalline, 3-D frameworks that can undergo structural transitions that enable a "breathing" architecture

CHAPTER 7

Conclusion

Inspired by assemblies in the natural world, researchers have prepared a diverse range of suprastructures with distinct spatial arrangements by artificial supramolecular assembly. Control over the size, shape, charge and composition of synthetic building blocks has enabled the formation of supramolecular architectures with substantial structural diversity. More importantly, harnessing noncovalent interactions to assemble structures in a controlled manner has lead to a better understanding of structure, function relationships and has better informed the complex formation energetics. Coordination-driven self-assembly provides a bottom-up approach to constructing various bioinspired supramolecular coordination complexes, which can—and have—been further exploited as building blocks with controllable shapes and sizes.

This dissertation focused on our recent advances in the construction of coordination-based supramolecular macrocycles and materials. A series of hemilabile ligands were developed for the assembly of a switchable macrocycle, which was first constructed through coordination-driven self-assembly. Then, further work investigated the complex switching behavior of this system, demonstrating a multi-state switch capable of responding to multiple molecular cues. Finally, the principles developed in this work, gave rise to switchable, supramolecular materials and higher-order structures. By changing the functional groups in the acceptors and donors in these coordination-based materials, different suprastructures, including nanoparticles, sheets, and crystalline chains, were prepared. These studies suggest that using stimuli-responsive, coordination-based complexes as building blocks is a highly efficient strategy to achieve complex architectures and functional materials for the development of desired stimuli-responsive biomimetic architectures and materials with high precision and fidelity.

REFERENCES

1. Rebek, J., Introduction to the Molecular Recognition and Self-Assembly Special Feature. *Proceedings of the National Academy of Sciences* **2009,** *106* (26), 10423.
2. Caro, J. A.; Harpole, K. W.; Kasinath, V.; Lim, J.; Granja, J.; Valentine, K. G.; Sharp, K. A.; Wand, A. J., Entropy in molecular recognition by proteins. *Proceedings of the National Academy of Sciences* **2017,** *114* (25), 6563.
3. Cleaves, H. J., Molecular Recognition. In *Encyclopedia of Astrobiology*, Gargaud, M.; Amils, R.; Quintanilla, J. C.; Cleaves, H. J.; Irvine, W. M.; Pinti, D. L.; Viso, M., Eds. Springer Berlin Heidelberg: Berlin, Heidelberg, 2011; pp 1079-1080.
4. Shashikala, H. B. M.; Chakravorty, A.; Alexov, E., Modeling Electrostatic Force in Protein-Protein Recognition. **2019,** *6* (94).
5. Zhu, H.; Sommer, I.; Lengauer, T.; Domingues, F. S., Alignment of Non-Covalent Interactions at Protein-Protein Interfaces. *PLOS ONE* **2008,** *3* (4), e1926.
6. Lodish, H. B., A.; Zipursky, S. L.; Matsudaira, P.; Baltimore, D.; Darnell, J., Noncovalent Bonds. In *Molecular Cell Biology*, 4th Ed.; W. H. Freeman: New York, 2000.
7. Frieden, E., Non-covalent interactions: Key to biological flexibility and specificity. *Journal of Chemical Education* **1975,** *52* (12), 754.
8. Laskowski, R. A.; Gerick, F.; Thornton, J. M., The structural basis of allosteric regulation in proteins. *FEBS Letters* **2009,** *583* (11), 1692-1698.
9. Biswas, K. H., Allosteric regulation of proteins. *Resonance* **2017,** *22* (1), 37-50.
10. Cui, Q.; Karplus, M., Allostery and cooperativity revisited. *Protein Science* **2008,** *17* (8), 1295-1307.

11. Monod, J.; Changeux, J. P.; Jacob, F., Allosteric Proteins and Cellular Control Systems. *J Mol Biol* **1963,** *6* (4), 306-&.

12. Monod, J.; Wyman, J.; Changeux, J. P., On Nature of Allosteric Transitions - a Plausible Model. *J Mol Biol* **1965,** *12* (1), 88-&.

13. Koshland, D. E.; Nemethy, G.; Filmer, D., Comparison of Experimental Binding Data and Theoretical Models in Proteins Containing Subunits. *Biochemistry-Us* **1966,** *5* (1), 365-&.

14. Perutz, M. F., Stereochemistry of cooperative effects in hemoglobin. Hem-hem interaction and the problem of allostery. *Nature (London)* **1970,** *228* (5273), 726-34.

15. Barford, D.; Johnson, L., The allosteric transition of glycogen phosphorylase. **1989**.

16. Saibil, H. R.; Fenton, W. A.; Clare, D. K.; Horwich, A. L., Structure and Allostery of the Chaperonin GroEL. *J. Mol. Biol.* **2013,** *425* (9), 1476-1487.

17. Wyman Jr, J.; Allen, D. W., The problem of the heme interactions in hemoglobin and the basis of the bohr effect. *Journal of Polymer Science* **1951,** *7* (5), 499-518.

18. Eaton, W. A.; Henry, E. R.; Hofrichter, J.; Mozzarelli, A., Is cooperative oxygen binding by hemoglobin really understood? *Nature Structural Biology* **1999,** *6* (4), 351-358.

19. Cornish-Bowden, A., Understanding allosteric and cooperative interactions in enzymes. *The FEBS Journal* **2014,** *281* (2), 621-632.

20. Kanaori, K.; Tajiri, Y.; Tsuneshige, A.; Yonetani, T., Allosteric Mechanism of Oxygen-Binding in Hemoglobin. *Biophysical Journal* **2011,** *100* (3), 380a.

21. Laskowski, R. A.; Luscombe, N. M.; Swindells, M. B.; Thornton, J. M., Protein clefts in molecular recognition and function. *Protein Science* **1996,** *5* (12), 2438-2452.

22. Liang, J.; Edelsbrunner, H.; Woodward, C., Anatomy of protein pockets and cavities: measurement of binding site geometry and implications for ligand design. *Protein Sci* **1998,** *7* (9), 1884-1897.

23. Stank, A.; Kokh, D. B.; Fuller, J. C.; Wade, R. C., Protein Binding Pocket Dynamics. *Accounts Chem Res* **2016,** *49* (5), 809-815.

24. Motojima, F., How do chaperonins fold protein? *Biophysics (Nagoya-shi)* **2015,** *11*, 93-102.

25. Saibil, H., Chaperone machines for protein folding, unfolding and disaggregation. *Nat Rev Mol Cell Biol* **2013,** *14* (10), 630-642.

26. Bhalla, V., Supramolecular Chemistry. *Resonance* **2018,** *23* (3), 277-290.

27. Lehn, J.-M., Supramolecular Chemistry—Scope and Perspectives Molecules, Supermolecules, and Molecular Devices (Nobel Lecture). *Angewandte Chemie International Edition in English* **1988,** *27* (1), 89-112.

28. Thompson, J. M. T.; Gale, P. A., Supramolecular chemistry: from complexes to complexity. *Philosophical Transactions of the Royal Society of London. Series A: Mathematical, Physical and Engineering Sciences* **2000,** *358* (1766), 431-453.

29. Cram, D. J., The Design of Molecular Hosts, Guests, and Their Complexes (Nobel Lecture). *Angewandte Chemie International Edition in English* **1988,** *27* (8), 1009-1020.

30. Pedersen, C. J., The Discovery of Crown Ethers (Noble Lecture). *Angewandte Chemie International Edition in English* **1988,** *27* (8), 1021-1027.

31. Pedersen, C. J., The Discovery of Crown Ethers. *Science* **1988,** *241* (4865), 536.

32. Wenz, G., An Overview of Host-Guest Chemistry and its Application to Nonsteroidal Anti-Inflammatory Drugs. *Clinical Drug Investigation* **2000,** *19* (2), 21-25.

33. Davis, F.; Higson, S., Chapter 3 Crown Ethers, Cryptands and Other Compounds. 2011; pp 34-76.

34. Gale, Philip A.; Howe, Ethan N. W.; Wu, X., Anion Receptor Chemistry. *Chem* **2016,** *1* (3), 351-422.

35. M. G. Antonisse, M.; N. Reinhoudt, D., Neutral anion receptors: design and application. *Chem Commun* **1998,** (4), 443-448.

36. Kovbasyuk, L.; Krämer, R., Allosteric Supramolecular Receptors and Catalysts. *Chemical Reviews* **2004,** *104* (6), 3161-3188.

37. Rebek, J.; Trend, J. E.; Wattley, R. V.; Chakravorti, S., Allosteric effects in organic chemistry. Site-specific binding. *J Am Chem Soc* **1979,** *101* (15), 4333-4337.

38. Rebek, J.; Wattley, R. V., Allosteric effects. Remote control of ion transport selectivity. *J Am Chem Soc* **1980,** *102* (14), 4853-4854.

39. Rebek, J.; Marshall, L., Allosteric effects: an on-off switch. *J Am Chem Soc* **1983,** *105* (22), 6668-6670.

40. Canary, J. W.; Gibb, B. C., Selective recognition of organic molecules by metallohosts. *Prog. Inorg. Chem.* **1997,** *45*, 1-81.

41. Gibb, B. C. In *Nano-capsules assembled by the hydrophobic effect*, Wiley-VCH Verlag GmbH & Co. KGaA: 2008; pp 291-304.

42. Jordan, J. H.; Gibb, B. C., Molecular containers assembled through the hydrophobic effect. *Chem. Soc. Rev.* **2015,** *44* (2), 547-585.

43. Natarajan, A. K., L. S.; Jockusch, S.;Gibb, C. L. D.; Gibb, B. C.; Turro, N. J.; Ramamurthy, V., Controlling Photoreactions with Restricted Spaces and Weak Intermolecular Forces: Exquisite Selectivity during Oxidation of Olefins by Singlet Oxygen. *J. Am. Chem. Soc.* **2007,** *129* (14), 4132-4133.

44. Chen, J.; Rebek, J., Selectivity in an Encapsulated Cycloaddition Reaction. *Organic Letters* **2002,** *4* (3), 327-329.

45. Dinolfo, P. H.; Hupp, J. T., Supramolecular Coordination Chemistry and Functional Microporous Molecular Materials. *Chemistry of Materials* **2001,** *13* (10), 3113-3125.

46. Chakrabarty, R.; Mukherjee, P. S.; Stang, P. J., Supramolecular Coordination: Self-Assembly of Finite Two- and Three-Dimensional Ensembles. *Chemical Reviews* **2011,** *111* (11), 6810-6918.

47. Lifschitz, A. M.; Rosen, M. S.; McGuirk, C. M.; Mirkin, C. A., Allosteric Supramolecular Coordination Constructs. *J Am Chem Soc* **2015,** *137* (23), 7252-7261.

48. Yoshizawa, M.; Tamura, M.; Fujita, M., Diels-Alder in Aqueous Molecular Hosts: Unusual Regioselectivity and Efficient Catalysis. *Science* **2006,** *312* (5771), 251.

49. Holliday, B. J.; Mirkin, C. A., Strategies for the Construction of Supramolecular Compounds through Coordination Chemistry. *Angewandte Chemie International Edition* **2001,** *40* (11), 2022-2043.

50. Kennedy, R. D.; Machan, C. W.; McGuirk, C. M.; Rosen, M. S.; Stern, C. L.; Sarjeant, A. A.; Mirkin, C. A., General Strategy for the Synthesis of Rigid Weak-Link Approach Platinum(II) Complexes: Tweezers, Triple-Layer Complexes, and Macrocycles. *Inorg Chem* **2013,** *52* (10), 5876-5888.

51. Gianneschi, N. C.; Bertin, P. A.; Nguyen, S. T.; Mirkin, C. A.; Zakharov, L. N.; Rheingold, A. L., A Supramolecular Approach to an Allosteric Catalyst. *J Am Chem Soc* **2003,** *125* (35), 10508-10509.

52. Wiester, M. J.; Ulmann, P. A.; Mirkin, C. A., Enzyme Mimics Based Upon Supramolecular Coordination Chemistry. *Angew Chem Int Edit* **2011,** *50* (1), 114-137.

53. Yoo, H.; Rosen, M. S.; Brown, A. M.; Wiester, M. J.; Stern, C. L.; Mirkin, C. A., Elucidating the mechanism of the halide-induced ligand rearrangement reaction. *Inorg. Chem.* **2012,** *51* (21), 11986-95.

54. Oliveri, C. G.; Ulmann, P. A.; Wiester, M. J.; Mirkin, C. A., Heteroligated supramolecular coordination complexes formed via the halide-induced ligand rearrangement reaction. *Acc. Chem. Res.* **2008,** *41* (12), 1618-29.

55. Rosen, M. S.; Spokoyny, A. M.; Machan, C. W.; Stern, C.; Sarjeant, A.; Mirkin, C. A., Chelating effect as a driving force for the selective formation of heteroligated Pt(II) complexes with bidentate phosphino-chalcoether ligands. *Inorg. Chem.* **2011,** *50* (4), 1411-9.

56. Gianneschi, N. C.; Bertin, P. A.; Nguyen, S. T.; Mirkin, C. A.; Zakharov, L. N.; Rheingold, A. L., A Supramolecular Approach to an Allosteric Catalyst. *J. Am. Chem. Soc.* **2003,** *125* (Copyright (C) 2013 American Chemical Society (ACS). All Rights Reserved.), 10508-10509.

57. Gianneschi, N. C.; Cho, S.-H.; Nguyen, S. B. T.; Mirkin, C. A., Reversibly addressing an allosteric catalyst in situ: Catalytic molecular tweezers. *Angew. Chem., Int. Ed.* **2004,** *43*

(Copyright (C) 2013 American Chemical Society (ACS). All Rights Reserved.), 5503-5507.

58. Yoon, H. J.; Heo, J.; Mirkin, C. A., Allosteric Regulation of Phosphate Diester Transesterification Based upon a Dinuclear Zinc Catalyst Assembled via the Weak-Link Approach. *J. Am. Chem. Soc.* **2007,** *129* (Copyright (C) 2013 American Chemical Society (ACS). All Rights Reserved.), 14182-14183.

59. Heo, J.; Mirkin, C. A., Pseudo-allosteric recognition of mandelic acid with an enantioselective coordination complex. *Angew. Chem., Int. Ed.* **2006,** *45* (Copyright (C) 2013 American Chemical Society (ACS). All Rights Reserved.), 941-944.

60. Gianneschi, N. C.; Nguyen, S. T.; Mirkin, C. A., Signal Amplification and Detection via a Supramolecular Allosteric Catalyst. *J. Am. Chem. Soc.* **2005,** *127* (Copyright (C) 2013 American Chemical Society (ACS). All Rights Reserved.), 1644-1645.

61. Masar, M. S., III; Gianneschi, N. C.; Oliveri, C. G.; Stern, C. L.; Nguyen, S. T.; Mirkin, C. A., Allosterically Regulated Supramolecular Catalysis of Acyl Transfer Reactions for Signal Amplification and Detection of Small Molecules. *J. Am. Chem. Soc.* **2007,** *129* (Copyright (C) 2013 American Chemical Society (ACS). All Rights Reserved.), 10149-10158.

62. Yoon, H. J.; Mirkin, C. A., PCR-like cascade reactions in the context of an allosteric enzyme mimic. *J. Am. Chem. Soc.* **2008,** *130* (Copyright (C) 2013 U.S. National Library of Medicine.), 11590-1.

63. Rosen, M. S.; Spokoyny, A. M.; Machan, C. W.; Stern, C.; Sarjeant, A.; Mirkin, C. A., Chelating Effect as a Driving Force for the Selective Formation of Heteroligated Pt(II)

Complexes with Bidentate Phosphino-Chalcoether Ligands. *Inorg. Chem.* **2010,** *50* (4), 1411-1419.

64. Rosen, M. S.; Stern, C. L.; Mirkin, C. A., Heteroligated Pt-II Weak-Link Approach complexes using hemilabile N-heterocyclic carbene-thioether and phosphino-thioether ligands. *Chem. Sci.* **2013,** *4* (11), 4193-4198.

65. Spokoyny, A. M.; Rosen, M. S.; Ulmann, P. A.; Stern, C.; Mirkin, C. A., Selective formation of heteroligated Pt(II) complexes with bidentate phosphine-thioether (P,S) and phosphine-Selenoether (P,Se) ligands via the halide-induced ligand rearrangement reaction. *Inorg. Chem.* **2010,** *49* (4), 1577-86.

66. Rosen, M. S.; Stern, C. L.; Mirkin, C. A., Heteroligated PtII Weak-Link Approach complexes using hemilabile N-heterocyclic carbene–thioether and phosphino–thioether ligands. *Chem Sci* **2013,** *4* (11), 4193-4198.

67. Lin, I. J. B.; Vasam, C. S., Preparation and application of N-heterocyclic carbene complexes of Ag(I). *Coord. Chem. Rev.* **2007,** *251* (5–6), 642-670.

68. de Frémont, P.; Scott, N. M.; Stevens, E. D.; Ramnial, T.; Lightbody, O. C.; Macdonald, C. L. B.; Clyburne, J. A. C.; Abernethy, C. D.; Nolan, S. P., Synthesis of Well-Defined N-Heterocyclic Carbene Silver(I) Complexes. *Organometallics* **2005,** *24* (26), 6301-6309.

69. Mendez-Arroyo, J.; Barroso-Flores, J.; Lifschitz, A. M.; Sarjeant, A. A.; Stern, C. L.; Mirkin, C. A., A Multi-State, Allosterically-Regulated Molecular Receptor With Switchable Selectivity. *J Am Chem Soc* **2014,** *136* (29), 10340-10348.

70. Mendez-Arroyo, J.; d'Aquino, A. I.; Chinen, A. B.; Manraj, Y. D.; Mirkin, C. A., Reversible and Selective Encapsulation of Dextromethorphan and beta-Estradiol Using an

Asymmetric Molecular Capsule Assembled via the Weak-Link Approach. *J Am Chem Soc* **2017,** *139* (4), 1368-1371.

71. Fabbrizzi, L.; Poggi, A., Sensors and Switches from Supramolecular Chemistry. *Chem Soc Rev* **1995,** *24* (3), 197-202.

72. Ashton, P. R.; Balzani, V.; Becher, J.; Credi, A.; Fyfe, M. C. T.; Mattersteig, G.; Menzer, S.; Nielsen, M. B.; Raymo, F. M.; Stoddart, J. F.; Venturi, M.; Williams, D. J., A three-pole supramolecular switch. *J Am Chem Soc* **1999,** *121* (16), 3951-3957.

73. Cook, T. R.; Stang, P. J., Coordination-Driven Supramolecular Macromolecules via the Directional Bonding Approach. *Adv Polym Sci* **2013,** *261*, 229-248.

74. Yoshizawa, M.; Klosterman, J. K.; Fujita, M., Functional Molecular Flasks: New Properties and Reactions within Discrete, Self-Assembled Hosts. *Angew Chem Int Edit* **2009,** *48* (19), 3418-3438.

75. Caulder, D. L.; Raymond, K. N., The rational design of high symmetry coordination clusters. *J Chem Soc Dalton* **1999,** (8), 1185-1200.

76. Caulder, D. L.; Raymond, K. N., Supermolecules by design. *Accounts Chem Res* **1999,** *32* (11), 975-982.

77. Smulders, M. M. J.; Riddell, I. A.; Browne, C.; Nitschke, J. R., Building on architectural principles for three-dimensional metallosupramolecular construction. *Chem Soc Rev* **2013,** *42* (4), 1728-1754.

78. Ronson, T. K.; Zarra, S.; Black, S. P.; Nitschke, J. R., Metal-organic container molecules through subcomponent self-assembly. *Chem Commun* **2013,** *49* (25), 2476-2490.

79. Oliveri, C. G.; Nguyen, S. T.; Mirkin, C. A., A highly modular and convergent approach for the synthesis of stimulant-responsive heteroligated cofacial porphyrin tweezer complexes. *Inorg Chem* **2008,** *47* (7), 2755-2763.

80. Yamanaka, M.; Yamada, Y.; Sei, Y.; Yamaguchi, K.; Kobayashi, K., Selective formation of a self-assembling homo or hetero cavitand cage via metal coordination based on thermodynamic or kinetic control. *J Am Chem Soc* **2006,** *128* (5), 1531-1539.

81. Schmittel, M.; Mahata, K., Diversity and complexity through reversible multiple orthogonal interactions in multicomponent assemblies. *Angew Chem Int Edit* **2008,** *47* (29), 5284-5286.

82. Dalgarno, S. J.; Power, N. P.; Atwood, J. L., Metallo-supramolecular capsules. *Coordin Chem Rev* **2008,** *252* (8-9), 825-841.

83. Gianneschi, N. C.; Masar, M. S., 3rd; Mirkin, C. A., Development of a coordination chemistry-based approach for functional supramolecular structures. *Acc Chem Res* **2005,** *38* (11), 825-37.

84. McGuirk, C. M.; Stern, C. L.; Mirkin, C. A., Small Molecule Regulation of Self-Association and Catalytic Activity in a Supramolecular Coordination Complex. *J Am Chem Soc* **2014,** *136* (12), 4689-4696.

85. McGuirk, C. M.; Mendez-Arroyo, J.; Lifschitz, A. M.; Mirkin, C. A., Allosteric Regulation of Supramolecular Oligomerization and Catalytic Activity via Coordination-Based Control of Competitive Hydrogen-Bonding Events. *J Am Chem Soc* **2014,** *136* (47), 16594-16601.

86. Yoon, H. J.; Kuwabara, J.; Kim, J. H.; Mirkin, C. A., Allosteric Supramolecular Triple-Layer Catalysts. *Science* **2010,** *330* (6000), 66-69.

87. Ulmann, P. A.; Braunschweig, A. B.; Lee, O. S.; Wiester, M. J.; Schatz, G. C.; Mirkin, C. A., Inversion of product selectivity in an enzyme-inspired metallosupramolecular tweezer catalyzed epoxidation reaction. *Chem Commun* **2009,** (34), 5121-5123.

88. McGuirk, C. M.; Mendez-Arroyo, J.; d'Aquino, A. I.; Stern, C. L.; Liu, Y.; Mirkin, C. A., A concerted two-prong approach to the in situ allosteric regulation of bifunctional catalysis. *Chem Sci* **2016,** *7* (11), 6674-6683.

89. Lifschitz, A. M.; Young, R. M.; Mendez-Arroyo, J.; Stern, C. L.; McGuirk, C. M.; Wasielewski, M. R.; Mirkin, C. A., An allosteric photoredox catalyst inspired by photosynthetic machinery. *Nat Commun* **2015,** *6*.

90. Lifschitz, A. M.; Young, R. M.; Mendez-Arroyo, J.; Roznyatovskiy, V. V.; McGuirk, C. M.; Wasielewski, M. R.; Mirkin, C. A., Chemically regulating Rh(I)-Bodipy photoredox switches. *Chem Commun* **2014,** *50* (52), 6850-6852.

91. Masar, M. S.; Mirkin, C. A.; Stern, C. L.; Zakharov, L. N.; Rheingold, A. L., Binuclear copper(I) macrocycles synthesized via the weak-link approach. *Inorg Chem* **2004,** *43* (15), 4693-4701.

92. Machan, C. W.; Spokoyny, A. M.; Jones, M. R.; Sarjeant, A. A.; Stern, C. L.; Mirkin, C. A., Plasticity of the Nickel(II) Coordination Environment in Complexes with Hemilabile Phosphino Thioether Ligands. *J Am Chem Soc* **2011,** *133* (9), 3023-3033.

93. Kuwabara, J.; Ovchinnikov, M. V.; Stem, C. L.; Mirkin, C. A., Reactivity of dinuclear rhodium(I) macrocycles formed via the weak-link approach. *Organometallics* **2008,** *27* (4), 789-792.

94. Khoshbin, M. S.; Ovchinnikov, M. V.; Mirkin, C. A.; Zakharov, L. N.; Rheingold, A. L., Binuclear ruthenium macrocycles formed via the weak-link approach. *Inorg Chem* **2005,** *44* (3), 496-501.

95. Rosen, M. S.; Stern, C. L.; Mirkin, C. A., Heteroligated Pt-II Weak-Link Approach complexes using hemilabile N-heterocyclic carbene-thioether and phosphino-thioether ligands. *Chem. Sci.* **2013,** *4* (11), 4193-4198.

96. Yoo, H.; Rosen, M. S.; Brown, A. M.; Wiester, M. J.; Stern, C. L.; Mirkin, C. A., Elucidating the Mechanism of the Halide-Induced Ligand Rearrangement Reaction. *Inorg. Chem.* **2012,** *51* (21), 11986-11995.

97. Brown, A. M.; Ovchinnikov, M. V.; Mirkin, C. A., Heteroligated Rh-I tweezer complexes. *Angew. Chem. Int. Ed.* **2005,** *44* (27), 4207-4209.

98. Oliveri, C. G.; Ulmann, P. A.; Wiester, M. J.; Mirkin, C. A., Heteroligated Supramolecular Coordination Complexes Formed via the Halide-Induced Ligand Rearrangement Reaction. *Acc. Chem. Res.* **2008,** *41* (12), 1618-1629.

99. Krevor, J. V. Z.; Simonis, U.; Richter, J. A., Structural-Analysis of Platinum Phosphine Complexes by 2-Dimensional P-31 Nmr-Spectroscopy. *Inorg. Chem.* **1992,** *31* (12), 2409-2414.

100. Pregosin, P. S., Pt-195 Nuclear Magnetic-Resonance. *Coord. Chem. Rev.* **1982,** *44* (2), 247-291.

101. Still, B. M.; Kumar, P. G.; Aldrich-Wright, J. R.; Price, W. S., 195Pt NMR--theory and application. *Chem. Soc. Rev.* **2007,** *36* (4), 665-86.

102. Kennedy, R. D.; Stern, C. L.; Mirkin, C. A., Zwitterionic Weak-Link Approach Complexes Based on Anionic Icosahedral Monocarbaboranes. *Inorg. Chem.* **2013,** *52* (24), 14064-14071.

103. Ulmann, P. A.; Brown, A. M.; Ovchinnikov, M. V.; Mirkin, C. A.; DiPasquale, A. G.; Rheingold, A. L., Spontaneous formation of heteroligated Pt-II complexes with chelating hemilabile ligands. *Chem. - Eur. J.* **2007,** *13* (16), 4529-4534.

104. Noda, K.; Sasaki, T.; Iwatsuki, S.; Kashiwabara, K.; Suzuki, T.; Takagi, H. D., Syntheses and first structural analyses of Cu(I)-PS complexes with bidentate 1,1-diphenyl-1-phospha-4-thiapentane (mtdpp) and quadridentate 5,9-diphenyl-5,9-diphospha-2,12-dithiatridecane (2,3,2-SPPS): successful synthetic route for monomeric [Cu(mtdpp)2]BF4 and dimeric [Cu-2(2,3,2-SPPS)(2)](BF4)(2). *Inorg. Chim. Acta* **2004,** *357* (2), 526-532.

105. Dolomanov, O. V.; Bourhis, L. J.; Gildea, R. J.; Howard, J. A. K.; Puschmann, H., OLEX2: a complete structure solution, refinement and analysis program. *J. Appl. Crystallogr.* **2009,** *42*, 339-341.

106. Sheldrick, G. M., SHELXT - Integrated space-group and crystal-structure determination. *Acta Crystallogr., Sect. A: Found. Adv.* **2015,** *71*, 3-8.

107. Sheldrick, G. M., Crystal structure refinement with SHELXL. *Acta Crystallogr., Sect. C: Struct. Chem.* **2015,** *71*, 3-8.

108. Wiester, M. J.; Braunschweig, A. B.; Yoo, H.; Mirkin, C. A., Solvent and Temperature Induced Switching Between Structural Isomers of Rh-I Phosphinoalkyl Thioether (PS) Complexes. *Inorg. Chem.* **2010,** *49* (15), 7188-7196.

109. Macchioni, A., Ion pairing in transition-metal organometallic chemistry. *Chem. Rev.* **2005,** *105* (6), 2039-2073.

110. Garrou, P. E., Delta-R Ring Contributions to P-31 Nmr Parameters of Transition-Metal-Phosphorus Chelate Complexes. *Chem. Rev.* **1981,** *81* (3), 229-266.

111. Abel, E. W.; Bhargava, S. K.; Orrell, K. G., The Stereodynamics of Metal-Complexes of Sulfur-Containing, Selenium-Containing, and Tellurium-Containing Ligands. *Prog. Inorg. Chem.* **1984,** *32*, 1-118.

112. Abel, E. W.; Bhargava, S. K.; Kite, K.; Orrell, K. G.; Sik, V.; Williams, B. L., Structural Dependencies of Pyramidal Inversion at Sulfur and Selenium in Thio-Ether and Seleno-Ether Complexes of Palladium(Ii) and Platinum(Ii) - a Nuclear Magnetic-Resonance Study. *Polyhedron* **1982,** *1* (3), 289-298.

113. Spokoyny, A. M.; Kim, D.; Sumrein, A.; Mirkin, C. A., Infinite coordination polymer nano- and microparticle structures. *Chem. Soc. Rev.* **2009,** *38* (5), 1218-27.

114. Ferey, G., Hybrid porous solids: past, present, future. *Chem. Soc. Rev.* **2008,** *37* (1), 191-214.

115. Park, K. H.; Jang, K.; Son, S. U.; Sweigart, D. A., Self-supported organometallic rhodium quinonoid nanocatalysts for stereoselective polymerization of phenylacetylene. *J. Am. Chem. Soc.* **2006,** *128* (27), 8740-8741.

116. Calabrese, C. M.; Merkel, T. J.; Briley, W. E.; Randeria, P. S.; Narayan, S. P.; Rouge, J. L.; Walker, D. A.; Scott, A. W.; Mirkin, C. A., Biocompatible Infinite-Coordination-Polymer Nanoparticle–Nucleic-Acid Conjugates for Antisense Gene Regulation. *Angew. Chem. Int. Ed.* **2015,** *54* (2), 476-480.

117. Jeon, Y. M.; Heo, J.; Mirkin, C. A., Dynamic interconversion of amorphous microparticles and crystalline rods in salen-based homochiral infinite coordination polymers. *J. Am. Chem. Soc.* **2007,** *129* (24), 7480-7481.

118. Oh, M.; Mirkin, C. A., Ion exchange as a way of controlling the chemical compositions of nano- and microparticles made from infinite coordination polymers. *Angew. Chem. Int. Ed.* **2006,** *45* (33), 5492-4.

119. Oh, M.; Mirkin, C. A., Chemically tailorable colloidal particles from infinite coordination polymers. *Nature* **2005,** *438* (7068), 651-4.

120. Jeon, Y. M.; Armatas, G. S.; Kim, D.; Kanatzidis, M. G.; Mirkin, C. A., Troger's-Base-Derived Infinite Co-ordination Polymer Microparticles. *Small* **2009,** *5* (1), 46-50.

121. Sun, X. P.; Dong, S. J.; Wang, E. K., Coordination-induced formation of submicrometer-scale, monodisperse, spherical colloids of organic-inorganic hybrid materials at room temperature. *J. Am. Chem. Soc.* **2005,** *127* (38), 13102-13103.

122. Imaz, I.; Maspoch, D.; Rodríguez-Blanco, C.; Pérez-Falcón, J. M.; Campo, J.; Ruiz-Molina, D., Valence-Tautomeric Metal–Organic Nanoparticles. *Angew. Chem. Int. Ed.* **2008,** *47* (10), 1857-1860.

123. Johnson, C. A.; Sharma, S.; Subramaniam, B.; Borovik, A. S., Nanoparticulate Metal Complexes Prepared with Compressed Carbon Dioxide: Correlation of Particle Morphology with Precursor Structure. *J. Am. Chem. Soc.* **2005,** *127* (27), 9698-9699.

124. Spokoyny, A. M.; Kim, D.; Sumrein, A.; Mirkin, C. A., Infinite coordination polymer nano- and microparticle structures. *Chem. Soc. Rev.* **2009,** *38* (5), 1218-1227.

125. Cho, W.; Lee, H. J.; Oh, M., Growth-Controlled Formation of Porous Coordination Polymer Particles. *J. Am. Chem. Soc.* **2008,** *130* (50), 16943-16946.

126. Jung, S.; Oh, M., Monitoring shape transformation from nanowires to nanocubes and size-controlled formation of coordination polymer particles. *Angew. Chem. Int. Ed.* **2008,** *47* (11), 2049-2051.

127. Farha, O. K.; Spokoyny, A. M.; Mulfort, K. L.; Galli, S.; Hupp, J. T.; Mirkin, C. A., Gas-Sorption Properties of Cobalt(II)-Carborane-Based Coordination Polymers as a Function of Morphology. *Small* **2009,** *5* (15), 1727-1731.

128. Zhang, Y.; Guo, Y. J.; Wu, S. Y.; Liang, H. J.; Xu, H. X., Photodegradable Coordination Polymer Particles for Light-Controlled Cargo Release. *Acs Omega* **2017,** *2* (6), 2536-2543.

129. Yoon, H. J.; Kuwabara, J.; Kim, J.-H.; Mirkin, C. A., Allosteric Supramolecular Triple-Layer Catalysts. *Science* **2010,** *330* (Copyright (C) 2013 American Chemical Society (ACS). All Rights Reserved.), 66-69.

130. Machan, C. W.; Adelhardt, M.; Sarjeant, A. A.; Stern, C. L.; Sutter, J.; Meyer, K.; Mirkin, C. A., One-Pot Synthesis of an Fe(II) Bis-Terpyridine Complex with Allosterically Regulated Electronic Properties. *J. Am. Chem. Soc.* **2012,** *134* (41), 16921-16924.

131. Dobrawa, R.; Ballester, P.; Saha-Möller, C. R.; Würthner, F., Thermodynamics of 2,2′:6′,2″-Terpyridine-Metal Ion Complexation. In *Metal-Containing and Metallosupramolecular Polymers and Materials*, American Chemical Society: 2006; Vol. 928, pp 43-62.

132. Andres, P. R.; Schubert, U. S., Metallo-Polymerization/-Cyclization of a C16-Bridged Di-Terpyridine Ligand and Iron(II) Ions. *Macromol. Rapid Commun.* **2004,** *25* (15), 1371-1375.

133. Li, X.; Chan, Y.-T.; Casiano-Maldonado, M.; Yu, J.; Carri, G. A.; Newkome, G. R.; Wesdemiotis, C., Separation and Characterization of Metallosupramolecular Libraries by Ion Mobility Mass Spectrometry. *Anal. Chem.* **2011,** *83* (17), 6667-6674.

134. Newkome, G. R.; Cho, T. J.; Moorefield, C. N.; Cush, R.; Russo, P. S.; Godínez, L. A.; Saunders, M. J.; Mohapatra, P., Hexagonal Terpyridine–Ruthenium and –Iron Macrocyclic Complexes by Stepwise and Self-Assembly Procedures. *Chem. - Eur. J.* **2002,** *8* (13), 2946-2954.

135. Perera, S.; Li, X.; Soler, M.; Schultz, A.; Wesdemiotis, C.; Moorefield, C. N.; Newkome, G. R., Hexameric Palladium(II) Terpyridyl Metallomacrocycles: Assembly with 4,4′-Bipyridine and Characterization by TWIM Mass Spectrometry. *Angew. Chem. Int. Ed.* **2010,** *49* (37), 6539-6544.

136. Jeon, Y. M.; Heo, J.; Mirkin, C. A., Dynamic interconversion of amorphous microparticles and crystalline rods in salen-based homochiral infinite coordination polymers. *J. Am. Chem. Soc.* **2007,** *129* (24), 7480-7481.

137. Ulmann, P. A.; Mirkin, C. A.; DiPasquale, A. G.; Liable-Sands, L. M.; Rheingold, A. L., Reversible Ligand Pairing and Sorting Processes Leading to Heteroligated Palladium(II) Complexes with Hemilabile Ligands. *Organometallics* **2009,** *28* (4), 1068-1074.

138. Ranaud, E.; Russell, R. B.; Fortier, S.; Brown, S. J.; Baird, M. C., Synthesis of a new family of water-soluble tertiary phosphine ligands and of their rhodium(I) complexes; olefin

hydrogenation in aqueous and biphasic media. *J. Organomet. Chem.* **1991,** *419* (3), 403-415.

139. Zhou, G.; Harruna, I. I., Synthesis and Characterization of Bis(2,2‘:6‘,2‘ ‘-terpyridine)ruthenium(II)-Connected Diblock Polymers via RAFT Polymerization. *Macromolecules* **2005,** *38* (10), 4114-4123.

140. Ernzerhof, M.; Scuseria, G. E., Assessment of the Perdew-Burke-Ernzerhof exchange-correlation functional. *J Chem Phys* **1999,** *110* (11), 5029-5036.

141. Abualia, M.; Schroeder, L.; Garcia, M.; Daubenmire, P. L.; Wink, D. J.; Clark, G. A., Connecting Protein Structure to Intermolecular Interactions: A Computer Modeling Laboratory. *Journal of Chemical Education* **2016,** *93* (8), 1353-1363.

142. Olsman, N.; Goentoro, L., Allosteric proteins as logarithmic sensors. *Proceedings of the National Academy of Sciences* **2016**, 201601791.

143. Barron, P. M.; Wray, C. A.; Hu, C.; Guo, Z.; Choe, W., A Bioinspired Synthetic Approach for Building Metal−Organic Frameworks with Accessible Metal Centers. *Inorganic Chemistry* **2010,** *49* (22), 10217-10219.

144. Mishra, R.; Patil, B.; Karadaş, F.; Yılmaz, E., Bioinspired Copper Coordination Polymer Catalysts for Oxygen Reduction Reaction. *ChemistrySelect* **2017,** *2* (27), 8296-8300.

145. Mishra, R.; Ülker, E.; Karadas, F., One-Dimensional Copper(II) Coordination Polymer as an Electrocatalyst for Water Oxidation. *ChemElectroChem* **2017,** *4* (1), 75-80.

146. Amo-Ochoa, P.; Castillo, O.; Gómez-García, C. J.; Hassanein, K.; Verma, S.; Kumar, J.; Zamora, F., Semiconductive and Magnetic One-Dimensional Coordination Polymers of Cu(II) with Modified Nucleobases. *Inorganic Chemistry* **2013,** *52* (19), 11428-11437.

147. Tatikonda, R.; Bulatov, E.; Özdemir, Z.; Nonappa; Haukka, M., Infinite coordination polymer networks: metallogelation of aminopyridine conjugates and in situ silver nanoparticle formation. *Soft Matter* **2019,** *15* (3), 442-451.

148. Loukopoulos, E.; Kostakis, G. E., Review: Recent advances of one-dimensional coordination polymers as catalysts. *Journal of Coordination Chemistry* **2018,** *71* (3), 371-410.

149. Uemura, K.; Matsuda, R.; Kitagawa, S., Flexible microporous coordination polymers. *Journal of Solid State Chemistry* **2005,** *178* (8), 2420-2429.

150. Kokado, K.; Ishiwata, T.; Anan, S.; Sada, K., Unidirectional compression and expansion of a crosslinked MOF crystal prepared via axis-dependent crosslinking and ligand exchange. *Polymer Journal* **2017,** *49*, 685.

151. Ishiwata, T.; Furukawa, Y.; Sugikawa, K.; Kokado, K.; Sada, K., Transformation of Metal–Organic Framework to Polymer Gel by Cross-Linking the Organic Ligands Preorganized in Metal–Organic Framework. *J Am Chem Soc* **2013,** *135* (14), 5427-5432.

152. Shimomura, S.; Higuchi, M.; Matsuda, R.; Yoneda, K.; Hijikata, Y.; Kubota, Y.; Mita, Y.; Kim, J.; Takata, M.; Kitagawa, S., Selective sorption of oxygen and nitric oxide by an electron-donating flexible porous coordination polymer. *Nature Chemistry* **2010,** *2*, 633.

153. Tanaka, D.; Henke, A.; Albrecht, K.; Moeller, M.; Nakagawa, K.; Kitagawa, S.; Groll, J., Rapid preparation of flexible porous coordination polymer nanocrystals with accelerated guest adsorption kinetics. *Nature Chemistry* **2010,** *2*, 410.

154. Horcajada, P.; Serre, C.; Maurin, G.; Ramsahye, N. A.; Balas, F.; Vallet-Regí, M.; Sebban, M.; Taulelle, F.; Férey, G., Flexible Porous Metal-Organic Frameworks for a Controlled Drug Delivery. *J Am Chem Soc* **2008,** *130* (21), 6774-6780.

155. Mason, J. A.; Oktawiec, J.; Taylor, M. K.; Hudson, M. R.; Rodriguez, J.; Bachman, J. E.; Gonzalez, M. I.; Cervellino, A.; Guagliardi, A.; Brown, C. M.; Llewellyn, P. L.; Masciocchi, N.; Long, J. R., Methane storage in flexible metal–organic frameworks with intrinsic thermal management. *Nature* **2015,** *527*, 357.

156. Farha, O. K.; Spokoyny, A. M.; Mulfort, K. L.; Galli, S.; Hupp, J. T.; Mirkin, C. A., Gas-Sorption Properties of Cobalt(II)–Carborane-Based Coordination Polymers as a Function of Morphology. *Small* **2009,** *5* (15), 1727-1731.

157. Li, J.-R.; Kuppler, R. J.; Zhou, H.-C., Selective gas adsorption and separation in metal–organic frameworks. *Chemical Society Reviews* **2009,** *38* (5), 1477-1504.

158. Souza, D. C. S.; Pralong, V.; Jacobson, A. J.; Nazar, L. F., A Reversible Solid-State Crystalline Transformation in a Metal Phosphide Induced by Redox Chemistry. *Science* **2002,** *296* (5575), 2012.

159. Lin, W.; Rieter, W. J.; Taylor, K. M. L., Modular Synthesis of Functional Nanoscale Coordination Polymers. *Angewandte Chemie International Edition* **2009,** *48* (4), 650-658.

160. d'Aquino, A. I.; Kean, Z. S.; Mirkin, C. A., Infinite Coordination Polymer Particles Composed of Stimuli-Responsive Coordination Complex Subunits. *Chemistry of Materials* **2017,** *29* (24), 10284-10288.

161. Lu, W.; Chui, S. S.-Y.; Ng, K.-M.; Che, C.-M., A Submicrometer Wire-to-Wheel Metamorphism of Hybrid Tridentate Cyclometalated Platinum(II) Complexes. *Angewandte Chemie International Edition* **2008,** *47* (24), 4568-4572.

162. Kaminker, R.; Popovitz-Biro, R.; van der Boom, M. E., Coordination-Polymer Nanotubes and Spheres: A Ligand-Structure Effect. *Angewandte Chemie* **2011,** *123* (14), 3282-3284.

163. Maeda, H.; Hasegawa, M.; Hashimoto, T.; Kakimoto, T.; Nishio, S.; Nakanishi, T., Nanoscale Spherical Architectures Fabricated by Metal Coordination of Multiple Dipyrrin Moieties. *J Am Chem Soc* **2006,** *128* (31), 10024-10025.

164. Tran, M.; Kline, K.; Qin, Y.; Shen, Y.; Green, M. D.; Tongay, S., 2D coordination polymers: Design guidelines and materials perspective. *Applied Physics Reviews* **2019,** *6* (4), 041311.

165. Wiester, M. J.; Ulmann, P. A.; Mirkin, C. A., Enzyme Mimics Based Upon Supramolecular Coordination Chemistry. *Angewandte Chemie International Edition* **2011,** *50* (1), 114-137.

166. Winter, S.; Weber, E.; Eriksson, L.; Csöregh, I., New coordination polymer networks based on copper(ii) hexafluoroacetylacetonate and pyridine containing building blocks: synthesis and structural study. *New Journal of Chemistry* **2006,** *30* (12), 1808-1819.

167. Graham, P. M.; Pike, R. D.; Sabat, M.; Bailey, R. D.; Pennington, W. T., Coordination Polymers of Copper(I) Halides. *Inorg Chem* **2000,** *39* (22), 5121-5132.

168. Rodgers, M. T.; Stanley, J. R.; Amunugama, R., Periodic Trends in the Binding of Metal Ions to Pyridine Studied by Threshold Collision-Induced Dissociation and Density Functional Theory. *J Am Chem Soc* **2000,** *122* (44), 10969-10978.

169. Balogh-Hergovich, É.; Speier, G., Reaction of copper(I) chloride pyridine complexes with dioxygen. A kinetic study. *Transition Metal Chemistry* **1982,** *7* (3), 177-180.

170. Marchetti, L. A.; Kumawat, L. K.; Mao, N.; Stephens, J. C.; Elmes, R. B. P., The Versatility of Squaramides: From Supramolecular Chemistry to Chemical Biology. *Chem* **2019,** *5* (6), 1398-1485.

Andrea d'Aquino

535 Hinman Ave. Apt. E1, Evanston, IL 60202 | 224-420-7097
andreadaquino2019@u.northwestern.edu

EDUCATION

Northwestern University, Evanston, IL 2014–December 2019
In Progress: Ph.D. Chemistry

Western Washington University, Bellingham, WA 2009–2014
B.S. Chemistry, Honors Thesis
Minor in Mathematics

RESEARCH AND PROFESSIONAL EXPERIENCE

2014 – Present | Northwestern University Department of Chemistry
Advisor: Dr. Chad Mirkin
Leadership Role: Organometallic Subgroup Leader
Conducting research on coordination based, supramolecular chemistry with a focus on constructing stimuli-responsive coordination constructs and extended networks.

Winter 2013 – July 2014 | Western Washington University Department of Chemistry
Advisor: Dr. Mark Bussell
Conducted research on heterogeneous catalysts for the production of ultra-low sulfur fuels and renewable biofuels. Developed a new synthetic route for preparing Ni_2P catalysts.

Summer 2013 | Western Washington University National Science Foundation REU
Advisor: Dr. Mark Bussell
Developed new synthetic routes for preparing nickel phosphide catalysts.

Summer 2012 | University of Washington Environmental & Occupational Health Sciences
Advisor: Dr. Christopher Simpson
Conducted studies on the stability of ozone and air pollutants in Seattle, WA through the Environmental Health Research Experience Program.

2011 – 2012 | Western Washington University, Vietnam and America Study Abroad
Advisor: Dr. Mart Stewart
Studied the effects of dioxin within fatty tissues and the environment; investigated the epidemiology associated with Agent Orange sprayed over 40 years ago during the war.

HONORS, AWARDS, FELLOWSHIPS & DISTINCTIONS

February 2019 | Accepted into Stanford's Postdoctoral Recruitment Initiative in Science and Medicine (PRISM) Program
Website: https://postdocs.stanford.edu/PRISM

April 16, 2018 | McBride Award
This award recognizes one outstanding graduate student for their contribution of excellence in the area of diversity, service, or engagement ($3,000).
Link to Northwestern's featured highlight.

April 2018 | PEO Scholars Award

These one-time, competitive, merit-based awards are for women pursuing a PhD and provides support to those who will make significant contributions in their field ($15,000).

April 1, 2014 – Present | National Science Foundation Graduate Research Fellowship
Recognizes and supports outstanding graduate students in science, technology, engineering, and mathematics disciplines ($138,000).

2016 – Present | Ryan Fellowship, Northwestern University
The Fellowship supports graduate students who have shown exceptional scientific talent and are dedicated to the exploration and advancement of nanoscale science.
Link to Andrea's fellowship bio.

April 2009 – Present | Gates Millennium Scholarship and Fellowship
Funded by Bill & Melinda Gates Foundation, the award provides outstanding underrepresented minorities an opportunity to earn a college and graduate education.

November 2016 | Selected to attend the 67th Lindau Nobel Laureate Meeting
Selected to participate in the 67th Lindau Nobel Laureate Meeting (June 25, 2017) in Lindau, Germany. Only the 400 most qualified scientists are selected.
(https://news.northwestern.edu/stories/2017/may/spring-honors-and-awards/)

March 2, 2017 | Gordon Research Conference Carl Storm Fellowship ($600)

June 2014 | Western Washington University Spring Commencement Speaker
The commencement speaker of WWU is granted to a student from WWU's entire graduating class. The award honors a graduating senior for their exceptional scholarship and service to the university and community.

April 2014 | Western Washington University Presidential Scholar Award
One award granted to a student from WWU's College of Science & Engineering. The award honors a senior for scholarship and service to the university/community.

April 2014 | WWU Outstanding Chemistry Department Graduate
One student from WWU's Department of Chemistry is honored as the Outstanding Graduate. Selected based on grades, research, writing, service, promise for the future.

February 2014 | Advanced Materials Science and Engineering (AMSEC) Kaiser–Borsari Scholarship for Women in Material Science
Awarded to one female undergraduate who has excelled in materials science and engineering research ($5,000).

March 17, 2014 | Outstanding Undergraduate Poster Prize – 247th American Chemical Society National Meeting, Dallas, TX
1st Place Poster Prize in the Division of Colloid and Surface Chemistry ($250)

September 19, 2013 | Outstanding Undergraduate Poster Prize – Pacific Northwest AVS Science and Technology Symposium, Troutdale, OR. 1st Place Poster Prize ($250)

September 2013 | All Nations Louis Stokes Alliance for Minority Participation Scholarship
The ANLSAMP program is funded by the NSF, with the goal of increasing the number of minority and Native American students successfully completing degrees in STEM.

May 2012 | Harvard Center for Communicable Disease Dynamics Conference Scholar

December 2011 | Vietnam Study Abroad Research Scholarship

June 2010 | TeachWashington NOYCE Summer Internship (WWU)
Funded by the NSF, this internship allowed me to teach summer school math and science.

LEADERSHIP POSITIONS

May 2017 – May 2019 | Chair of the 2019 Self-Assembly and Supramolecular Chemistry Gordon Research Seminar; *Les Diablerets, Switzerland*

March 2016 – Present | Mirkin Lab Organometallic Subgroup Leader, Northwestern Univ.
I facilitate subgroup meetings, delegate group responsibilities, I take leadership of instrument repairs/maintenance, write grants, mentor students and develop projects.

January 2019 – Present | Northwestern Prison Education Program (NPEP) Graduate Student Advisory Committee Member and Volunteer and Director of Student Wellness
I travel to Stateville Correctional Center once a week to tutor a broad range of subjects and develop programs for incarcerated NPEP students.
(https://sites.northwestern.edu/npep/andrea-daquino/)

September 2015 – 2019 | Co-Director of HerStory, Northwestern University
I helped establish HerStory: an annual event aimed to inspire middle/high school girls to pursue careers in science. (http://nuherstory.weebly.com/2017-organizers.html)

September 2015 – 2018 | Director of ChemUnity
I helped establish this mentoring program and I organize meetings, plan and execute events, and apply for grants.

September 2015 – Present | Member and Organizer of NU BonD (Building on Diversity)
I helped establish NU BonD, and as a board member I organize meetings, plan and execute events and apply for grants. (http://nubond.weebly.com/organizers.html)

September 2015 – Present | Organizer of Northwestern University's Faces of Science
I helped establish and run the Faces of Science Seminar series at Northwestern University. (https://nubond.weebly.com/faces-of-science.html)

PUBLICATIONS

1. **d'Aquino, A. I.**; Gosavi, A.; Paul, M.; Kleunder, E.; Mirkin, C. A. Spectroscopic Investigation into the Formation of Metallic Nanoparticles Prepared *via* Scanning Probe Block Co-Polymer Lithography. *In preparation*, **2019**.
2. **d'Aquino, A. I.**; Kean, Z.; Mirkin, C. A. Single-Chain Coordination Polymers Enabled by Chemically Tunable Metal–Ligand Interactions. *In preparation*, **2019**.
3. Topalian, P.; Liyanage, D. R.; Danforth, S.; **d'Aquino, A. I.**; Brock, S.; Bussell, M. Effect of Particle Size on the Deep HDS Properties of Ni_2P Catalysts. *J. Phys. Chem. C.* **2019**. *Just Accepted*. Link
4. **d'Aquino, A. I.**; Cheng, H. F.; Barroso-Flores, J.; Kean, Z. S.; Mendez-Arroyo, J. E.; McGuirk, C. M.; Mirkin, C. A. An Allosterically-Regulated, Four-State Macrocycle. *Inorg. Chem*. **2018**, *57*, 3568–3578. DOI: 10.1021/acs.inorgchem.7b02745. Link

5. Cheng, H-F.; **d'Aquino, A. I.**; Barroso-Flores, J.; Mirkin, C. A. A Redox-Switchable, Allosteric Coordination Complex. *J. Am. Chem. Soc.* **2018**, *140*, 14590–14594. DOI: 10.1021/jacs.8b09321. Link

6. Wang, S.; McGuirk, C. M.; **d'Aquino, A. I.**; Mason, J.; Mirkin, C. A. Metal-Organic Framework Nanoparticles. *Adv. Mater.* **2018**, *30*, 1800202. Link

7. **d'Aquino, A. I.**; Kean, Z. S.; Mirkin, C. A. Infinite Coordination Polymer Particles Composed of Stimuli-Responsive Coordination Complex Subunits. *Chem. Mater*. **2017**, *29*, 10284–10288. DOI: 10.1021/acs.chemmater.7b03638. Link

8. Liu, Y.; Kean, Z. S.; **d'Aquino, A. I.**; Manraj, Y.; Mendez-Arroyo, J. E.; Mirkin, C. A. Pd^{II} Weak-Link Approach Complexes Bearing Hemilabile N-heterocyclic Carbene-Thioether Ligands. *Inorganic Chem.* **2017***, 56*, 5902–5910. Article. DOI: 10.1021/acs.inorgchem.7b00543. Link

9. Mendez-Arroyo, J. E.; **d'Aquino, A. I.**; Chinen, A. B.; Manraj, Y.; Mirkin, C. A., Reversible and Selective Encapsulation of Dextromethorphan and B-Estradiol Using an Asymmetric Molecular Capsule Assembled via the Weak-Link Approach. *J. Am. Chem. Soc*. **2017**, 139, 1368–1371. DOI: 10.1021/jacs.6b10027. Link

10. McGuirk, C. M.; Mendez-Arroyo, J. E.; **d'Aquino, A. I.**, Stern, C. L.; Mirkin, C. A., A Concerted Two-Prong Approach to the *in-Situ* Allosteric Regulation of Bifunctional Catalysis. *Chem. Sci.* **2016**, *7*, 6674–6683. Link

11. **d'Aquino, A. I.**; Danforth, S. J.; Clinkingbeard, T. R.; Ilic, B.; Pullan, L.; Reynolds, M. A.; Murray, B. D.; Bussell, M. E., Highly-Active Nickel Phosphide Hydrotreating Catalysts Prepared In Situ Using Nickel Hypophosphite Precursors. *J. Catal.* **2016,** *335*, 2014–214. Link

12. Anne E. d'Aquino, **Andrea I. d'Aquino**, Lauren Sutton, Mart Stewart, "Agent Orange and Narratives of Suffering," *Occam's Razor* 2 (**2012**): 36–64.

CONFERENCE PRESENTATIONS

1. "Molecular Design of Supramolecular Compounds and Nanomaterials"
   Poster Presentation, 2019 Self-Assembly and Supramolecular Chemistry Gordon Research Conference – May 17-24, 2019.

2. "Navigating the Energy Landscape of Graduate School"
   Oral Presentation, Invited speaker for the 2018 Western Washington University REU Symposium. Bellingham, WA.

3. "An Allosterically Regulated, Four-State Macrocycle"
   Oral Presentation, 255th American Chemical Society National Meeting; March 18-22, 2018

4. "Molecular Geometry and Bond-Strength Effects in Infinite Coordination Polymer Particles Bearing Weak-Link Approach Subunits"
   Oral Presentation, 2017 Self-Assembly and Supramolecular Chemistry Gordon Research Seminar; May 20, 2017, Les Diablerets, Switzerland

5. "Molecular Geometry and Bond-Strength Effects in Infinite Coordination Polymer Particles Bearing Weak-Link Approach Subunits"

Poster Presentation, 2017 Self-Assembly and Supramolecular Chemistry Gordon Research Conference, May 2017, Les Diablerets, Switzerland

6. "Stimuli-Responsive Supramolecular Assemblies *via* the Weak-Link Approach."
   Poster Presentation, April 21, 2016, National Science Foundation Mathematical and Physical Sciences Directorate Visit Poster Session

7. "Optimizing the Synthesis of Nickel Phosphide Catalysts for Heteroatom Removal Reactions."
   Oral Presentation, 2014 Western Washington University Honors Thesis Presentation

8. "Optimizing the Synthesis of Nickel Phosphide Catalysts for Heteroatom Removal Reactions."
   Poster Presentation, 2014 Pacific Northwest ACS Symposium

9. "Optimizing the Synthesis of Nickel Phosphide Catalysts for Heteroatom Removal Reactions."
   Poster Presentation, 2014 National ACS Conference (Best poster award, $250)

10. "Optimizing the Synthesis of Nickel Phosphide Catalysts for Heteroatom Removal Reactions."
    Oral Presentation, November 2013 MJ Murdock College Science Conference (Finalist for the John Van Zytveld award for best oral presentation in the physical sciences)

11. "Nickel Phosphide Hydrotreating Catalysts."
    Poster Presentation, September 2013 Pacific Northwest – AVS Science and Technology Symposium (Best undergraduate research poster award, $250)

12. "Nickel Phosphide Hydrotreating Catalysts."
    Poster Presentation, July 2013 WWU REU Undergraduate Research Symposium

13. "Investigating Ozone Stability: Ogawa Holding Time Experiment in Seattle, WA."
    Poster Presentation, August 2012 University of Washington Research Symposium

14. "Investigating Ozone Stability: Ogawa Holding Time Experiment in Seattle, WA."
    Poster Presentation, October 2012 SACNAS National Conference, Seattle, WA.

COMMUNITY & VOLUNTEER SERVICE

Fall 2018 – Present | Northwestern Prison Education Program (NPEP)
Northwestern University, Volunteer, Advisory Committee Member and Teacher. I help incarcerated students with coursework they are taking towards their Associates degree, at Stateville Correctional Center.

September 2015 – Present | HerStory Outreach Program
Northwestern University, Lead organizer and Volunteer. I organized "HerStory" in collaboration with the Museum of Science and Industry. The event is geared towards young minority females with a goal to inspire young women in science.

September 2015 – Present | NU Bond (*Building on Diversity*)
Northwestern University, Organizer, Board Member. Established NU BonD, with a goal of fostering a community built on inclusivity and diversity of thought, ideas and backgrounds.

January 2017 – Present | Faces of Science Seminar Series

Northwestern University, Organizer and board Member. Faces of Science is a 2-day lecture series recognizing leading scientists who are committed to science and diversity.

June 2019 | Museum of Science and Industry Engineer Your Future Event
As a scientist, I connected with youth and families through meaningful scientific conversations, hands-on activities and science demos.

February 2018–2019 | MSI Black Creativity Career Showcase
Interacted with kids and families through demonstrations, hands-on activities and one-on-one conversations about science at the Museum of Science and Industry.

2015 – 2019 | Science Club
Northwestern University, Volunteer. I develop and implement hands-on science lessons for underserved populations. This is a mentor-driven afterschool program for middle school youth in high need communities.

September 2015 – 2018 | Northwestern University ChemUnity
Northwestern University Department of Chemistry, Organizer, Board Member. Organized NU Chemistry Dept.'s first graduate student mentoring program.

September 2015 – 2016 | Northwestern's Science in the Classroom (SITC)
Northwestern University, 4th grade classroom leader and Volunteer. I taught 4th grade students basic concepts in science. I lead demonstrations and hands-on activities.

2014 – 2016 | Jugando con la Ciencia (JCLC – Translates to "Playing with Science")
Northwestern University, Volunteer. I design science lessons in Spanish for 3rd/4th grade Latino and minority students.

September 2014 – 2016 | Science in Society HELIX Magazine
Scientific writer/blogger, Northwestern University
(https://helix.northwestern.edu/entities/andrea-daquino)

GRANTS

June 2017 | National Science Foundation Research Grant from the Macromolecular, Supramolecular and Nanochemistry Program | Awarded for four years for a total of $595,000 with a start date of 08/01/17.

February 2016 | The Alumnae of Northwestern University Grant ($4,880) | This grant was awarded to NU BonD for the *Faces of Science* Seminar Series.

September 2016 | Northwestern ASCB COMPASS Outreach Grant ($688) | This grant was awarded to *Jugando con la Ciencia* for a science outreach event at Oakton Elementary, entitled "*Science Show in Spanish*".

TEACHING

Fall 2019 | Teaching general chemistry and general chemistry lab at Stateville Correctional Center with the Northwestern Prison Education Program (NPEP)

Fall 2014 – Winter 2015 | Organic Chemistry Teaching Assistant, Northwestern University

Spring 2015 |General Chemistry Teaching Assistant, Northwestern University

Spring 2015, Spring 2016 | Instrumental Analysis Teaching Assistant, Northwestern

Winter 2012 – Spring 2014 | Chemistry Tutor, Western Washington University

Fall 2013 | Laboratory Teaching Assistant, Western Washington University

PROFESSIONAL SOCIETY MEMBERSHIPS

2018 – Present | P.E.O. Member
2014 – Present | Women in Science and Engineering Research (WISER)
2016 – Present | Phi Lambda Upsilon Alpha Gamma Chapter Northwestern University
September 2012 – 2015 | Society for the Advancement of Hispanics/Chicanos and Native Americans in Science (SACNAS)
September 2012 – Present | American Chemical Society
February 2017 – Present | AAAS Member